

# **A NEW CLASS OF HIGH EFFICIENCY MULTIPHASE DC-DC CONVERTERS**

Teză destinată obținerii  
titlului științific de doctor inginer  
la  
Universitatea Politehnica Timișoara  
în domeniul  
INGINERIE ELECTRONICĂ ȘI TELECOMUNICAȚII  
de către

**Ing. Ioana-Monica Pop**

Conducător științific: prof.univ.dr.ing. Viorel Popescu  
Referenți științifici: prof.univ.dr.ing. Folker Renken  
prof.univ.dr.ing. Dorin Petreus  
prof.univ.dr.ing. Dan Lascu

Ziua susținerii tezei: 29 Iunie 2015

Seriile Teze de doctorat ale UPT sunt:

- |   |  |
|---|--|
| 1. Automatică                               | 9. Inginerie Mecanică                      |
| 2. Chimie                                   | 10. Știința Calculatoarelor                |
| 3. Energetică                               | 11. Știința și Ingineria Materialelor      |
| 4. Ingineria Chimică                        | 12. Ingineria sistemelor                   |
| 5. Inginerie Civilă                         | 13. Inginerie energetică                   |
| 6. Inginerie Electrică                      | 14. Calculatoare și tehnologia informației |
| 7. Inginerie Electronică și Telecomunicații | 15. Ingineria materialelor                 |
| 8. Inginerie Industrială                    | 16. Inginerie și Management                |

Universitatea Politehnica Timișoara a inițiat seriile de mai sus în scopul diseminării expertizei, cunoștințelor și rezultatelor cercetărilor întreprinse în cadrul Școlii doctorale a universității. Seriile conțin, potrivit H.B.Ex.S Nr. 14 / 14.07.2006, tezele de doctorat susținute în universitate începând cu 1 octombrie 2006.

Copyright © Editura Politehnica – Timișoara, 2015

Această publicație este supusă prevederilor legii dreptului de autor. Multiplicarea acestei publicații, în mod integral sau în parte, traducerea, tipărirea, reutilizarea ilustrațiilor, expunerea, radiodifuzarea, reproducerea pe microfilme sau în orice altă formă este permisă numai cu respectarea prevederilor Legii române a dreptului de autor în vigoare și permisiunea pentru utilizare obținută în scris din partea Universității Politehnica Timișoara. Toate încălcările acestor drepturi vor fi penalizate potrivit Legii române a drepturilor de autor.

România, 300159 Timișoara, Bd. Republicii 9,  
Tel./fax 0256 403823  
e-mail: editura@edipol.upt.ro

## Acknowledgment

“This work was partially supported by the strategic grant POSDRU 107/1.5/S/77265, inside POSDRU Romania 2007-2013 co-financed by the European Social Fund-Investing in People.”

The research project was carried out under the supervision of Professor PhD. Eng. Viorel Popescu from the Power Electronics Department, Faculty of Electronics and Telecommunications Engineering from the Politehnica University of Timisoara. First of all, I am deeply grateful to him for the professional support and direction he gave me starting with my master study and finishing with my PhD.

I would like to express my sincere heartfelt gratitude to Professor PhD. Eng. Folker Renken for his valuable guidance, constant encouragement, timely suggestions and constructive feedback during my research abroad period at University of Applied Science, Wilhelmshaven. It was a privilege for me to be my coordinator professor and work with him. I would like to extend my gratitude to Eng. Udo Schürmann for the support he gave me during building and testing the laboratory prototypes. It was a remarkable experience to work and learn from him.

I would like to thank PhD Peter van Duijsen from Simulation Research for providing me the license for CASPOC package, and his advice during my PhD period. Also, to Eng. Alexandru Pătru for his advice related to Saber simulator.

I would also like to express my appreciation to Professor PhD. Eng. Dan Lascu for his useful comments and suggestions regarding the thesis. My sincere appreciation also extends to my committee member Professor PhD. Eng. Dorin Petreuş.

To Professor PhD Eng. Ivan Bogdanov, I would like to thank for all the support, guidance and encouragement during the years, at the Politehnica University of Timisoara.

Particular thanks go to all my professors and my colleagues from the both university.

I would like to mention Tom Anna and his family. I thank them for their generous help and for all those unforgettable moments that always kept me positive even through hard times. Also, I would like to thank to the AKA team.

A big thank to all my friends and Sosdean family, that helps me and encouragement to continue and finish this work.

And finally, to my family, I would like to articulate my deepest gratitude for the unceasing confidence and encouragement which I have received from them.

I would like to dedicate this thesis to my husband Marius Pop-Călimanu and our daughter Aida. I thank him for unlimited understanding, profound love, and all the sacrifices he made during our doctoral studies.

*... any omissions in this brief acknowledgment does not mean lack of gratitude.*

Timișoara,  
June, 2015

Ioana-Monica Pop (căs. Pop-Călimanu)

Pop (căș. Pop-Călimanu), Ioana-Monica

**A New Class of High Efficiency Multiphase DC-DC Converters**

Teze de doctorat ale UPT, Seria 7, Nr. YY, Editura Politehnica, 2015, 205 pagini, 153 figuri, 8 tabele.

ISSN: 1842-7014

ISBN: 978-606-554-972-2

Keywords:

multiphase converter, interleaved converters, hybrid converters, L-switching cell, coupled inductors, high efficiency.

Abstract:

The present thesis wishes to offer a new class of high efficiency multiphase DC-DC converters. A brief presentation of the L- and C-switching structures proposed in the literature by Boris Axelrod, Yefim Berkovich and Adrian Ioinovici which are inserted in classical and bidirectional converters resulting 17 new hybrid structures, has been presented in the thesis. After a comparative study of the hybrid converters, one topology has been chosen and a method for increasing the efficiency, reducing the size through reducing the numbers of inductors without affecting the circuit operation and the dc voltage transfer function have been proposed. Analytical study, operating modes, simulation and experimental results have been included in the thesis. A synthesizing method for getting new multiphase hybrid converters is proposed. Also, 11 new topologies of multiphase hybrid DC-DC converter were proposed by the author. The validation of one of the multiphase hybrid converter proposed by the author is realised. Analytical study, system description, operating modes, simulation and experimental results have been included in the thesis for two-phase converter, and the deduction of the relationship was extended to n-phase converter. Simulation was realised in CASPOC Simulation Program and SABER Simulator. The proposed converter can be used as an interface between the renewable energy system (PV or fuel cell system) and the dc load/inverter/battery.

## Table of contents

<b>Nomenclature</b> .....	7
<b>List of tables</b> .....	10
<b>List of figures</b> .....	11
<b>Introduction</b> .....	16
<b>CHAPTER 1. DC-DC Converters for RE Systems – A General Review</b> .....	19
1.1. Introduction.....	19
1.2. Classical converters .....	20
1.2.1. Step-up Boost Converter.....	20
1.2.2. Step-down Buck converter .....	22
1.2.3. Buck–Boost converter.....	23
1.3. Bidirectional DC-DC converters.....	25
1.3.1. Bidirectional Boost/Buck DC-DC converter.....	25
1.3.2. Bidirectional Boost/Buck DC-DC converter with coupled inductors .....	26
1.3.3. Bidirectional Zeta-Sepic DC-DC converter .....	29
1.3.4. Bidirectional half-bridge/current-fed push-pull DC-DC converter .....	31
1.4. Other DC-DC converter structures .....	33
1.4.1. Forward Converter .....	33
1.4.2. Ćuk converter.....	34
1.4.3. Sepic converter.....	36
1.4.4. Zeta Converter .....	37
1.4.5. Flyback Converter .....	38
1.5. Association of power converters .....	41
1.5.1. Cascaded converters .....	41
1.5.2. Series converters .....	43
1.5.3. Parallel converters .....	46
1.6. Multiphase converter.....	46
1.7. Boost converter used for a measuring system .....	51
1.8. Conclusions and contributions .....	53
<b>CHAPTER 2. Multiphase Converters with Wide Conversion Ratio Using Hybrid Structures</b> .....	55
2.1. Introduction.....	55
2.2. Hybrid Buck converter with C-switching structure step-down 1.....	66
2.3. Hybrid Buck converter with L-switching structure step-down 1 .....	71

2.4. Hybrid Sepic converter with L-switching structure step-down 2 .....	75
2.5. Hybrid Boost converter with C-switching structure step-up 1.....	80
2.6. Hybrid Ćuk converter with C-switching structure step-up 2 .....	85
2.7. Hybrid Boost converter with L-switching structure step-up 1 .....	90
2.8. Multiphase DC-DC converters synthesis using hybrid structures .....	96
2.9. Conclusions and contributions .....	103
<b>CHAPTER 3. Hybrid Boost converter with L-switching structure step-up</b>	<b>1104</b>
3.1. Hybrid Boost DC-DC L-converter – input circuit .....	105
3.2. Hybrid Boost DC-DC L-converter – output circuit .....	111
3.3. Simulation of the Hybrid Boost DC-DC L-converter .....	114
3.4. Experimental results for the hybrid Boost DC-DC L-converter.....	121
3.5. Conclusions and contributions .....	136
<b>CHAPTER 4. Multiphase Hybrid Boost DC/DC L-converter</b> .....	<b>138</b>
4.1. Multiphase hybrid Boost DC-DC L-converter – input circuit.....	139
4.2. Multiphase hybrid Boost DC-DC L-converter – output circuit.....	144
4.3. Simulation of the two-phase hybrid Boost DC-DC L-converter .....	150
4.4. Practical Measurements for the two-phase hybrid Boost DC-DC L-converter .....	171
4.5. Conclusions and contributions .....	188
<b>CHAPTER 5. Conclusions and Contributions</b> .....	<b>191</b>
5.1. Conclusions .....	191
5.2. Contributions .....	191
5.3. Future works.....	192
<b>References</b> .....	<b>194</b>
<b>Author’s papers related to the thesis</b> .....	<b>204</b>

# Nomenclature

## List of notations

AC- alternative current

DC- direct current

DC-DC- direct current- direct current

d- duty cycle in steady state

$d_1$ - duty cycle of the first converter in steady state

$d_2$ - duty cycle of the second converter in steady state

$D, D_0, D_1, D_2, D_3, D_4, D_5, D_6$ - diodes

$D_{11}, D_{21}, D_{31}$ - diodes of phase one

$D_{12}, D_{22}, D_{32}$ - diodes of phase two

$D_{O1}$ - output diode of phase one

$D_{O2}$ - output diode of phase two

$f_s$ - switching frequency

$F_{Out}$ - output frequency

n- number of phases

$t_{off}$ - time period when the power switch is off

$t_{on}$ - conduction time, time period when the power switch is on

$S, S_1, S_2, S_3$ - power switches

$T_s$ - power switch period

## List of Abbreviations, Acronyms

CCM- continuous conduction mode

DCM- discontinuous conduction mode

DSP- digital signal processing

e.g.- for example

IGBT- insulated-gate bipolar transistor

M- voltage gain(dc voltage transfer function)

MOSFET- metal-oxide-semiconductor field-effect transistor

PCB- printed circuit board

PFC- power factor correction

PV- photovoltaic

PWM- pulse width modulation

RE- renewable energy

RMS- root mean square

## List of Symbols

$C, C_0, C_1, C_2, C_a, C_b, C_{ab}$ - capacitors [F]

$C_I$ - input capacitor [F]

$C_O$ - output capacitor [F]

$GS, GS_1, GS_2, GS_3, GS_4$  - gate signal

$i$ - current [A]

$i_C, i_{C1}, i_{C_a}, i_{C_b}, i_{C_{ab}}$ - capacitor current

$i_{iC}$ - input capacitor current

$i_{iP}$ - input phase current

$i_{IP1}$ - input current of phase one  
 $i_{IP2}$ - input current of phase two  
 $i_{IPN}$ - input current of phase N  
 $i_L, i_{L0}, i_{L1}, i_{L2}$ - inductor current  
 $i_{L11}, i_{L21}$ - currents in inductances of phase one  
 $i_{L12}, i_{L22}$ - currents in inductances of phase two  
 $i_{OC}$ - output capacitor current  
 $i_{OP}$ - output phase current  
 $i_{OP1}$ - output current of phase one  
 $i_{OP2}$ - output current of phase two  
 $i_{OPN}$ - output current of phase N  
 $i_S, i_{S1}, i_{S2}$ - switch current  
 $I_D$ - RMS current in the diode  
 $I_{DAV}$ -average current value in the diode  
 $I_{DO}$ - RMS current in the output diode  
 $I_{DOAV}$ - average current value in the output diode  
 $I_{IC}$ - RMS current in the input capacitor  
 $I_{IC \Pi}$ - RMS current in the input capacitor, rectangular part  
 $I_{IC \Delta}$ - RMS current in the input capacitor, triangular part  
 $I_{In}$ - input current of the converter  
 $I_L$ - RMS current in the inductors  
 $I_{L1AV}$ - dc inductor current of the phase one  
 $I_{LAV}$ - average current in the inductor  
 $I_{LAVR}$ - rated average inductance current  
 $I_{LnAV}$ - dc inductor current of the individual phases  
 $I_{LnAVR}$ - dc inductor current of the individual phases at rated power  
 $I_{out}$ - output current of the converter  
 $I_S$ - RMS current in the switch  
 $I_{SAV}$ - average current value in the power switch  
 $L, L_1, L_2$ - inductors [H]  
 $L_{11}, L_{21}$ - inductors of phase one [H]  
 $L_{12}, L_{22}$ - inductors of phase two [H]  
 $L_{1n}, L_{2n}$ - inductors of individual phases [H]  
 $L_{EQ}$ - equivalent inductor value  
 $L_m$ - transformer magnetizing inductance  
 $M$ - mutual inductance  
 $n_1, n_2, n_3$ - windings turns number of the transformer  
 $N_p, N_{p1}$ - number of turns in the primary coil  
 $N_s$ - number of turns in the secondary coil  
 $P_{InR}$ - rated input power [W]  
 $R, R_a, R_b$ - converters resistance [ $\Omega$ ]  
 $t$ - time  
 $u_L, u_{L0}, u_{L1}, u_{L2}$ - inductor voltage or voltage across inductor [V]  
 $u_{S1}, u_{S2}, u_{S3}, u_{S4}$ - switch voltage [V]  
 $U_a, U_b$ - input/output voltage for bidirectional converter [A]  
 $U_{in}$ - input voltage [V]  
 $U_{out}$ - output voltage [V]  
 $U_{bat}$ - battery voltage [V]  
 $U_{in1}$ - input voltage (source) 1[V]  
 $U_{in2}$ - input voltage (source) 2[V]  
 $U_{inR}$ - input voltage at rated power



$U_{outR}$  - output voltage at rated power

$\Delta i_{Lmax}$  - maximum inductor current variation

$\Delta i_{Ln}$  - current variation in n inductors

$\Delta u_{Inmax}$  - maximum acceptable static input voltage variation

$\Delta i_{Lnmax}$  - maximum current variation of the dc-phase current in the inductances

$\Delta u_{Outmax}$  - maximum acceptable output voltage variation.

## List of tables

Table 2.1. Hybrid converter [3]- [4] [5] .....	57
Table 2.2. Output voltage equation for hybrid converters [3]-[4][5] .....	63
Table 2.3. Possible combination for multiphase converters with hybrid structure...	97
Table 2.4. Output voltage equations for multiphase hybrid converters .....	102
Table 4.1. Simulation results for uncoupled and directly coupled inductor $d=1/3$ .	150
Table 4.2. Simulation results for uncoupled and directly coupled inductor $d=1/2$ .	151
Table 4.3. Simulation results for uncoupled and directly coupled inductor $d=2/3$ .	151
Table 4.4. Simulation results for the coupled inductor single and two-phase Boost L-converters when $d=1/3$ .....	169

## List of figures

Figure 1.1. Circuit diagram of the Boost converter [70] .....	20
Figure 1.2. Main waveforms associated to the Boost converter [70] .....	21
Figure 1.3. Circuit diagram of the Buck converter [70] .....	22
Figure 1.4. Main waveforms associated to the Buck converter [70] .....	23
Figure 1.5. Circuit diagram of the Buck-Boost converter [70] .....	24
Figure 1.6. Main waveforms associated to the Buck-Boost Converter [70] .....	24
Figure 1.7. Circuit diagram of the bidirectional Boost/Buck DC-DC converter [77].	25
Figure 1.8. Equivalent circuit of the converter in step-up mode [77] .....	26
Figure 1.9. Equivalent circuit of the converter in step-down mode [77] .....	26
Figure 1.10. Circuit diagram of the bidirectional Boost/Buck converter with coupled inductors [77] .....	27
Figure 1.11. Equivalent circuit of the Boost/Buck converter in step-up mode [77].	27
Figure 1.12. Equivalent circuit of the Boost/Buck converter in step-down mode [77] .....	28
Figure 1.13. Waveforms of the Boost/Buck converter in step-up and step-down modes [77] .....	28
Figure 1.14. Circuit diagram of the Zeta-Sepic converter [79] .....	29
Figure 1.15. Equivalent circuit of the Zeta-Sepic converter when switch S1 is conducting [79] .....	29
Figure 1.16. Equivalent circuit of the Zeta-Sepic converter when switch S2 is conducting [79] .....	30
Figure 1.17. Main waveforms when Zeta converter is active, and when Sepic converter is active [79] .....	30
Figure 1.18. Circuit diagram of the bidirectional half-bridge/current-fed push-pull converter [80] .....	31
Figure 1.19. Equivalent circuit of the bidirectional half-bridge/current-fed push-pull converter in forward/charging mode [80] .....	31
Figure 1.20. Equivalent circuit of the bidirectional half-bridge/current-fed push-pull converter in current-fed/backup mode [80] .....	32
Figure 1.21. Waveforms of the bidirectional half-bridge/current-fed push-pull converter during the forward/charging mode and current-fed/backup mode [80] .	32
Figure 1.22. Circuit diagram of the Forward converter [7] .....	33
Figure 1.23. Main waveforms of Forward converter [7] .....	34
Figure 1.24. Circuit diagram of the Ćuk converter [70] .....	35
Figure 1.25. Main waveforms of Ćuk converter [70] .....	35
Figure 1.26. Circuit diagram of the Sepic converter [6] .....	36
Figure 1.27. Main waveforms of the SEPIC converter [6] .....	37
Figure 1.28. Circuit diagram of the Zeta converter [6] .....	37
Figure 1.29. Main waveforms of the Zeta converter [6] .....	38
Figure 1.30. Circuit diagram of the Flyback converter [6] .....	39
Figure 1.31. Main waveforms of the Flyback converter [6] .....	40
Figure 1.32. Cascaded connection of power converters [68] .....	41
Figure 1.33. Circuit diagram of cascade of two Buck converters [87] .....	42
Figure 1.34. Circuit diagram of cascade of two Buck converter with a single switch [87] .....	42
Figure 1.35. Circuit diagram of cascade of two Boost converters [90] .....	43
Figure 1.36. Cascade of two Boost converter with single switch [88] .....	43

Figure 1.37. Series connection of power converter [85].....	44
Figure 1.38. Circuit diagram of the integrated Buck/ Buck converter [96] .....	45
Figure 1.39. Waveforms of the integrated Buck/ Buck converter [96].....	45
Figure 1.40. Parallel connection of power converters [85].....	46
Figure 1.41. Switching signals for a 2-phase converter [59].....	47
Figure 1.42. Circuit diagram of the two-phase Buck converter [111].....	47
Figure 1.43. Waveforms of the two-phase Buck converter [111] .....	48
Figure 1.44. Circuit diagram of a two-phase Buck converter with coupled inductors [111].....	49
Figure 1.45. Waveforms of two-phase Buck converter with coupled inductors [111] .....	49
Figure 1.46. Circuit diagram of the two-phase Boost converter [112].....	50
Figure 1.47. Waveforms of the two-phase Boost converter [112] .....	50
Figure 1.48. Block diagram of the monitoring system .....	51
Figure 1.49. Block scheme of the measuring system .....	52
Figure 1.50. Design circuit of Boost converter [71] .....	52
Figure 1.51. General scheme of the monitoring system [67] .....	53
Figure 2.1. C-switching structures: a) Step-up 1; b) Step-up 2; c) Step-down 1[4] .....	55
Figure 2.2. L-switching structures: a) Step- down 1; b) Step- down 2; c) Step-up 1[4].....	56
Figure 2.3. Comparison between conversion ratios of the step-up hybrid converter64	
Figure 2.4. Comparison between conversion ratios of the step-down hybrid converter.....	66
Figure 2.5. Hybrid Buck converter with C-switching structure step-down 1: a) circuit diagram; b) switched-on ( $t_{on}$ ) state; c) switched-off ( $t_{off}$ ) state [4] .....	67
Figure 2.6. Comparison between conversion ratios of a hybrid Buck DC-DC C-converter and a classical Buck DC/DC converter .....	68
Figure 2.7. CASPOC simulation diagram for the hybrid Buck DC-DC C-converter... 69	
Figure 2.8. Simulation results for the hybrid Buck DC-DC C-converter .....	69
Figure 2.9. Hybrid Buck converter with L-switching structure step-down 1: a) circuit diagram; b) switched-on ( $t_{on}$ ) state; c) switched-off ( $t_{off}$ ) state [4] .....	72
Figure 2.10. CASPOC simulation diagram for the hybrid Buck converter with L-switching structure step-down 1 .....	73
Figure 2.11. Simulation results for the hybrid Buck DC-DC L-converter.....	74
Figure 2.12. Hybrid Sepic DC-DC L-converter: a) circuit diagram; b) switched-on ( $t_{on}$ ) state; c) switched-off ( $t_{off}$ ) state [5].....	76
Figure 2.13. Comparison between conversion ratio of a hybrid Sepic DC-DC L-converter and classical Sepic DC/DC converter .....	77
Figure 2.14. CASPOC simulation diagram for the hybrid Sepic DC-DC L-converter. 78	
Figure 2.15. Simulation results for the hybrid Sepic DC-DC L-converter .....	78
Figure 2.16. Hybrid Boost DC-DC C-converter: a) circuit diagram; b) switched-on ( $t_{on}$ ) state; c) switched-off ( $t_{off}$ ) state [1].....	81
Figure 2.17. Comparison between conversion ratio of a hybrid Boost DC-DC C-converter and classical Boost DC/DC converter.....	82
Figure 2.18. CASPOC simulation diagram for the hybrid Boost DC-DC C-converter 83	
Figure 2.19. Simulation results for the hybrid Boost DC-DC C-converter .....	83
Figure 2.20. Hybrid Ćuk DC-DC C-converter: a) circuit diagram; b) switched-on ( $t_{on}$ ) state; c) switched-off ( $t_{off}$ ) state [4].....	86
Figure 2.21. Comparison between conversion ratio of a hybrid Ćuk DC-DC C-converter and classical Ćuk DC/DC converter .....	87

Figure 2.22. CASPOC simulation diagram of the hybrid Ćuk DC-DC C-converter....	88
Figure 2.23. Simulation results for the hybrid Ćuk DC-DC C-converter.....	88
Figure 2.24. Hybrid Boost DC-DC L-converter: a) circuit diagram; b) switched-on ( $t_{on}$ ) state; c) switched-off ( $t_{off}$ ) state [103].	91
Figure 2.25. CASPOC circuit diagram for the hybrid Boost DC-DC L-converter .....	92
Figure 2.26. Simulation results for the hybrid Boost DC-DC L-converter.....	93
Figure 3.1. Circuit diagram of hybrid Boost DC-DC L-converter [103] .....	105
Figure 3.2. Current waveforms at the input of a single phase hybrid Boost DC/DC converter a) $d=0.3$ b) $d=0.5$ c) $d=0.7$ [103] .....	106
Figure 3.3. Maximum power transfer in case of fixed output voltage [103] .....	108
Figure 3.4. RMS current in the input capacitor of a single phase hybrid Boost DC/DC converter [103] .....	110
Figure 3.5. Current waveforms at the output of a single phase hybrid Boost DC/DC converter a) $d=0.3$ b) $d=0.5$ c) $d=0.7$ [103] .....	111
Figure 3.6. RMS Current in the output capacitor of a single phase hybrid Boost DC/DC converter [103] .....	114
Figure 3.7. CASPOC simulation diagram for the hybrid Boost DC-DC L-converter coupled inductor .....	115
Figure 3.8. Simulation results for the hybrid Boost DC-DC L-converter with coupled inductors, $U_{in}=40V$ and $d=50\%$ .....	116
Figure 3.9. Simulation results for the hybrid Boost DC-DC L-converter with coupled inductors, $U_{in}=60V$ and $d=33.3\%$ .....	119
Figure 3.10. Image of the experimental hybrid Boost DC-DC L-converter .....	122
Figure 3.11. Input voltage waveform when $d=1/3$ .....	123
Figure 3.12. MOSFET current waveform when $d=1/3$ .....	123
Figure 3.13. Input phase current waveform when $d=1/3$ .....	124
Figure 3.14. The current in the inductors when $d=1/3$ .....	124
Figure 3.15. Output phase current waveform when $d=1/3$ .....	125
Figure 3.16. Output current waveform when $d=1/3$ .....	125
Figure 3.17. Output voltage waveform when $d=1/3$ .....	126
Figure 3.18. Input voltage waveform when $d=1/2$ .....	127
Figure 3.19. MOSFET current waveform when $d=1/2$ .....	127
Figure 3.20. Input phase current waveform when $d=1/2$ .....	128
Figure 3.21. Current in the inductors when $d=1/2$ .....	128
Figure 3.22. Output phase current waveform when $d=1/2$ .....	129
Figure 3.23. Output current waveform when $d=1/2$ .....	129
Figure 3.24. Output voltage waveform when $d=1/2$ .....	130
Figure 3.25. Input voltage waveform when $d=2/3$ .....	131
Figure 3.26. MOSFET current waveform when $d=2/3$ .....	131
Figure 3.27. Input phase current waveform when $d=2/3$ .....	132
Figure 3.28. Current in the inductors when $d=2/3$ .....	132
Figure 3.29. Output phase current waveform when $d=2/3$ .....	133
Figure 3.30. Output current waveform when $d=2/3$ .....	133
Figure 3.31. Output voltage waveform when $d=2/3$ .....	134
Figure 3.32. Saber simulation diagram for the hybrid Boost DC-DC L-converter ..	134
Figure 3.33. Simulation results for the hybrid Boost DC-DC L-converter.....	135
Figure 3.34. Efficiency vs output power $d=1/3$ .....	135
Figure 4.1. The architecture of a multiphase hybrid boost DC/DC converter [120] .....	138
Figure 4.2. Schematics of a two-phase hybrid boost DC/DC converter [120].....	139

Figure 4.3. Input currents of a two-phase DC/DC converter with duty cycles a) $d=0.3$ , b) $d=0.5$ , c) $d=0.7$ [120] .....	140
Figure 4.4. Output currents of a two-phase DC/DC converter with duty cycles: a) $d=0.3$ , b) $d=0.5$ , c) $d=0.7$ [120] .....	144
Figure 4.5. RMS input capacitor currents of a one-, two- and three-phase converter [103].....	148
Figure 4.6. RMS output capacitor currents of a one-, two- and three-phase converter [103].....	149
Figure 4.7. CASPOC circuit diagram for the two-phase hybrid Boost DC-DC L-converter coupled inductor.....	152
Figure 4.8. Simulation results for the two-phase hybrid Boost DC-DC L-converter with coupled inductors, $d=33.3\%$ .....	153
Figure 4.9. Simulation results for the two-phase hybrid Boost DC-DC L-converter with coupled inductors, $d=50\%$ .....	158
Figure 4.10. Simulation results for the two-phase hybrid Boost DC-DC L-converter with coupled inductors, $d=66.7\%$ .....	163
Figure 4.11. Simulation waveform for input current for the single phase hybrid Boost L-converter in the case of $d=50\%$ .....	168
Figure 4.12. Simulation waveform for input current for the two-phase hybrid Boost L-converter in the case of $d=50\%$ .....	168
Figure 4.13. Simulation waveform for output current for a single phase hybrid Boost L-converter in the case of $d=50\%$ .....	169
Figure 4.14. Simulation waveform for output current for a two-phase hybrid Boost L-converter in the case of $d=50\%$ .....	169
Figure 4.15. Image of the experimental two-phase hybrid Boost DC-DC L-converter [120].....	171
Figure 4.16. Input current and voltage waveforms when $d=1/3$ [120] .....	173
Figure 4.17. MOSFET current and voltage of first phase switch when $d=1/3$ [120] .....	174
Figure 4.18. MOSFET current and voltage of second phase switch when $d=1/3$ ... ..	174
Figure 4.19. Input current and input phase current of the first and second phase when $d=1/3$ [120].....	175
Figure 4.20. Current in the inductors of the first phase and second phases when $d=1/3$ [120] .....	175
Figure 4.21. Output phase current of the first and second phases when $d=1/3$ ... ..	176
Figure 4.22. Output current and output voltage waveforms when $d=1/3$ [120] .. ..	176
Figure 4.23. Input current and voltage waveforms when $d=1/2$ [120] .....	177
Figure 4.24. MOSFET current of first and second phase when $d=1/2$ .....	178
Figure 4.25. MOSFET current and voltage of the first phase when $d=1/2$ [120] .. ..	178
Figure 4.26. MOSFET voltage and current for the second phase when $d=1/2$ .....	179
Figure 4.27. Input current and input phase current of first and second phases when $d=1/2$ [120] .....	179
Figure 4.28. Current in the inductors of first and second phase when $d=1/2$ [120] .....	180
Figure 4.29. Output phase current of first phase when $d=1/2$ .....	180
Figure 4.30. Output phase current of second phase when $d=1/2$ .....	181
Figure 4.31. Output current and voltage waveforms when $d=1/2$ [120] .....	181
Figure 4.32. Input voltage and current waveforms when $d=2/3$ .....	182
Figure 4.33. MOSFET voltage and current of the first phase when $d=2/3$ .....	183
Figure 4.34. MOSFET voltage and current of the second phase when $d=2/3$ .....	183

Figure 4.35. Input current and input phase current of the first and second phase when $d=2/3$ .....	184
Figure 4.36. Current in the inductors of first phase and second phase when $d=2/3$ .....	184
Figure 4.37. Output phase current of first and second phase when $d=2/3$ .....	185
Figure 4.38. Output current and voltage waveforms when $d=2/3$ .....	185
Figure 4.39. Saber circuit diagram for the two-phase hybrid Boost DC-DC L-converter .....	186
Figure 4.40. Simulation results for the two-phase hybrid Boost DC-DC L-converter, output and input power .....	187
Figure 4.41. Efficiency vs output power $d=1/3$ .....	187
Figure 4.42. Efficiency vs output power $d=1/2$ .....	188

# Introduction

## Motivation

The evolution of modern power electronics is of main concern in the modern economy. Many applications starting from automotive and continuing with industrial and renewable energy require step-up or step-down converters respectively, with a higher/lower conversion ratio.

In a DC-DC converter the input voltage is converted to an output voltage having larger or smaller amplitude, opposite or, the same and isolated or nonisolated polarity, with respect to the input side. Classical DC-DC converters are unable to provide very high step-up or step-down conversion ratios. On the other side, utilization of transformers to achieve higher/lower conversion ratios comes with a decrease in efficiency.

Boris Axelrod, Yefim Berkovich and Adrian Ioinovici [1]-[6], propose several simple switching structures, consisting by either two capacitors and two-three diodes (C-switching), or two inductors and two-three diodes (L-switching) that can be inserted in classical converters in order to get new converter topologies. The new structures have a very large step-up or step-down conversion ratio compared to the classical converters.

The multiphase converter is a circuit where the same "n"- converter topology are connected in parallel both at the input and at the output, at a common input and output capacitor of the converter, forming the different phases that are controlled with phase shift.

One basic goal of this study is to try to extend the existing knowledge and techniques obtained from classical multiphase converters to the hybrid multiphase converters.

## Thesis outline

In this work, different hybrid multiphase DC-DC converter topologies are proposed, analytically studied, digitally simulated and validated through practical experiments. The dissertation consists of 5 chapters and is organized as follows.

**Chapter 1** was thought as a general introduction to DC-DC converters. Different structures of DC-DC converters for renewable energy systems encountered in the literature are presented by the author through a comprehensive literature survey.

The survey was done via a classification of these DC-DC converters in three classes: classical converters, bidirectional converters and association of converters.

A special focus was made on the parallel and multiphase converters that are the subject of the thesis.

**Chapter 2** presents the L and C-switching structures proposed by Boris Axelrod, Yefim Berkovich and Adrian Ioinovici. These structures are inserted in classical and bidirectional converters resulting in new hybrid structures. The possible hybrid structures are presented in Table 2.1, and the new conversion ratios are presented in Table 2.2.

A comparative analysis of the hybrid converters is performed by the author. Such an analysis is very important before making a choice for a hybrid converter.



Different hybrid DC-DC converter topologies, with switched capacitor or switched inductor cells inserted in the classical or bidirectional converters are studied and simulated. From this study a synthesizing method for multiphase hybrid converters is proposed.

A method for increasing the efficiency, reducing the size through reducing the numbers of inductors in the hybrid L-converter without affecting the circuit operation and the dc voltage transfer function, is also proposed.

In Table 2.3 eleven new multiphase converters with hybrid structures that are possible to be implemented are proposed by the author.

In **Chapter 3** one hybrid step-up structure has been chosen due to its advantages and a complete description with an analytical study, operating modes, waveforms, and design parameters is provided. A method for improving the drawbacks of the circuit is also described and compared with the help of digital simulation.

The digital simulation results are validated by experimental results obtained from a laboratory prototype.

In **Chapter 4** the hybrid step-up structure that was analyzed in Chapter 3, is used to build multiphase converter. A two-phase hybrid Boost L-converter is designed.

The new converter is analytically studied, the operating modes are presented, together with the main waveforms and design parameters. Experimental results validated the simulation and theoretical analyses for these types of converters. An analysis and a comparison between single phase structures and two-phase structures are also performed. The main features of the multiphase converters are evaluated at the end of this chapter.

The thesis ends with **Chapter 5**, that summarizes the conclusions, original contributions of the author and possible future work.

### **Thesis objectives**

- to perform a review of the main DC-DC converters used for renewable energy systems developed in the literature;
- to analyse and compare the switching cells structures;
- to analyse and compare the hybrid converters;
- to present the main methods and rules (synthesizing method) to generate new multiphase hybrid converters;
- to propose a new class of multiphase DC-DC converter topologies based on hybrid structures;
- to study both analytically and through digital simulation the proposed converters;
- to build and test laboratory prototypes in order to practically validate the theoretical results and simulations.

Theoretical concepts developed throughout the chapters are supported and validated by simulations as a preliminary phase.

Single phase hybrid Boost L-converter and two-phase hybrid Boost L-converter are compared through experimental results obtained from a laboratory prototype. The laboratory prototypes were built at the University of Applied Science Wilhelmshaven, in the Power Electronic laboratory, number L122a.

For experimental results and efficiency calculation of the converters the following technical equipment was used:

- LeCroy waverunner LT354M Oscilloscope;
- LeCroy AP015 Current Probe;

- Universal Waveform Generator Wavetek 40 MHz;
- Electronic Load EA-EL 9160-100;
- Multichannel Precision Power Meter Electronic Systems ZES ZIMMER LMG 450.

For text editing, design and simulation media the author used the following tools:

- for text editing: Microsoft Office Word 2007;
- for calculations and graphics: Mathcad Prime 2.0, Matlab R2011a and Microsoft Office Excel 2007;
- for circuit simulation program: CASPOC package, Saber Simulator;
- for schematic and layout design: EAGLE PCB design software.

# CHAPTER 1. DC-DC Converters for RE Systems – A General Review

## 1.1. Introduction

The growing market for renewable energy technologies has resulted in a rapid growth in the need of power electronics. Most of the renewable energy technologies produce dc power and hence power electronics and control equipment to process this power, or, to convert the DC into AC power [7] - [8] is required.

The task of a power converter is to process and control the flow of electric energy by supplying voltages and currents in a form that is optimally suited for user loads [9] - [10].

An ideal converter controls the flow of power between the input and output with 100% efficiency [11] - [12]. To define basic topologies, it is assumed that no losses occur in power processing. A power converter is composed by:

- non-linear elements, mainly electronic switches used in commutation mode;
- linear reactive elements, like capacitors, inductances and transformers.

These components are used for intermediate energy storage but also for voltage and current filtering, and represent an important part of the size, weight, and cost of the converter, and can reduce its lifetime [13].

The power converter can be designed with different topologies and with one or several intermediate conversion stages. The topology will mainly depend on the type of the load, dc level of the input and the output voltage and the power level processed.

In a RE system, the DC-DC converter converts a dc input voltage, to a dc output voltage, with a magnitude lower or higher than the input voltage.

The DC-DC converter is always presented in a stand-alone PV system. In this type of system, the PV energy has to be stored in a battery, to guarantee the energy when the sun is not present. In grid connected systems is widely used to extract the maximum PV energy from the PV module/array.

Different DC-DC converters, with different constraints are required due to the distinction between stand alone and grid connected PV systems.

Several DC-DC converters for PV systems and their corresponding control have been presented in literature. Between them the most remarkable are:

- the classical converters - Boost, Buck, Buck-Boost;
- bidirectional converters - Boost/Buck, Zeta-Sepic, half-bridge/current-fed push-pull, full-bridge/center tapped push-pull;
- association of converters - multi-input connection, multilevel connection, cascaded connection, series connection, parallel connection and multiphase connection.

The first converters used in PV systems were the classical Boost, Buck and Buck-Boost converters [14] - [19]. These converters are still adequate and are used in photovoltaic applications for battery charging or for a system in which high-step-up/down of the voltage is not needed.

The bidirectional DC-DC converter along with energy storage has become a widely used option not just for PV systems and renewable energy [20]-[27], but also for hybrid vehicles, fuel cell vehicles, in automotive domain and so forth [28] -

[34]. It reduces the cost, improves efficiency and also improves the performance of the system.

The different associations of power converters are widely used solutions today in various applications, not just in PV systems. For instance, the multi-input DC-DC converters are used in renewable energy generation systems and automotive industry [35] - [44]. The multilevel converter can be used in the utility interface for renewable energy systems, high-power applications, flexible AC transmission systems, traction drive systems and industrial voltage motor drives [45] - [51]. In embedded fields such as computers and satellites, in order to achieve more robust architectures through the concept of redundancy, we can note complex distributed architectures with more than three stages in cascade connection [52] - [54], and in parallel connection. In railway systems, there are new series topologies linked to the parallel ones that achieve high voltage levels and supply locomotive motors. Parallel connection is also used in the systems of low voltage levels but with high current levels, in the case of point of load or voltage regulator modules and for uninterruptible power supplies [55] - [58].

The multiphase configuration is very popular in battery storage systems for small renewable energy [59]. Also it can be used as power supply for high performance microprocessors [60] - [61], in applications such as motor drives, power factor correction equipment and for uninterruptible power supplies [62] - [66].

A lot of electrical problems are solved through interconnection of power converters. New optimized structures with new or even improved characteristics can be achieved with new techniques of inter-connections.

This chapter is an overview of the DC-DC converters for PV Systems described in the literature.

## 1.2. Classical converters

### 1.2.1. Step-up Boost Converter

The simplest step-up DC-DC converter structure used for RE systems is the Boost converter [17], [19], [67]-[68]. The circuit diagram of Boost converter is presented in Figure 1.1, [69] - [70].

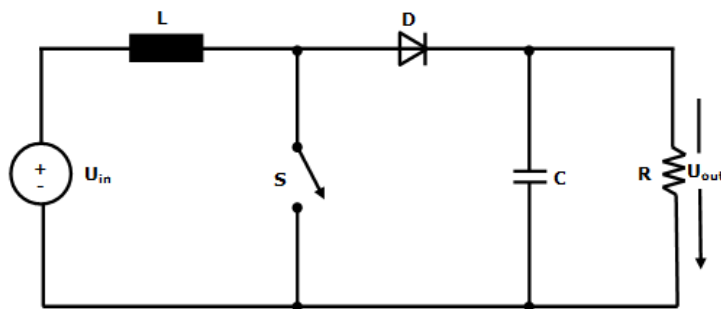


Figure 1.1. Circuit diagram of the Boost converter [70]

As the name of the converter suggests, the converter is able to produce a dc output voltage that is higher in magnitude than the dc input voltage.

When the switch  $S$  is in the on state, diode  $D$  is off, and the current in the Boost inductor increase linearly. When the switch  $S$  is turned off, the energy stored in the

inductor L is released into the output through the diode D, adding to the input voltage source, and setting the output voltage to the desired value as a function of the converter's duty cycle [70] - [72]. The author is using this converter in [72]. The converter waveforms in CCM are presented in Figure 1.2.

According to the inductor volt-second balance, product over a period of steady-state operation is zero. For the Boost converter this implies that:

$$U_{in} \cdot dT_s = (U_{out} - U_{in}) \cdot (1-d) \cdot T_s \quad (1.1)$$

from which the dc voltage transfer function (voltage gain), defined as the ratio of the dc output voltage to the dc input voltage turns out to be:

$$M = \frac{U_{out}}{U_{in}} = \frac{1}{1-d} \quad (1.2)$$

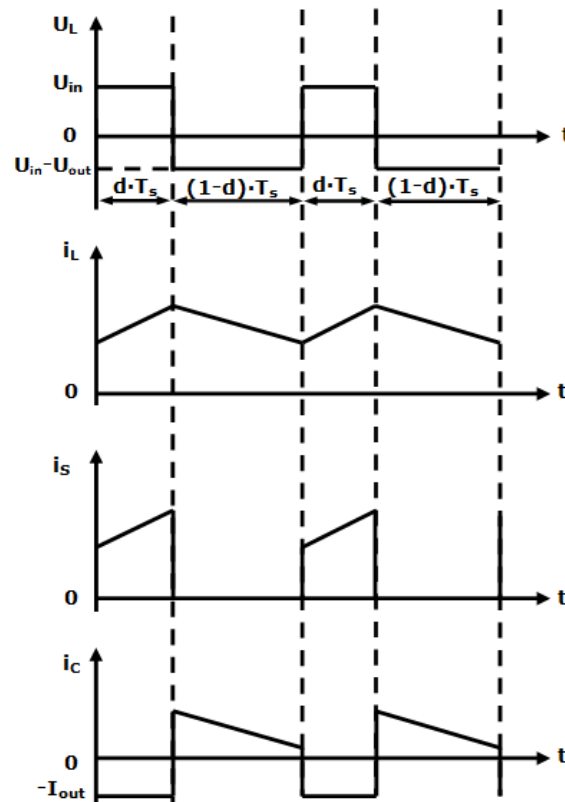


Figure 1.2. Main waveforms associated to the Boost converter [70]

Advantages [73]:

- simplicity;
- low number of components;
- the ability to achieve up conversion without a transformer;
- low cost;
- and, a good efficiency.

Disadvantages [73]:

- limited power level;
- high output ripple due to all of the off-time energy coming from the output capacitor C;
- difficult control at start-up as the energy is delivered to the load in the off state of the transistor and the switch is in parallel to the input.

### 1.2.2. Step-down Buck converter

The Buck converter is one of the most basic and simple topologies of step-down converter. As the name of the converter suggests, the main function is to reduce or “buck” the dc input voltage to a lower dc output voltage. The circuit diagram of Buck converter is presented in Figure 1.3, and, the converter waveforms are presented in Figure 1.4.

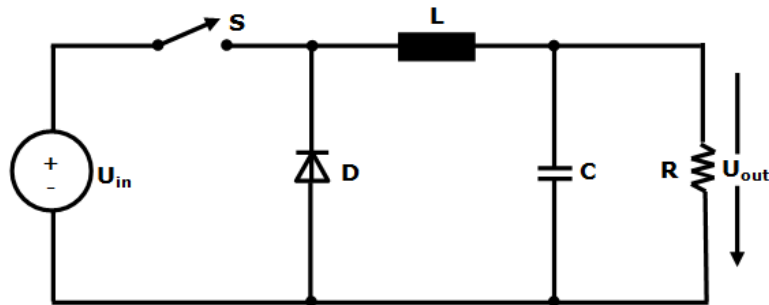


Figure 1.3. Circuit diagram of the Buck converter [70]

When the switch S is in the on state the diode D is reverse biased. When the switch S is in the off state, the diode conducts to sustain an uninterrupted current in the inductor [7], [70].

According with the inductor volt-second balance, product over a period of steady-state operation is zero. For the Buck converter this is written as:

$$(U_{in} - U_{out}) \cdot dT_s = -U_{out}(1 - d) \cdot T_s \quad (1.3)$$

from which the dc voltage transfer function turns out to be:

$$M = \frac{U_{out}}{U_{in}} = d \quad (1.4)$$

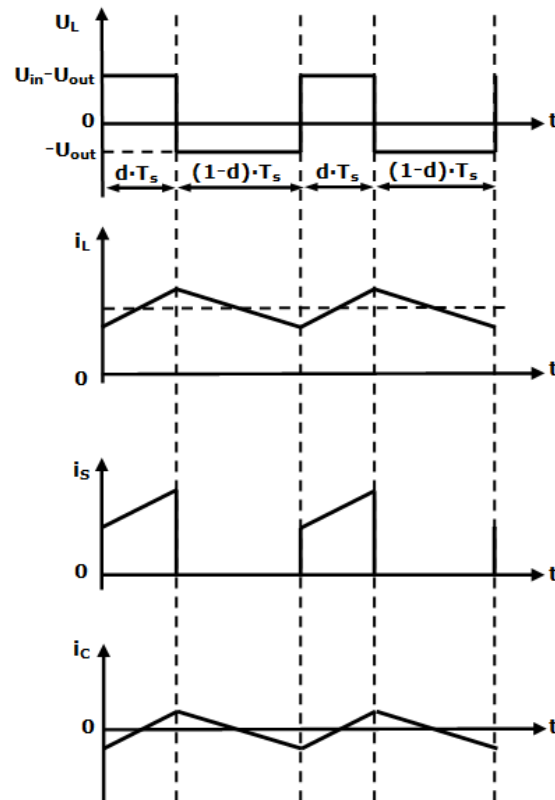


Figure 1.4. Main waveforms associated to the Buck converter [70]

**Advantages [73]:**

- simplicity;
- low number of components;
- the facility for control;
- the ability to achieve down conversion without a transformer;
- low cost.

**Disadvantages [73]:**

- limited power level;
- dc path from input to output in the event of a shorted switch element, which can make secondary circuit protection more difficult.

**1.2.3. Buck–Boost converter**

As the name of the converter suggests, the converter is able to produce an output voltage magnitude that can be either higher or lower than the input voltage. With the switch on, input voltage is applied across the inductor and the inductor current increases, while the diode is maintained off. When the switch is turned off, the voltage across the inductor reverses in polarity and the diode conducts. During this interval the energy stored in the inductor supplies the load and recharges the capacitor.

The circuit diagram of Buck-Boost converter is presented in Figure 1.5 and, the converter waveforms are presented in Figure 1.6.

The polarity of the output voltage is opposite to that of the input voltage [7], [70].

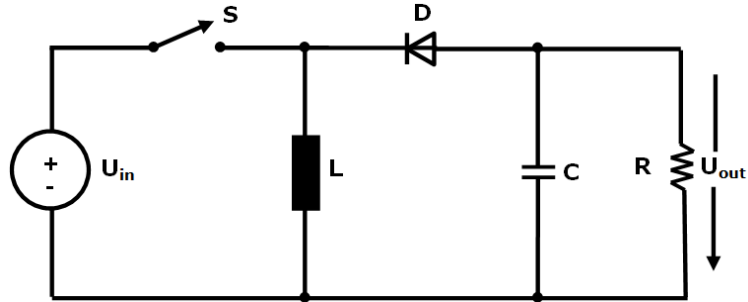


Figure 1.5. Circuit diagram of the Buck-Boost converter [70]

According with the inductor volt-second balance, product over a period of steady-state operation is zero. For the Buck-Boost converter one obtains:

$$U_{in} \cdot dT_s = -U_{out}(1-d) \cdot T_s \quad (1.5)$$

Hence, the dc voltage transfer function of the buck-boost converter is:

$$M = \frac{U_{out}}{U_{in}} = -\frac{d}{1-d} \quad (1.6)$$

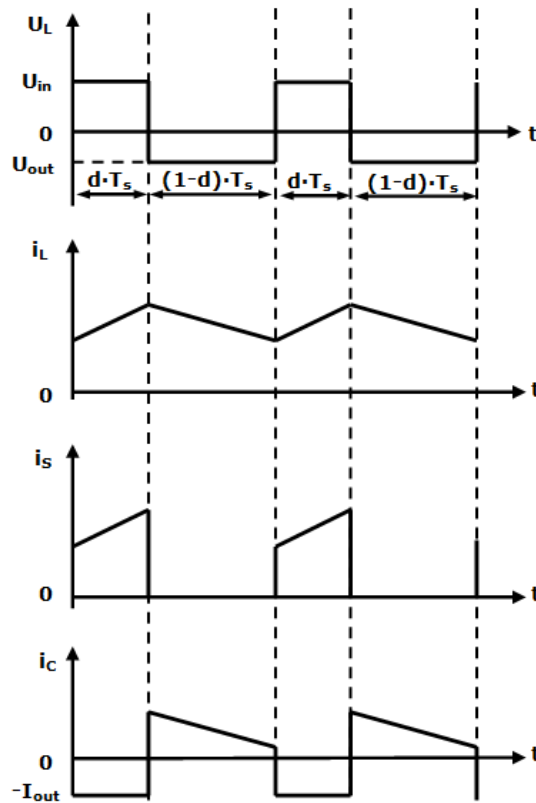


Figure 1.6. Main waveforms associated to the Buck-Boost Converter [70]



Advantages:

- the ability to combine the functions of a step-up and step-down converter;
- simplicity;
- low number of components;
- the polarity of the output voltage is opposite, without using a transformer.

Disadvantages:

- higher semiconductor stresses than in Buck or Boost converter;
- does not provide electrical isolation between input and output.

### 1.3. Bidirectional DC-DC converters

The developments of bidirectional DC-DC converters becomes an important topic in power electronics and are playing an important role in the applications involving renewable energy generating systems such as fuel cells and photovoltaic systems.

The bidirectional converters have the capability of reversing the direction of the current flow and thereby the power flow, while maintaining the voltage polarity of both dc sources. Due to this ability they are being used in the applications for renewable energy systems for energy storage devices such as batteries or super-capacitors.

High efficiency, lightweight, compact size and high reliability are some important requirements for the bidirectional converter.

#### 1.3.1. Bidirectional Boost/Buck DC-DC converter

The converter in Figure 1.7 is a combination of two well-known topologies, Boost and Buck. The converter requires just one inductor. To obtain the double sided power flow in bidirectional DC-DC converters, the switch should carry the current on both directions. The bidirectional power flow is achieved by replacing the switch and the diode from a classical Boost/Buck converter, with a MOSFET/IGBT in parallel with a diode [74] - [77].

The equivalent circuit of the converter in step-up mode, and, step-down mode are presented in Figure 1.8 and Figure 1.9 respectively.

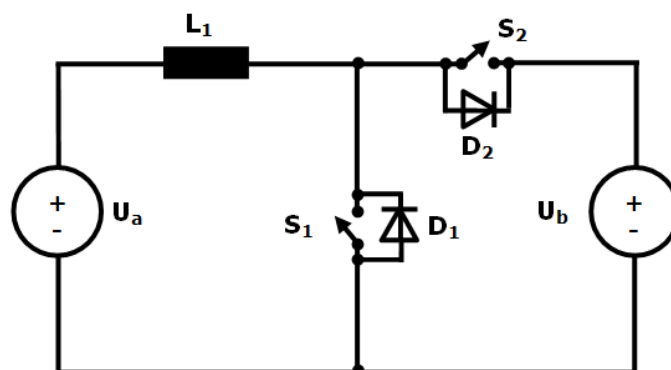


Figure 1.7. Circuit diagram of the bidirectional Boost/Buck DC-DC converter [77]

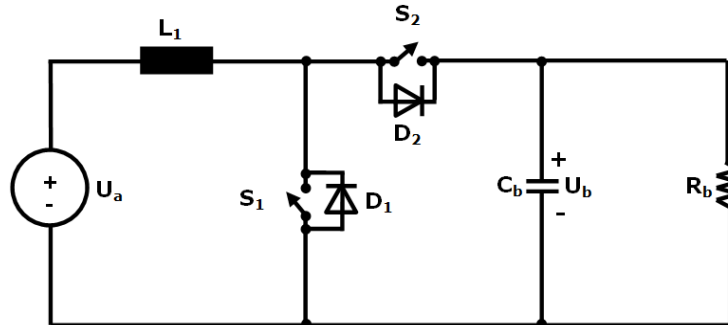


Figure 1.8. Equivalent circuit of the converter in step-up mode [77]

The voltage gain in step-up mode is:

$$\frac{U_b}{U_a} = \frac{1}{1-d} \quad (1.7)$$

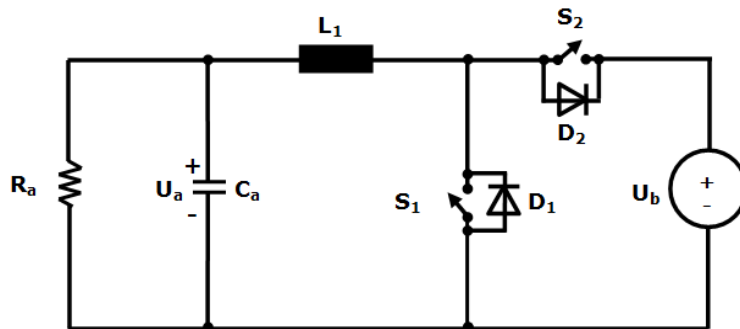


Figure 1.9. Equivalent circuit of the converter in step-down mode [77]

The voltage gain in step-down mode is:

$$\frac{U_a}{U_b} = d \quad (1.8)$$

This converter has the advantage of simple structure and easy control.

### 1.3.2. Bidirectional Boost/Buck DC-DC converter with coupled inductors

The bidirectional converter presented in Figure 1.10, employs coupled inductors with the same winding turns in the primary and secondary sides. The switches are synchronously controlled with duty cycle  $d$ .

In step-up mode, Figure 1.11, to achieve a high step-up voltage gain, the primary and secondary windings of the coupled inductor are charged in parallel and discharged in series.

In step-down mode, Figure 1.12, to achieve high step-down voltage gain, the primary and secondary windings of the coupled inductor are charged in series and discharged in parallel [77].

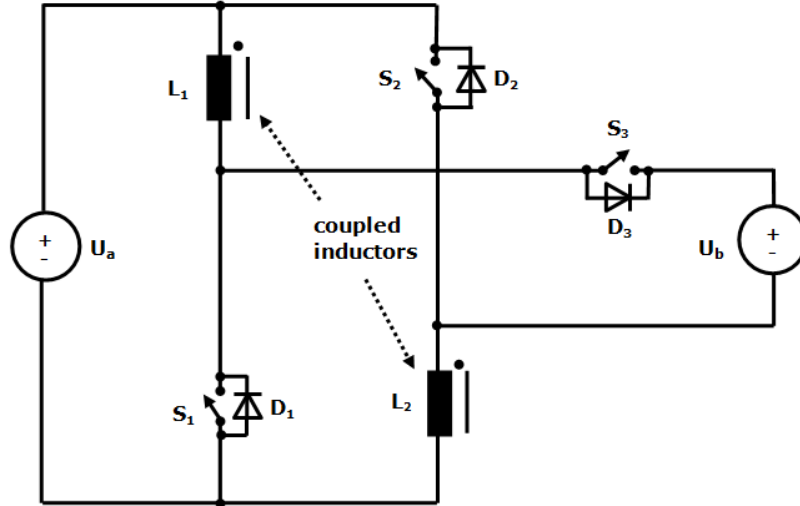


Figure 1.10. Circuit diagram of the bidirectional Boost/Buck converter with coupled inductors [77]

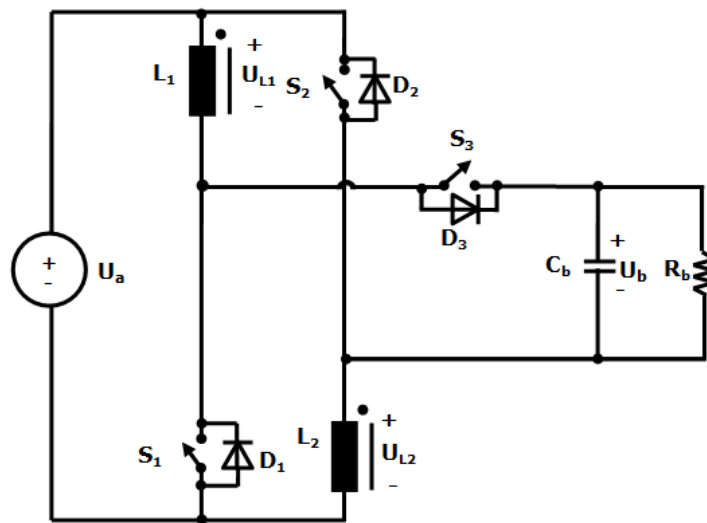


Figure 1.11. Equivalent circuit of the Boost/Buck converter in step-up mode [77]

The voltage gain in step-up mode is:

$$\frac{U_b}{U_a} = \frac{1+d}{1-d} \quad (1.9)$$

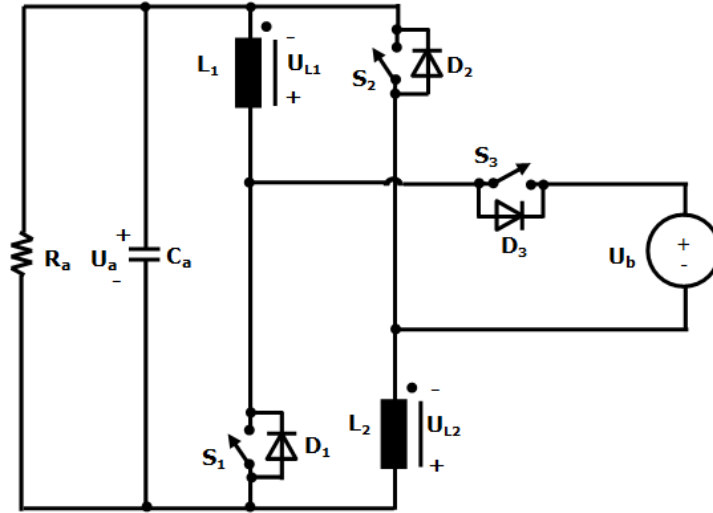


Figure 1.12. Equivalent circuit of the Boost/Buck converter in step-down mode [77]

The voltage gain in step-down mode is:

$$\frac{U_a}{U_b} = \frac{d}{2-d} \quad (1.10)$$

The waveforms of this converter are presented in Figure 1.13.

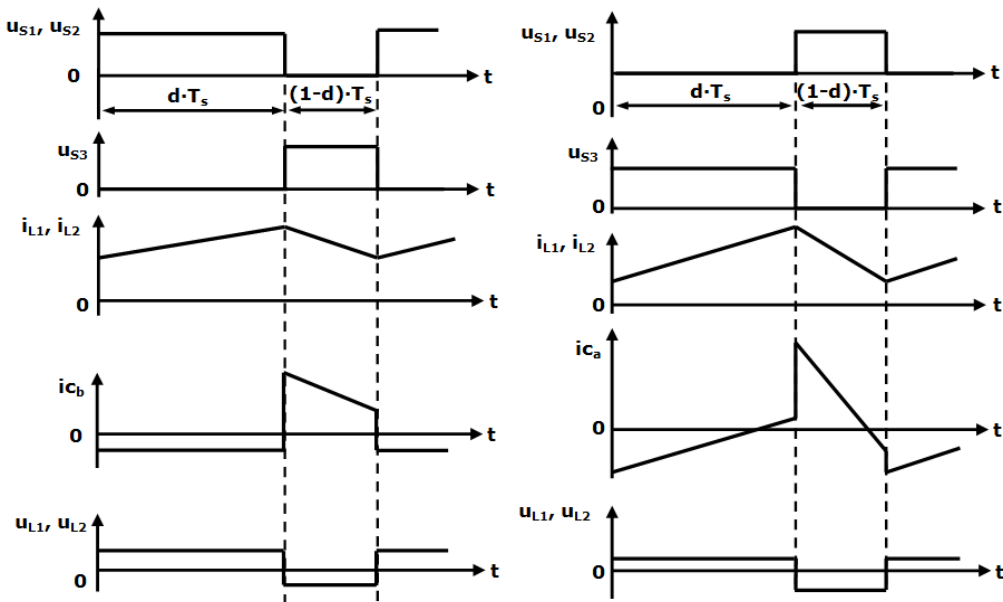


Figure 1.13. Waveforms of the Boost/Buck converter in step-up and step-down modes [77]

This converter exhibits higher step-up and lower step-down voltage gains and lower average values for the switch current compared to the conventional bidirectional DC-DC Boost/Buck converter.

### 1.3.3. Bidirectional Zeta-Sepic DC-DC converter

The bidirectional converter presented in Figure 1.14 is a combination of the Zeta and Sepic converters. The active converter, depends on what direction the power flows. When power flows from source  $U_a$  to  $U_b$ , the Zeta converter is active, and when power flows from source  $U_b$  to  $U_a$  the SEPIC converter is active. The authors [78] - [79], consider that this converter is a possible candidate to substitute the conventional bidirectional buck-boost converter in some practical applications, such as renewable power supply systems.

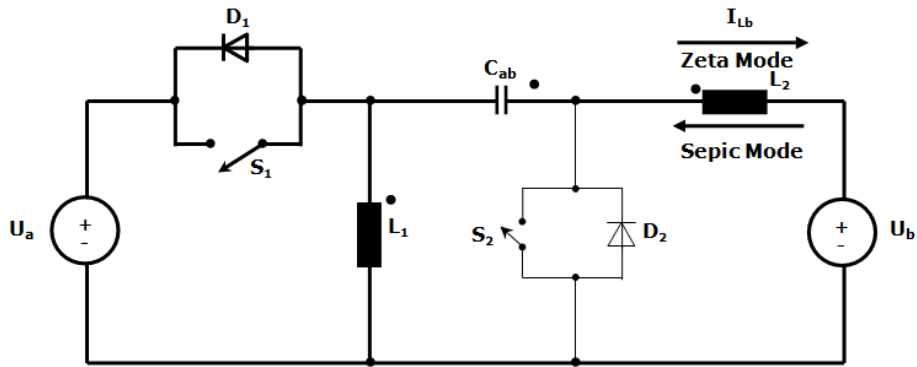


Figure 1.14. Circuit diagram of the Zeta-Sepic converter [79]

The voltage gain is for both converter modes the same, namely:

$$\frac{U_b}{U_a} = \frac{d}{1-d} \tag{1.11}$$

The equivalent circuit of the converter when switch  $S_1$  is conducting is presented in Figure 1.15, and when switch  $S_2$  is conducting is depicted in Figure 1.16.

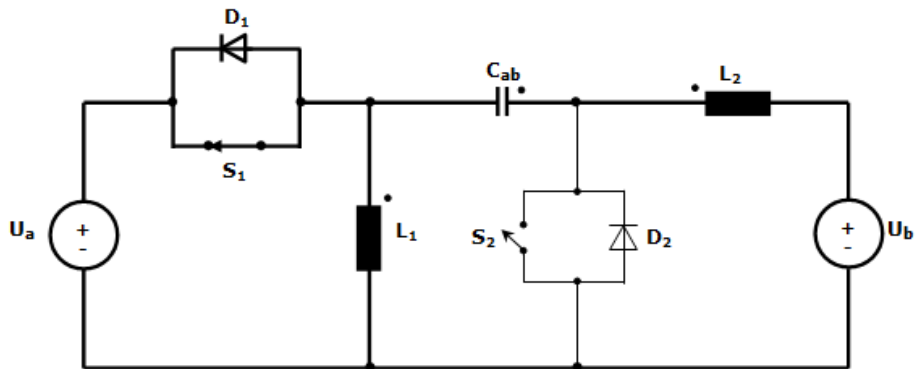


Figure 1.15. Equivalent circuit of the Zeta-Sepic converter when switch  $S_1$  is conducting [79]

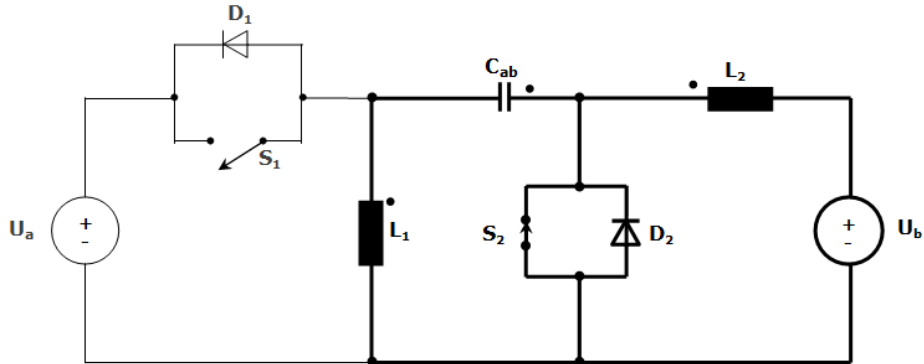


Figure 1.16. Equivalent circuit of the Zeta-Sepic converter when switch S2 is conducting [79]

The Zeta-Sepic converter waveforms are similar to the ones for the Zeta when the Zeta converter is active, and to the Sepic converter, when the Sepic converter is active, as shown in Figure 1.17.

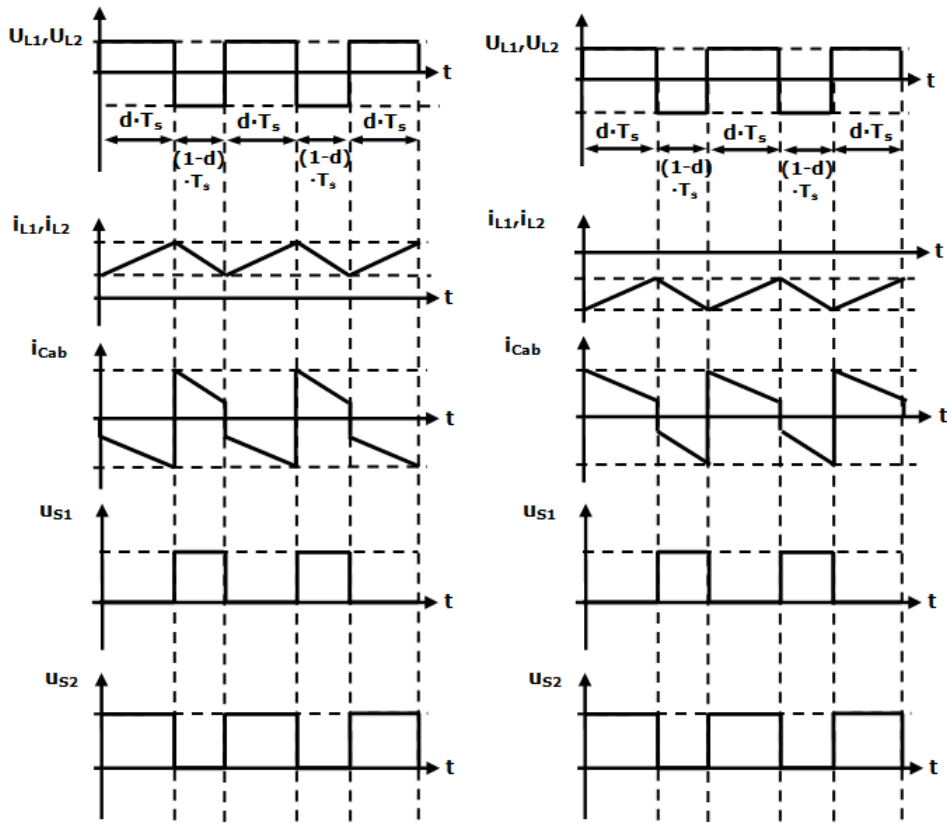


Figure 1.17. Main waveforms when Zeta converter is active, and when Sepic converter is active [79]

The main advantage of this converter is that it has the capability to operate in step-up and step-down modes no matter in what direction the power is flowing.

### 1.3.4. Bidirectional half-bridge/current-fed push-pull DC-DC converter

The bidirectional converter presented in Figure 1.18 is a combination of two topologies namely half-bridge and current-fed push-pull, and it can be used in PV applications as a battery charger/discharger. The primary side of the converter is a half bridge and is connected to the dc mains. The secondary side, connected to the battery, represents current-fed push-pull. The transformer provides galvanic isolation between the dc mains and the battery [80]. This bidirectional DC-DC converter provides the desired bidirectional flow of power for battery charging and discharging using only one transformer.

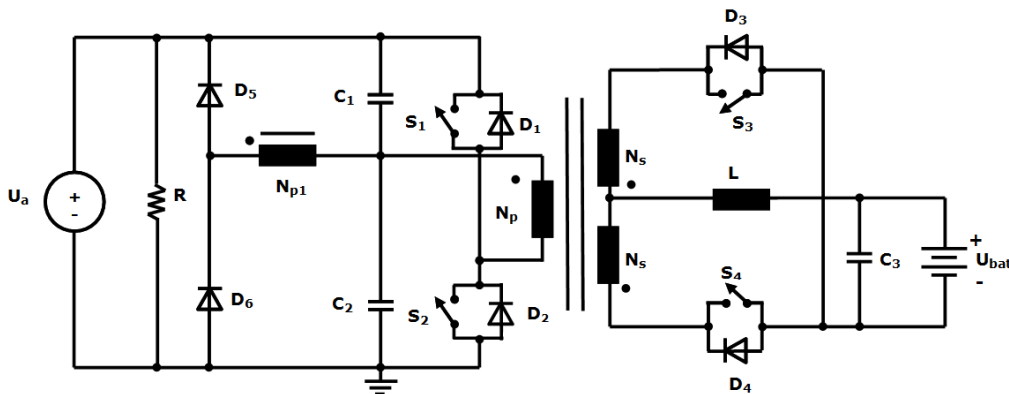


Figure 1.18. Circuit diagram of the bidirectional half-bridge/current-fed push-pull converter [80]

This converter has two modes of operation:

- forward/charging mode - the dc mains powers the load converters and provides the battery charging current, Figure 1.19;
- backup/current-fed mode - the converter operates in this mode on failure of the dc mains, the battery discharges to supply the load power, Figure 1.20.

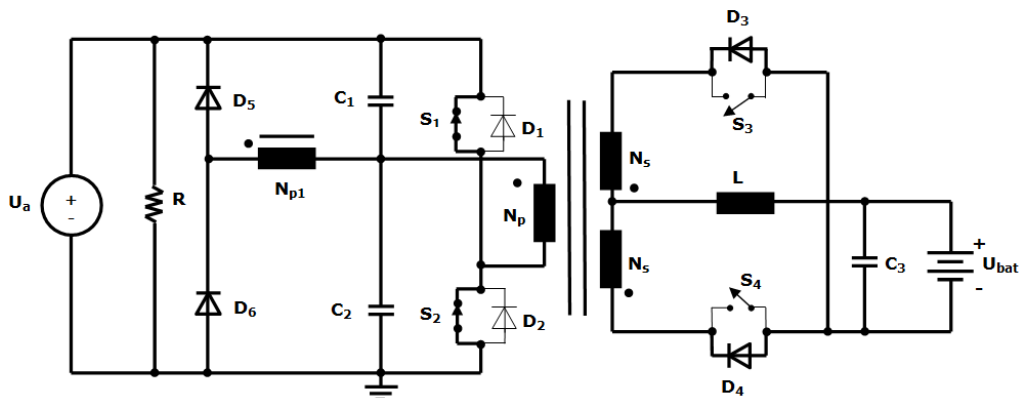


Figure 1.19. Equivalent circuit of the bidirectional half-bridge/current-fed push-pull converter in forward/charging mode [80]

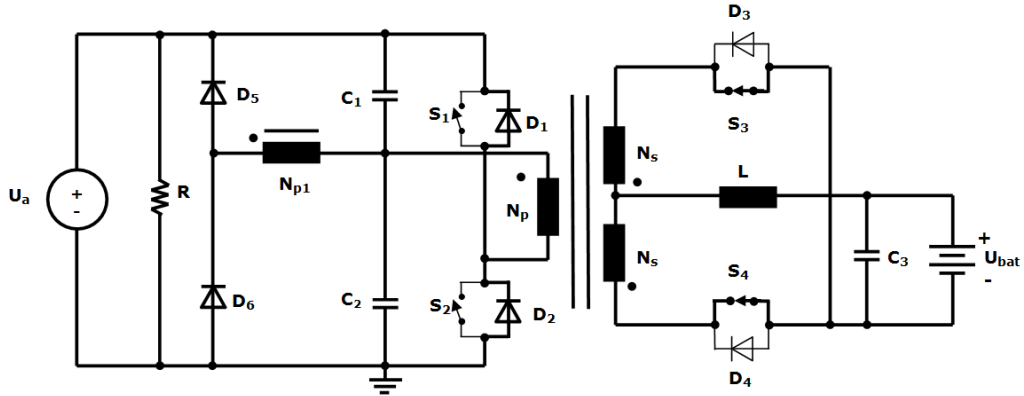


Figure 1.20. Equivalent circuit of the bidirectional half-bridge/current-fed push-pull converter in current-fed/backup mode [80]

The waveforms corresponding to operating modes are presented in the next figure.

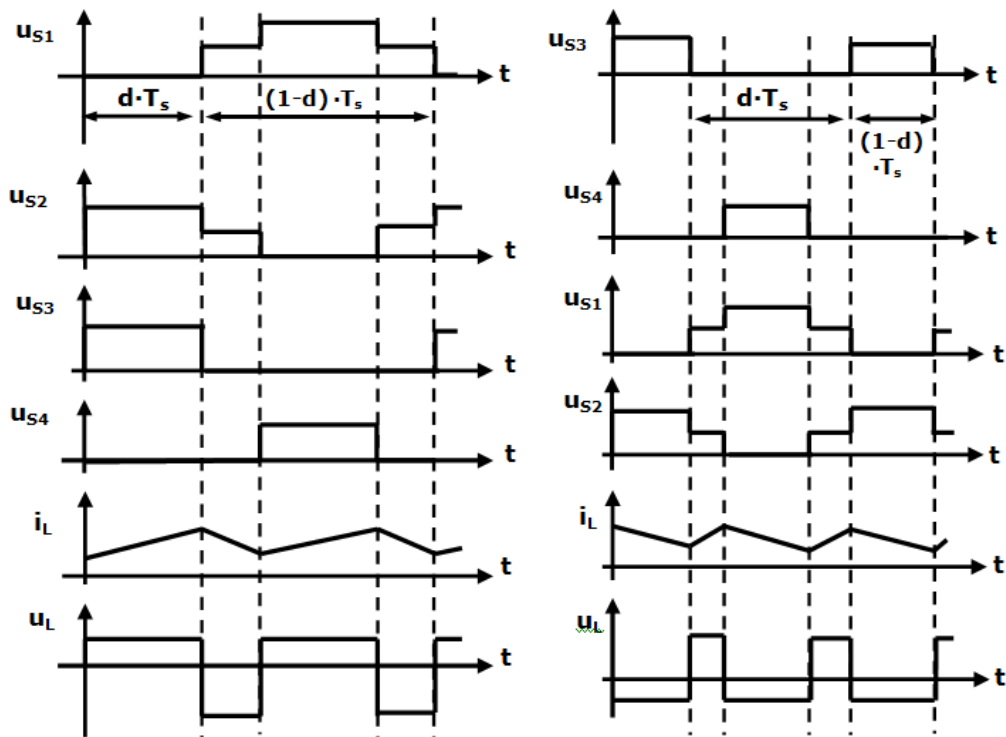


Figure 1.21. Waveforms of the bidirectional half-bridge/current-fed push-pull converter during the forward/charging mode and current-fed/backup mode [80]

Advantages [80], [81]:

- reduced part count due to use of the same components in both directions of power flow;
- low stresses on the switches;



- galvanic isolation;
- low ripple in the battery charging current;
- minimal number of active switches.

## 1.4. Other DC-DC converter structures

There are many researches in this field of power converter looking for efficient high step-up or step-down converter suitable for RE systems. Below are presented some different structures.

### 1.4.1. Forward Converter

The Forward converter, Figure 1.22, is a derived version of the Buck converter, by adding the transformer and diode  $D_2$  between the switch and the diode  $D_3$ . Due to the transformer, the forward topology can be used as either a step-up or a step-down converter. The transformer is reset while switch  $S$  is in the off state. While switch  $S$  conducts, the input voltage  $U_{in}$  is applied across the transformer primary winding. This causes the transformer magnetizing current to increase. When switch  $S$  turns off, the transformer magnetizing current forward biases diode  $D_1$ , and hence voltage  $U_{in}$  is applied to the second winding. This negative voltage causes the magnetizing current to decrease, and when it reaches zero, diode  $D_1$  turns off. If the number of turns of the primary and tertiary is the same, the voltage stress on the transistor is twice the dc input voltage and the duty cycle  $d$  must be less than 0.5. Because its core size requirements are smaller, it is popular in low-medium- power applications (up to several hundreds of watts) [7], [15],[73], [82] - [84].

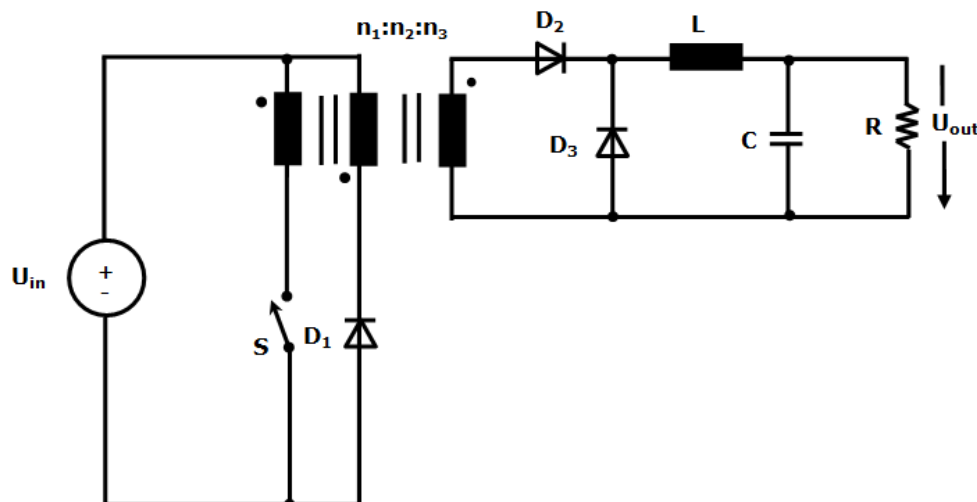


Figure 1.22. Circuit diagram of the Forward converter [7]

In Figure 1.23 the main waveforms for the Forward converter are presented.

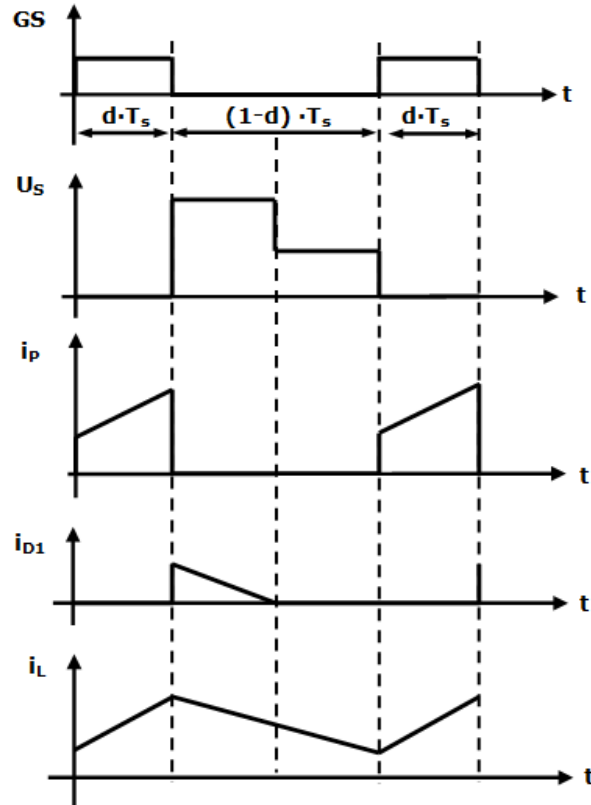


Figure 1.23. Main waveforms of Forward converter [7]

A disadvantage of the Forward converter is that the input current is pulsating. A non pulsating input current can be obtained by inserting an input LC filter between the input dc source and the switch [7], [15], [82], [83]. The main advantages of the forward topology are its simplicity and flexibility [73].

### 1.4.2. Ćuk converter

Named after its inventor, the Ćuk converter, Figure 1.24, can be obtained by using the duality principle of the Buck-Boost circuit. Similar to the Buck-Boost, the Ćuk converter provides a negative-polarity output voltage with respect to the common terminal of the input voltage. When the switch is on, the diode is off and the capacitor  $C_1$  is discharged by the inductor  $L_2$  current. With the switch in the off state, the diode conducts the currents of the inductors  $L_1$  and  $L_2$  whereas capacitor  $C_1$  is charged by the inductor  $L_1$  current [7], [14], [15], [70], [73].

The dc voltage transfer function of the Ćuk converter is the same to that of the Buck-Boost converter:

$$M = \frac{U_{out}}{U_{in}} = -\frac{d}{1-d} \quad (1.12)$$

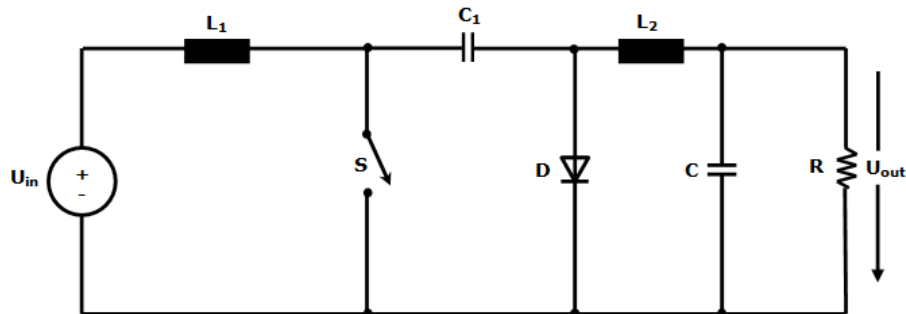


Figure 1.24. Circuit diagram of the Ćuk converter [70]

In Figure 1.25 the waveforms for the Ćuk converter are presented.

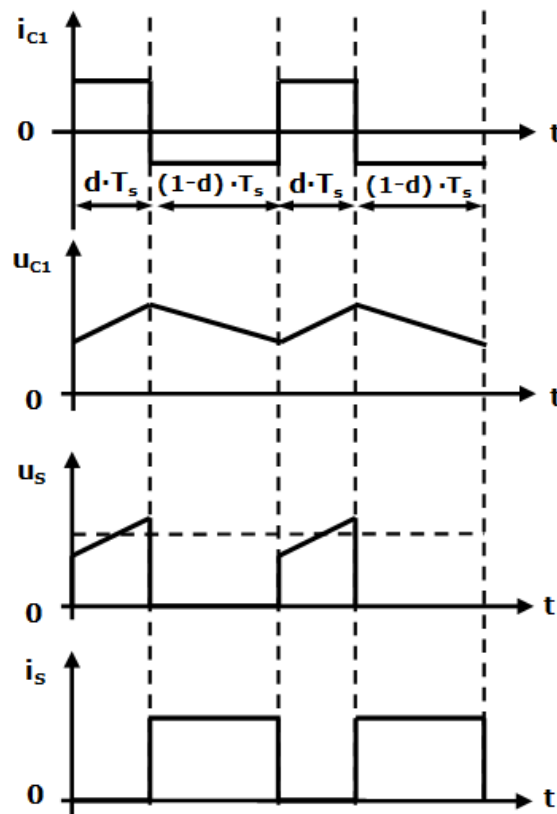


Figure 1.25. Main waveforms of Ćuk converter [70]

The topology is unique in that the primary and secondary are connected through a capacitor, even this does not represent galvanic isolation.

Continuous currents at both the input and the output of the converter, is an important advantage of this topology. A transformer (isolated) version of the Ćuk converter can be obtained by splitting capacitor  $C_1$  and inserting a high frequency transformer between the splitted capacitors [70].

Disadvantages of the Ćuk converter include a high number of passive devices and high current stresses related to the switch, diode, and capacitor  $C_1$ .

### 1.4.3. Sepic converter

The SEPIC - Single-Ended Primary Inductance Converter, Figure 1.26, has many similarities to the Ćuk converter:

- contains two inductors and two capacitors;
- can realize a step-down and a step-up voltage conversion, depending on the value of the duty cycle;
- draws a non-pulsating input current;
- also, exhibits the desirable feature that the switch control terminal is connected to ground[6].

The main difference between them is that the Sepic is a non-inverting converter, and, due to the pulsating output current requires a large output capacitor for filtering [7], [14], [15], [70], [82].

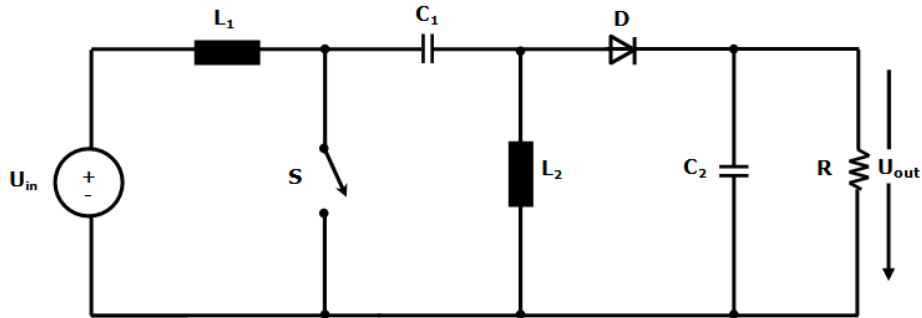


Figure 1.26. Circuit diagram of the Sepic converter [6]

The dc voltage transfer function of the Sepic converter is the same to that of the Buck-Boost converter, with, the difference that now the load voltage has the same polarity as the input voltage.

$$M = \frac{U_{out}}{U_{in}} = \frac{d}{1-d} \quad (1.13)$$

In Figure 1.27 the waveforms for the Sepic converter are presented.

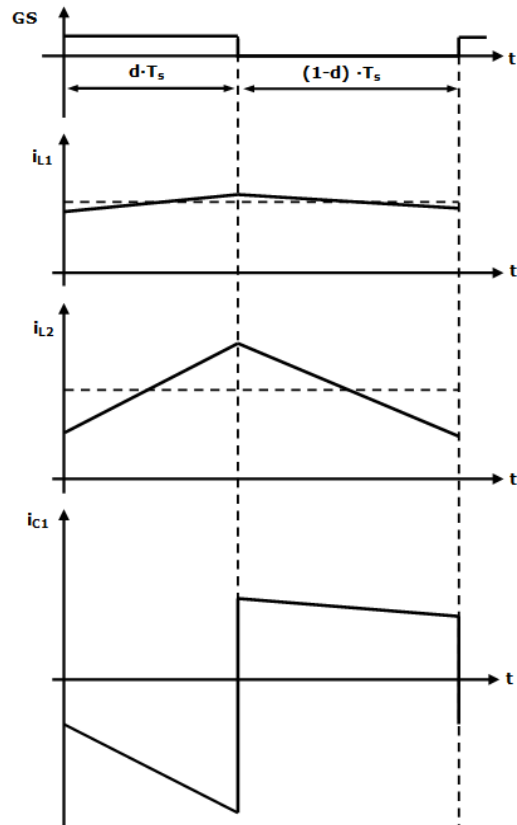


Figure 1.27. Main waveforms of the SEPIC converter [6]

An isolated version of the SEPIC converter is also reported.

#### 1.4.4. Zeta Converter

The Zeta converter is known as the inverse-SEPIC, because this converter can be obtained by interchanging the power input and the power output ports of the SEPIC converter.

The non-isolated version is presented in Figure 1.28, and it is obvious that it is a cascade of a Buck-Boost and a Buck stage in which the redundant switches were removed. The switch is positioned as in a buck converter [6], [14], [82].

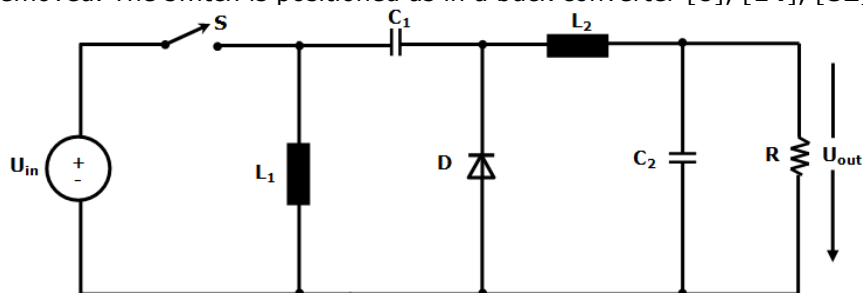


Figure 1.28. Circuit diagram of the Zeta converter [6]

The dc voltage transfer function of the Zeta converter is the same to that of the SEPIC converter:

$$M = \frac{U_{out}}{U_{in}} = \frac{d}{1-d} \quad (1.14)$$

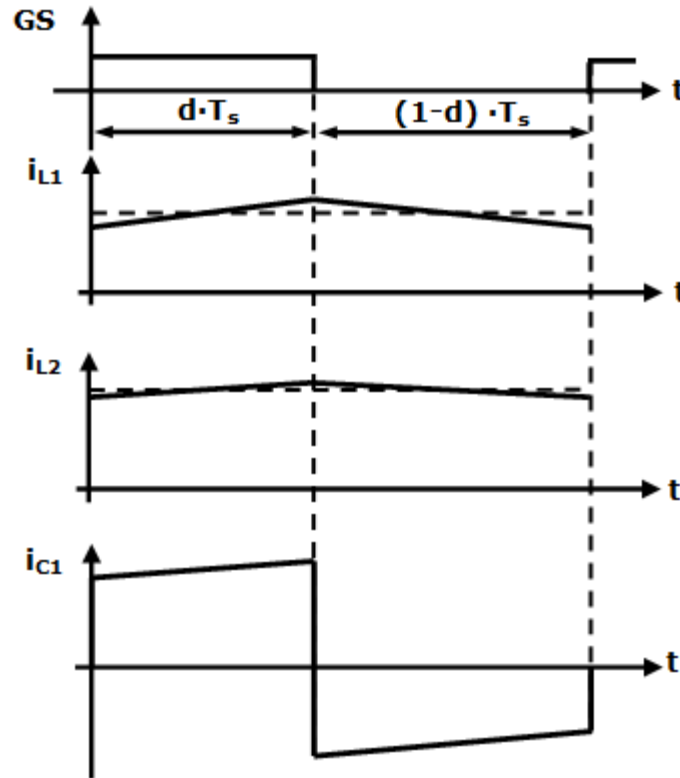


Figure 1.29. Main waveforms of the Zeta converter [6]

The disadvantage of the Zeta converter is that exhibits a pulsating input current.

An isolated version of Zeta converter can be obtained by inserting a high frequency transformer, replacing inductor  $L_1$  by two windings.

#### 1.4.5. Flyback Converter

The Flyback converter, Figure 1.30, [6] is one of the oldest converters. This converter is an isolated version of the Buck-Boost converter. The inductor of Buck-Boost converter has been replaced by a transformer, and for this reason this converter is sometimes also called a "Flyback transformer". Also, it contains a switch, a diode and a filter capacitor  $C$ . The transformer is modelled by an ideal transformer and its magnetizing inductance  $L_m$ . The transformer magnetizing inductance  $L_m$  can be used to store the magnetic energy, and is a very important design parameter. Its value determines the boundary between CCM and DCM, [6], [14], and [82].

An inverting Flyback converter is obtained if the diode, the filter capacitor, and the polarity of the transformer are reversed.

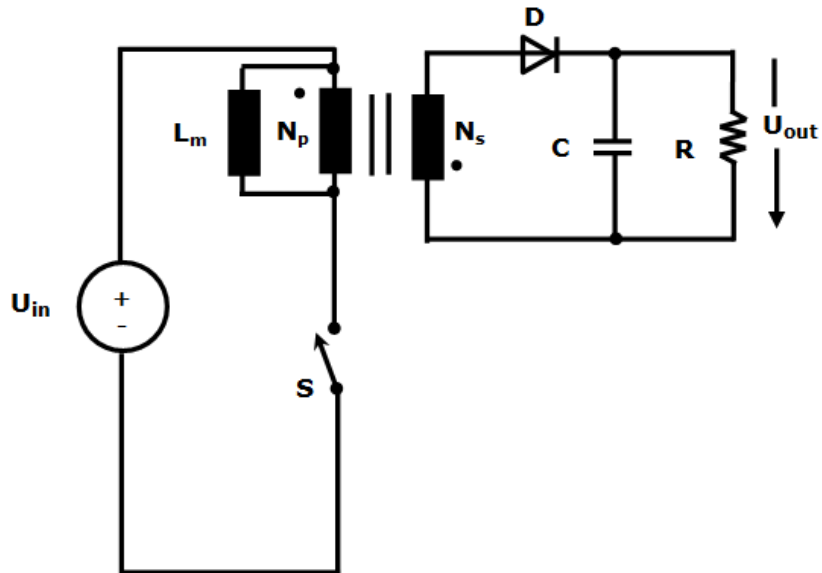


Figure 1.30. Circuit diagram of the Flyback converter [6]

The dc voltage transfer function of the converter is:

$$M = \frac{U_{out}}{U_{in}} = \frac{d}{(1-d)} \cdot \frac{N_s}{N_p} \quad (1.15)$$

In Figure 1.31 the waveforms for the Flyback converter are presented.

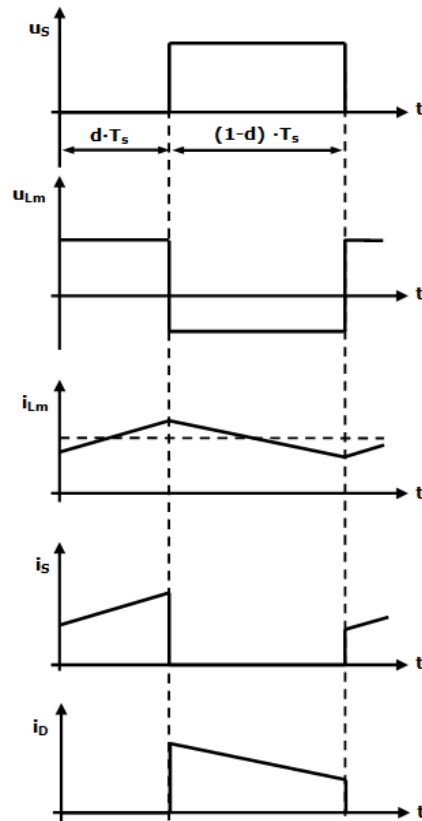


Figure 1.31. Main waveforms of the Flyback converter [6]

Advantages [6], [82]:

- the simplest isolated topology;
- very low parts count;
- the transformer provides dc isolation;
- can be used as either a step-down or a step-up converter;
- can be either an inverting or non-inverting converter;
- multiple outputs can be obtained by adding additional secondary windings to the transformer, each with its own rectifier and output low-pass filter.

Disadvantages [6], [82]:

- the Flyback converter has poor cross regulation in comparison with buck-derived transformer-isolated converters such as the Full Bridge and Forward circuits.



## 1.5. Association of power converters

The inter-connection of power converters is the response to the request of the industry for designing new and more advantageous power conversion structures that must support the continued development of the converters to avoid failures. The inter-connection of these converters can consist of multi-input connection, multilevel connection, cascaded connection, series connection, paralleled connection and multiphase connection of power converters.

This new conversion structures with improved performances offer new electrical characteristics that with only one converter are not possible to be achieved. Because in this work the author is focused only on converters that are used for renewable systems and their control, only the cascaded, series, and the parallel association are analysed and their main principles will be mentioned below [68].

### 1.5.1. Cascaded converters

Cascaded architectures is presented in Figure 1.32 [85]. Two power converters can be cascaded if the output port of the first power converter is directly connected to the input of the second one.

The cascaded converters can be both of same characteristic and structure, or totally different structures depending on applications. By association of the same DC-DC converters higher voltage ratio and reduced current ripple can be achieved. The cascaded converters are used where it is necessary to achieve a very high conversion ratio without transformers or, to assure several different functions in the structure [68].

For instance, in photovoltaic systems this cascaded connection can be composed by a simple DC-DC structure with its MPPT control and another simple DC-AC structure which allows the grid connection [86].

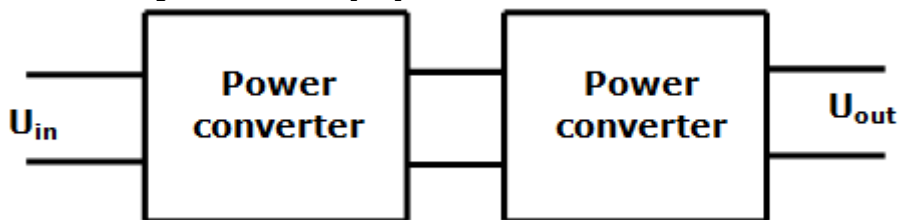


Figure 1.32. Cascaded connection of power converters [68]

Below are enumerated some different structures of cascaded converters with application in PV systems.

#### a) Buck-Boost converter

The simplest cascaded converter is the classical Buck-Boost converter, presented in Figure 1.5, which can be obtained by cascade connection of a Buck and Boost converter.

#### b) Ćuk converter

Another simple structure of the cascade converter is the Ćuk converter, Figure 1.24, which can be obtained by cascade connection of a Boost and Buck converter.

#### c) Zeta converter

Zeta converter it is a cascade of a Buck-Boost and a Buck stage, Figure 1.28.

#### d) Cascaded Buck converters

In Figure 1.33 are presented two Buck converters in a cascade [87].

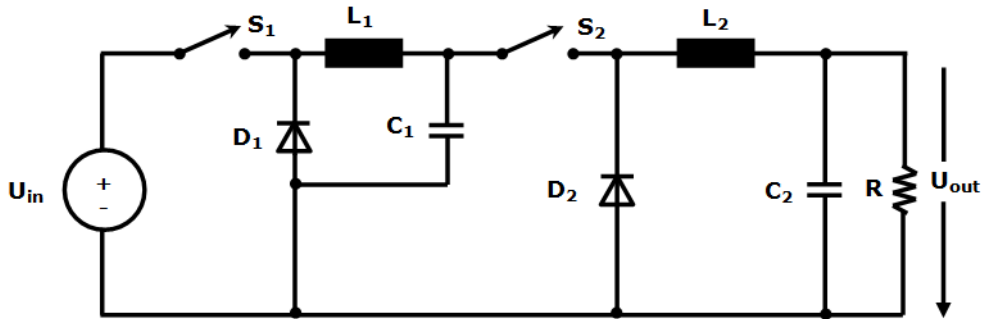


Figure 1.33. Circuit diagram of cascade of two Buck converters [87]

The converter provides a larger step-down ratio than a normal Buck, but requires two switches.

The dc voltage transfer function of the converter is:

$$M = \frac{U_{out}}{U_{in}} = d^2 \tag{1.16}$$

This converter is also known as a quadratic converter. A slight modification in the position of the switch  $S_1$  results in a single switch converter with the same voltage transfer function.

The cascaded two Buck converter with single switch is presented in Figure 1.34.

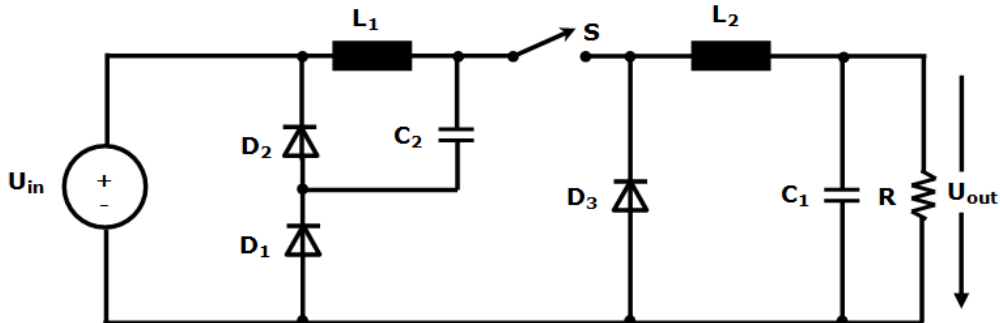


Figure 1.34. Circuit diagram of cascade of two Buck converter with a single switch [87]

This converter is less efficient than the classical Buck converter due to the two-stages [87] - [88], but is very useful for high frequency applications when large step-down conversion ratios are needed.

**e) Cascade Boost converter**

This cascade topology of two Boost converters, Figure 1.35, can be attractive for large-scale PV systems due to its high-voltage-gain. The main advantages of this topology are that it can meet the requirements of generating a high output voltage with a relatively high efficiency and can be operated with high switching frequency to improve power density.

The voltage stresses of the first stage are low and, to reduce the switching losses, the second stage can be designed to operate at a lower switching frequency [89] - [91].

The converter requires two switches which results in increased complexity and cost.

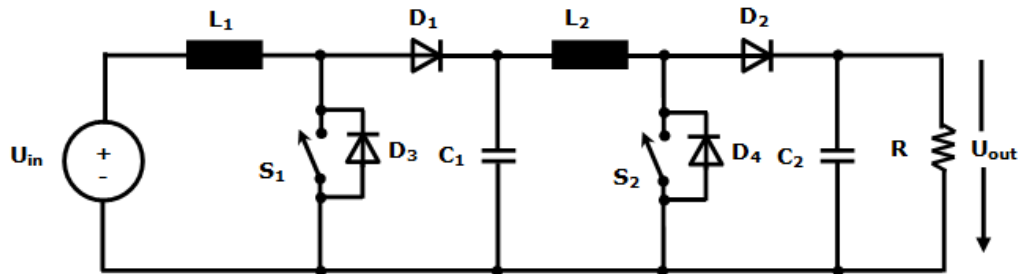


Figure 1.35. Circuit diagram of cascade of two Boost converters [90]

To reduce the complexity and cost, in the same manner like for cascaded Buck converter, the two switches can be integrated into one switch, Figure 1.36, [91] - [93].

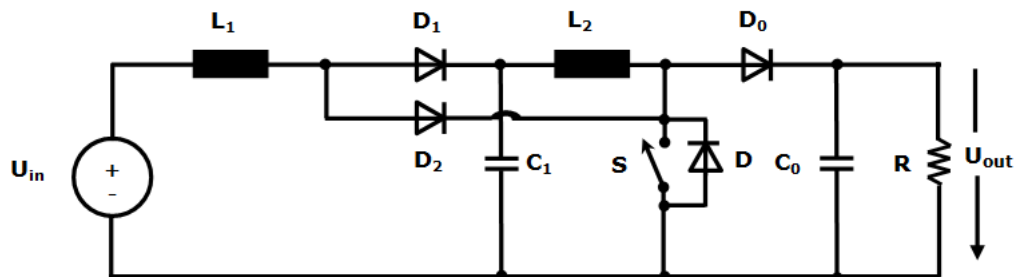


Figure 1.36. Cascade of two Boost converter with single switch [88]

The circuit is simplified compared to two Boost converters.

### 1.5.2. Series converters

Figure 1.37 shows the block diagrams of series power converters. As the name of the connection suggests, two power converters can be connected in series when the input and/or output port of the first power converter is series connected to the input and/or output port of the second one, creating a new structure.

The series connections increase/decrease the voltage and involve a major power transfer capability. For this reason, in PV systems the output port can be directly connected to an inverter and in order to adapt the output voltage according to the requirements, this kind of structures normally use converters that can operate in step-up and step-down mode [85], [94].

In Figure 1.37 a) is presented a series-input series-output connection, also called SISO connection. This can be used in high voltage converters, where converter modules share the input and output voltages.

In Figure 1.37 b) is depicted a series-input parallel-output connection, also called SIPO connection. This can be used in step-down applications, where input converter modules share the input voltages, and due to the outputs that are parallel connected the output current handling capability is increased.

In Figure 1.37 c) is shown a parallel-input series-output connection, also called PISO connection. This can be used in step-up applications, where the high input current is split and shared among several modules of the converter, while the

output voltage is built-up from output voltages of the modules. The main disadvantage of this connection is that the system requires a complex control.

In Figure 1.37d), output port of the first converter is series connected to the output port of the second one, and so on. The main advantage of this series connection compared to the series connection in Figure 1.37a), b) and c) is that it has the possibility to use different sources at each input, because the input port is not connected in series. One example is presented in Figure 1.38, and is known as integrated Buck/Buck converter [85], [94].

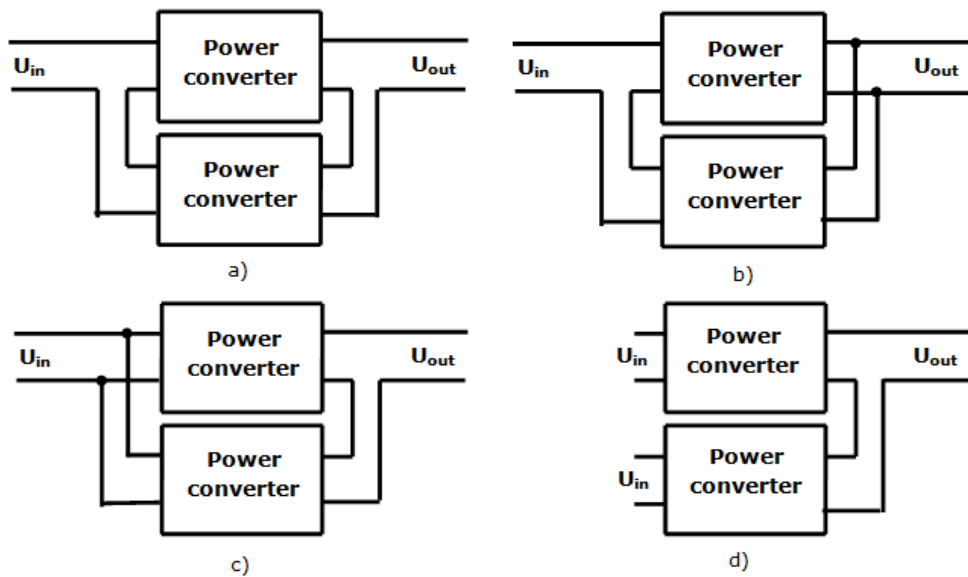


Figure 1.37. Series connection of power converter [85]

### The Integrated Buck/Buck Converter

The input sources of the converter can provide power to the load simultaneously or individually, [38], [40], [95] - [96].

Due to this, it is obvious that it exhibits four operating modes:

- input source  $U_{in1}$  provides power to the load - switch  $S_1$  is on and the switch  $S_2$  is off;
- input source  $U_{in2}$  provides power to the load - switch  $S_2$  is on and the switch  $S_1$  is off;
- the energy stored in the inductor  $L$  is being released to the load - both switches,  $S_1$  and  $S_2$  are off;
- input sources  $U_{in1}$  and  $U_{in2}$  provide power to the load - both switches,  $S_1$  and  $S_2$  are on [96].

The output voltage of the converter is:

$$U_{out} = U_{in1} \cdot d_1 + U_{in2} \cdot d_2 \quad (1.17)$$

where  $d_1$  is the duty cycle of switch  $S_1$  and  $d_2$  is the duty cycle of switch  $S_2$ .

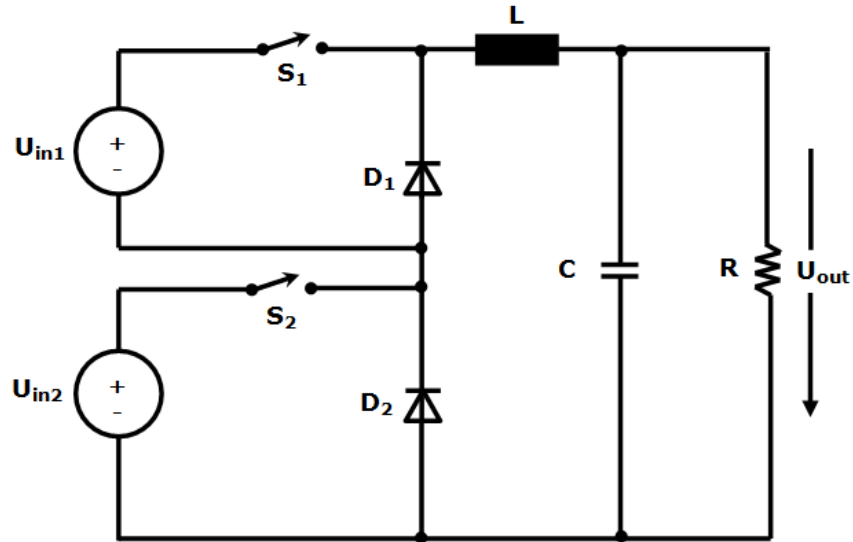


Figure 1.38. Circuit diagram of the integrated Buck/ Buck converter [96]

In Figure 1.39 the waveforms of the integrated Buck/Buck converter are presented.

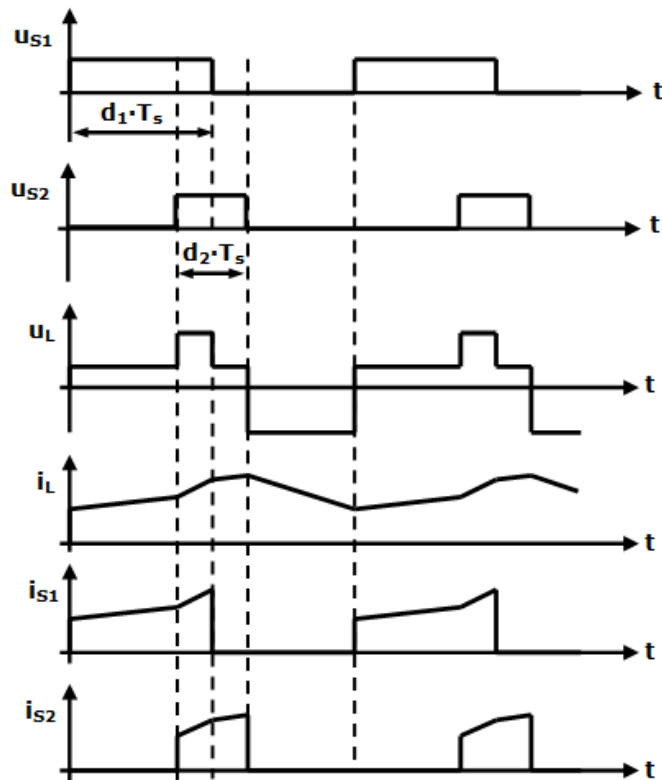


Figure 1.39. Waveforms of the integrated Buck/ Buck converter [96]

Switches  $S_1$  and  $S_2$  have different turn-on and turn-off times, at the same switching frequency.

The main advantages of this converter is that more power is available, it has the possibility to combine different renewable energy sources with the electric grid and the energy storage units, and the power flow in the system can be continuous even if one of the voltage sources is damaged.

### 1.5.3. Parallel converters

One of the most used interconnection techniques is the parallel connection of converters. It can be used for isolated and non-isolated converters. First time this connection, was used in the inverter uninterruptible power systems to increase output power capacity and system reliability [57].

Figure 1.40 shows the block diagram of a parallel power converter.

As the name of the connection suggests, two power converters are connected in parallel when the input and output ports of the first power converter are parallel connected to the input and output ports of the second one. The input and output voltage of all the phases is the same, as they are connected in parallel.

The main characteristic of this kind of structures is the distribution of current between the branches. This distribution can be identical or not and depends on the current control strategy that is used as well as the mismatches that exist between different phases.

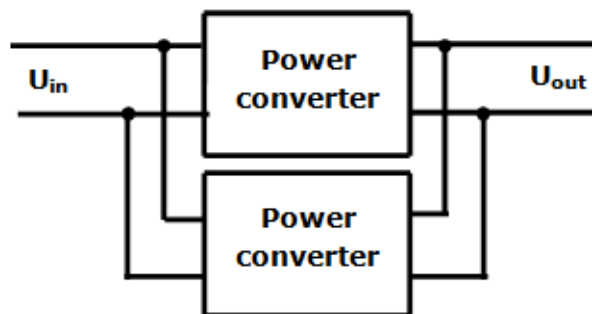


Figure 1.40. Parallel connection of power converters [85]

The parallel connection of converters involves a major power transfer capability, simplicity of control, reduction of the thermal and electric stresses in the components, gain in robustness and reliability [68], [85], [97] - [98].

### 1.6. Multiphase converter

Several solutions and their control were presented in the literature for interconnection of the converters [59], [99]- [103].

The physical connection of the multiphase looks exactly the same like parallel connection, Figure 1.40.

We make distinction between parallel configurations and multiphase configurations. The main difference is the method of how their main switches are controlled.

The parallel configuration is operated by having the main switches synchronously controlled (e.g. when a switch from first power converter turns on, so does the switch from the second power converter and vice versa). The main

advantage of parallel configuration is that the control circuit must only provide a single switching signal [103].

In multiphase converters the switch are asynchronously controlled with a phase shift between the switch gate drivers [59], but with a common frequency.

Figure 1.41 shows the switching signals for 2-phase converter. The result of the phase delay allows multiphase configurations to exhibit higher overall efficiency due to ripple cancellation, smaller output filter requirements and smaller output voltage ripple [104]-[107]. The output voltage ripple is reduced because the output frequency is increased by the number of phases. Higher output frequency makes the output ripple easier to be filtered which allows smaller components and further increase in efficiency [59], [103], [108]-[110].

In a parallel configuration since both main switches are synchronized, the input and output currents will be the same frequency as in the components inside each converter and this makes both input and output filtering requirements more challenging than in multiphase configurations [59] where frequency is doubled.

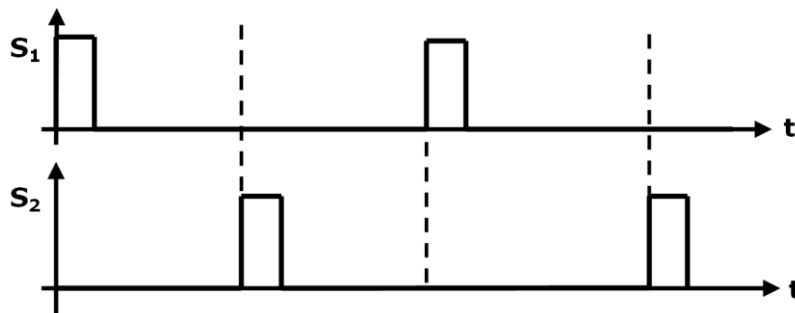


Figure 1.41. Switching signals for a 2-phase converter [59]

**a) The two-phase Buck converter**

In Figure 1.42 is presented a two-phase buck converter [111].

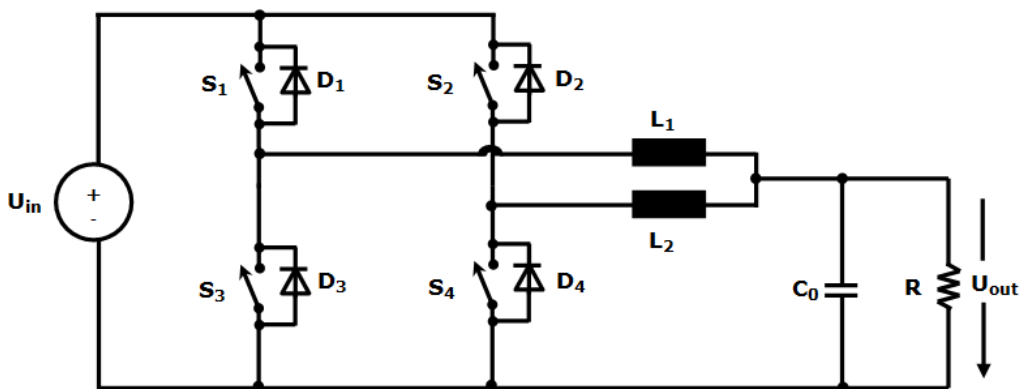


Figure 1.42. Circuit diagram of the two-phase Buck converter [111]

The main advantage of this converter compared to the single phase Buck converter is that this converter can significantly reduce the output current ripple.

If the number of phases is increased the output current ripple will be even smaller.

The main disadvantage of this converter is the individual inductor current

ripple, which is the same like in single phase Buck converter. Large inductor current ripples decrease the converter efficiency. One way to solve this problem is to use coupled inductors, like in [111]. The coupled inductors are represented as an ideal 1:1 transformer, two leakage inductances, and a magnetizing inductance. The ideal transformer is out of phase connected with the polarity dots on opposite ends.

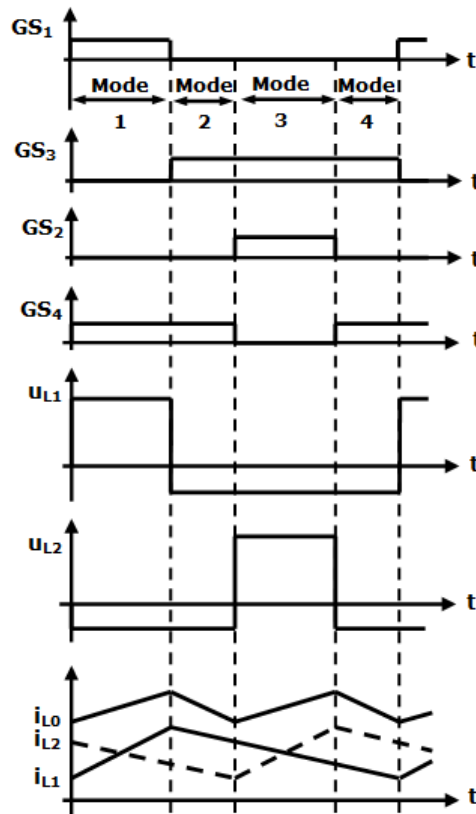


Figure 1.43. Waveforms of the two-phase Buck converter [111]

The circuit diagram of the two-phase Buck converter with coupled inductors is presented in Figure 1.44.

Figure 1.45 shows the waveforms of two-phase Buck converter with coupled inductors.



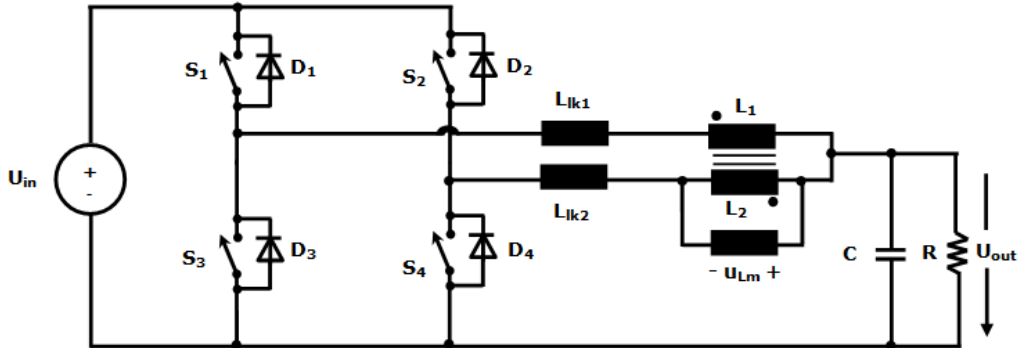


Figure 1.44. Circuit diagram of a two-phase Buck converter with coupled inductors [111]

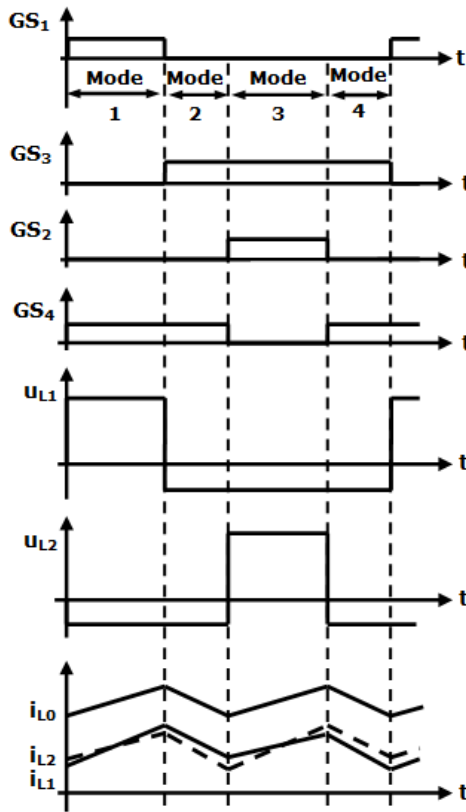


Figure 1.45. Waveforms of two-phase Buck converter with coupled inductors [111]

Both circuits have four operating modes. The coupling coefficient has a significant effect on the inductor current ripples although it does not affect output current ripple [111].

**b) The two-phase Boost converter**

In Figure 1.46 a two-phase Boost converter is presented. Due to the multiphase configuration, at the output the circuit will have just a single capacitor

and the output voltage will have the ripple twice than operating switching frequency of each individual Boost converter. The frequency multiplication effect also occurs in the input side of the converter, and will reduce the input filters and improving the quality of the input current [112] - [113].

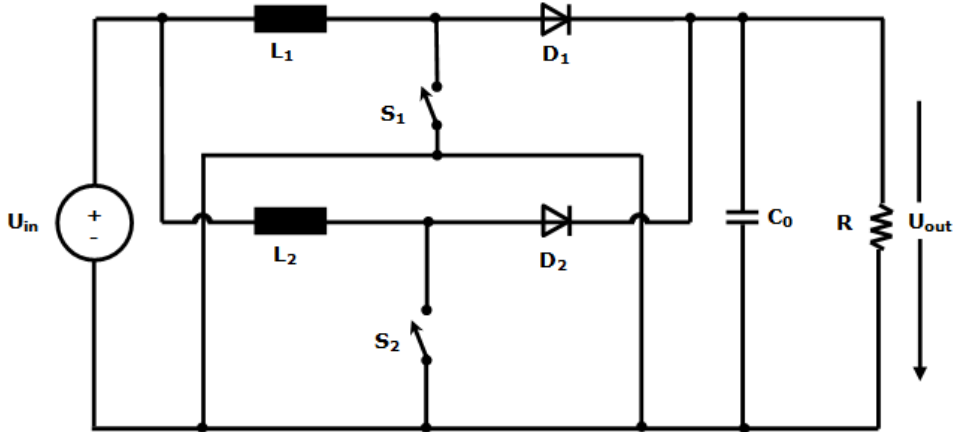


Figure 1.46. Circuit diagram of the two-phase Boost converter [112]

Figure 1.47 shows the waveforms of the two-phase Boost converter.

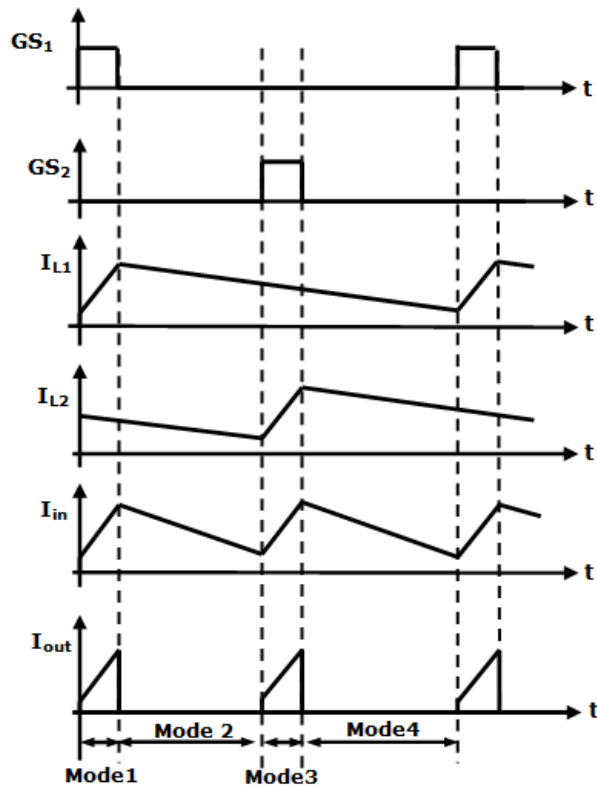


Figure 1.47. Waveforms of the two-phase Boost converter [112]

One advantage is the amount of peak to peak ripple on the input current that should be half of each individual inductor current [112].

The dc voltage transfer function of the two-phase Boost converter is the same as that for the Boost converter:

$$M = \frac{U_{out}}{U_{in}} = \frac{1}{1-d} \quad (1.18)$$

### 1.7. Boost converter used for a measuring system

In [71] and [67], the author presents the development of a low cost system for testing and monitoring the performance of PV modules in outdoor conditions. This system was used to ensure the performance of the PV module through testing and monitoring, as well as saving collected data to a database.

This database can be accessed through a graphical interface on a laptop connected to the system using serial interface. The error sources of this system are reduced to minimum because the human operators interfering with the system only through the graphical user interface.

Also, a Two Diode Model with series and parallel resistances was used to estimate the parameters of the electrical equivalent circuit for the PV module. This model was simulated in CASPOC 2009. The outdoor measurements were compared with the performances obtained through simulation, to prove the efficiency of the model. Figure 1.48 shows the block diagram of the system which is based on a PV cell, a step-up DC-DC converter and the measuring system.

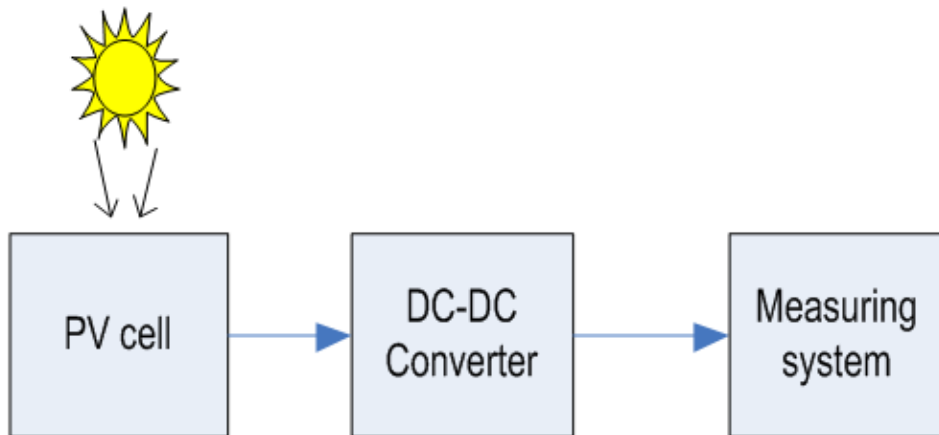


Figure 1.48. Block diagram of the monitoring system

The measuring system consists of one master unit and a variable number of slave units. The communication between master and slave is realized through RS485, and the slaves are powered through the communication cable, Figure 1.49.

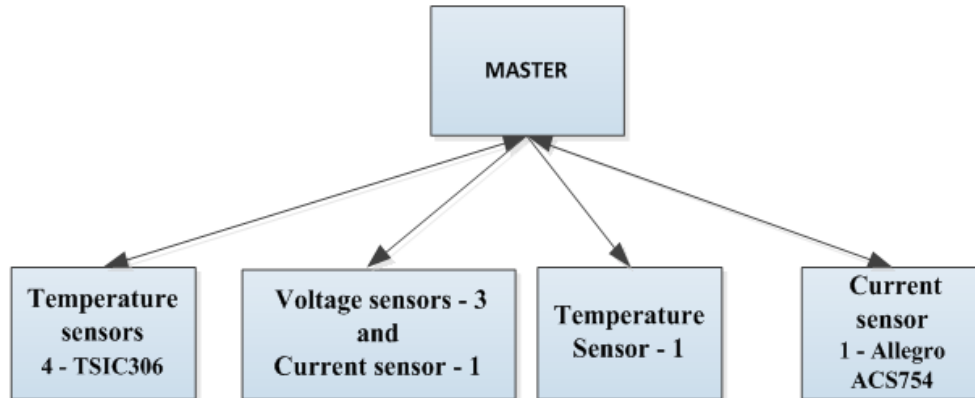


Figure 1.49. Block scheme of the measuring system

The measuring system is supplied with 12 V, energy taken from a DC-DC converter. As only 5V are needed to supply the integrated circuits, a voltage regulator is used.

The purpose of the DC-DC converter is to ensure that the output voltage will be step-up from an unregulated 5V to a constant 12V at a switching frequency of 21 kHz. The 5V input voltage is from PV cell and the 12V output voltage will be the input voltage for the measurements system. We chose a classical Boost converter to step-up the voltage. We design, simulate and construct this DC-DC Boost converter which is one of the main modules in the solar measuring system, and in Figure 1.50, is presented the circuit that we used.

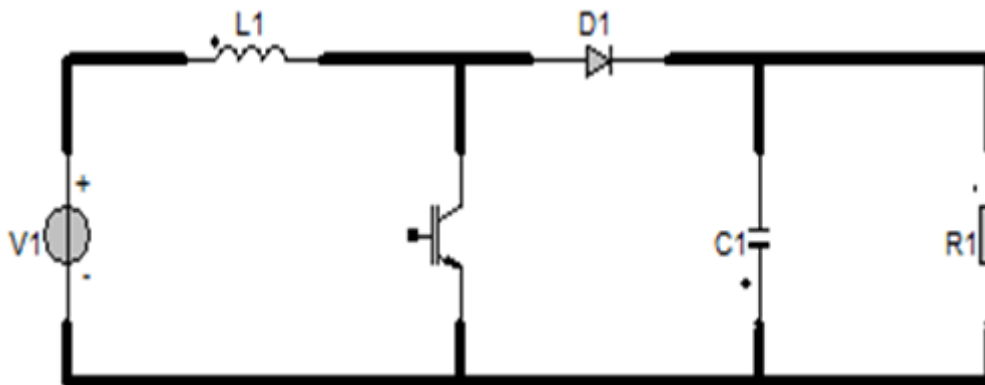


Figure 1.50. Design circuit of Boost converter [71]

For the beginning of the simulation we consider for the input voltage a fix value of 5V and for this value the duty cycle that we used is  $d=0,583$ . The Boost converter consists of inductor  $L_1=35\mu\text{H}$ , switching device IGBT which is driven by a typically PWM signal, diode  $D_1$ , capacitor  $C_1=5\text{mF}$ , and a resistance  $R_1=10\Omega$  (measuring system it is like a load for the Boost converter, and we show this through the  $R_1$ ). In Figure 1.51 is presented a picture with the image of practical implementation of the monitoring system.

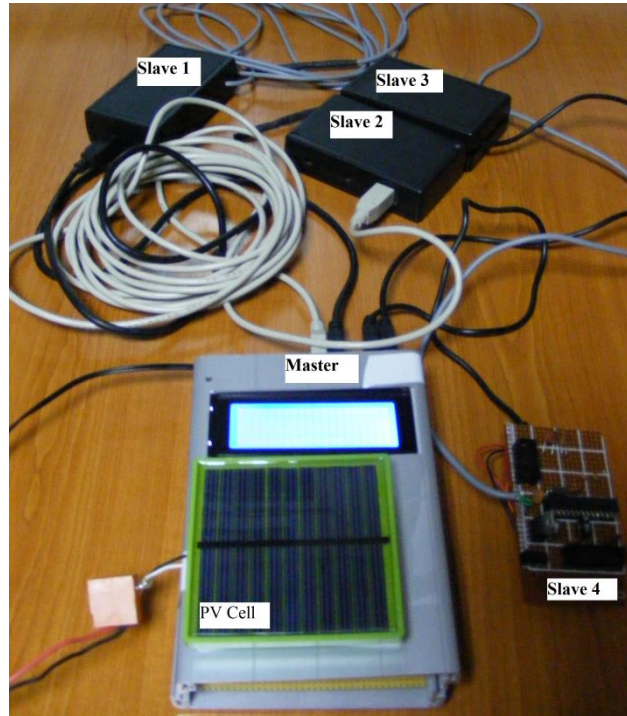


Figure 1.51. General scheme of the monitoring system [67]

Details about this system proposed and implemented by the author can be found in the articles [71], [67] and [114].

## 1.8. Conclusions and contributions

The present chapter was thought as an introduction to DC-DC converters for RE systems. The author presented an overview of some of the most popular, more complex and more challenging DC-DC converters for RE systems, described in the literature.

A special focus was made on the classical and multiphase converters, which is the subject of the thesis.

For each converter is presented a short description of the circuit, diagram of the circuit, the transfer function and the waveforms. Also, are presented the advantages and disadvantages of the presented converters.

Throughout this chapter it was shown that circuit diagram of some of the converters are very simple, with few components, and some of them very complex. Such an analysis is very important before making a choice for a converter.

This chapter is a survey of the DC-DC converters used in RE systems and therefore all the author's contributions in this chapter are theoretical.

The main author's personal contribution is the comprehensive literature survey in the DC-DC converters from all the points of view discussed in this chapter. The author made a summary of the current status of the converters used in RE systems, from a theoretical and practical point of view and the most important features of each of the converters are highlighted.

Also the author implemented a low cost system for testing and monitoring the performance of PV modules in outdoor conditions, and is using a classical Boost converter like that one presented in this chapter. Details of this systems and converter simulation have been published in [67] and [71].

[67] is **ISI** – Web of Knowledge – Thomson Reuters indexed, and published in “Advances in Electrical and Computer Engineering”, in 2013, and [71] is **ISI** – Web of Knowledge – Thomson Reuters and IEEE Explore 2013 indexed and published at 2012 10<sup>th</sup> International Symposium on Electronics and Telecommunications Proceedings (ISETC '12).

## CHAPTER 2. Multiphase Converters with Wide Conversion Ratio Using Hybrid Structures

### 2.1. Introduction

The multiphase converters generated with the methods presented in chapter 1.6, include in their architectures classical converters. As a major contribution of this thesis, the concept of synthesizing multiphase DC-DC converters will be extended, from classical to hybrid structures. For this reason the operation of these hybrid converters is analysed and simulated. A comparative study of the hybrid converters is performed before making a choice for a hybrid structure.

A hybrid structure is characterized by a higher input to output voltage conversion ratio compared to a classical converter in step-up, and a lower conversion ratio in step-down mode.

The hybrid DC-DC converters result from classical Buck, Boost, Buck-Boost, Ćuk, Sepic and Zeta structures by inserting a switching cell. These switching cells structures can be of two types: "step-down" or "step-up" [3]-[5].

The C-switching cells presented in Figure 2.1 are a structure, including two capacitors and two or three diodes.

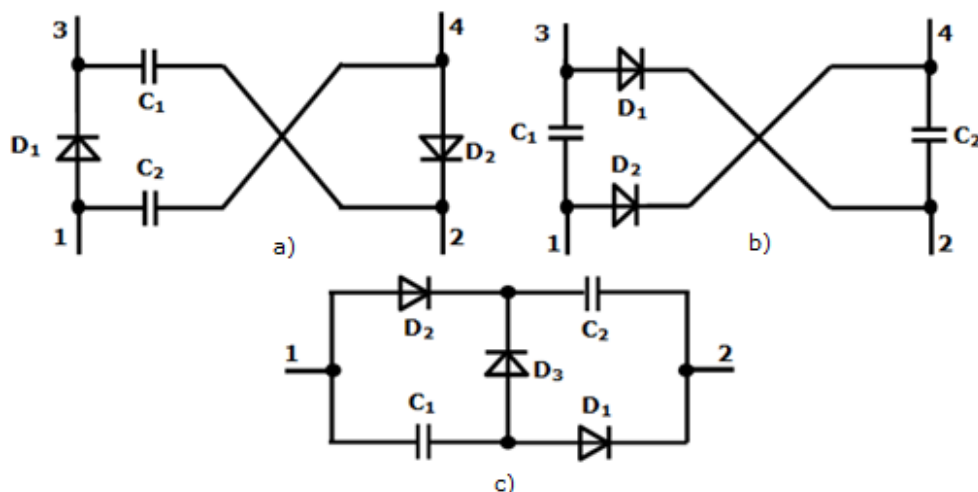


Figure 2.1. C-switching structures: a) Step-up 1; b) Step-up 2; c) Step-down 1[4]

The "step-up" C- or L-switching structures are combined with the Boost, Buck-Boost, Ćuk, Zeta and Sepic converters, to get a step-up dc transfer function [3], [4].

The "step-down" C- or L-switching structures can be combined with the Buck, Buck-Boost, Ćuk, Zeta and Sepic converters in order to get a step-down dc transfer function [4] - [5].

The L-switching cells presented in Figure 2.2, include two inductors and two-three diodes.

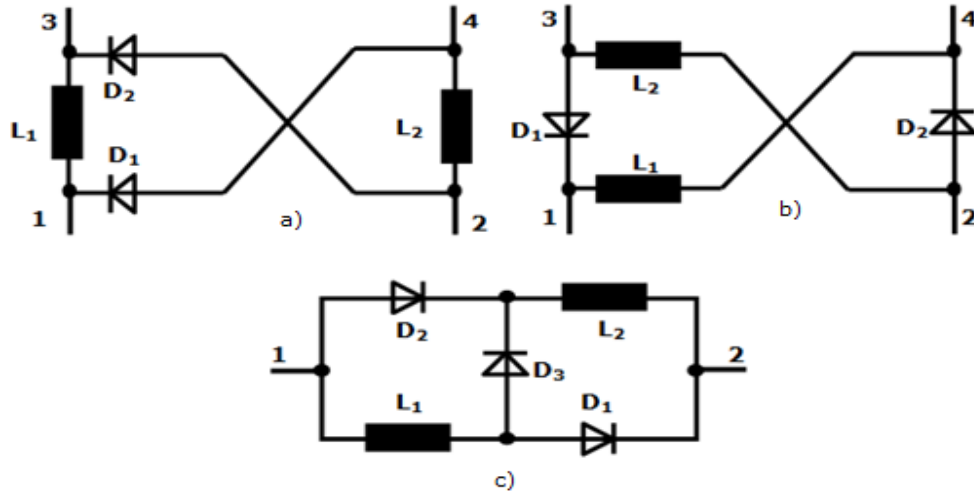


Figure 2.2. L-switching structures: a) Step- down 1; b) Step- down 2; c) Step-up 1[4]

As will be seen further, in the step-down C-switching structures the capacitors are discharged in parallel when the active switch is "on", and the capacitors are charged in series when the active switch is "off".

In the step-up C-switching structures, when the active switch of the converter is "on" the capacitors are discharged in series, and when the active switch is "off", the capacitors are charged in parallel [4], [6].

In the step-down L-switching structures when the active switch is "on", the inductors are charged in series and when the active switch is "off", the inductors are discharged in parallel.

The inductors are charged in parallel, in the step-up L-switching structures when the active switch is "on", and when the active switch is "off" the inductors are discharged in series [4], [6].

In Table 2.1 the hybrid converters topologies are presented as they result after inserting the L or C - switching structures in the classical converters, while, in Table 2.2 the output voltage equation is provided [3] - [5], [115] - [117].



Table 2.1. Hybrid converter [3] - [5]

Converter name	Converter diagram
<p>1. Hybrid Buck converter with C-switching structure step-down 1</p>	
<p>2. Hybrid Buck converter with L-switching structure step-down 1</p>	

<p>3. Hybrid Boost converter with C-switching structure step-up 1</p>	
<p>4. Hybrid Boost converter with L-switching structure step-up 1</p>	
<p>5. Hybrid Buck-Boost converter with C-switching structure step-down 1</p>	

Table 2.1. (continued 1) Hybrid converter [3] - [5]

<p>6. Hybrid Buck-Boost converter with C-switching structure step-up 1</p>	
<p>7. Hybrid Buck-Boost converter with L-switching structure step-up 1</p>	
<p>8. Hybrid Ćuk converter with C-switching structure step-down 1</p>	

Table 2.1. (continued 2) Hybrid converter [3] - [5]

<p>9. Hybrid Ćuk converter with L-switching structure step-up 1</p>	
<p>10. Hybrid Ćuk converter with L-switching structure step-down 1</p>	
<p>11. Hybrid Ćuk converter with C-switching structure step-up 2</p>	
<p>Table 2.1. (continued 3) Hybrid converter [3] - [5]</p>	

<p>12. Hybrid Sepic converter with C-switching structure step-down 1</p>	
<p>13. Hybrid Sepic converter with L-switching structure step-down 2</p>	
<p>14. Hybrid Sepic converter with L-switching structure step-up 1</p>	
<p>Table 2.1. (continued 4) Hybrid converter [3] - [5]</p>	

<p>15. Hybrid Zeta converter with C-switching structure step-up 2</p>	
<p>16. Hybrid Zeta converter with L-switching structure step-down 1</p>	
<p>17. Hybrid Zeta converter with L-switching structure step-up 1</p>	
<p>Table 2.1. (continued 5) Hybrid converter [3] - [5]</p>	

Table 2.2. Output voltage equation for hybrid converters [3] - [5]

Converter name	Output voltage
1. Hybrid Buck converter with C-switching structure step-down 1	$U_{out} = \frac{d}{2-d} \cdot U_{in}$
2. Hybrid Buck converter with L-switching structure step-down 1	$U_{out} = \frac{d}{2-d} \cdot U_{in}$
3. Hybrid Boost converter with C-switching structure step-up 1	$U_{out} = \frac{1+d}{1-d} \cdot U_{in}$
4. Hybrid Boost converter with L-switching structure step-up 1	$U_{out} = \frac{1+d}{1-d} \cdot U_{in}$
5. Hybrid Buck-Boost converter with C-switching structure step-down 1	$U_{out} = \frac{d}{(1-d) \cdot (2-d)} \cdot U_{in}$
6. Hybrid Buck-Boost converter with C-switching structure step-up 1	$U_{out} = \frac{2 \cdot d}{1-d} \cdot U_{in}$
7. Hybrid Buck-Boost converter with L-switching structure step-up 1	$U_{out} = \frac{2 \cdot d}{1-d} \cdot U_{in}$
8. Hybrid Ćuk converter with C-switching structure step-down 1	$U_{out} = \frac{d}{2 \cdot (1-d)} \cdot U_{in}$
9. Hybrid Ćuk converter with L-switching structure step-up 1	$U_{out} = \frac{(1+d) \cdot d}{1-d} \cdot U_{in}$
10. Hybrid Ćuk converter with L-switching structure step-down 1	$U_{out} = \frac{d}{2 \cdot (1-d)} \cdot U_{in}$
11. Hybrid Ćuk converter with C-switching structure step-up 2	$U_{out} = \frac{1+d}{1-d} \cdot U_{in}$
12. Hybrid Sepic converter with C-switching structure step-down 1	$U_{out} = \frac{d}{(1-d) \cdot (2-d)} \cdot U_{in}$
13. Hybrid Sepic converter with L-switching structure step-down 2	$U_{out} = \frac{d}{2 \cdot (1-d)} \cdot U_{in}$
14. Hybrid Sepic converter with L-switching structure step-up 1	$U_{out} = \frac{(1+d) \cdot d}{1-d} \cdot U_{in}$
15. Hybrid Zeta converter with C-switching structure step-up 2	$U_{out} = \frac{2 \cdot d}{1-d} \cdot U_{in}$
16. Hybrid Zeta converter with L-switching structure step-down 1	$U_{out} = \frac{d}{2 \cdot (1-d)} \cdot U_{in}$
17. Hybrid Zeta converter with L-switching structure step-up 1	$U_{out} = \frac{(1+d) \cdot d}{1-d} \cdot U_{in}$

As it is obvious from the formulae above, a hybrid structure can be characterised by a higher or lower input to output voltage conversion ratio compared to the classical converter it is derived from in step-up/step-down mode. Also it can be seen that some of the converters exhibit the same formula for the output voltage, even if they have different structures.

## 64 Multiphase Converters with Wide Conversion Ratio Using Hybrid Structures

We will highlight which converters have the same output voltage and which one has the highest/lowest conversion ratio.

Step-up hybrid converters with the same output voltage are:

- hybrid Boost converter with C-switching structure step-up 1, hybrid Boost converter with L-switching structure step-up 1 and hybrid Ćuk converter with C-switching structure step-up 2;

$$U_{out} = \frac{1+d}{1-d} \cdot U_{in} \quad (2.1)$$

- hybrid Buck-Boost converter with C-switching structure step-up 1, hybrid Buck-Boost converter with L-switching structure step-up 1 and hybrid Zeta converter with C-switching structure step-up 2;

$$U_{out} = \frac{2 \cdot d}{1-d} \cdot U_{in} \quad (2.2)$$

- hybrid Ćuk converter with L-switching structure step-up 1, hybrid Sepic converter with L-switching structure step-up 1 and hybrid Zeta converter with L-switching structure step-up 1;

$$U_{out} = \frac{(1+d) \cdot d}{1-d} \cdot U_{in} \quad (2.3)$$

A comparison between the conversion ratios of the step-up hybrid converters it is presented in Figure 2.3.

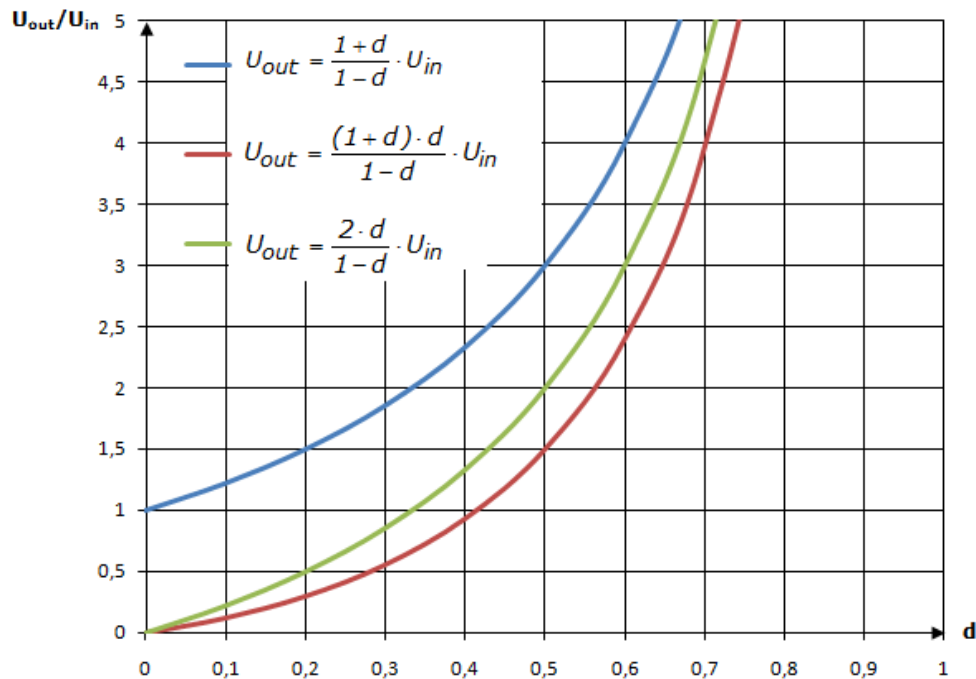


Figure 2.3. Comparison between conversion ratios of the step-up hybrid converter



As it can be seen from equations above and from the comparison between the conversion ratios of the step-up hybrid converters, the highest conversion ratio is achieved for the converters that use equation 2.1.

The converters that have the same formula from the hybrid converter in step-down configuration are:

- hybrid Buck converter with C-switching structure step-down 1 and hybrid Buck converter with L-switching structure step-down 1;

$$U_{out} = \frac{d}{2-d} \cdot U_{in} \quad (2.4)$$

- hybrid Buck-Boost converter with C-switching structure step-down 1, and hybrid Sepic converter with C-switching structure step-down 1;

$$U_{out} = \frac{d}{(1-d) \cdot (2-d)} \cdot U_{in} \quad (2.5)$$

- hybrid Ćuk converter with C-switching structure step-down 1, hybrid Ćuk converter with L-switching structure step-down 1, hybrid Sepic converter with L-switching structure step-down 2, and hybrid Zeta converter with L-switching structure step-down 1;

$$U_{out} = \frac{d}{2 \cdot (1-d)} \cdot U_{in} \quad (2.6)$$

A comparison between the conversion ratios of the step-down hybrid converters is performed in Figure 2.4.

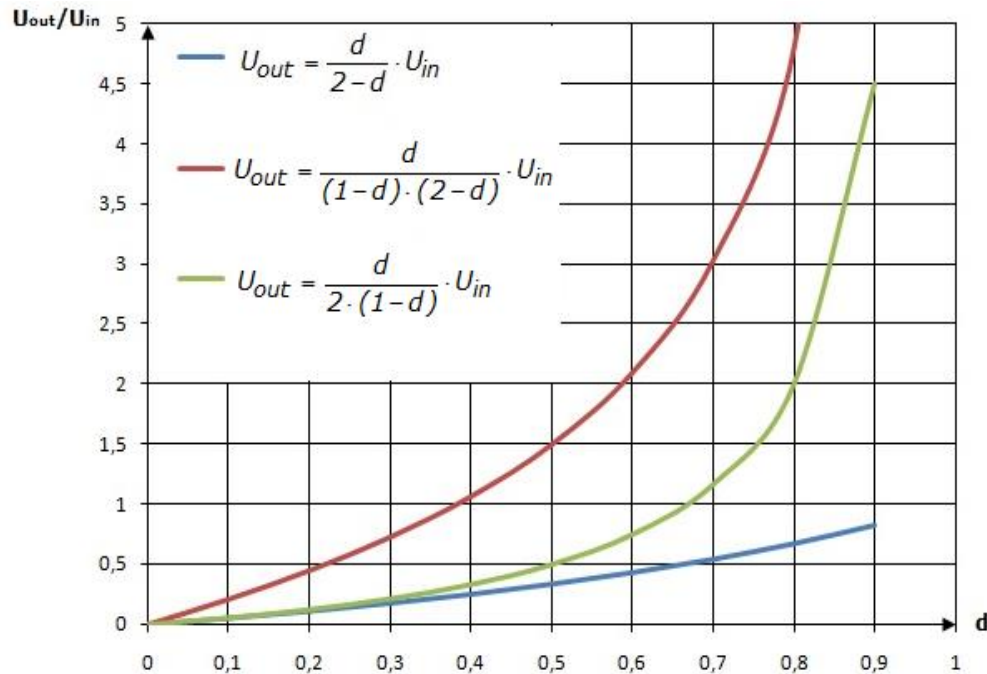


Figure 2.4. Comparison between conversion ratios of the step-down hybrid converter

As it can be seen from equations above and from the comparison between the conversion ratios of the step-down hybrid converters, the lowest conversion ratio it is achieved for the converters that used equation 2.4.

This chapter continues with the analysis of the hybrid converters.

## 2.2. Hybrid Buck converter with C-switching structure step-down 1

The hybrid Buck converter with C-switching structure step-down 1 consists of a classical Buck converter in which is inserted a C-switching cell step-down 1. In order to reduce the input current ripple, an input inductor  $L_1$  is inserted.

Figure 2.5 shows the circuit diagram with the corresponding on and off states [4], [116]-[117]. While the power switch turns off, the capacitors are charged in series from the input voltage source. When the switch is on these two capacitors are discharged in parallel.

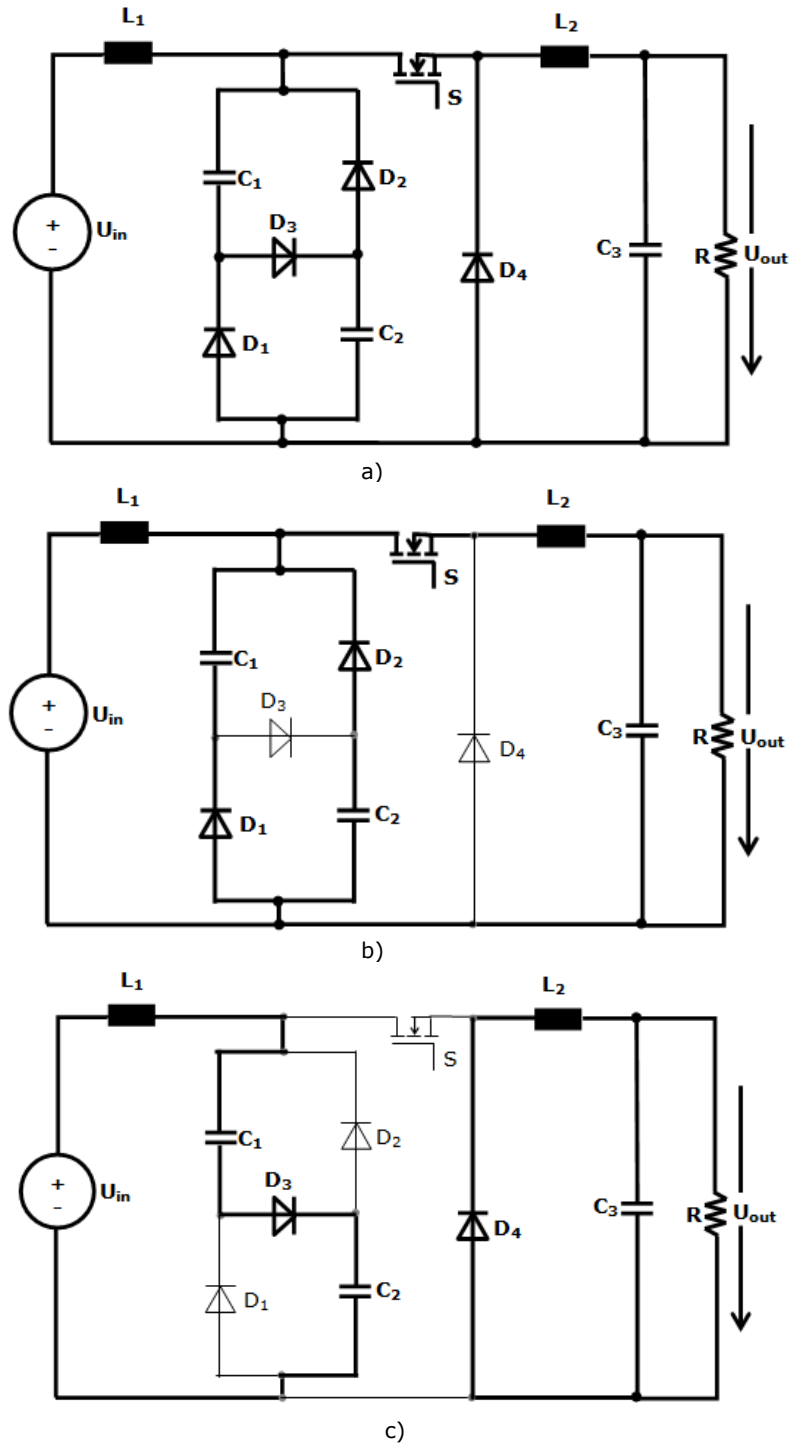


Figure 2.5. Hybrid Buck converter with C-switching structure step-down 1: a) circuit diagram; b) switched-on ( $t_{on}$ ) state; c) switched-off ( $t_{off}$ ) state [4]

Writing the voltage-second balance across the inductors it results that:

$$U_{out} = \frac{d}{2-d} \cdot U_{in} \quad (2.7)$$

In Figure 2.6 a comparison between conversion ratios as function of the duty cycle, for the classical Buck and hybrid Buck C-converter it is presented.

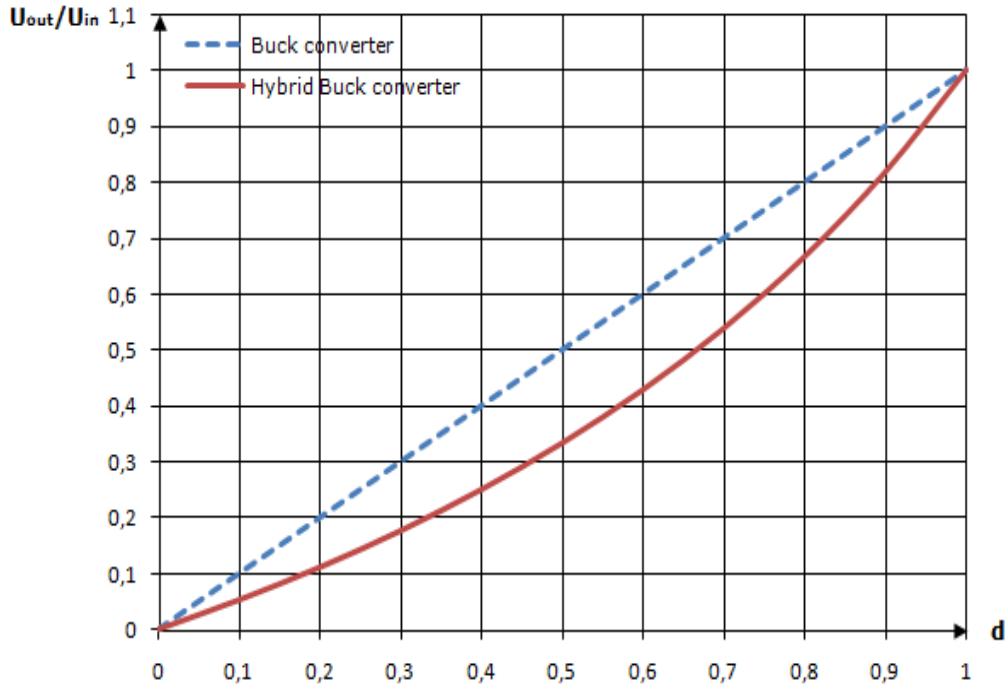


Figure 2.6. Comparison between conversion ratios of a hybrid Buck DC-DC C-converter and a classical Buck DC-DC converter

As it can be seen from equation 2.7 and from Figure 2.6, a lower conversion ratio can be achieved compared to classical Buck converter. The output voltage is reduced  $(2-d)$  times than in a classical Buck converter. For this reason, this converter have been reported in [116]-[117], as an alternative to high frequency transformer converters. Also, it can be used in automotive applications where extremely large ranges of voltage conversion ratios are necessary, in RE systems, and in power DC sources. The disadvantage of this converter compared to the classical Buck is that the number of the component is increased.

The hybrid Buck C-converter is simulated in the Caspoc package.

Figure 2.7 depicts the simulation schematic, while Figure 2.8 enfaces the simulated waveforms for the gate signal of the switch  $S$ , the current through the inductor  $L_1$ , the voltage across inductor  $L_1$ , the current through the inductor  $L_2$ , the voltage across the inductor  $L_2$ , and the output voltage. The converter was simulated for a duty cycle of 50% with an input voltage of 120V.

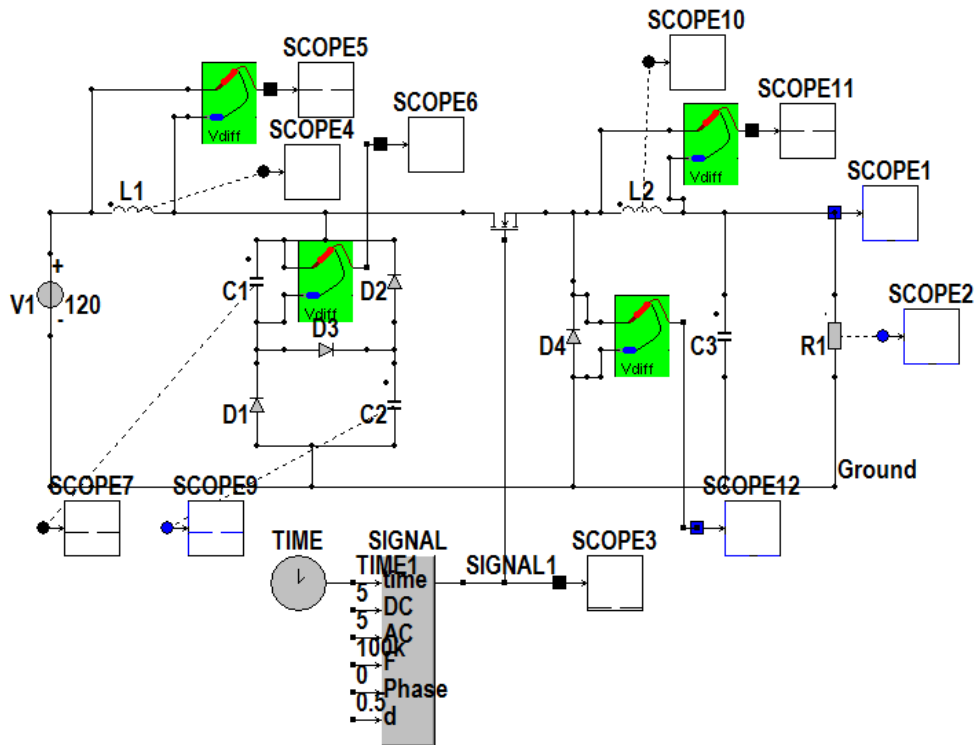


Figure 2.7. CASPOC simulation diagram for the hybrid Buck DC-DC C-converter

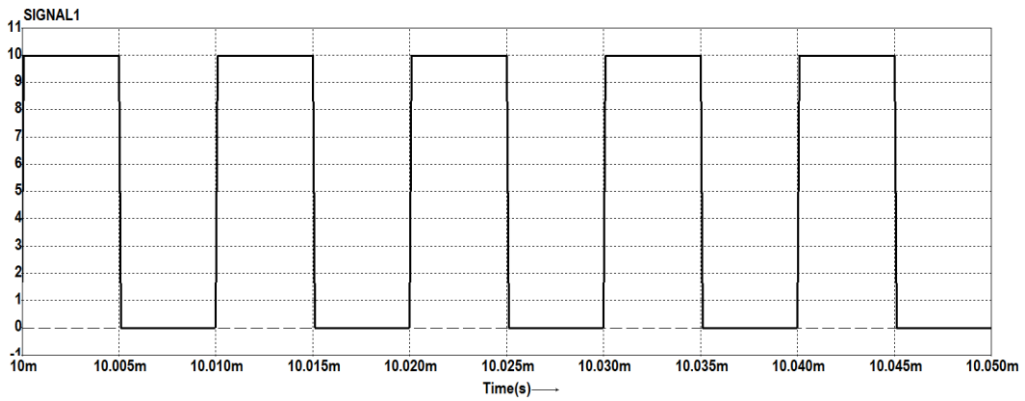


Figure 2.8. Simulation results for the hybrid Buck DC-DC C-converter

## 70 Multiphase Converters with Wide Conversion Ratio Using Hybrid Structures

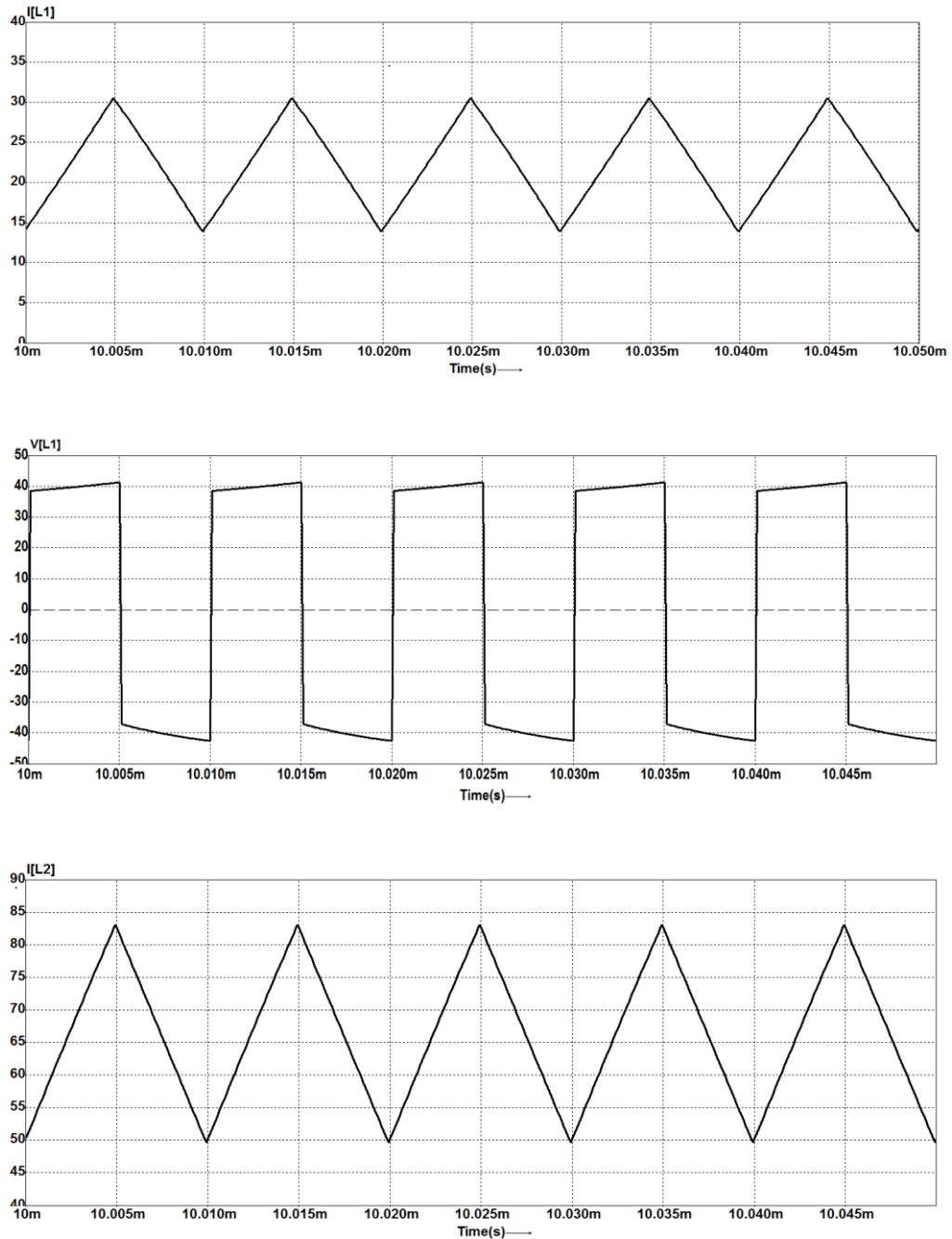


Figure 2.8. (continued 1) Simulation results for the hybrid Buck DC-DC C-converter

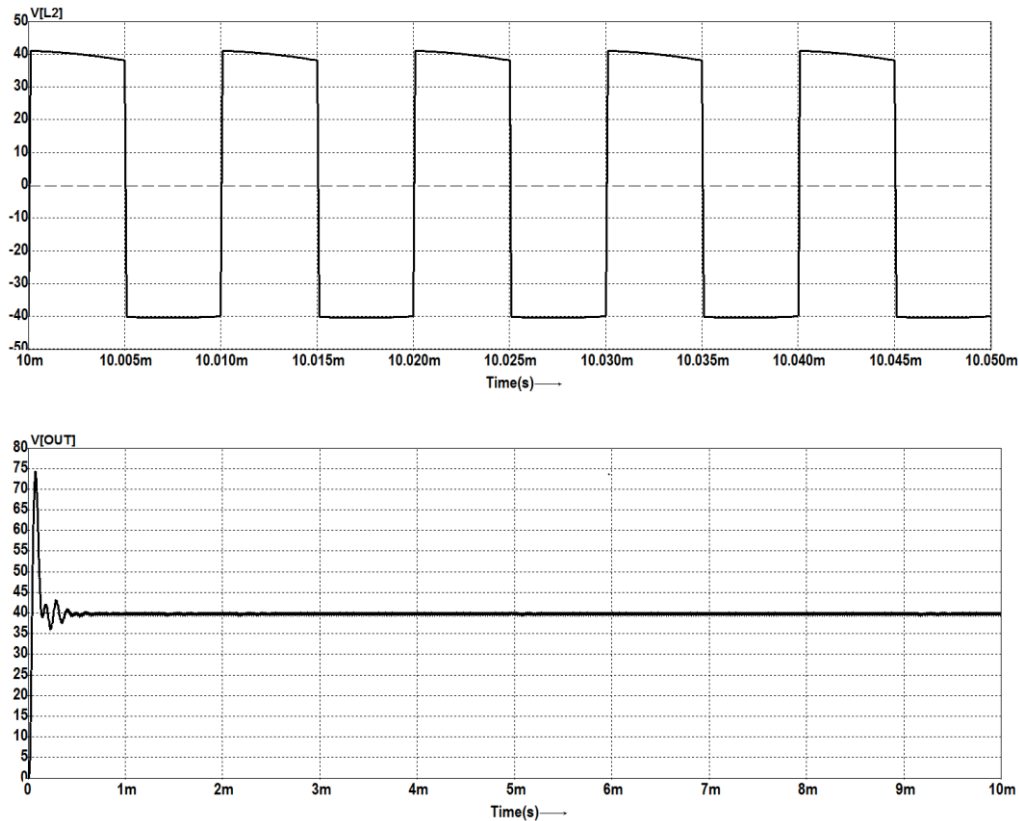


Figure 2.8. (continued 2) Simulation results for the hybrid Buck DC-DC C-converter  
This up to down order: signal,  $i_{L1}$ ,  $u_{L1}$ ,  $i_{L2}$ ,  $u_{L2}$ , and  $U_{out}$

### 2.3. Hybrid Buck converter with L-switching structure step-down 1

The hybrid Buck converter with L-switching structure step-down 1 consists of a classical Buck converter in which an L-switching cell step-down 1 is inserted. The L-switching cell consists of two inductors and two diodes. The output inductor and the diode from the classical Buck converter are replaced by the two inductors and two diodes from the L-switching structure.

Figure 2.9 shows the circuit diagram with the corresponding on and off state [4], [115] - [118].

While the power switch turns on, the inductors are charged in series from the input voltage source. When the switch is off these two inductors are discharged in parallel.

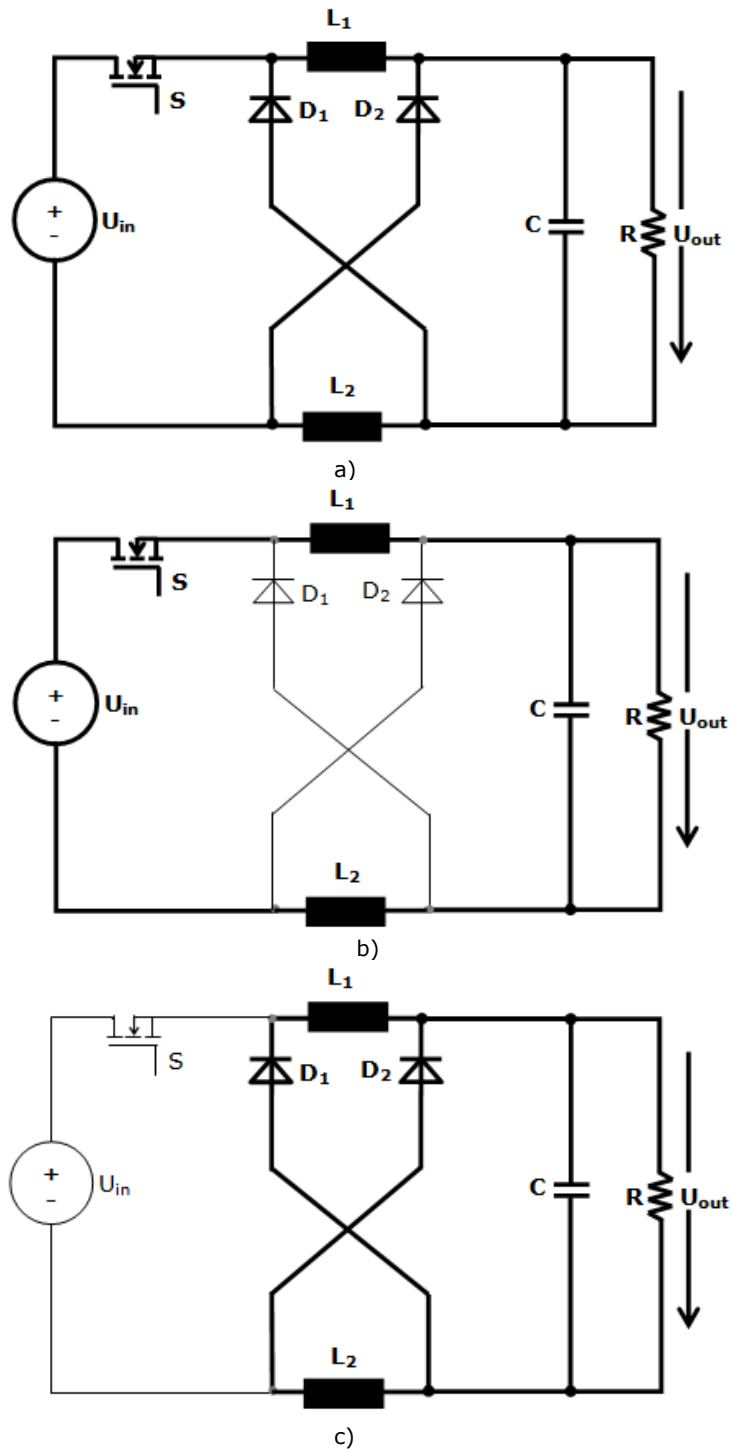


Figure 2.9. Hybrid Buck converter with L-switching structure step-down 1: a) circuit diagram; b) switched-on ( $t_{on}$ ) state; c) switched-off ( $t_{off}$ ) state [4]



Applying the voltage-second balance across inductors, the same output voltage equation to that one for the Buck converter with C-switching structure is obtained:

$$U_{out} = \frac{d}{2-d} \cdot U_{in} \quad (2.8)$$

As it can be seen from equation (2.8) and from Figure 2.6 a lower conversion ratio can be achieved compared to classical Buck converter.

The hybrid Buck L-converter is simulated in Caspoc Simulation program, Figure 2.10. The output voltage is reduced (2-d) times than in a classical Buck converter.

In Figure 2.11, the simulated waveforms for the gate signal of the switch S, the current through inductor L<sub>1</sub> (which is the same with the current through L<sub>2</sub>), the voltage across inductor L<sub>1</sub>, the current through the output capacitor and the output voltage are depicted. The converter was simulated for a duty cycle of 40% with an input voltage of 120V.

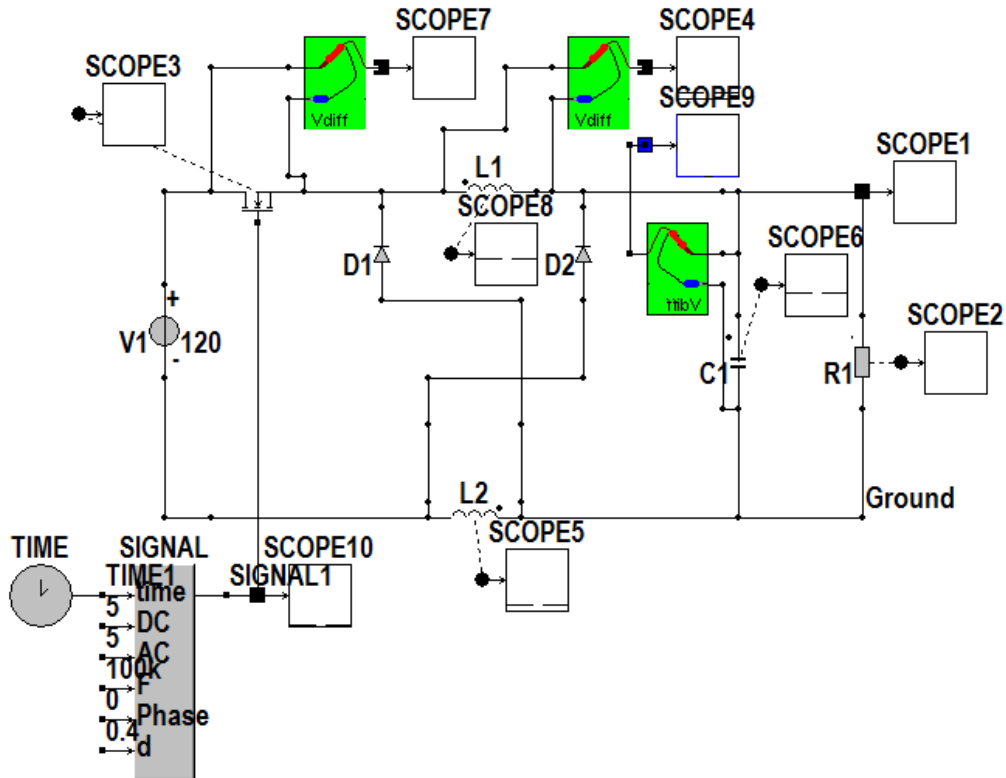


Figure 2.10. CASPOC simulation diagram for the hybrid Buck converter with L-switching structure step-down 1

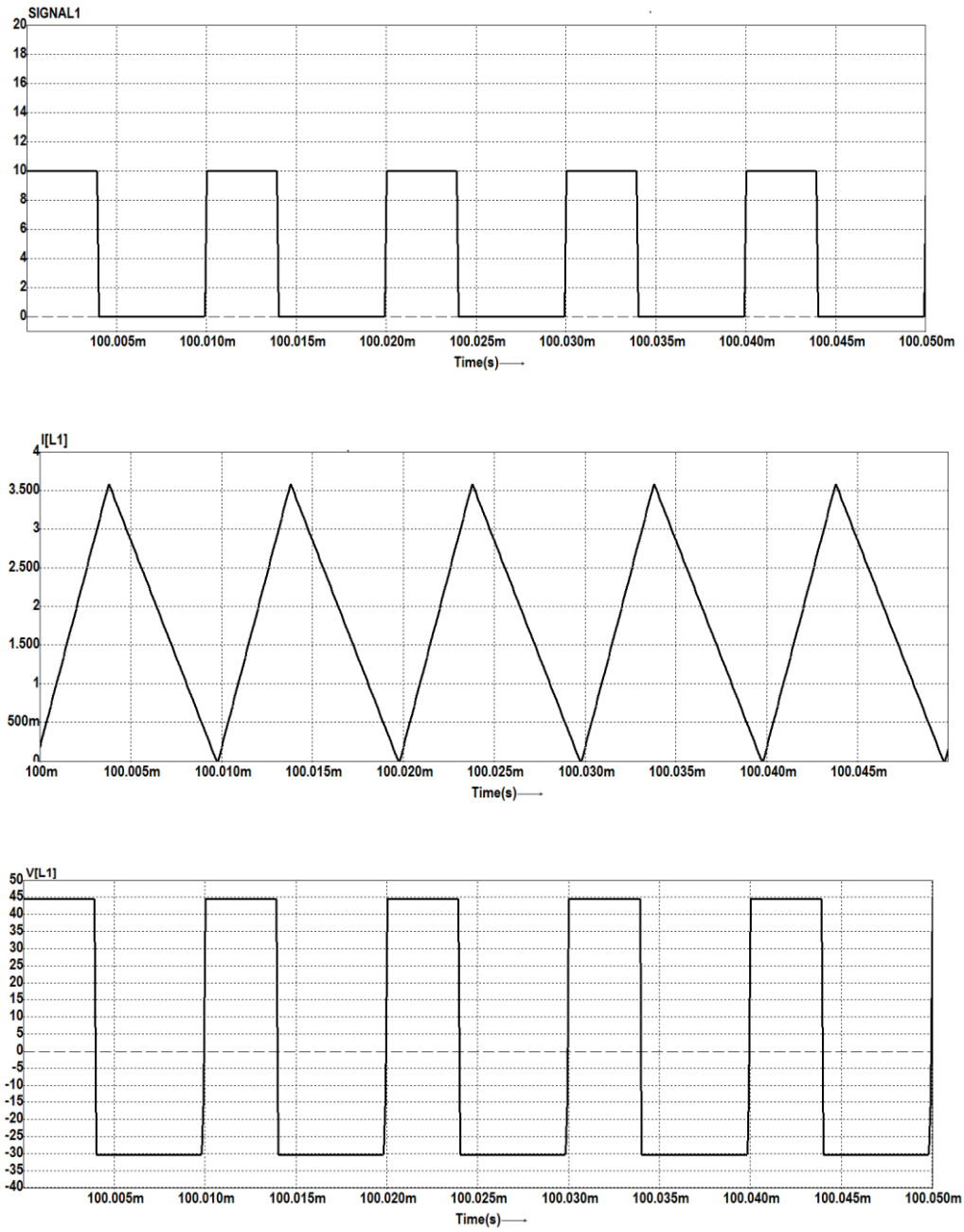


Figure 2.11. Simulation results for the hybrid Buck DC-DC L-converter

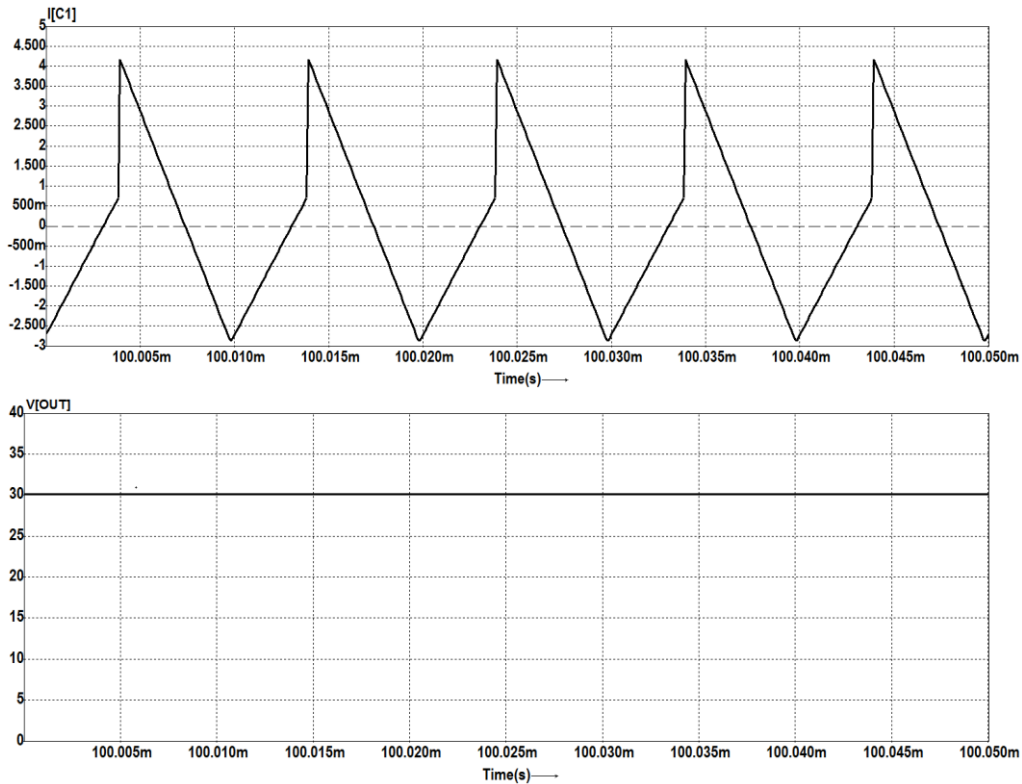


Figure 2.11. (continued 1) Simulation results for the hybrid Buck DC-DC L-converter  
This up to down order: signal,  $i_{L1}$ ,  $u_{L1}$ ,  $i_{C1}$  and  $U_{out}$

## 2.4. Hybrid Sepic converter with L-switching structure step-down 2

The hybrid Sepic converter with L-switching structure step-down 2 consists of a classical Sepic converter in which an L-switching cell step-down 2 is inserted. The L-switching cell consists of two inductors and two diodes. The output inductor and the diode from the classical Sepic converter are replaced by the two inductors and the two diodes from L-switching structure.

Figure 2.12 presents the circuit diagram with the corresponding on and off states [4], [5].

While the power switch turns on, the inductors are charged in series, and when the switch is off the inductors are discharged in parallel.

Voltage-second balance equation across the inductor leads to:

$$U_{out} = \frac{d}{2 \cdot (1-d)} \cdot U_{in} \quad (2.9)$$

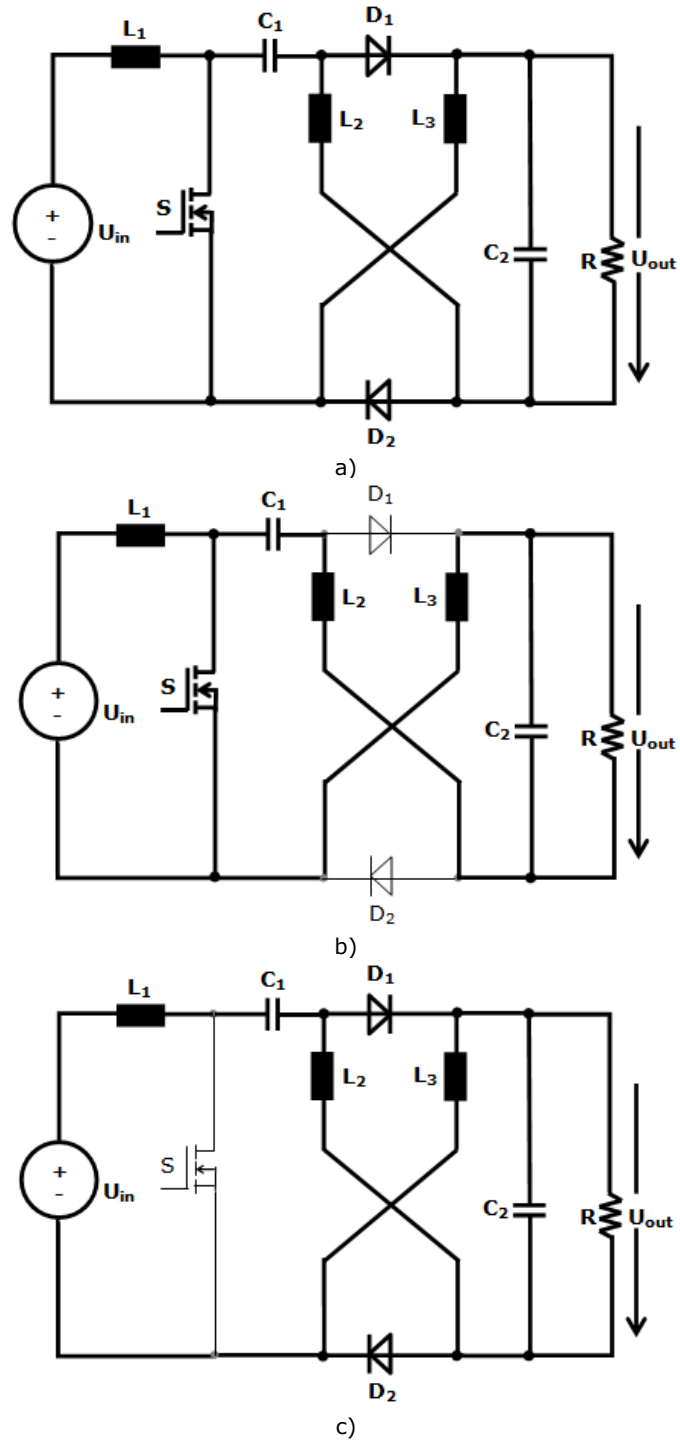


Figure 2.12. Hybrid Sepic DC-DC L-converter: a) circuit diagram; b) switched-on ( $t_{on}$ ) state; c) switched-off ( $t_{off}$ ) state [5]

In Figure 2.13 a comparison between conversion ratio as a function of the duty cycle, for classical Sepic and hybrid Sepic L-converter is presented.

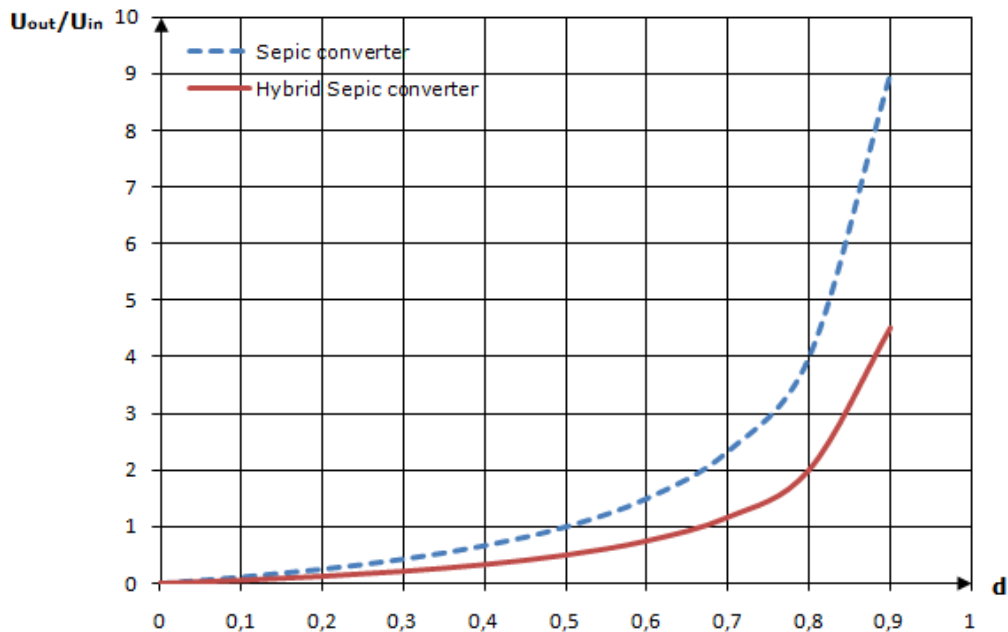


Figure 2.13. Comparison between conversion ratio of a hybrid Sepic DC-DC L-converter and classical Sepic DC-DC converter

As it can be seen from equation (2.9) and from Figure 2.13, a lower conversion ratio can be achieved compared to the classical Sepic converter. These hybrid converters presented many advantages: good efficiency, less voltage stress on the switches, allowing for a choice of lower-rated transistors and diodes, what conducted to lower conduction losses, and good transient performance. The Sepic converter is used in many low power applications where there is no need of DC isolation [4]-[5].

In Figure 2.14 the Caspoc simulation diagram of the hybrid Sepic L-converter is presented. Figure 2.15 enfoces the simulated waveforms for the gate signal of the switch S, the current through inductor  $L_1$ , the voltage across inductor  $L_1$ , the current through  $L_2$  (which is the same to the current through  $L_3$ ), the voltage across inductor  $L_2$ , and the output voltage. The converter was simulated for a duty cycle of 50% and with an input voltage of 120V.

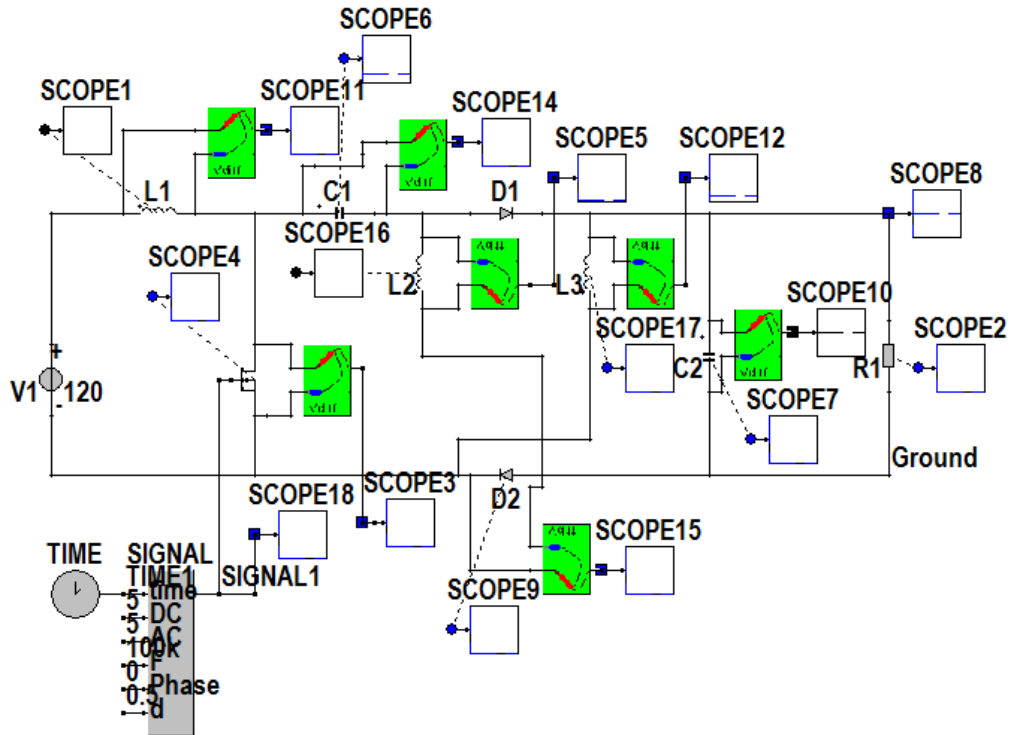


Figure 2.14. CASPOC simulation diagram for the hybrid Sepic DC-DC L-converter

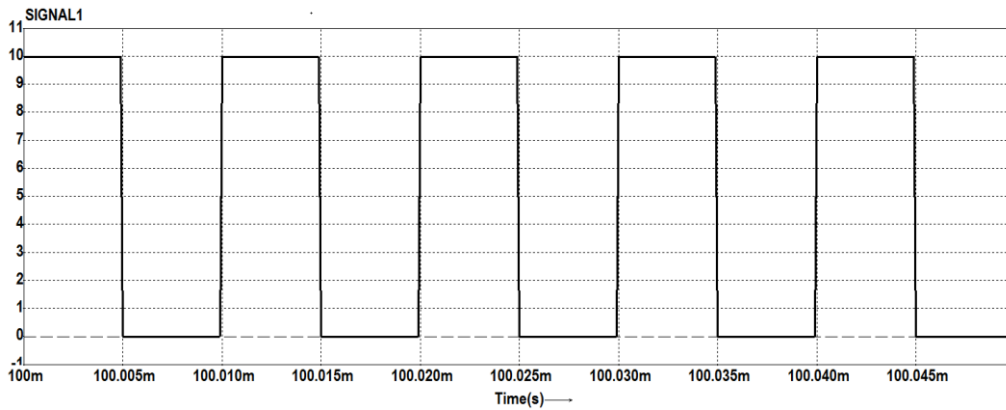


Figure 2.15. Simulation results for the hybrid Sepic DC-DC L-converter

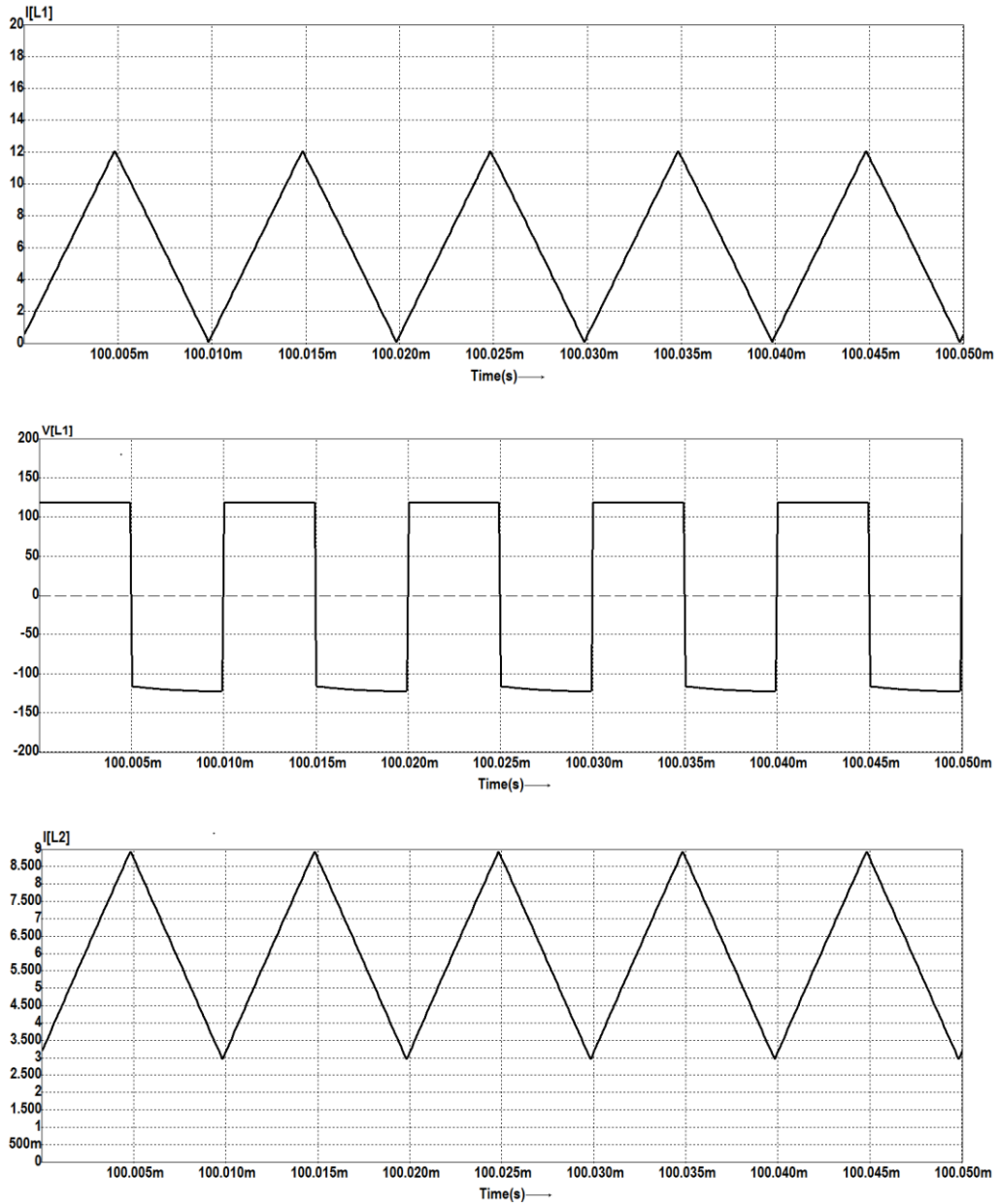


Figure 2.15. (continued 1 ) Simulation results for the hybrid Sepic DC-DC L-converter

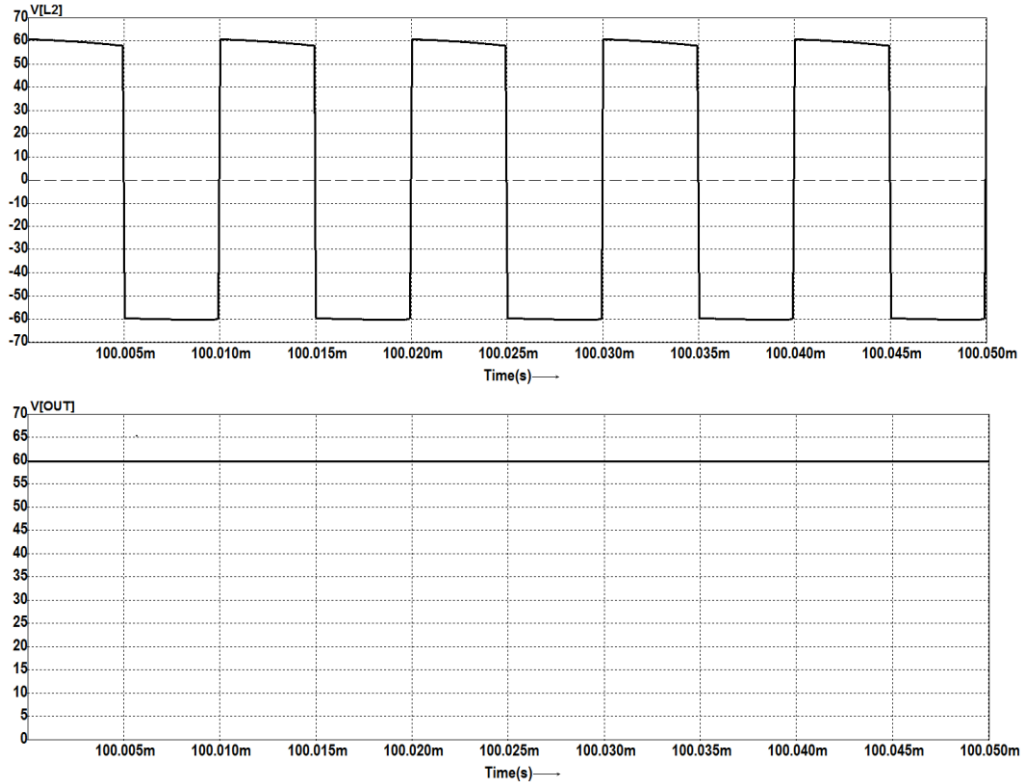


Figure 2.15. (continued 2) Simulation results for the hybrid Sepic DC-DC L-converter  
This up to down order: signal,  $i_{L1}$ ,  $u_{L1}$ ,  $i_{L2}$ ,  $u_{L2}$  and  $U_{out}$

The output voltage is two times lower than in a classical Sepic converter.

## 2.5. Hybrid Boost converter with C-switching structure step-up 1

The hybrid Boost converter with C-switching structure step-up 1 consists of a classical Boost converter in which a C-switching cell step-up 1 is inserted. The C-switching cell consists of two capacitors and two diodes. The output capacitor from a classical Boost converter was splitted into two capacitors, and the rectifier diode was duplicated. Also for reducing the output current ripple, an output inductor is inserted.

Figure 2.16 presents the circuit diagram with the corresponding on and off states, [1]- [2], [4], [119].

While the power switch turns off, the capacitors are equally charged by the energy stored in the inductor  $L_1$ . When the switch is on these two capacitors are discharged in series to the load.



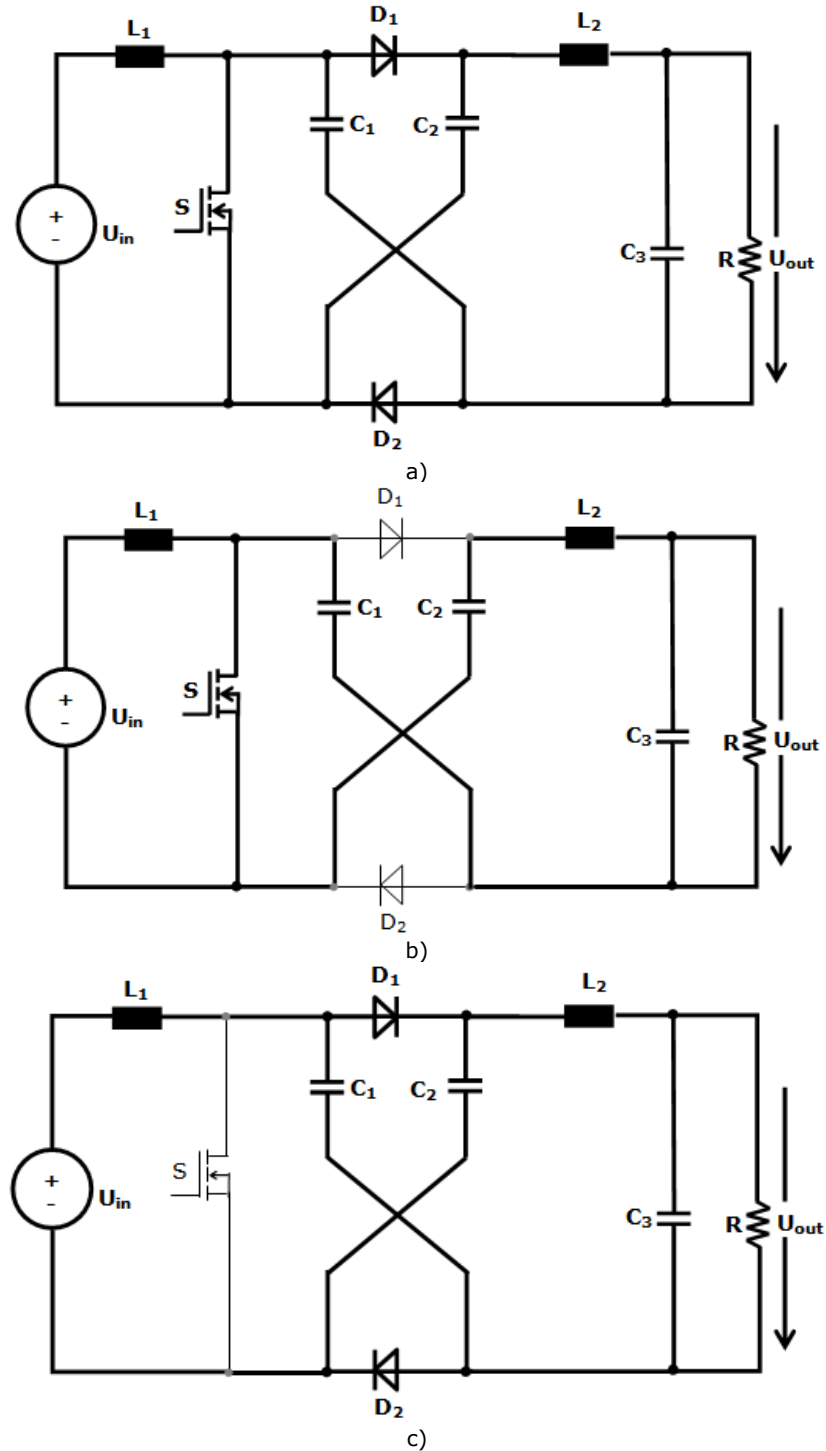


Figure 2.16. Hybrid Boost DC-DC C-converter: a) circuit diagram; b) switched-on ( $t_{on}$ ) state; c) switched-off ( $t_{off}$ ) state [1]

Applying the voltage-second balance on the inductors results that:

$$U_{out} = \frac{1+d}{1-d} \cdot U_{in} \quad (2.10)$$

In Figure 2.17 it is presented a comparison between conversion ratio against the duty cycle, for classical Boost and hybrid Boost C-converter.

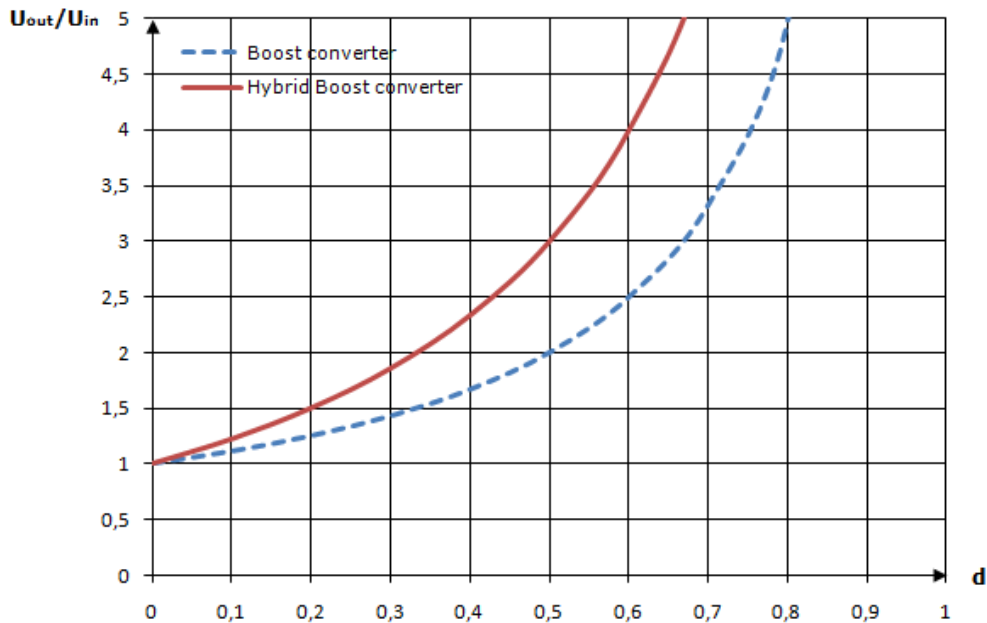


Figure 2.17. Comparison between conversion ratio of a hybrid Boost DC-DC C-converter and classical Boost DC-DC converter

As it can be seen from equation 2.10 and from Figure 2.17, the output voltage is increased  $(1+d)$  times compared to classical Boost converter. The circuit is simple and has some significant features of extended output voltage, less output voltage ripple and less input current ripple as compared with the classical Boost. This converter can be used in UPS applications, for charging the batteries, or for power conditioners for fuel cell systems [1]- [2], [119].

The Caspoc simulation diagram of the hybrid Boost C-converter is shown in Figure 2.18. The converter has been simulated for a duty cycle of 60% with an input voltage of 40V and switching frequency  $f_s=100$  kHz.

The simulated waveforms for the gate signal of the switch S, the current through inductor  $L_1$ , the voltage across inductor  $L_1$ , the current through  $L_2$ , the voltage across inductor  $L_2$ , and the output voltage are presented in Figure 2.19.

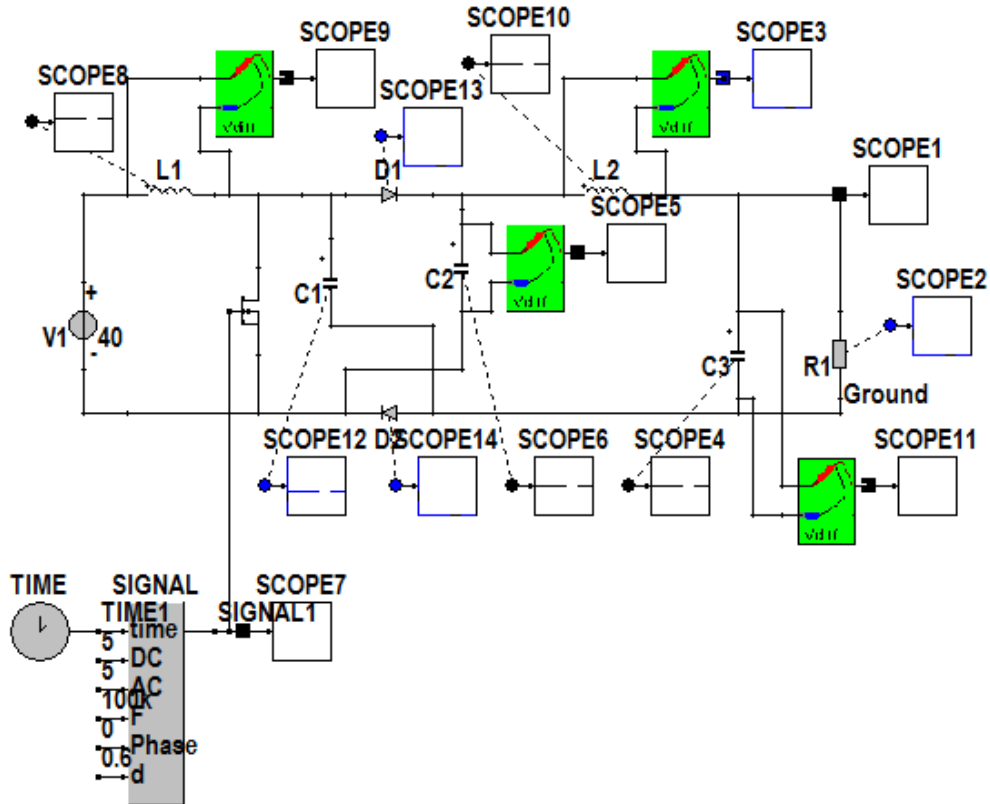


Figure 2.18. CASPOC simulation diagram for the hybrid Boost DC-DC C-converter

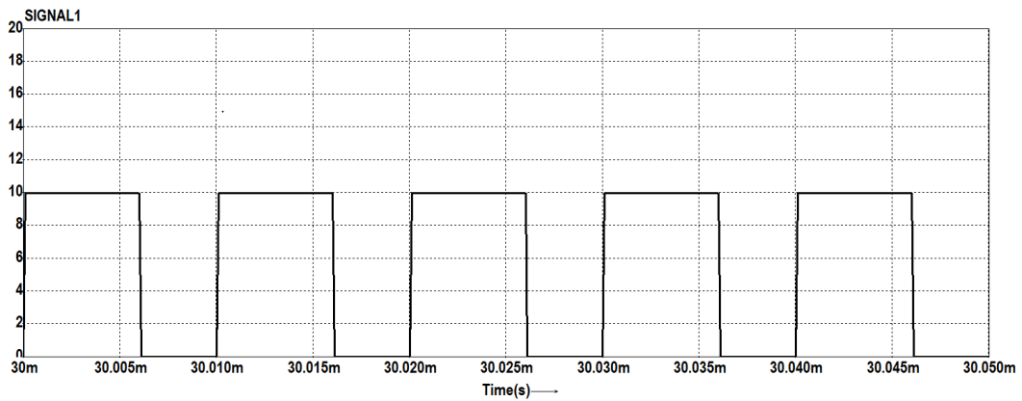


Figure 2.19. Simulation results for the hybrid Boost DC-DC C-converter

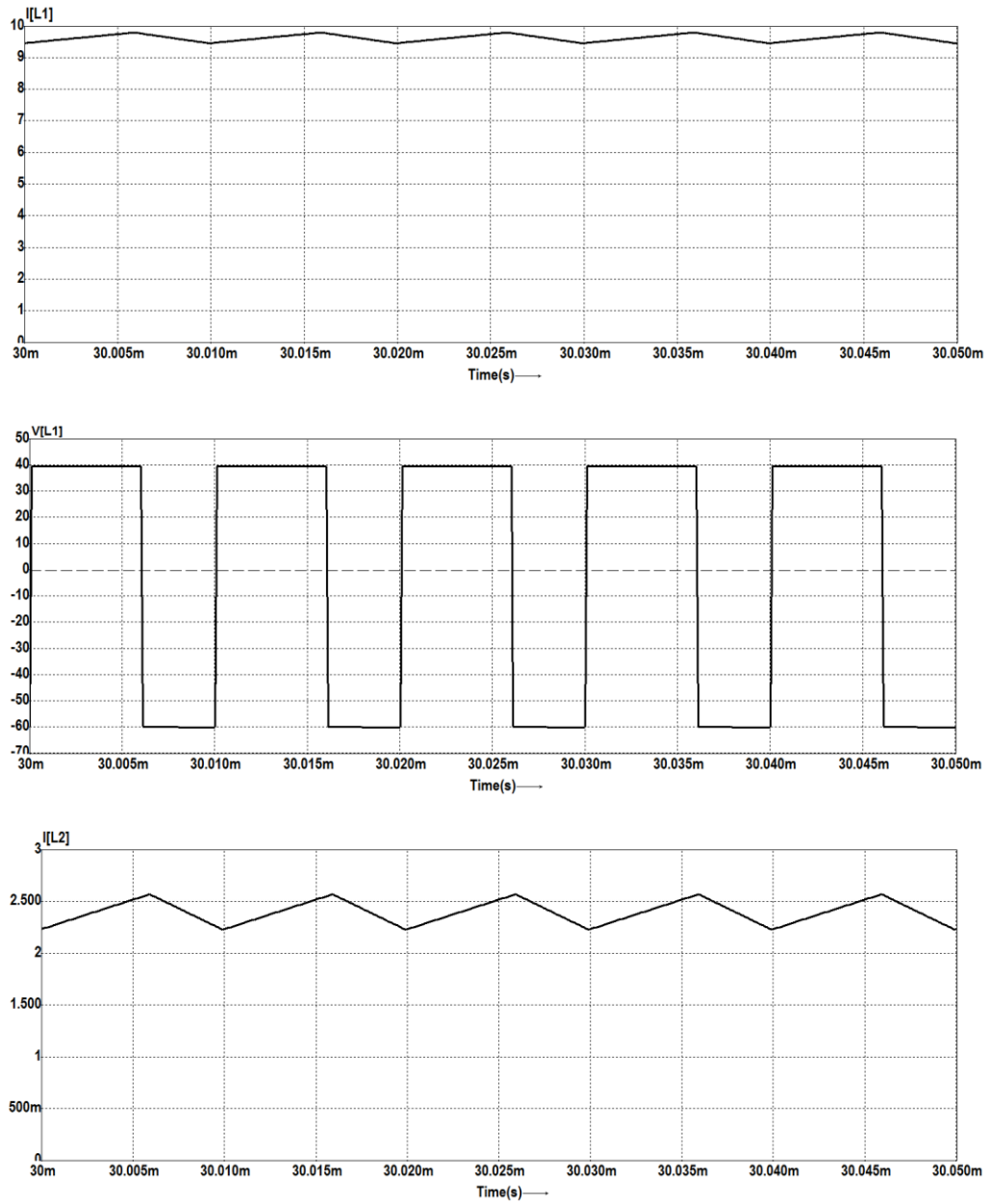


Figure 2.19. (continued 1) Simulation results for the hybrid Boost DC-DC C-converter

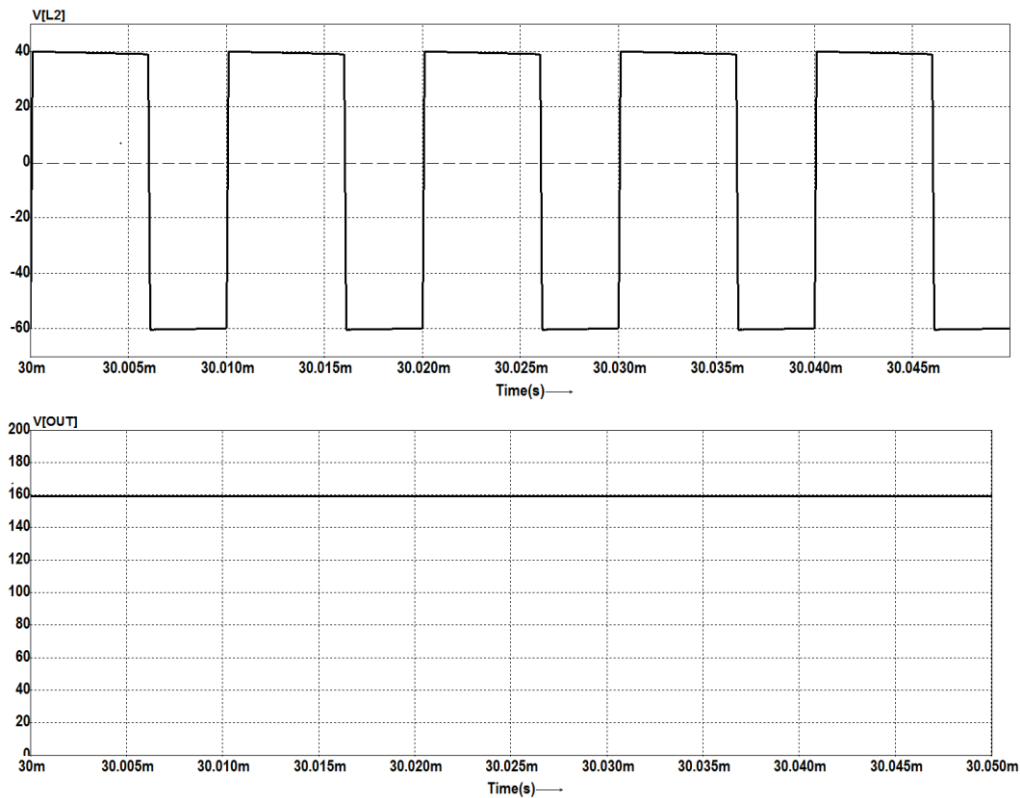


Figure 2.19. (continued 2) Simulation results for the hybrid Boost DC-DC C-converter  
This up to down order: signal,  $i_{L1}$ ,  $u_{L1}$ ,  $i_{L2}$ ,  $u_{L2}$  and  $U_{out}$

## 2.6. Hybrid Ćuk converter with C-switching structure step-up 2

The hybrid Ćuk converter with C-switching structure step-up 2 consists of a classical Ćuk converter in which a C-switching cell step-up 2 is inserted. The C-switching cell consists of two capacitors and two diodes. This C-switching cell only plays the role of the original energy-transfer capacitor, and is not cascaded with the original converter. The capacitor from a classical Ćuk converter was splitted in two capacitors, and the rectifier diode was duplicated.

Figure 2.20 presents the circuit diagram with the corresponding on and off state [3]-[4].

While the power switch turns off, the capacitors are equally charged by the energy stored in inductor  $L_1$ . When the switch is on these two capacitors are discharged in series to the load.

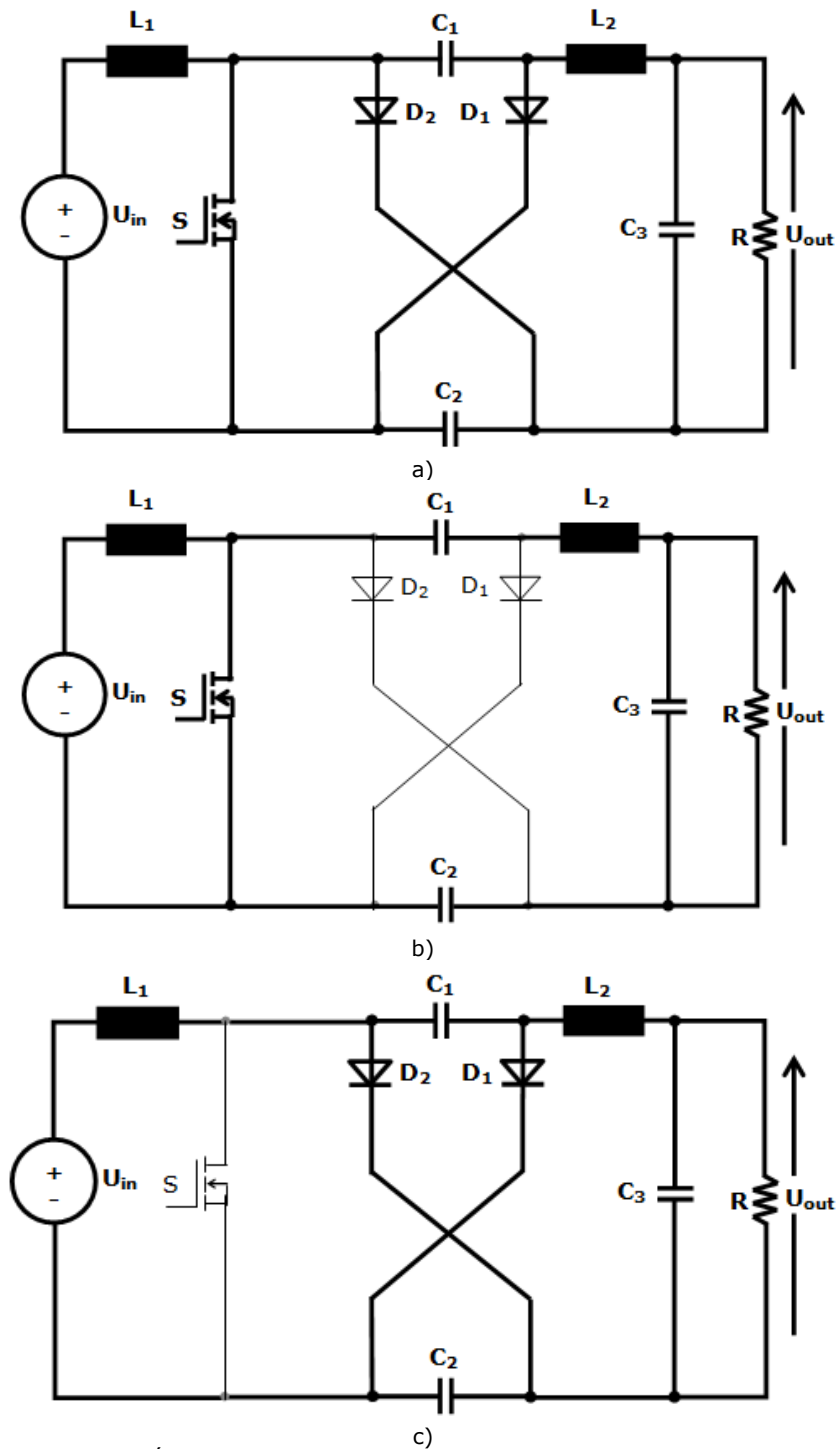


Figure 2.20. Hybrid Ćuk DC-DC C-converter: a) circuit diagram; b) switched-on ( $t_{on}$ ) state; c) switched-off ( $t_{off}$ ) state [4]

Invoking voltage-second balance principle across inductors one obtains:

$$U_{out} = \frac{1+d}{1-d} \cdot U_{in} \quad (2.11)$$

In Figure 2.21 a comparison between conversion ratio as function of the duty cycle, for classical Ćuk and hybrid Ćuk C-converter is presented.

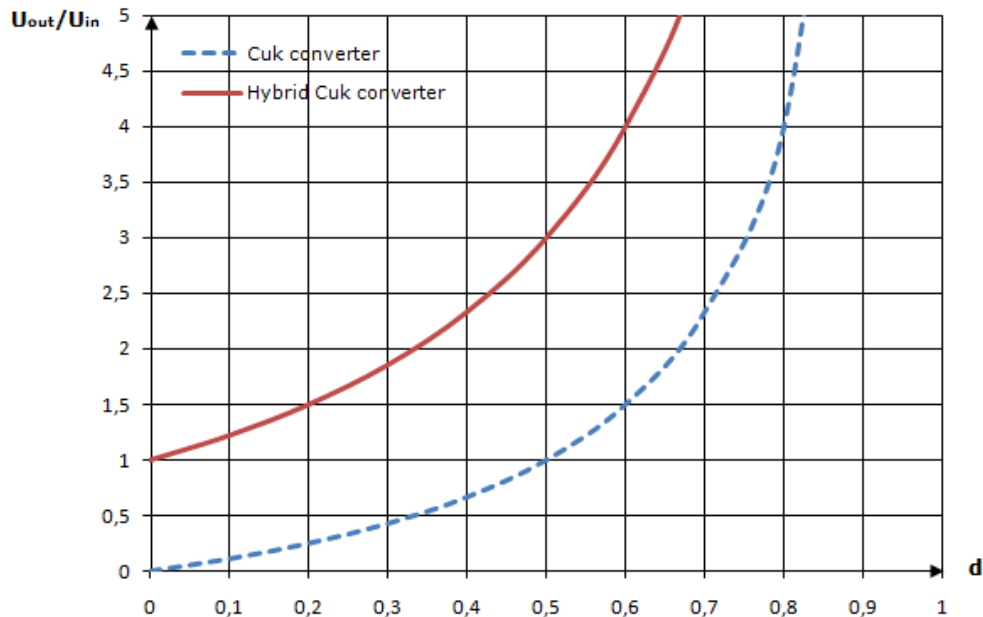


Figure 2.21. Comparison between conversion ratio of a hybrid Ćuk DC-DC C-converter and classical Ćuk DC-DC converter

As it can be seen from equation 2.11 and from Figure 2.21 a higher conversion ratio can be achieved compared to classical Ćuk converter.

The simulation circuit diagram of the hybrid Ćuk C-converter is presented in Figure 2.22. The output voltage is increased  $(1+d)/d$  times than in a classical Ćuk converter.

Figure 2.23 exhibits the simulated waveforms for the gate signal of the switch S, the current through inductor  $L_1$ , the voltage across inductor  $L_1$ , the current through  $L_2$ , the voltage across inductor  $L_2$ , and the output voltage. The converter was simulated for a duty cycle of 60% with 40V input voltage and switching frequency of  $f_s=50$  kHz.

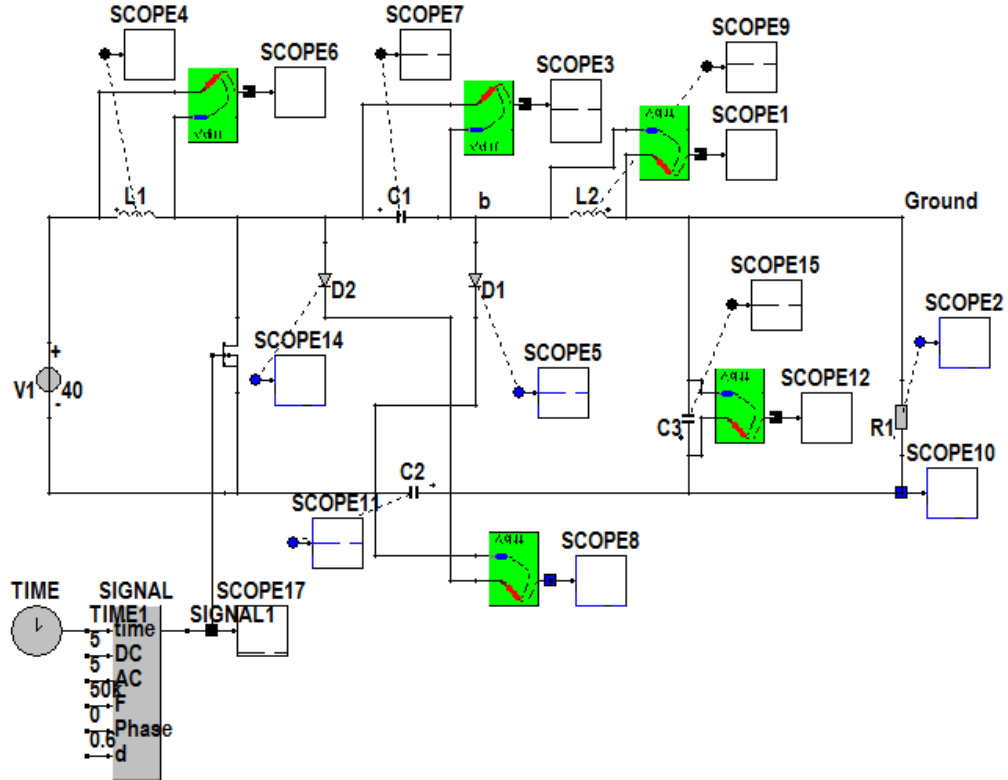


Figure 2.22. CASPOC simulation diagram of the hybrid Ćuk DC-DC C-converter

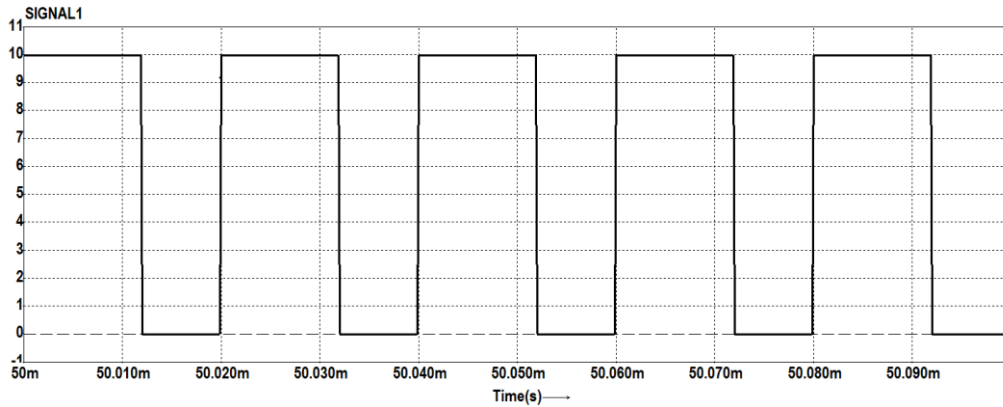


Figure 2.23. Simulation results for the hybrid Ćuk DC-DC C-converter



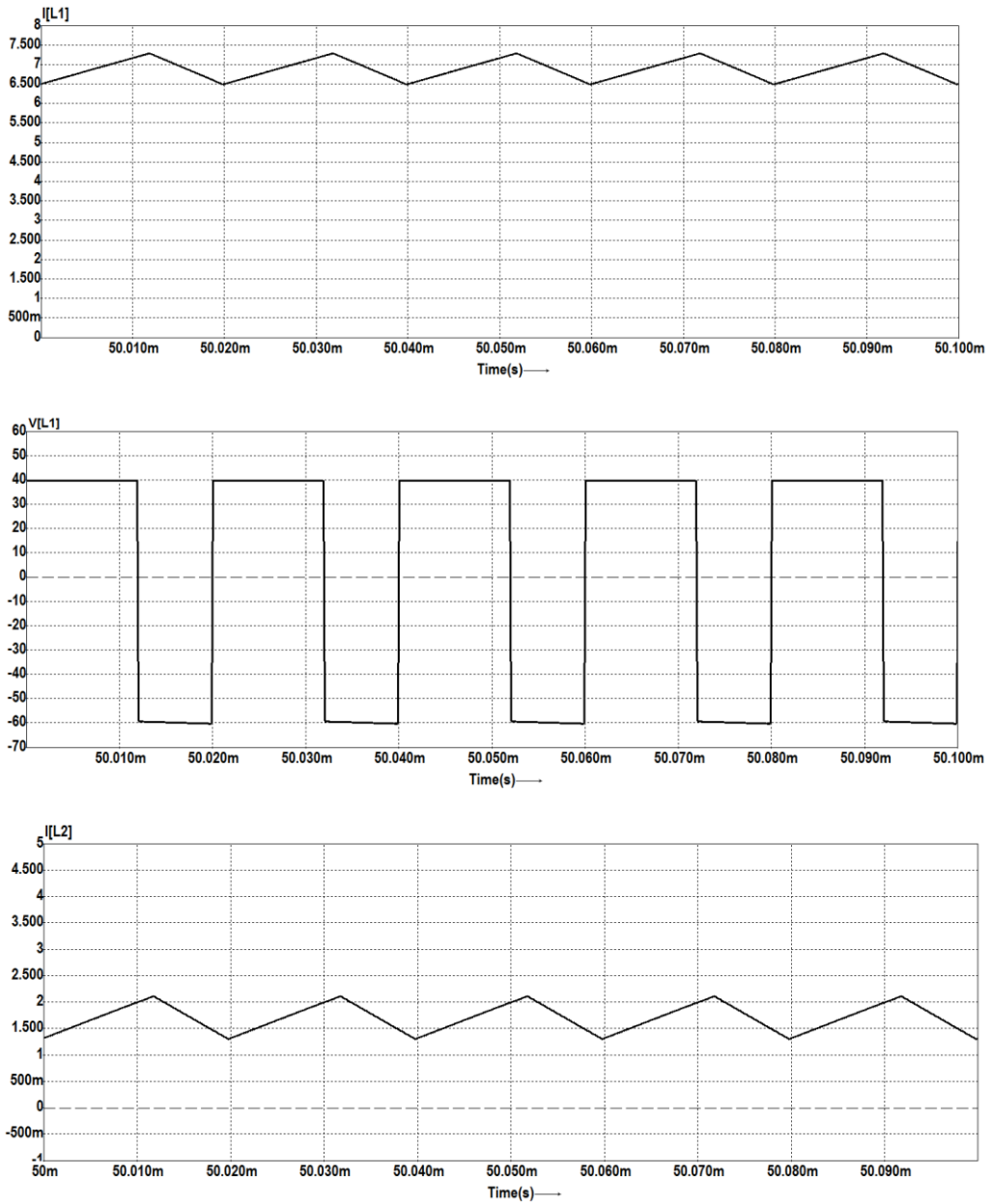


Figure 2.23. (continued 1) Simulation results for the hybrid Ćuk DC-DC C-converter

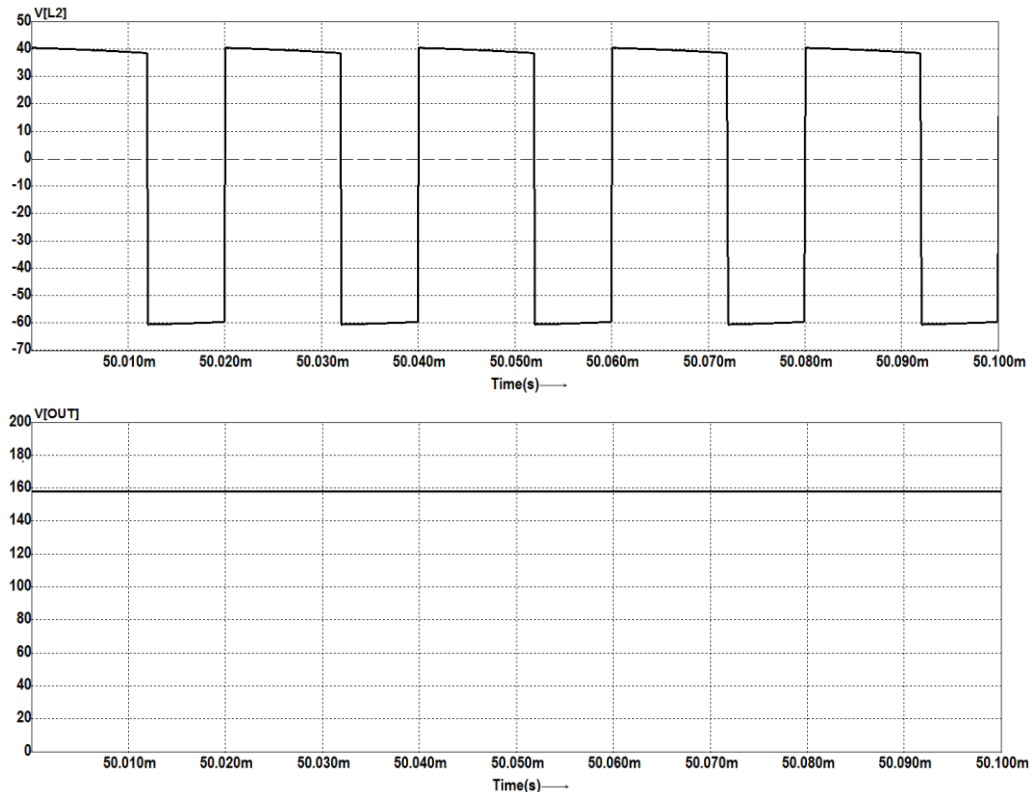


Figure 2.23. (continued 2) Simulation results for the hybrid Ćuk DC-DC C-converter  
This up to down order: signal,  $i_{L1}$ ,  $u_{L1}$ ,  $i_{L2}$ ,  $u_{L2}$  and  $U_{out}$

## 2.7. Hybrid Boost converter with L-switching structure step-up 1

The hybrid Boost converter with L-switching structure step-up 1 consists of a classical Boost converter in which an L-switching cell step-up 1 is inserted. The L-switching cell consists of two inductors and three diodes. The input inductor from the classical Boost converter is replaced by the two inductors in the new hybrid converter [4], [103], [120] - [122].

Figure 2.24 presents the circuit diagram with the corresponding on and off states [103], [121].

While the power switch turns on, the inductors are charged in parallel from the input voltage source. When the switch is off these two inductors are discharged in series.

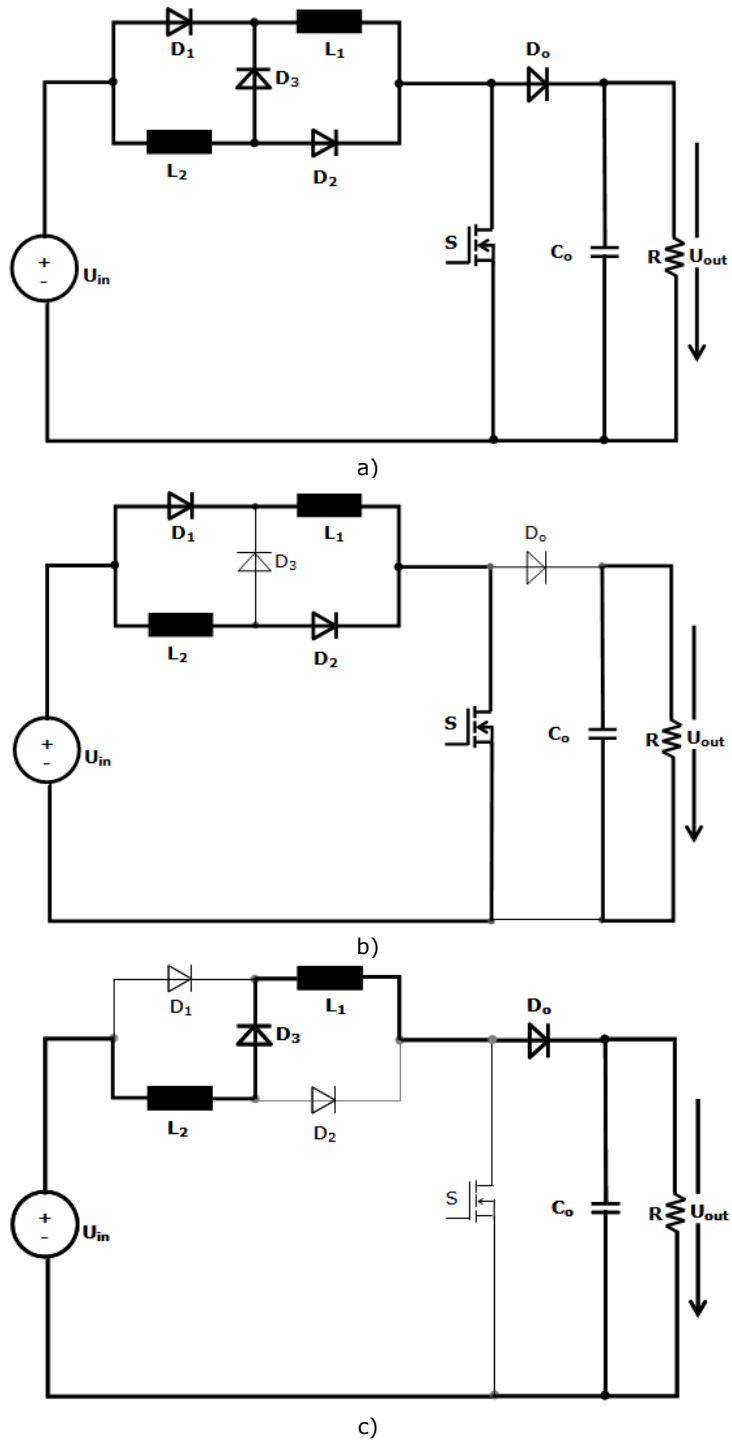


Figure 2.24. Hybrid Boost DC-DC L-converter: a) circuit diagram; b) switched-on ( $t_{on}$ ) state; c) switched-off ( $t_{off}$ ) state [103].

Applying the voltage-second balance on inductors the output voltage is obtained as:

$$U_{out} = \frac{1+d}{1-d} \cdot U_{in} \quad (2.12)$$

As it can be seen from equation 2.12 and from Figure 2.17 a higher conversion ratio can be achieved compared to classical Boost converter. This converter can be used as a interface between the PV system and the load, as a high-intensity-discharge lamp ballast for automobile headlamps, fuel cell conversion systems and battery back-up systems for UPS [121] - [122].

Figure 2.25 shows the Caspoc circuit diagram for the hybrid Boost L-converter. The output voltage is increased (1+d) times than in a classical Boost converter. The converter was simulated for a duty cycle of 50% with 40V input voltage and a switching frequency of  $f_s=100$  kHz.

Figure 2.26 presents the simulated waveforms for the gate signal of the switch S, the input phase current  $i_{iP}$ , the current through diode  $D_1$ , the current through inductor  $L_1$  (which is the same with the current through inductor  $L_2$ ), the voltage across inductor  $L_1$ , the current through switch S, the output phase current  $i_{oP}$ , the current through the output capacitor  $C_o$  (in simulation denoted  $C_2$ ), the output current and the voltage of the circuit.

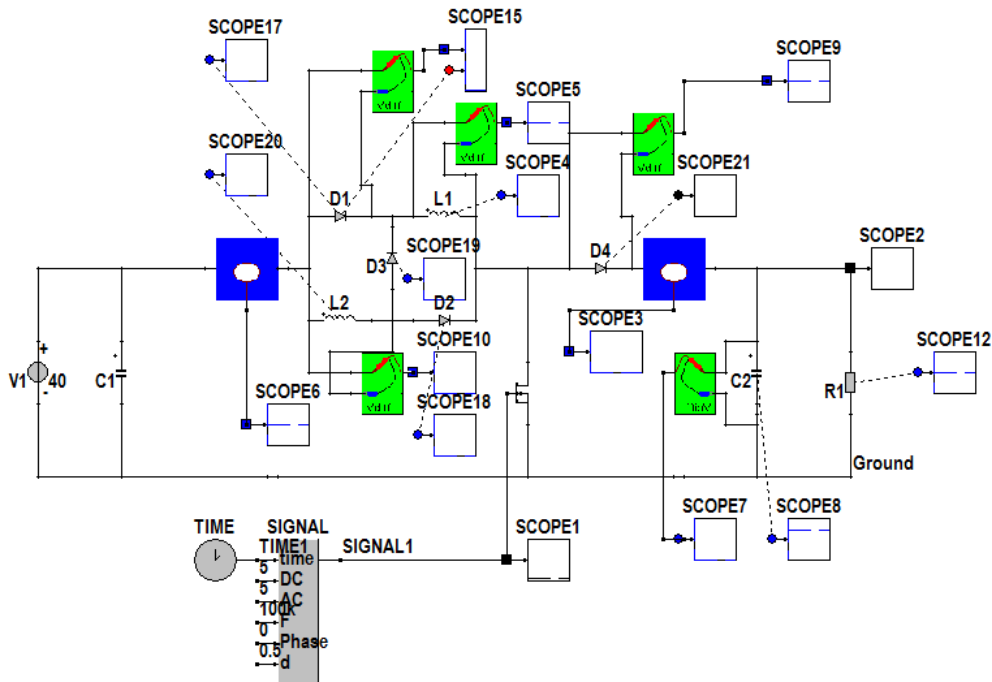


Figure 2.25. CASPOC circuit diagram for the hybrid Boost DC-DC L-converter

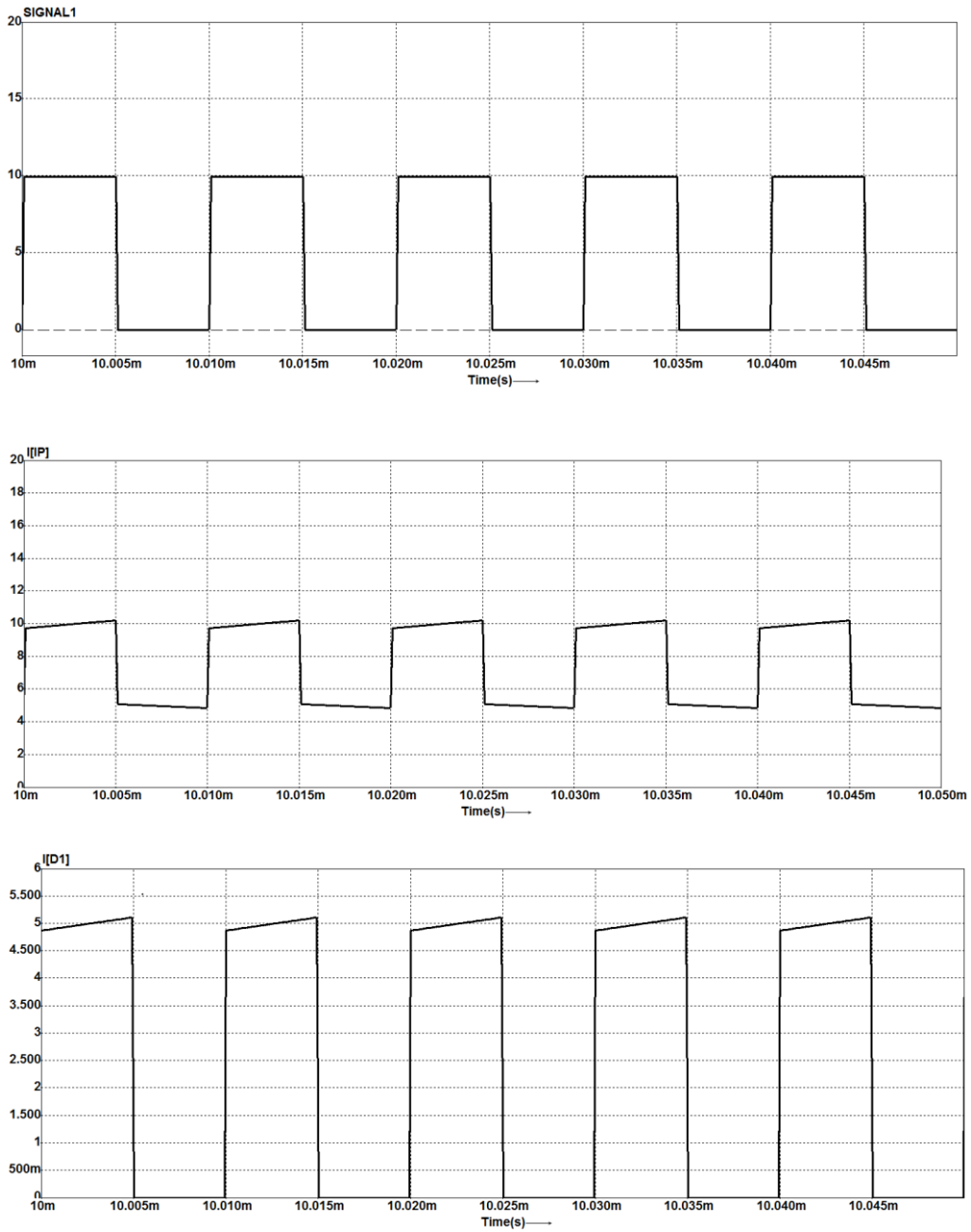


Figure 2.26. Simulation results for the hybrid Boost DC-DC L-converter

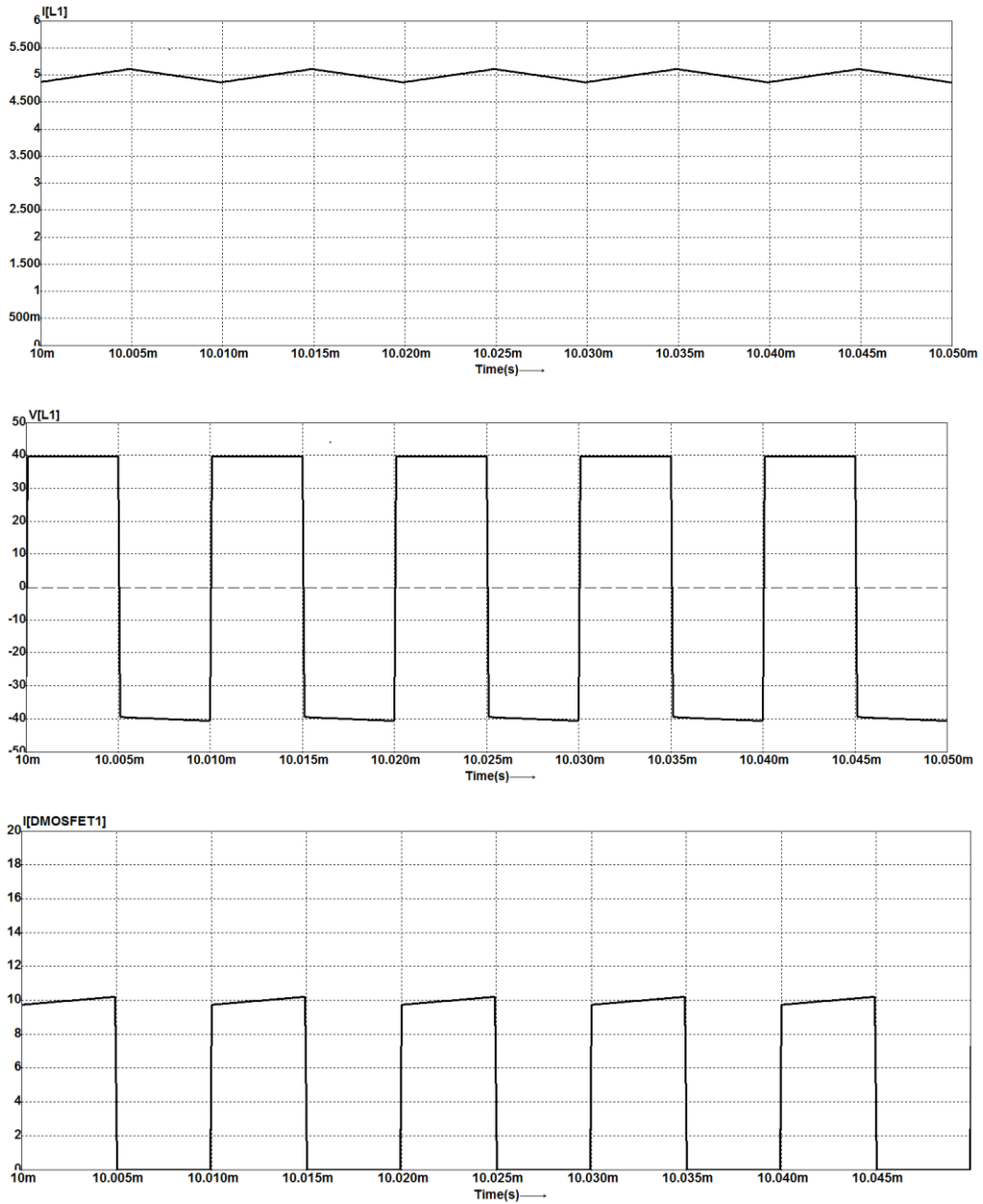


Figure 2.26. (continued 1) Simulation results for the hybrid Boost DC-DC L-converter

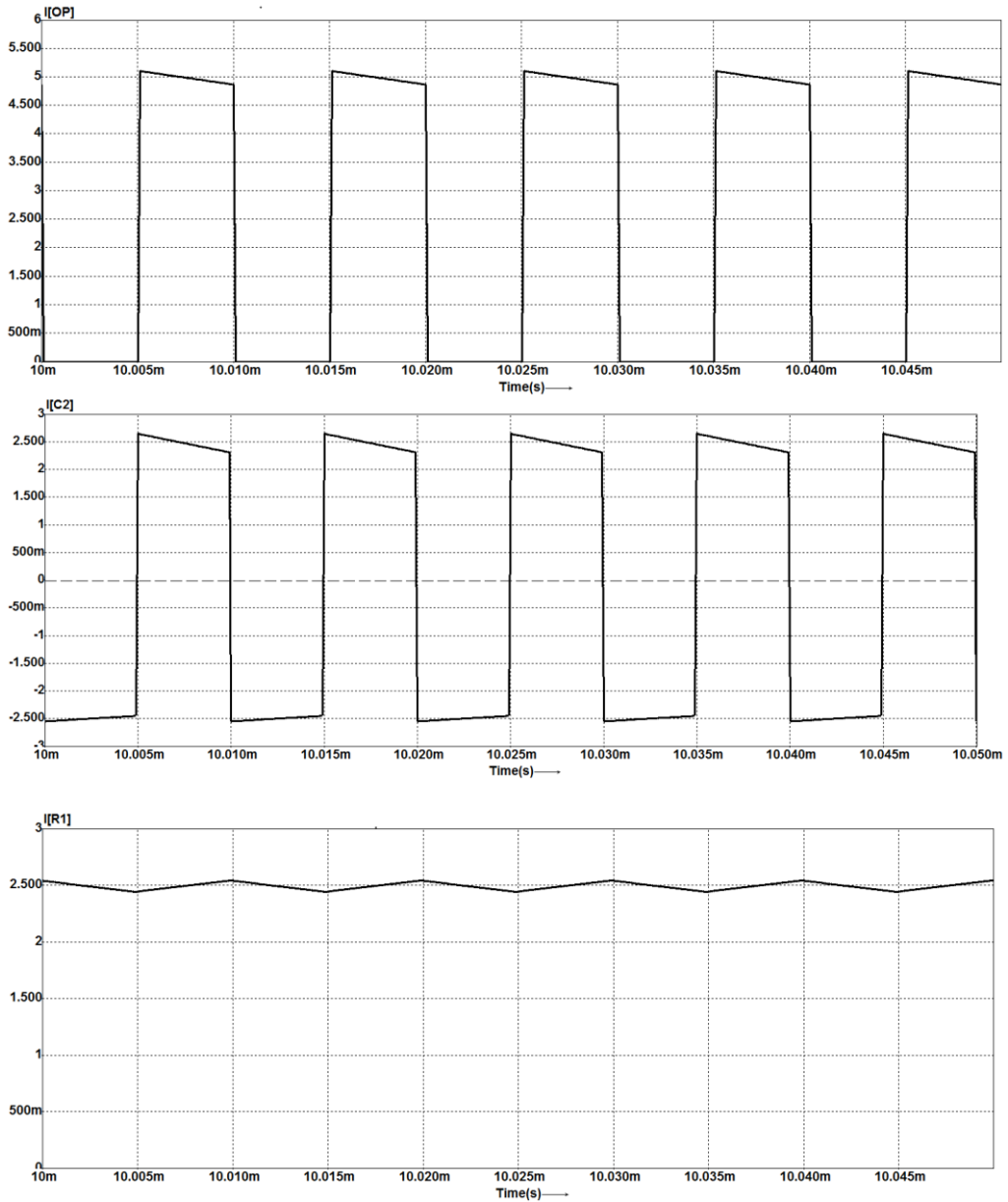


Figure 2.26. (continued 2) Simulation results for the hybrid Boost DC-DC L-converter

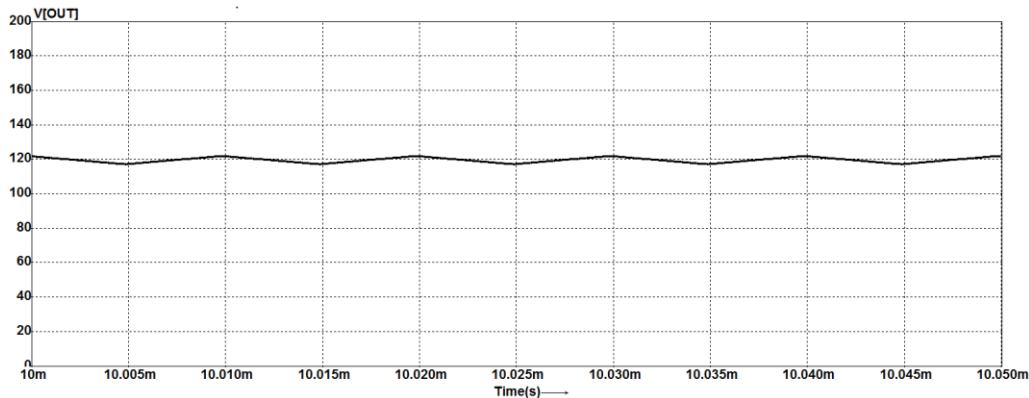


Figure 2.26. (continued 3) Simulation results for the hybrid Boost DC-DC L-converter  
This up to down order: signal,  $i_{IP}$ ,  $i_{D1}$ ,  $i_{L1}$ ,  $u_{L1}$ ,  $i_s$ ,  $i_{oP}$ ,  $i_{oC}$ ,  $i_{out}$  and  $U_{out}$

For the hybrid Boost L-converter extended study, digital simulation and practical implementation have been carried out, and are presented in detail in the next chapter.

## 2.8. Multiphase DC-DC converters synthesis using hybrid structures

The hybrid DC-DC converters presented in the previous sections, Table 2.1, will be used in multiphase configurations.

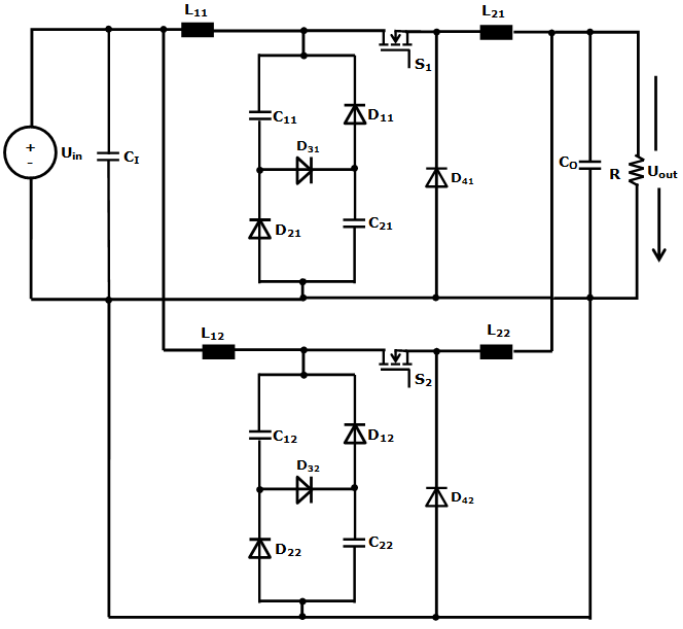
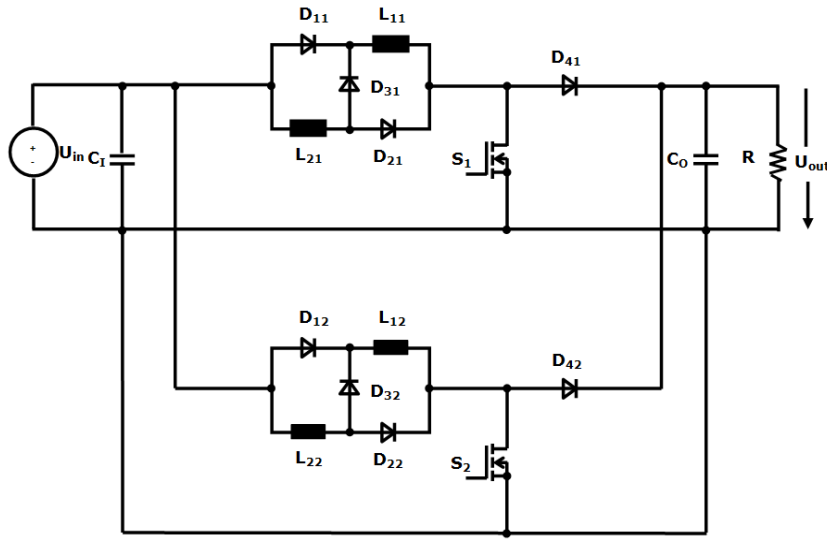
The rules to generate multiphase converters are the same as presented in the previous chapter. The input and output port of the first power converter is parallel connected to the input and output port of the second one, Figure 1.40. The converters used for paralleling are assumed to be identical topologies. Each converter is controlled by interleaved switching signals, which means that each switch switches at a different time moment, with a phase shift between the switch gate drivers ( $360^\circ/n$  against one to another), Figure 1.41, but with the same frequency and the same value of the duty cycle. In these circuits the different phases are connected to a common input source and a common output capacitor/filter of the converter.

The dc voltage transfer function of the multiphase converter is the same to that of the hybrid converter that is using and the equation is provided in Table 2.4.

Based on these rules, and using the hybrid converters mentioned above, eleven new multiphase converters with hybrid structures are possible to be implemented. The result of this analysis is presented in Table 2.3. The structure that cannot be integrated in the multiphase converters are the C-switching structure step-up 1, that is integrated in Boost and Buck-Boost converter forming the hybrid Boost and Buck-Boost converter, the L-switching structure step-down 1 integrated in Buck, Cuk and Zeta, and also the L-switching structure step-down 2 that is integrated in Sepic converter.



Table 2.3. Possible combination for multiphase converters with hybrid structure

Converter name	Converter diagram
<p>1. Multiphase hybrid Buck converter with C-switching structure step-down 1</p>	
<p>2. Multiphase hybrid Boost converter with L-switching structure step-up 1</p>	

<p>3. Multiphase hybrid Buck-Boost converter with C-switching structure step-down 1</p>	
<p>4. Multiphase hybrid Buck-Boost converter with L-switching structure step-up 1</p>	

Table 2.3. (cont.1) Possible combination for multiphase converters with hybrid structure

<p>5. Multiphase hybrid Ćuk converter with C-switching structure step-down 1</p>	
<p>6. Multiphase hybrid Ćuk converter with L-switching structure step-up 1</p>	

Table 2.3. (cont.2) Possible combination for multiphase converters with hybrid structure

<p>7. Multiphase hybrid Ćuk converter with C-switching structure step-up 2</p>	
<p>8. Multiphase hybrid Sepic converter with C-switching structure step-down 1</p>	

Table 2.3. (cont.3) Possible combination for multiphase converters with hybrid structure

<p>9. Multiphase hybrid Sepic converter with L-switching structure step-up 1</p>	
<p>10. Multiphase hybrid Zeta converter with C-switching structure step-up 2</p>	

Table 2.3. (cont.4) Possible combination for multiphase converters with hybrid structure

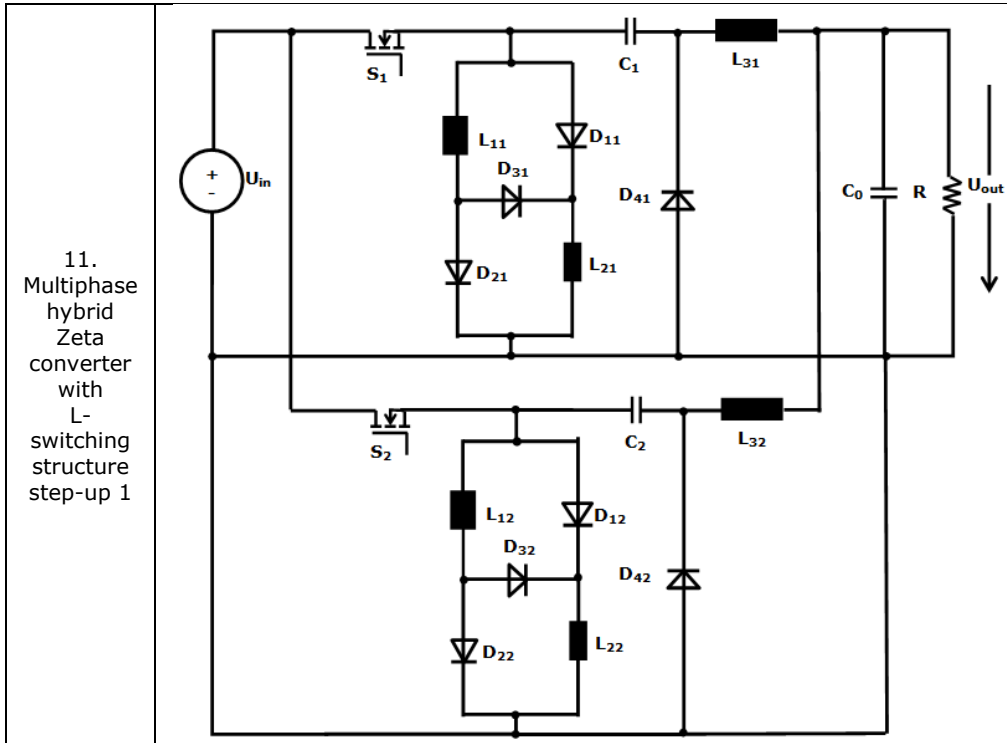


Table 2.3. (cont.5) Possible combination for multiphase converters with hybrid structure

Table 2.4. Output voltage equations for multiphase hybrid converters

Converter name	Output voltage
1. Multiphase hybrid Buck converter with C-switching structure step-down 1	$U_{out} = \frac{d}{2-d} \cdot U_{in}$
2. Multiphase hybrid Boost converter with L-switching structure step-up 1	$U_{out} = \frac{1+d}{1-d} \cdot U_{in}$
3. Multiphase hybrid Buck-Boost converter with C-switching structure step-down 1	$U_{out} = \frac{d}{(1-d) \cdot (2-d)} \cdot U_{in}$
4. Multiphase hybrid Buck-Boost converter with L-switching structure step-up 1	$U_{out} = \frac{2 \cdot d}{1-d} \cdot U_{in}$
5. Multiphase hybrid Ćuk converter with C-switching structure step-down 1	$U_{out} = \frac{d}{2 \cdot (1-d)} \cdot U_{in}$
6. Multiphase hybrid Ćuk converter with L-switching structure step-up 1	$U_{out} = \frac{(1+d) \cdot d}{1-d} \cdot U_{in}$
7. Multiphase hybrid Ćuk converter with C-switching structure step-up 2	$U_{out} = \frac{1+d}{1-d} \cdot U_{in}$
8. Multiphase hybrid Sepic converter with C-switching structure step-down 1	$U_{out} = \frac{d}{(1-d) \cdot (2-d)} \cdot U_{in}$

9. Multiphase hybrid Sepic converter with L-switching structure step-up 1	$U_{out} = \frac{(1+d) \cdot d}{1-d} \cdot U_{in}$
10. Multiphase hybrid Zeta converter with C-switching structure step-up 2	$U_{out} = \frac{2 \cdot d}{1-d} \cdot U_{in}$
11. Multiphase hybrid Zeta converter with L-switching structure step-up 1	$U_{out} = \frac{(1+d) \cdot d}{1-d} \cdot U_{in}$

Table 2.4. (continued 1) Output voltage equations for multiphase hybrid converters

## 2.9. Conclusions and contributions

At the beginning of this chapter the author presented the structure of the C- and L-switching cells proposed by A. Ioinovici et al. These C- and L-switching cells are inserted in the classical structures of Buck, Boost, Buck-Boost, Ćuk, Sepic and Zeta converters, resulting in new hybrid class of converters.

Throughout this chapter it was shown that the circuit diagram of some of these converters are very simple, with a few components, and some of them are very complex. A hybrid structure is characterized by a higher or lower input to output voltage conversion ratio compared to a classical converter in step-up or step-down mode. A comparison between conversion ratios of hybrid converter structures and classical converter structures is made. Even if they have different topologies some of the converters exhibit the same formula for the output voltage. The author highlights which converters have the same output voltage and which one has the highest or lowest conversion ratio.

The author analysis all the 17 converters, but in this thesis just 6 converters, one with each switching cells and with highest or lowest conversion ratio are presented. From author viewpoint, for each selected converter a short description of the circuit, diagram of the circuit, the transfer function and the waveforms from simulation are presented. Also, the advantages and disadvantages of the dc converters are emphasized.

At the end of the chapter, the concept of synthesizing multiphase DC-DC converters was extended, from classical to hybrid structures. The possible combinations to obtain multiphase converters with hybrid structure are presented in Table 2.3, and the output voltage equations are presented in Table 2.4.

The author contributions in this chapter can be summarized as follows:

- comparative analysis of the hybrid with classical converters;
- deduction of the dc voltage transfer function for hybrid converters;
- the analytical study, validated by simulation of the hybrid converters, made in Caspoc Simulation Program;
- a synthesizing method for multiphase hybrid converters is proposed;
- 11 new multiphase converters with hybrid structures that are possible to be implemented, are proposed by the author;
- deduction of the dc voltage transfer function for multiphase hybrid converters, confirmed by simulation.

## CHAPTER 3. Hybrid Boost converter with L-switching structure step-up 1

The hybrid Boost L-converter is one of the converters that have the possibility to be implemented in multiphase configuration.

This converter provides higher gain and higher efficiency than the traditional Boost, and is used for many applications such as power factor correction (PFC), generation of backlight voltages for LCD displays, solar cell energy conversion systems [121], fuel cell energy conversion systems, battery back-up systems for uninterruptible power supplies, and high intensity discharge lamp ballast for automobile head lamps [89].

This chapter describes the step by step process wherein a hybrid Boost L-converter, which originally uses non-coupled inductors, is modified to use coupled inductors resulting in both efficiency increase and lower price. To validate the operation of the converter [4], an analytical description is provided together with design equations, digital simulations and experimental results.

In Figure 2.24 the circuit diagram is presented with the corresponding on and off states [103], [121].

The converter diagram with currents of this hybrid converter is presented in Figure 3.1.

In the on state the inductors are connected in parallel and the current of both inductors flows through the input phase and through the switch element. In the off state the inductors are connected in series and the inductor current flows through the output diode.

The voltage across the inductors is given by:

$$t_{\text{on}}: u_L = U_{in} \quad (3.1)$$

$$t_{\text{off}}: u_L = -\frac{U_{out} - U_{in}}{2} \quad (3.2)$$

It can be seen from the above formulae, that the voltage across the inductors is positive in the on state, and negative in the off state. In circuit operation the positive and negative voltage-time-area across the inductors must always be the same.

With this condition the conversion ratio of the hybrid boost DC-DC L-converter can be calculated as:

$$U_{out} = \frac{1+d}{1-d} \cdot U_{in} \quad (3.3)$$

It can be observed that the hybrid Boost DC-DC L-converter exhibits the same conversion ratio like hybrid Boost DC-DC C-converter.

Compared to classical Boost converter, a higher conversion ratio can be achieved as it can be seen from equation 3.3 and from Figure 2.17.

The dc gain of the hybrid Boost DC-DC L-converter is higher than that of the traditional Boost converter by a factor of (1+d).



To ensure a better understanding, this chapter continues by presenting and discussing the power part of the hybrid converter.

The power part consists of an input network with two inductors and three diodes, a step up circuit with the power switch  $S$  and diode  $D_o$ , and dc-link capacitors at the input and output sides of the converter. Based on the circuit structure, we can observe that the energy can be transferred only in one direction from input to output (left to right) [103].

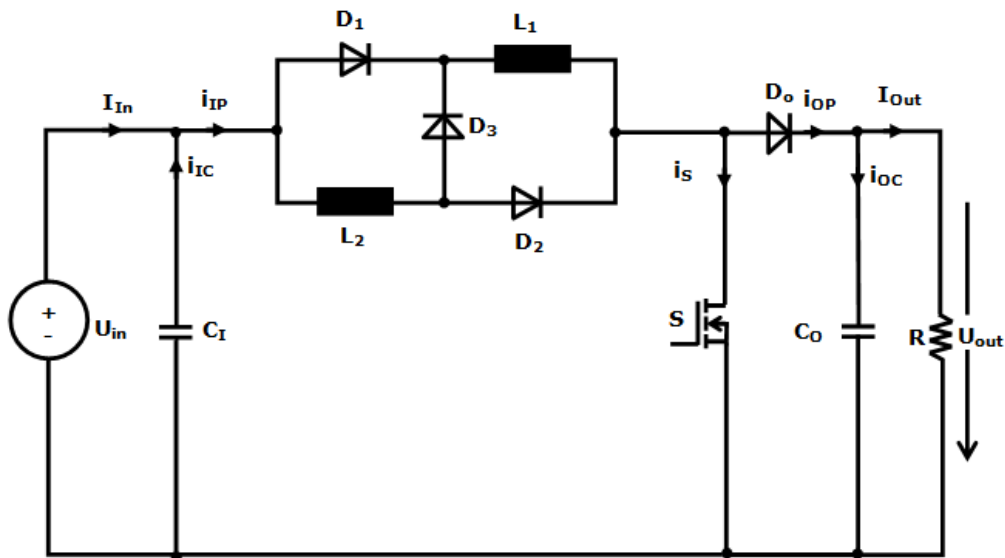


Figure 3.1. Circuit diagram of hybrid Boost DC-DC L-converter [103]

For calculations it is assumed that all elements of the converter are lossless, the voltage and currents at the input and output are ideally dc-values, and the converter is pulse width modulation controlled [103], [123].

### 3.1. Hybrid Boost DC-DC L-converter – input circuit

As presented above, in the on state the inductors are connected in parallel and the current of both inductors flows in the input phase and through the switching element. In the off state the inductors are connected in series and the current flows through the inductors and the output diode. In this topological state, the input phase current  $i_{IP}$  is the same to the inductor current. It is assumed that only the average value of the input phase current will determine converter input current,  $I_{In}$ , while the AC-current component will flow through capacitor  $C_I$  [103], [123].

The current waveforms at the input of the hybrid Boost converter are presented in Figure 3.2, for  $d < 0.5$ ,  $d = 0.5$ , and  $d > 0.5$ .

The first waveform shows that the currents through inductors  $L_1$  ( $i_{L1}$ ) and  $L_2$  ( $i_{L2}$ ) are the same. The inductor current rises in the on state and falls in the off state, therefore a triangular current is generated.

In the middle is presented the input phase current  $i_{IP}$ , which in switched-on state is double than the inductor current.

The lower waveform presents the input capacitor current,  $i_{IC}$ .

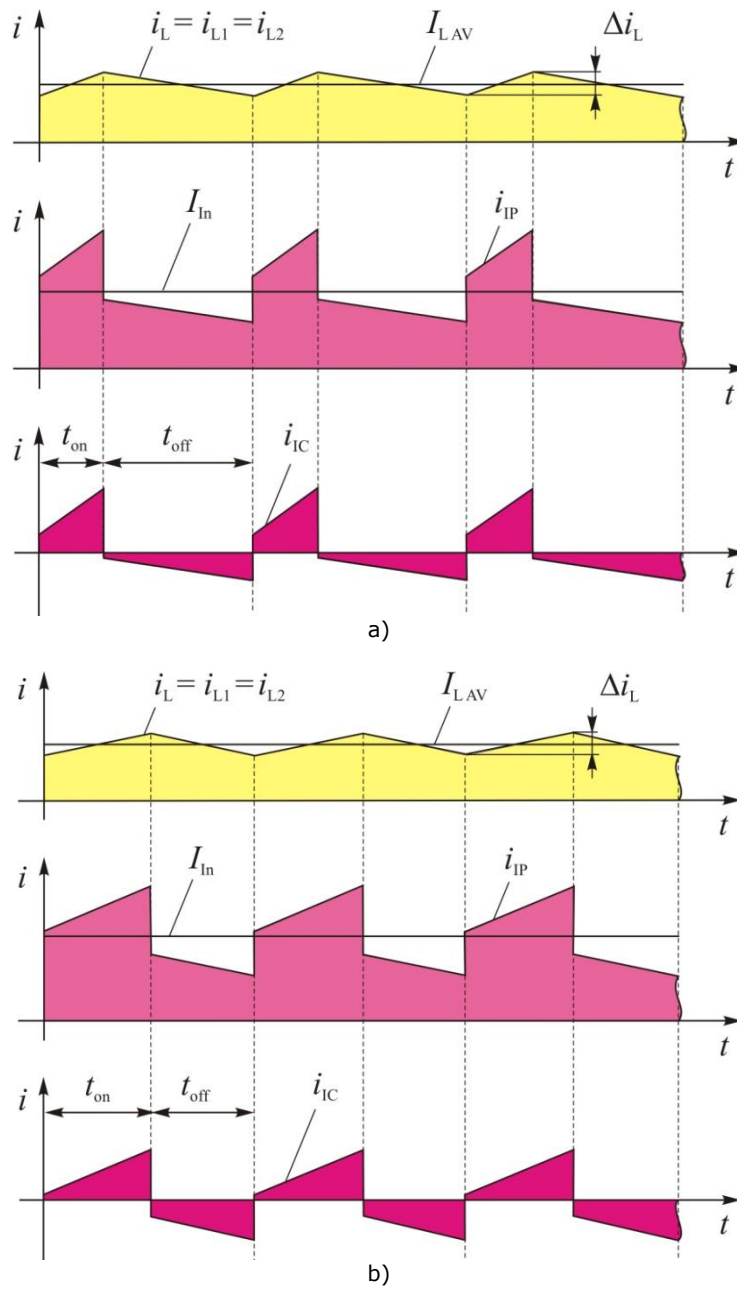


Figure 3.2. Current waveforms at the input of a single phase hybrid Boost DC-DC converter  
 a)  $d=0.3$  b)  $d=0.5$  c)  $d=0.7$  [103]

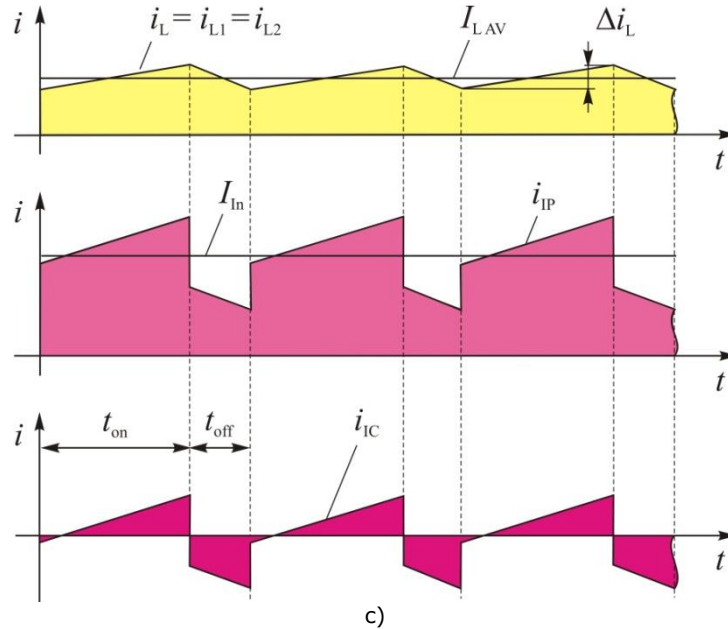


Figure 3.2. (continued 1) Current waveforms at the input of a single phase hybrid Boost DC-DC converter a)  $d=0.3$  b)  $d=0.5$  c)  $d=0.7$  [103]

In order to calculate the required inductance and capacitance in the circuit, it is necessary to state the conditions for circuit operation. First, we need to know the rated output voltage and also the minimum input voltage at rated power that should be transferred. With these conditions, the conversion ratio of the circuit for rated input power  $P_{InR}$  transfer is fixed.

In this operation point the dc-input current and the average current  $I_{L,AV}$  in the inductors can be calculated. It is assumed that this average current  $I_{L,AV}$  is the maximum dc-value in the inductors. This means that the possible power of the converter is lower in case of higher and higher in case of lower duty cycles.

The average current value  $I_{L,AV}$  depends on the duty cycle  $d$  according to the relationship [103].

$$I_{L,AV} = \frac{I_{In}}{1+d} \quad (3.4)$$

In Figure 3.3 is shown the possible power transfer that depends on the duty cycle for three different converter designs.

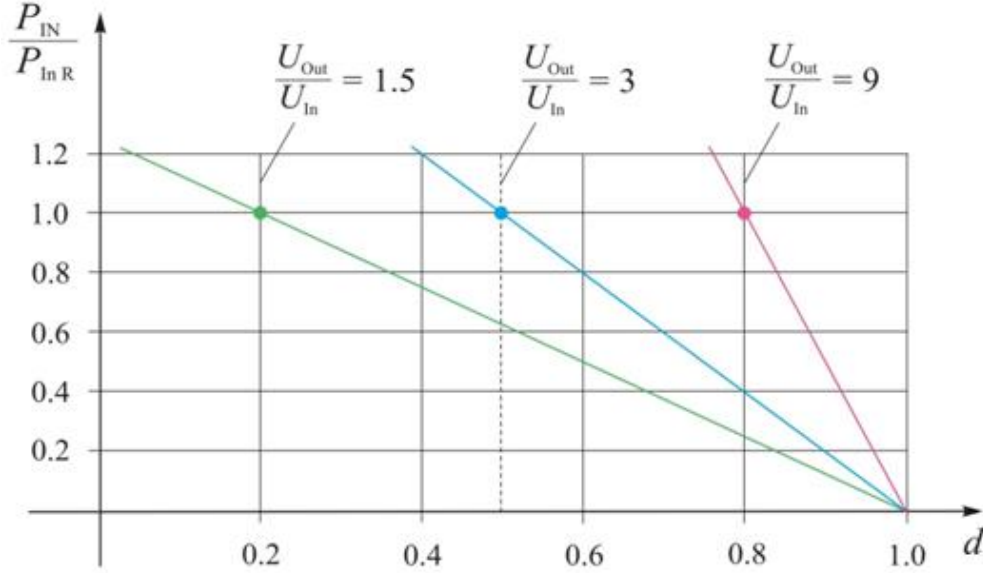


Figure 3.3. Maximum power transfer in case of fixed output voltage [103]

The inductivity must be calculated for the maximum inductor voltage-time-area within the pulse periods and the maximum acceptable current variation during this time. In the switched-on state  $t_{on}$ , the input voltage  $U_{in}$ , is connected across the inductors and therefore [103]:

$$L_1 = L_2 = \frac{U_{in} \cdot t_{on}}{\Delta i_L} \quad (3.5)$$

The input voltage  $U_{in}$ , is expressed in the formula below as a function of the output voltage and the duty cycle and thus (3.5) becomes [103]:

$$L_1 = L_2 = \frac{U_{out} \cdot T_s}{\Delta i_L} \cdot \frac{d \cdot (1-d)}{1+d} \quad (3.6)$$

Considering the full duty cycle range, after calculation, the voltage-time-area within the pulse periods reaches its maximum for a duty cycle of approximately 41%. For this duty cycle the converter inductance is specified as:

$$L_1 = L_2 = \frac{U_{out} \cdot T_s}{\Delta i_{L_{max}}} \cdot (3 - 2\sqrt{2}) \quad (3.7)$$

The maximum acceptable current variation  $\Delta i_{L_{max}}$  is chosen normally between 10%-30% of the rated average inductance current  $I_{LAVR}$  similar to CCM design:

$$\Delta i_{L_{max}} = (0.1 \div 0.3) \cdot I_{LAVR} \quad (3.8)$$

The RMS current in the inductors  $L_1$  and  $L_2$ , is given by the equation:

$$I_L = \sqrt{I_{LAV}^2 + \frac{\Delta i_L^2}{12}} \quad (3.9)$$

These inductors can be built as individual or mutually coupled inductors. Using coupled inductors can help in ripple current reduction and in getting lower dimension/size of the inductors.

It is continued with the calculation of the input side capacitor value. The worst case scenario could happen when the converter input current is ideally dc, and the overall AC-current of the input phase flows in the capacitor. This AC-current in the capacitor produces an AC-voltage at the input that is over imposed in the dc-input voltage. For this reason the maximum acceptable voltage variation across the capacitor must be chosen during the capacitor dimension [103].

$$C_I = \frac{i_C \cdot t_{on}}{\Delta u_C} \quad (3.10)$$

or

$$C_I = \frac{I_{LAV} \cdot T_S \cdot d \cdot (1-d)}{\Delta u_{Inmax}} \quad (3.11)$$

The current-time-area depends on the duty cycle having its maximum at 50% and at the rated inductance current  $I_{LAVR}$ .

In practice, the acceptable static voltage variation at the converter input is chosen lower than 1% of the rated input voltage  $U_{inR}$  [103]. Hence

$$C_I = \frac{I_{LAVR} \cdot T_S}{4 \cdot \Delta u_{Inmax}} \quad \text{with } \Delta u_{Inmax} \leq 0.01 \cdot U_{inR} \quad (3.12)$$

At the input of the DC-DC converters electrolytic capacitors are often used. The main design criteria for these capacitors are their RMS-current values [103]. The RMS-current in the input capacitor is calculated as a function of the duty cycle given the average inductance current  $I_{LAV}$  and the maximum current ripple  $\Delta i_{Lmax}$ .

$$I_{IC} = I_{LAV} \cdot \sqrt{d \cdot (1-d) + \left( \frac{\Delta i_{Lmax}}{I_{LAV}} \right)^2 \cdot \frac{d^2 \cdot (1-d)^2 \cdot (1+3 \cdot d)}{12 \cdot (1+d)^2 \cdot (3-2 \cdot \sqrt{2})}} \quad (3.13)$$

The result can be split into two. One is dependent on the average current  $I_{LAV}$ , and the other is dependent on the triangular current variation in the inductors.

In the next figure the RMS current in the capacitor is shown. The maximum value of the capacitor current is higher than the half of the dc inductor current  $I_{LAV}$ . However the current variation has only a small influence on the total RMS current in the capacitor.

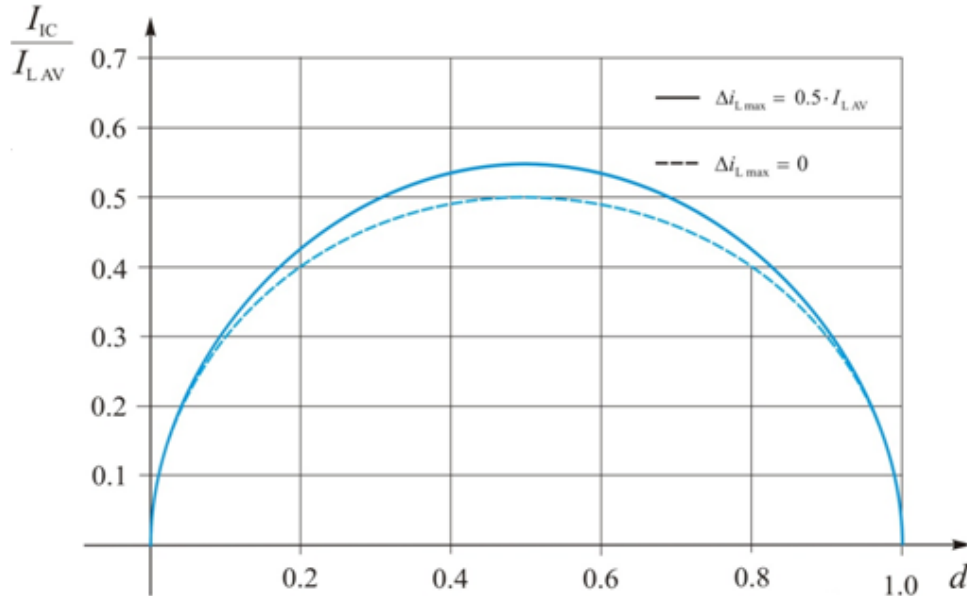


Figure 3.4. RMS current in the input capacitor of a single phase hybrid Boost DC-DC converter [103]

It is continued with the calculation of the other currents in the circuit. The current through diodes  $D_1$  and  $D_2$  is the same. The average current value of diodes  $D_1$  and  $D_2$ ,  $I_{DAV}$ , depends on the duty cycle  $d$ , and the average current  $I_{LAV}$ .

$$I_{DAV} = I_{LAV} \cdot d \quad (3.14)$$

The RMS-current in the diodes  $D_1$  and  $D_2$  is described by the formula below:

$$I_D = \sqrt{\left( I_{LAV}^2 + \frac{\Delta i_L^2}{12} \right)} \cdot d \quad (3.15)$$

The current through the diodes  $D_3$  and the output diode  $D_0$  is the same. The average current value of diode  $D_3$  and  $D_0$ ,  $I_{DOAV}$  depends on the duty cycle  $d$ , and the average current  $I_{LAV}$ .

$$I_{DOAV} = I_{LAV} \cdot (1 - d) \quad (3.16)$$

The RMS-current in the diodes  $D_3$  and  $D_0$  is described by the formula below:

$$I_{DO} = \sqrt{\left( I_{LAV}^2 + \frac{\Delta i_L^2}{12} \right)} \cdot (1 - d) \quad (3.17)$$

The average current value of the switch  $S$ ,  $I_{SAV}$ , also depends on the duty cycle  $d$ , and the average current  $I_{LAV}$ .

$$I_{SAV} = 2 \cdot I_{LAV} \cdot d \quad (3.18)$$

The RMS-current in the switch S is described by the formula below:

$$I_S = 2 \cdot \sqrt{\left( I_{LAV}^2 + \frac{\Delta i_L^2}{12} \right)} \cdot d \quad (3.19)$$

### 3.2. Hybrid Boost DC-DC L-converter – output circuit

As has been presented, in the on state, the current in the output phase  $i_{OP}$  is zero, because the inductors are connected in parallel, and the current of both inductors flows in the input phase and through the switching element. In the switched-off state the inductors are connected in series and the current flows through the inductors and the output diode. In this topological state the output phase current  $i_{OP}$  is the same as the inductor current.

It is assumed that only the average value of the input phase current would flow in the converter input current,  $I_{In}$ , while the AC-current component would flow through the capacitor  $C_I$  and the average value of the output phase current will flow in the converter output  $I_{Out}$  [103], [123].

In Figure 3.5, the current waveforms at the output of the hybrid Boost converter are presented, for  $d < 0.5$ ,  $d = 0.5$ , and  $d > 0.5$ .

A triangular current shape is generated by the currents through the inductors  $L_1$  ( $i_{L1}$ ) and  $L_2$  ( $i_{L2}$ ), that are the same and are presented in the first waveform. In the middle is presented the output phase current  $i_{OP}$ .

The lowest waveform presents the AC-current in the output capacitor. This current can be calculated by subtraction of output phase current  $i_{OP}$  and output current  $I_{Out}$ .

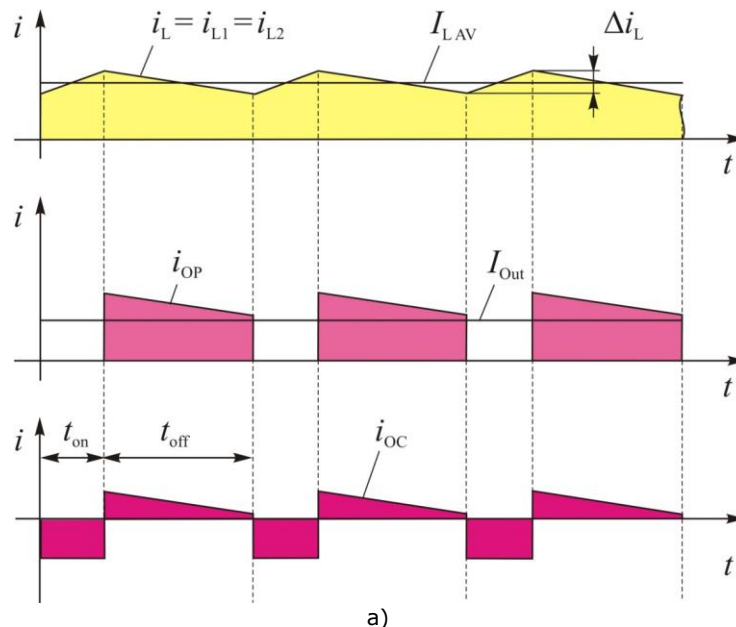


Figure 3.5. Current waveforms at the output of a single phase hybrid Boost DC-DC converter  
 a)  $d = 0.3$  b)  $d = 0.5$  c)  $d = 0.7$  [103]

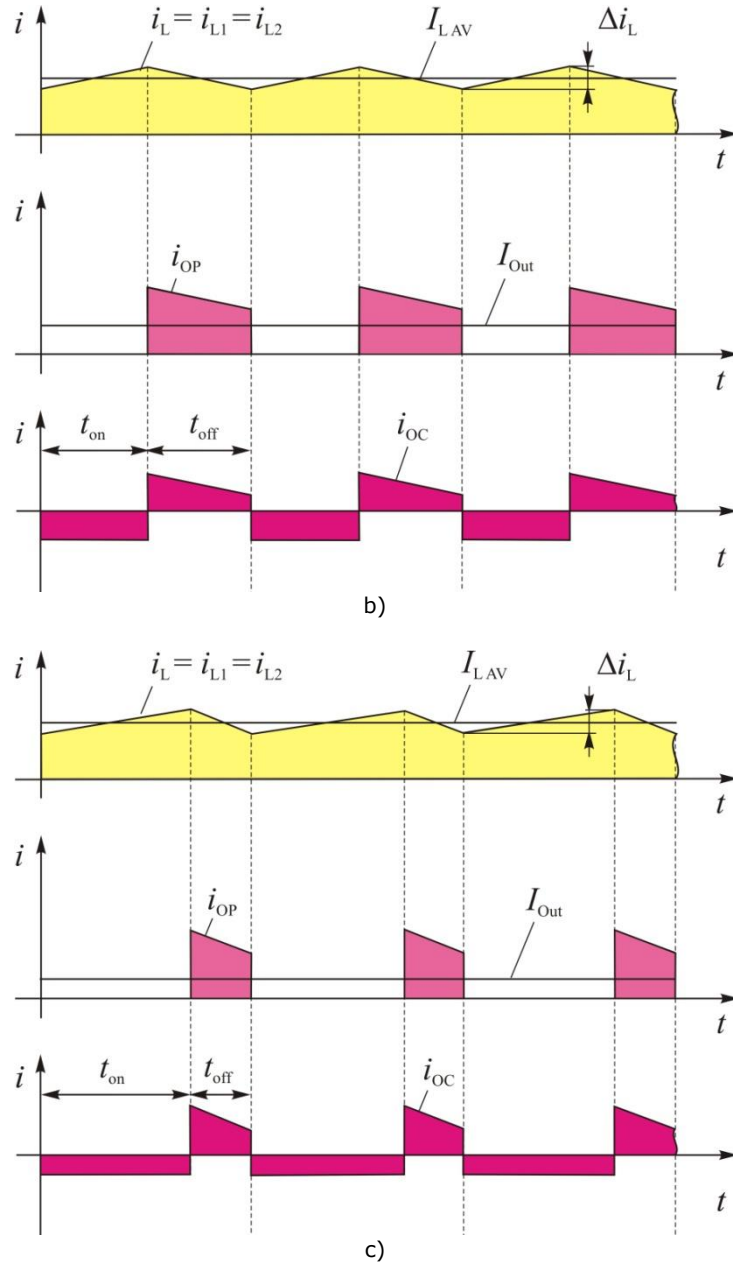


Figure 3.5. (continued 1) Current waveforms at the output of a single phase hybrid Boost DC-DC converter a)  $d=0.3$  b)  $d=0.5$  c)  $d=0.7$  [103]

It is continued with the calculation of the of the output capacitor value. The worst case scenario could happen when the converter output current is an ideally DC value, and the entire AC component of the output phase current flows through the capacitor. This AC-current in the capacitor produces an AC-voltage at the output that is over imposed in the dc component. For this reason the maximum acceptable



voltage variation across the capacitor must be chosen in order to calculate the output capacitor value.

The current-time-area in the capacitor within the pulse periods can be describe as a function of the output current and the duty cycle resulting in [103]:

$$C_O = \frac{I_{Out} \cdot T_s}{\Delta U_{Out_{max}}} \cdot d \quad (3.20)$$

or, equivalently

$$C_O = \frac{I_{LAV} \cdot T_s}{\Delta U_{Out_{max}}} \cdot d \cdot (1-d) \quad (3.21)$$

The current-time-area depends on the duty cycle exhibiting its maximum at 50% duty cycle and at the rated inductor current  $I_{LAVR}$ .

In practice, the acceptable steady state voltage variation at the converter output is chosen lower than 1% of the rated output voltage  $U_{outR}$  [103]. Thus the output capacitor value is:

$$C_O = \frac{I_{LAVR} \cdot T_s}{4 \cdot \Delta U_{Out_{max}}} \text{ with } \Delta U_{Out_{max}} \leq 0.01 \cdot U_{outR} \quad (3.22)$$

Also, on the output side of the hybrid Boost converters electrolytic capacitors are often used.

For the capacitors design [103], the RMS-current in the output must be calculated. In the next formula the RMS-current is derived as a function of the duty cycle for dc inductor current  $I_{LAV}$  and a maximum inductor current ripple  $\Delta i_{L_{max}}$ .

$$I_{OC} = I_{LAV} \cdot \sqrt{d \cdot (1-d) + \left( \frac{\Delta i_{L_{max}}}{I_{LAV}} \right)^2 \cdot \frac{d^2 \cdot (1-d)^3}{12 \cdot (1+d)^2 \cdot (3-2\sqrt{2})}} \quad (3.23)$$

The result can also be split in two parts. One is dependent on the average inductor current  $I_{LAV}$ , and the other is dependent on the triangular current variation in the inductances.

In Figure 3.6 the RMS capacitor current,  $C_O$ , is shown.

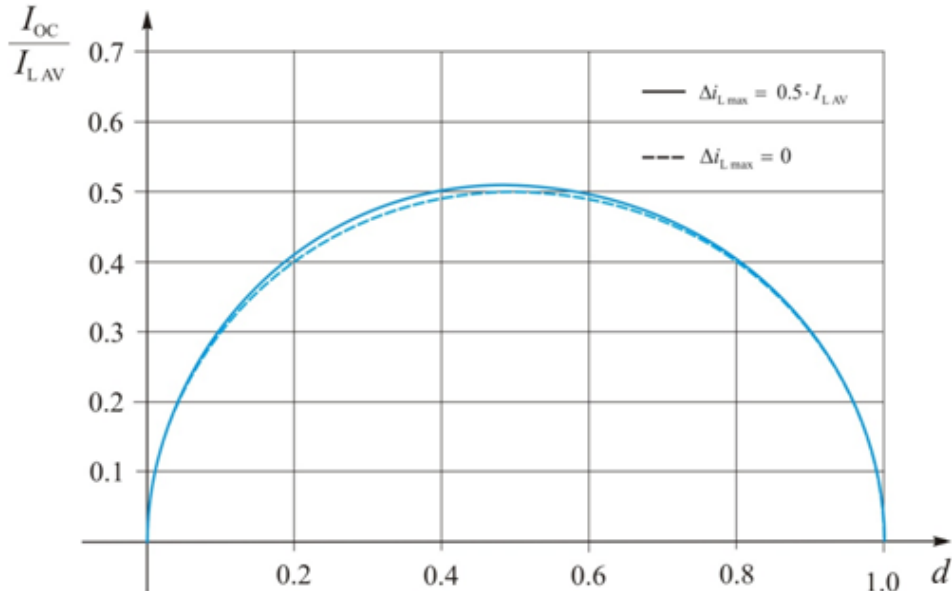


Figure 3.6. RMS Current in the output capacitor of a single phase hybrid Boost DC-DC converter [103]

The maximum value is a little bit higher than half of the dc inductor current  $I_{LAV}$ . The current variation  $\Delta i_{Lmax}$  also has only a small influence on the total RMS current in the output capacitor.

### 3.3. Simulation of the Hybrid Boost DC-DC L-converter

The simulation models of the hybrid Boost L-converter shown in Figure 2.25 were created in Caspoc simulation program in order to verify its theoretical properties. The input power supply is modelled by a constant voltage source  $U_{in}$ . The gate signal for the MOSFET is generated by using a squarewave signal generator. In Figure 2.25 the inductors of the converter are not coupled.

Figure 3.7 shows the simulation diagram of the hybrid Boost DC-DC L-converter with coupled inductors. Based on the ripple current, it is made a comparison between the Boost L-converter in the case of individual or mutually coupled inductors.

If the inductors are magnetically coupled, saw they can improve the electrical performance and reducing the cost, through the reducing the weight and size of the converter.

On the "coupling mode" of the inductors, inductors  $L_1$  and  $L_2$  are coupled together and share the same winding orientation. Consequently, the equivalent inductor value  $L_{EQ}$  is given by:

$$L_{EQ} = L_1 + L_2 + 2 \cdot M \quad (3.24)$$

where  $M$  is the mutual inductance.

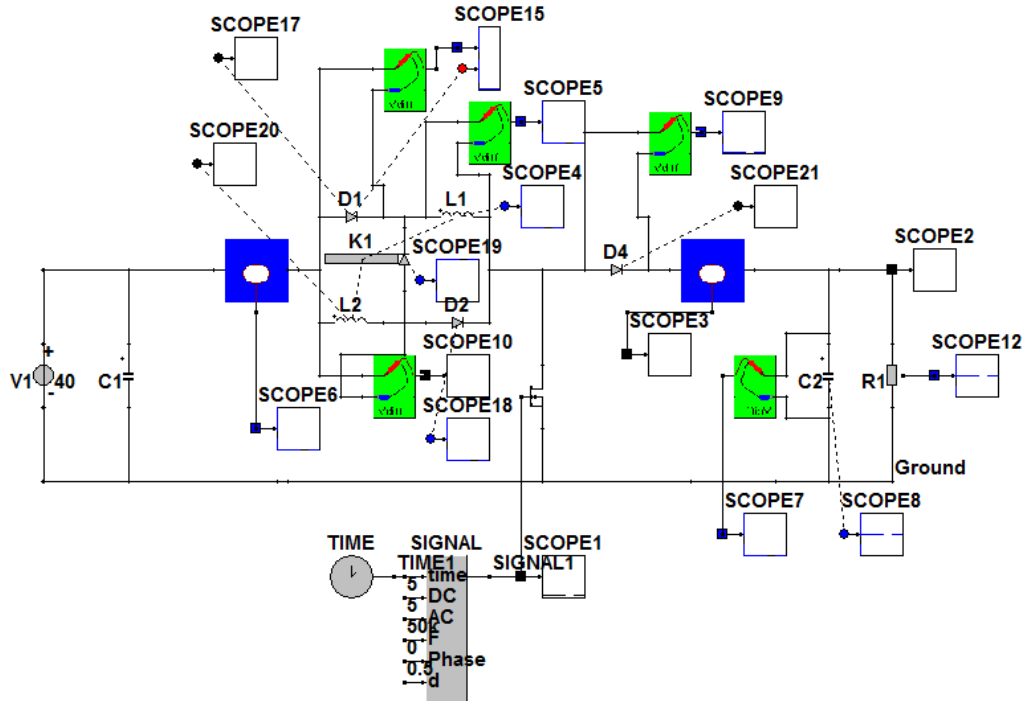


Figure 3.7. CASPOC simulation diagram for the hybrid Boost DC-DC L-converter coupled inductor

The hybrid Boost DC-DC L-converter with coupled inductors is simulated in CASPOC Simulation Program. All the components including MOSFET, diodes, coupled inductors are assumed to be ideal.

Two different levels for the input voltage were chosen to compare the properties of simulation models of the hybrid converter. The simulated values of input voltage were  $U_{in}=40V$  and  $U_{in}=60V$ , and the duty cycles were  $d=50\%$  and  $d=33.3\%$  respectively with  $f_s=50\text{ KHz}$ .

After calculation, the following parameters resulted for the Boost L-converter:  $L_1=L_2=411.775\mu\text{H}$ ,  $C_1=62.5\mu\text{F}$ ,  $C_0=20.833\mu\text{F}$ .

Figure 3.8 presents the simulated waveforms in the case of coupled inductors with the input voltage  $U_{in}=40V$ . They are presented as follows: the input phase current  $i_{IP}$ , the current through the switch  $S$ , the current through the inductor  $L_2$  (which is the same with the  $L_1$ ), the current through the diode  $D_1$ , the output phase current  $i_{OP}$ , the current through the output capacitor  $C_0$  (in simulation noted  $C_2$ ), and the output current and voltage of the circuit.

116 Hybrid Boost converter with L-switching structure step-up 1

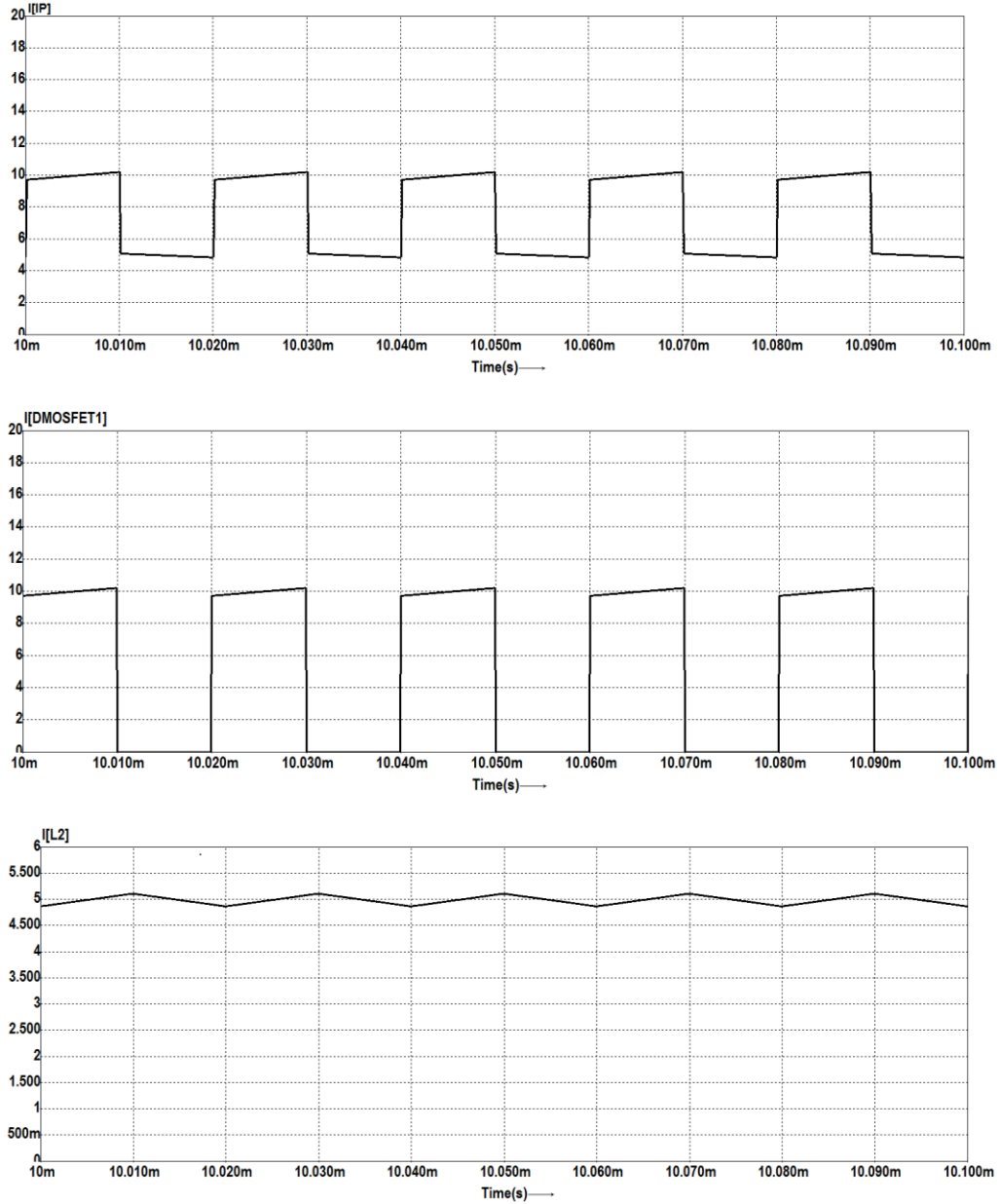


Figure 3.8. Simulation results for the hybrid Boost DC-DC L-converter with coupled inductors,  $U_{in}=40V$  and  $d=50\%$

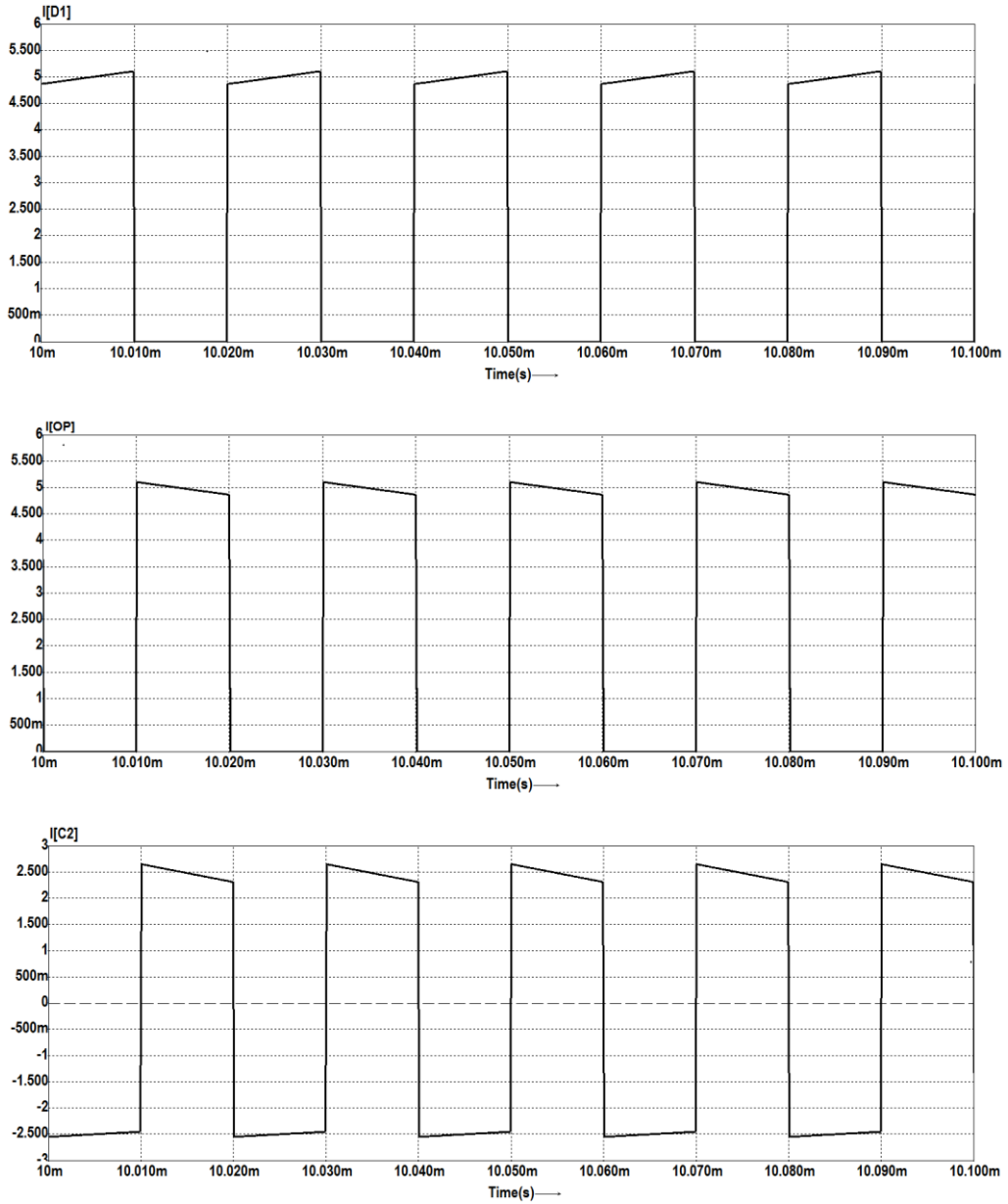


Figure 3.8. (continued 1) Simulation results for the hybrid Boost DC-DC L-converter with coupled inductors,  $U_{in}=40V$  and  $d=50\%$

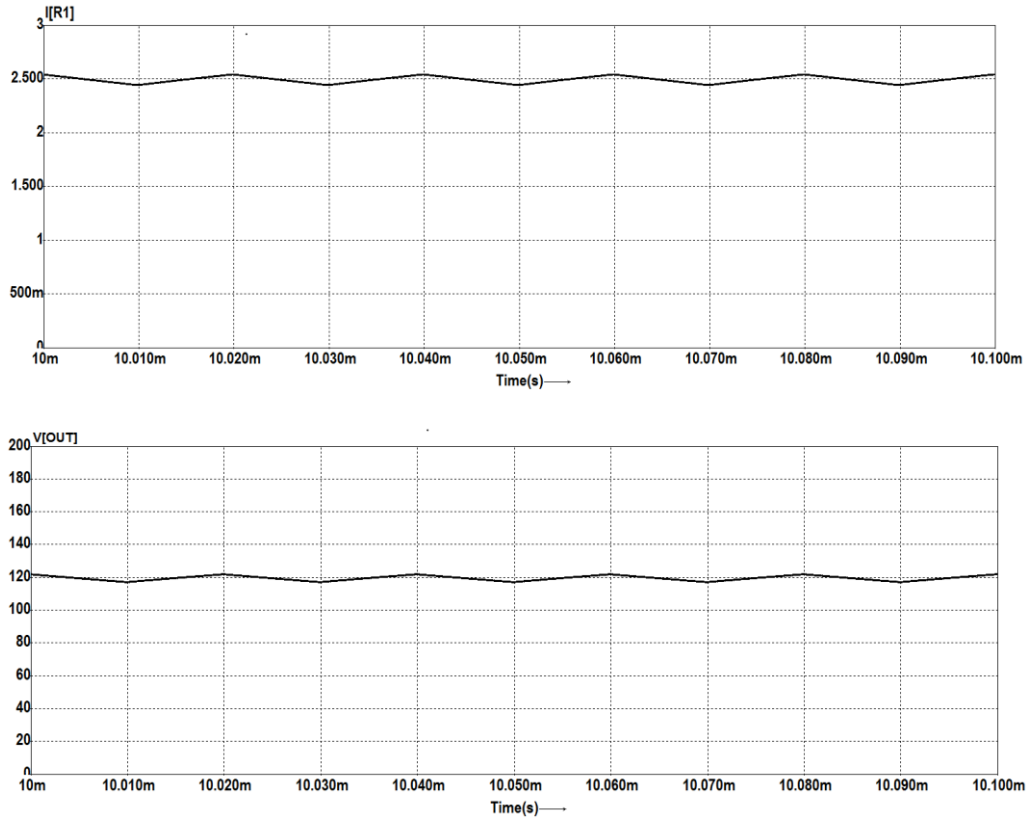


Figure 3.8. (continued 2) Simulation results for the hybrid Boost DC-DC L-converter with coupled inductors,  $U_{in}=40V$  and  $d=50\%$   
This up to down order: signal,  $i_{IP}$ ,  $i_S$ ,  $i_{L2}$ ,  $i_{D1}$ ,  $i_{OP}$ ,  $i_{OC}$ ,  $i_{out}$  and  $U_{out}$

The inductor current in the case of coupled inductors swings between 4.875 and 5.118A that is 0.243Ap-p. The dc value is 4.9965 A, with a ripple of 4.75%. In the case of individual inductors, the swing is between 4.753A to 5.239A that is 0.486Ap-p (at the same frequency of 50 kHz). This dc value is 4.996A with a ripple of 9.28%. Through this is demonstrated that the coupled inductors reduces the current ripple compared to that of uncoupled inductors. Also, from Figure 3.8 and Figure 2.26 we can see that the converter using coupled inductors will have the same current ripple as the original non-coupled inductors, at a reduced switching frequency (only 50kHz for coupled inductors, instead of 100kHz for uncoupled) which leads to a boost in efficiency.

As it was anticipated, using coupled inductors helps with the reduction of the ripple current leading to smaller size of the inductors.

This chapter continues with the simulation of hybrid Boost converter with coupled inductors, for  $U_{in}=60V$ , duty cycle  $d=33.3\%$ , and switching frequency  $f_s=50$  kHz, which will be compared with the results of uncoupled inductors.

Figure 3.9 presents the simulated waveforms in the case of coupled inductors for the input phase current  $i_{IP}$ , the current through switch S, the current through inductor  $L_2$  (which is the same with current through  $L_1$ ), the current through diode  $D_1$ , the output phase current  $i_{OP}$ , the current through the output

capacitor  $C_O$  (in simulation denoted as  $C_2$ ), the output current and the output voltage of the circuit.

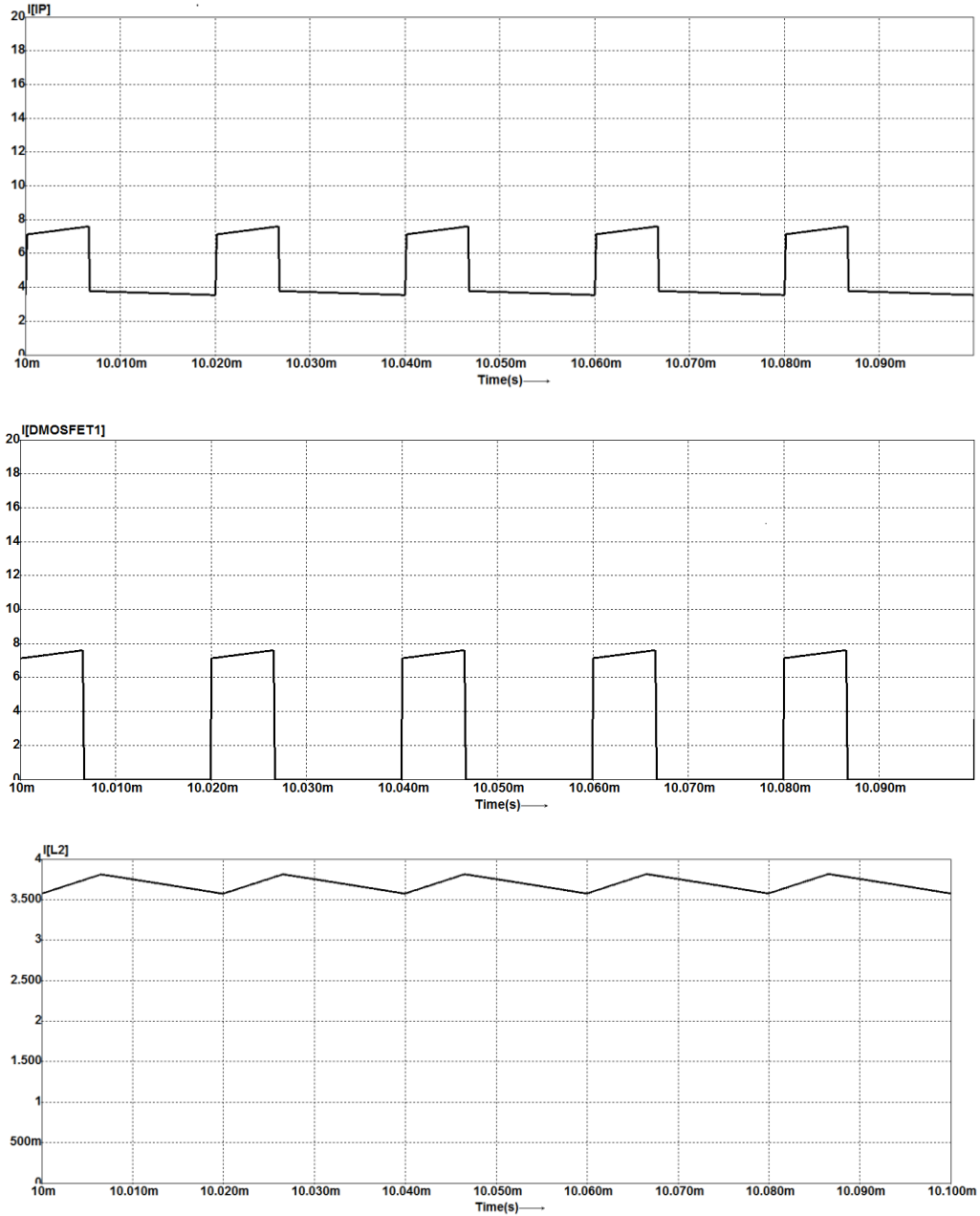


Figure 3.9. Simulation results for the hybrid Boost DC-DC L-converter with coupled inductors,  $U_{in}=60V$  and  $d=33.3\%$

120 Hybrid Boost converter with L-switching structure step-up 1

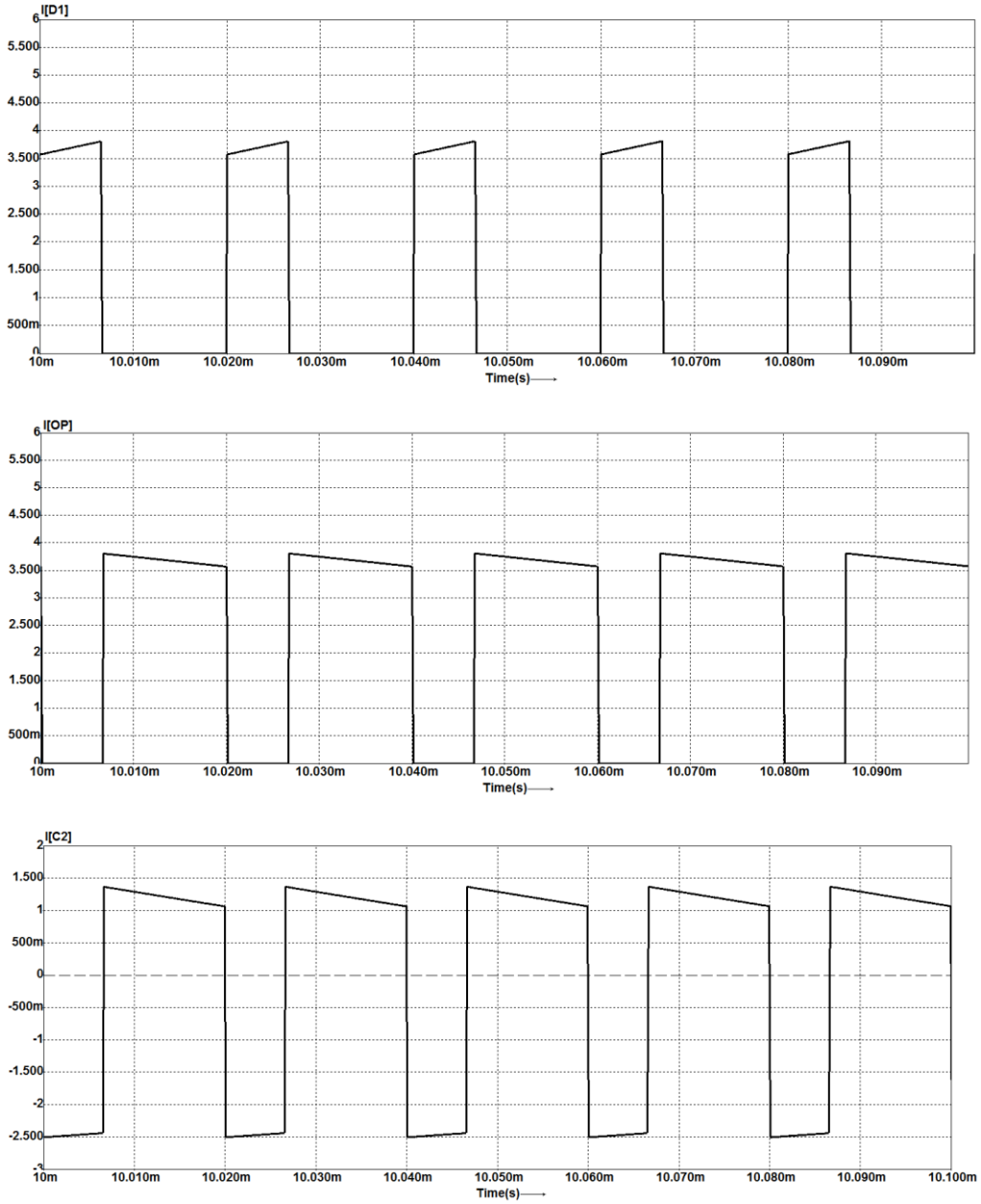


Figure 3.9. (continued 1) Simulation results for the hybrid Boost DC-DC L-converter with coupled inductors,  $U_{in}=60V$  and  $d=33.3\%$



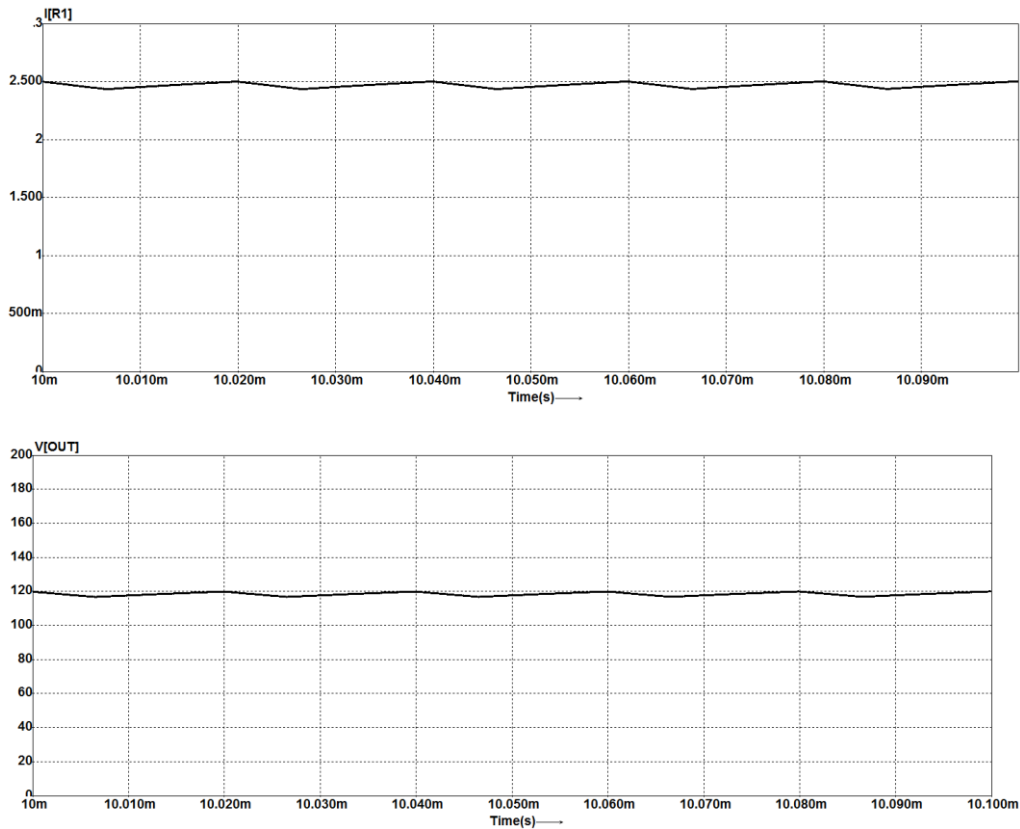


Figure 3.9. (continued 2) Simulation results for the hybrid Boost DC-DC L-converter with coupled inductors,  $U_{in}=60V$  and  $d=33.3\%$   
 This up to down order:  $i_{LP}$ ,  $i_S$ ,  $i_{L2}$ ,  $i_{D1}$ ,  $i_{OP}$ ,  $i_{OC}$ ,  $i_{out}$  and  $U_{out}$

The inductor current in the case of coupled inductors swings between 3.580A and 3.824A that is 0.244Ap-p. The dc is 3.702 A, with a ripple of 6.380%. In the case of individual inductors, the swing is between 3.466A to 3.956A that is 0.49Ap-p (at the same frequency of 50 kHz). This dc is 3.711A with a ripple of 12.39%. These results again confirm that using coupled inductors helps in the reduction of the ripple current with positive effect in inductors size and weight.

In order to verify the simulation results presented above a prototype of hybrid Boost DC-DC L-converter was built.

### 3.4. Experimental results for the hybrid Boost DC-DC L-converter

The laboratory prototype of the hybrid Boost L-converter was built and tested in order to verify the theoretical assumptions and simulation results. This prototype, from Figure 3.10, operates at 50 kHz. The schematic and layout design were done using EAGLE PCB design software. The semiconductor devices chosen for constructing the hybrid Boost converter are the HiPerFET power MOSFETs,

## 122 Hybrid Boost converter with L-switching structure step-up 1

---

IXFH50N20, and HiPerFRED diode DPG10J200PM. Arduino Uno is employed to generate the control pulses required for MOSFET. The rated power of the circuit is 300W and the output voltage is 120V, and 150V. The currents are measured with current probes.

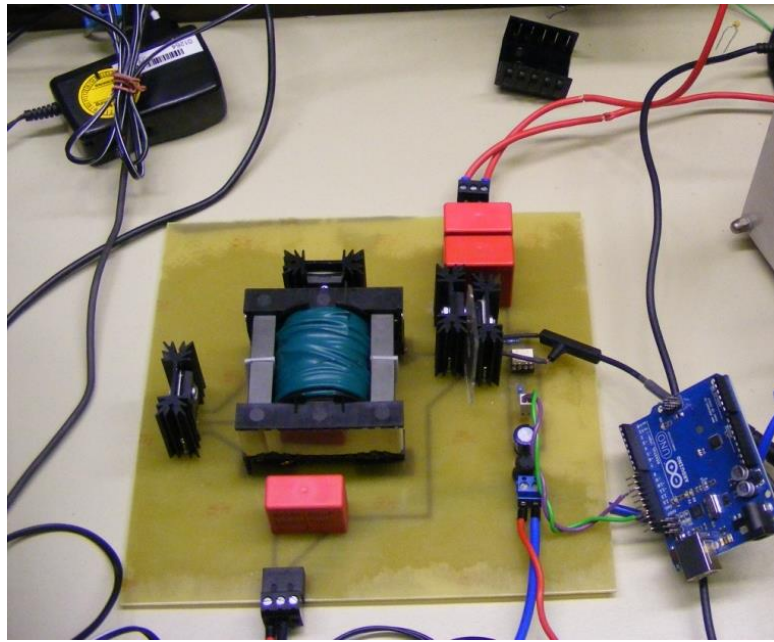


Figure 3.10. Image of the experimental hybrid Boost DC-DC L-converter

In Figure 3.11, the input voltage waveform of the converter with duty cycle  $d=1/3$  is shown.

The duty cycle of the converter is obvious from the Figure 3.12, where the current of the switch is represented. In Figure 3.13 the input phase current is depicted. The current in the two inductors is represented in Figure 3.14. The output phase current is presented in Figure 3.15. In Figure 3.16 and Figure 3.17, the output current and output voltage respectively are shown.

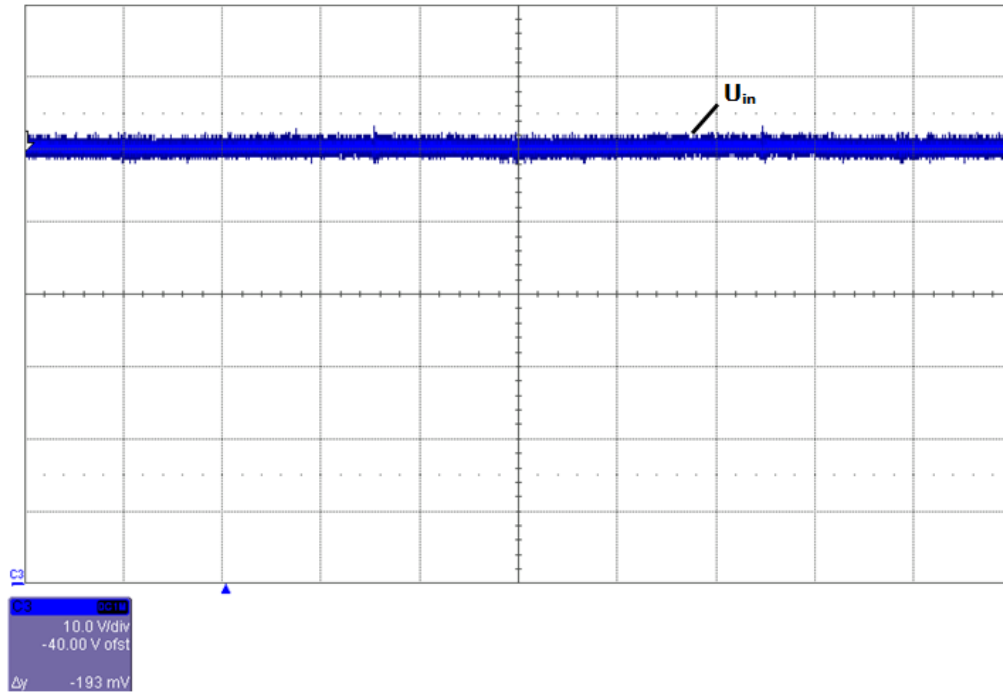


Figure 3.11. Input voltage waveform when  $d=1/3$

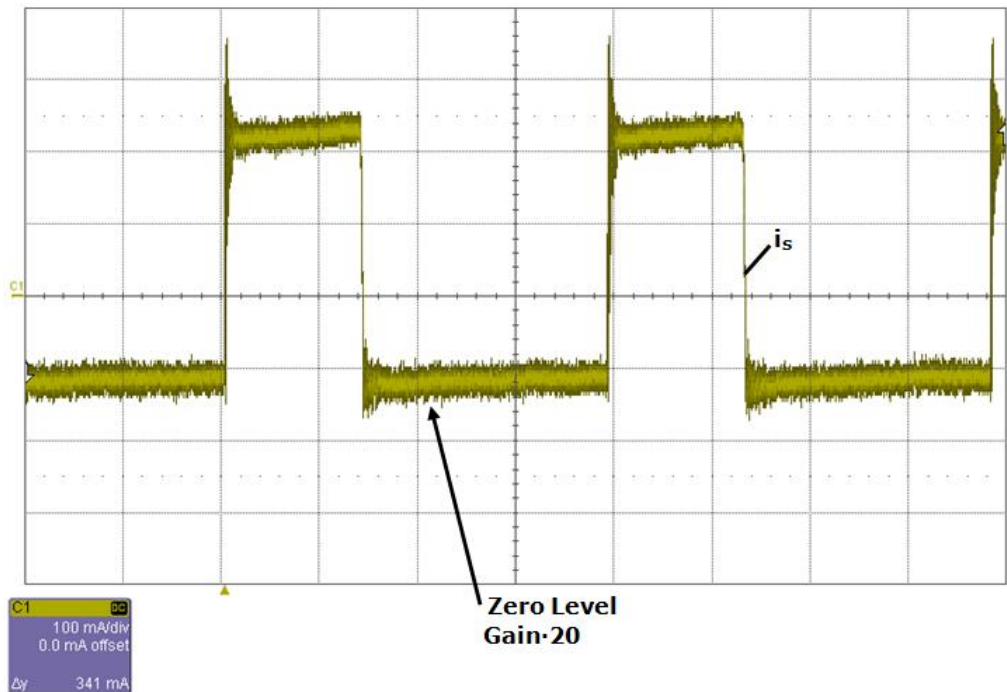


Figure 3.12. MOSFET current waveform when  $d=1/3$

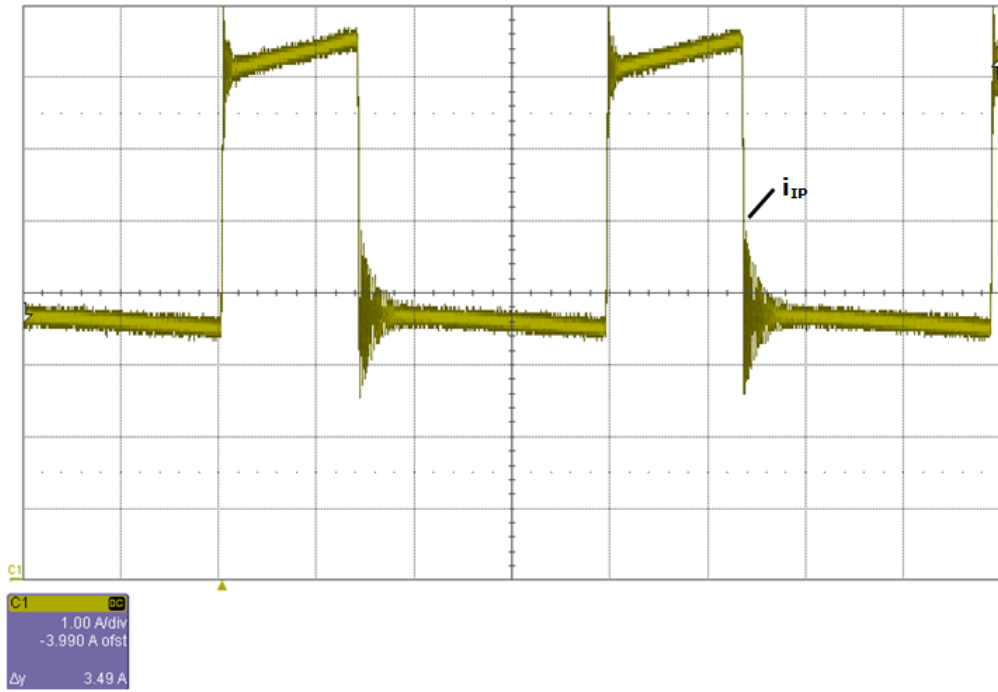


Figure 3.13. Input phase current waveform when  $d=1/3$

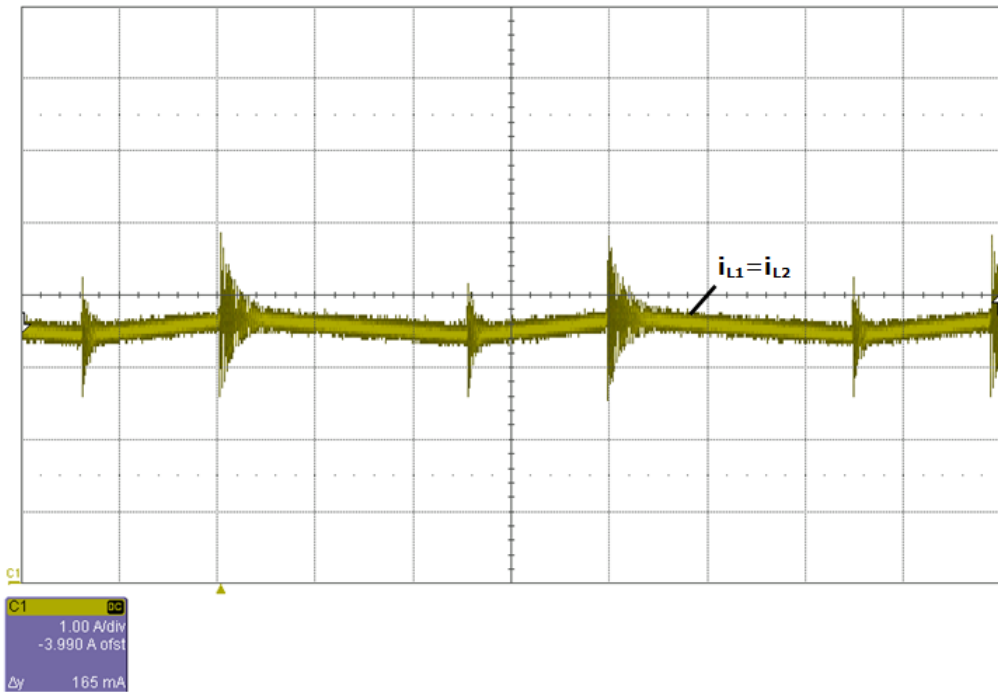


Figure 3.14. The current in the inductors when  $d=1/3$

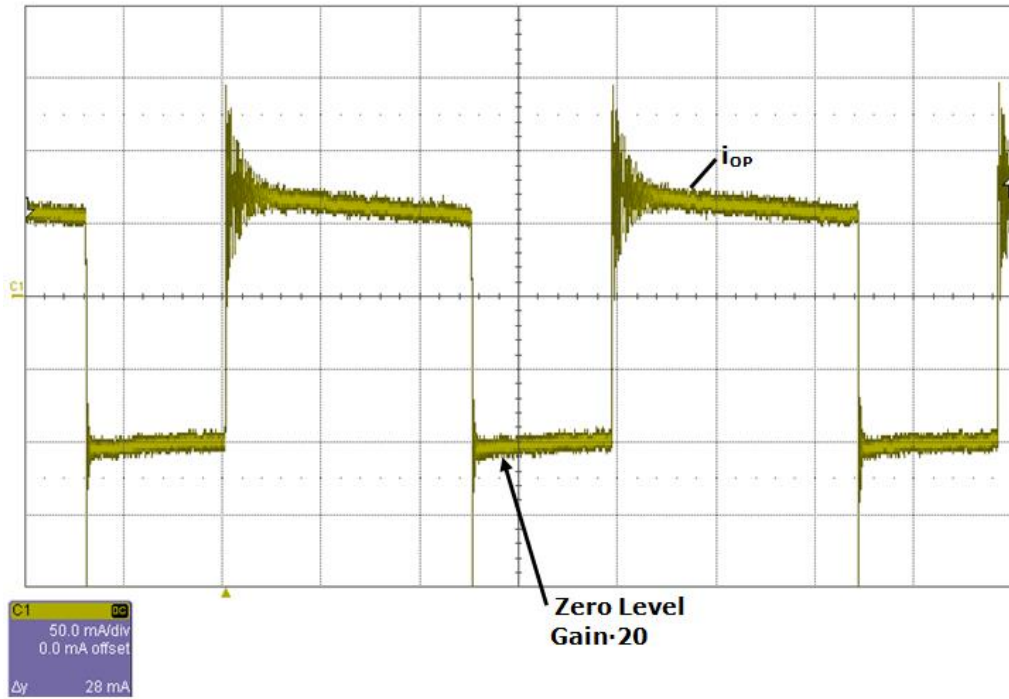


Figure 3.15. Output phase current waveform when  $d=1/3$

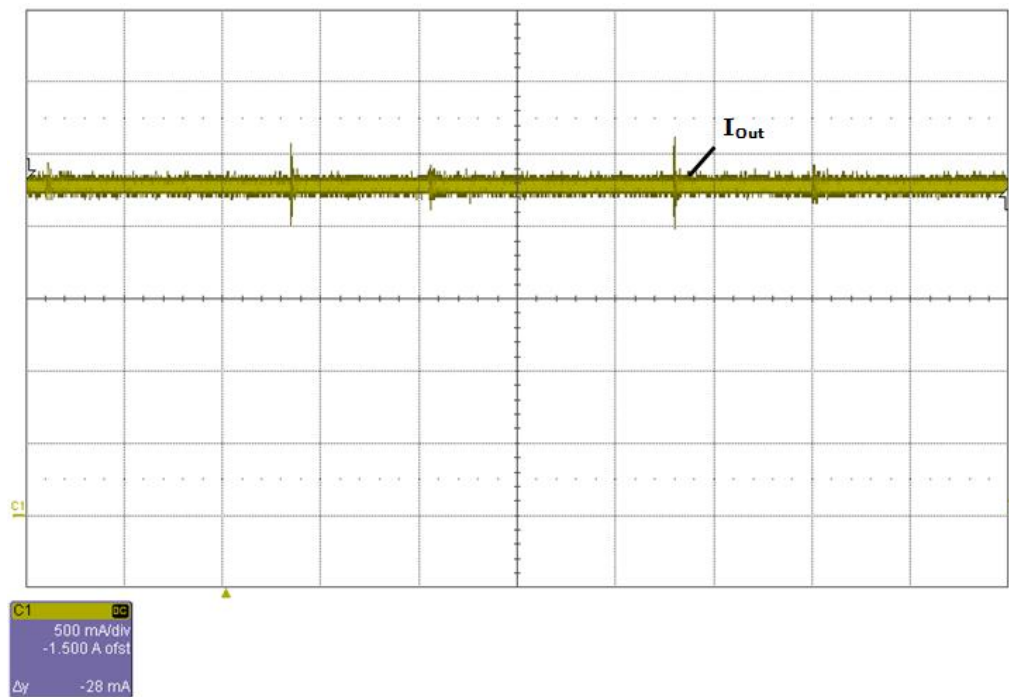
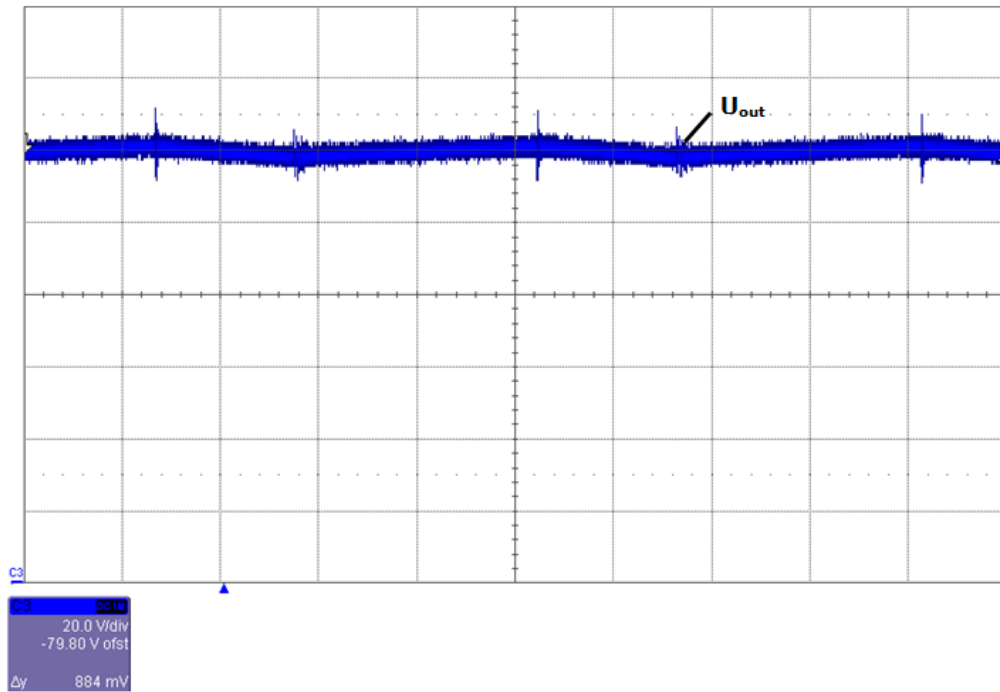


Figure 3.16. Output current waveform when  $d=1/3$

Figure 3.17. Output voltage waveform when  $d=1/3$ 

Then, the waveforms of the converter when a duty cycle  $d=1/2$  is used are presented. In Figure 3.18, the input voltage is shown. The duty cycle of the converter results from Figure 3.19, where the current of the switch is represented. In Figure 3.20 the input phase current is enfaced. The current in the two inductors is represented in Figure 3.21. The output phase current is presented in Figure 3.22. In Figure 3.23 and Figure 3.24, the current and output voltage respectively is shown.

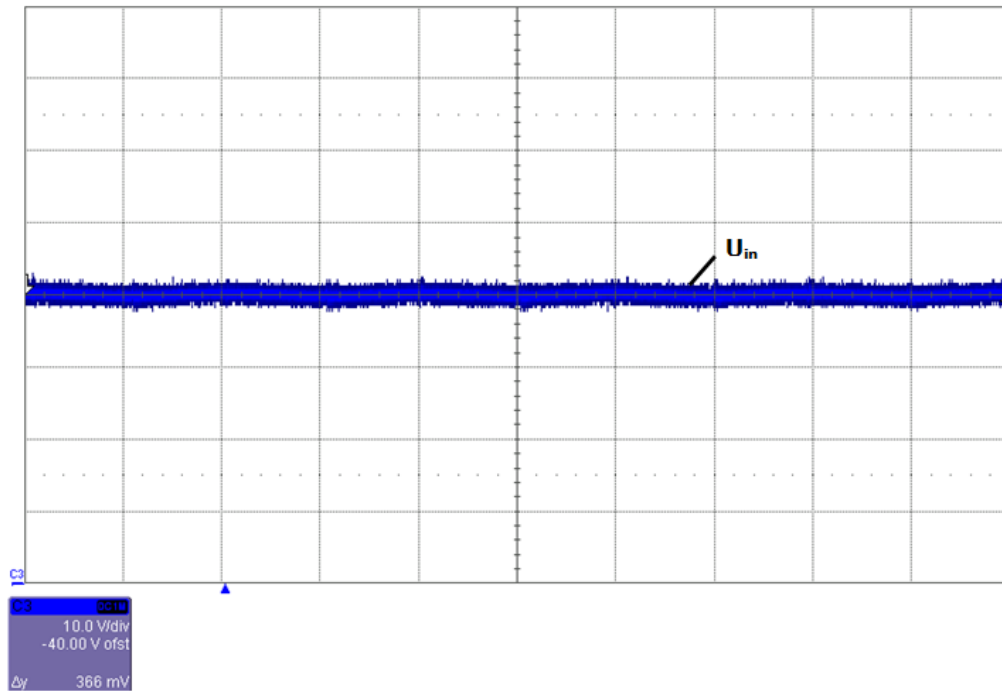


Figure 3.18. Input voltage waveform when  $d=1/2$

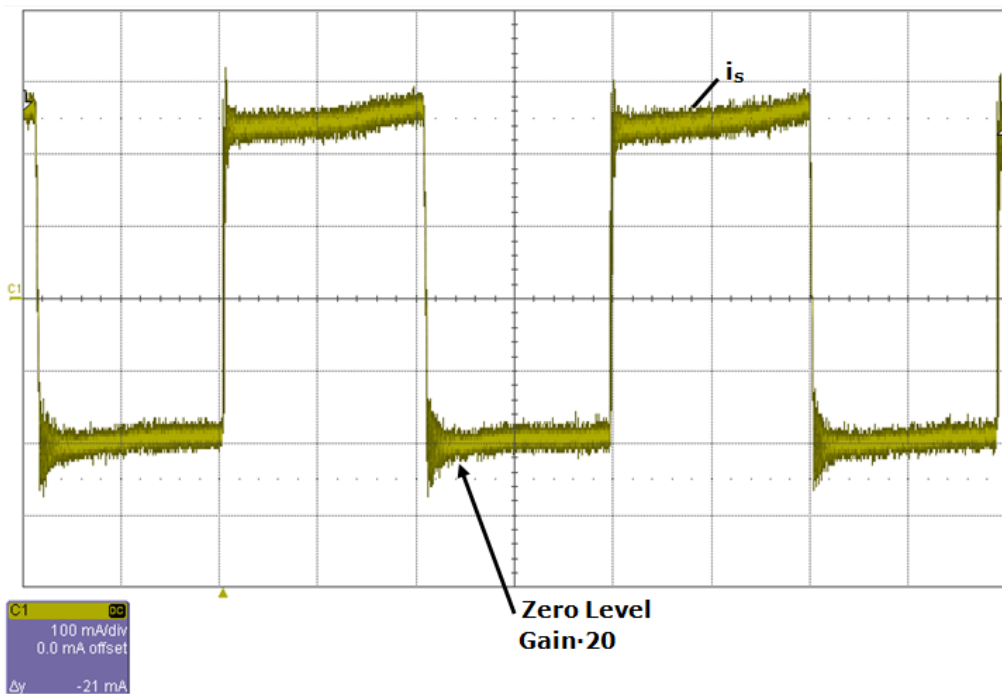


Figure 3.19. MOSFET current waveform when  $d=1/2$

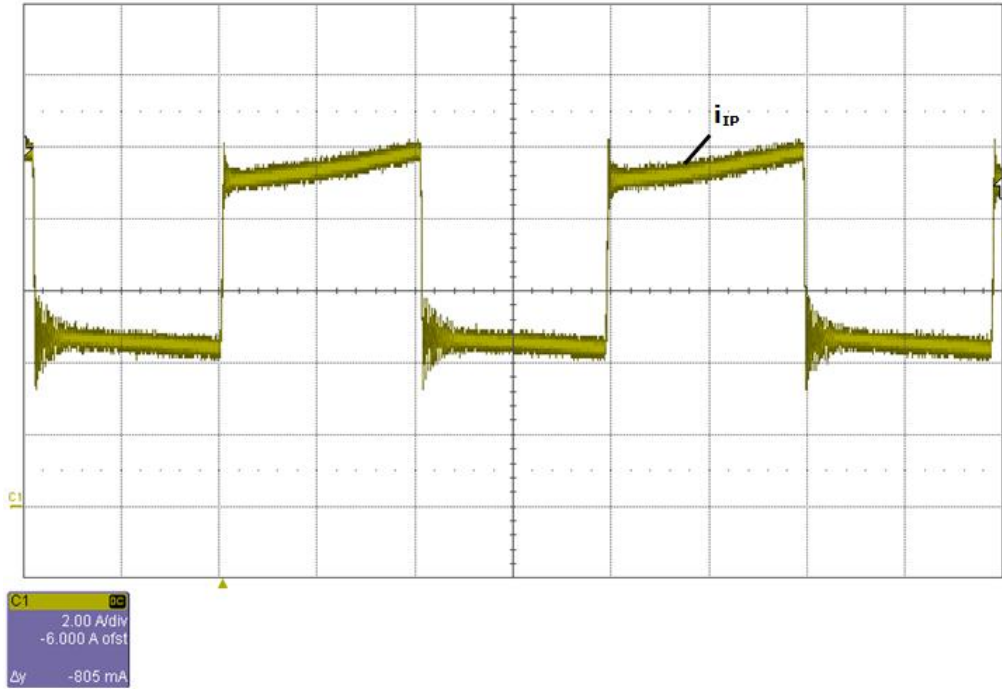


Figure 3.20. Input phase current waveform when  $d=1/2$

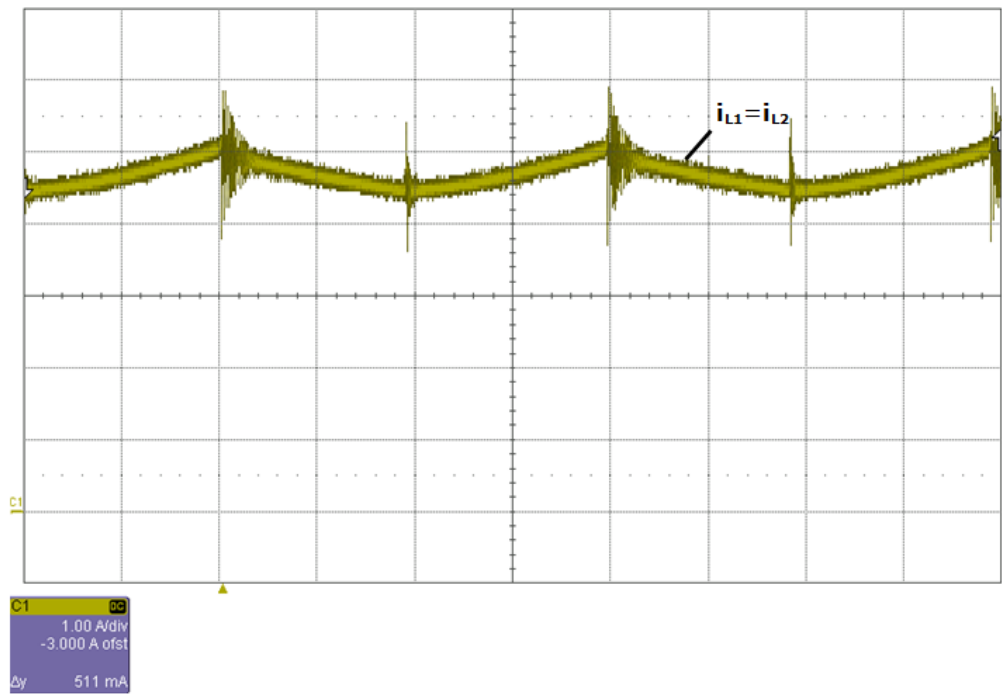


Figure 3.21. Current in the inductors when  $d=1/2$



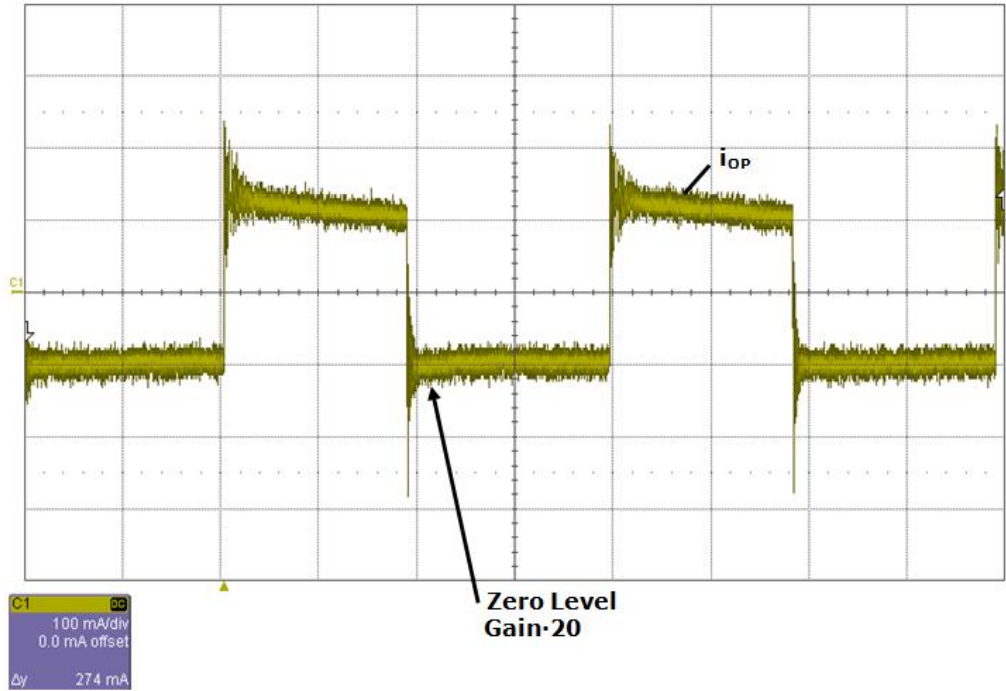


Figure 3.22. Output phase current waveform when  $d=1/2$

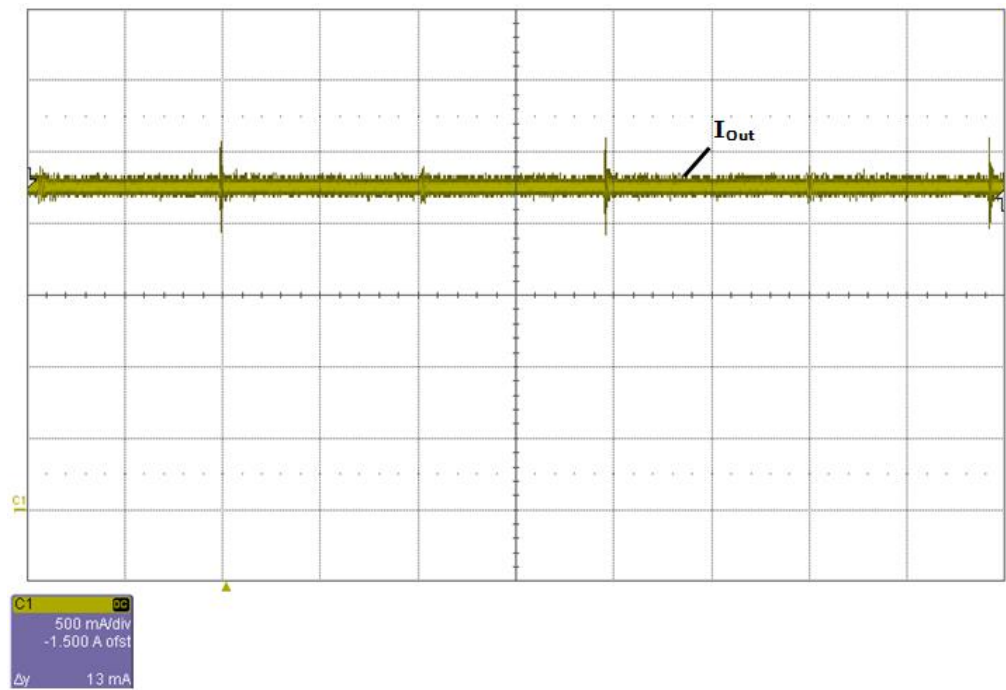
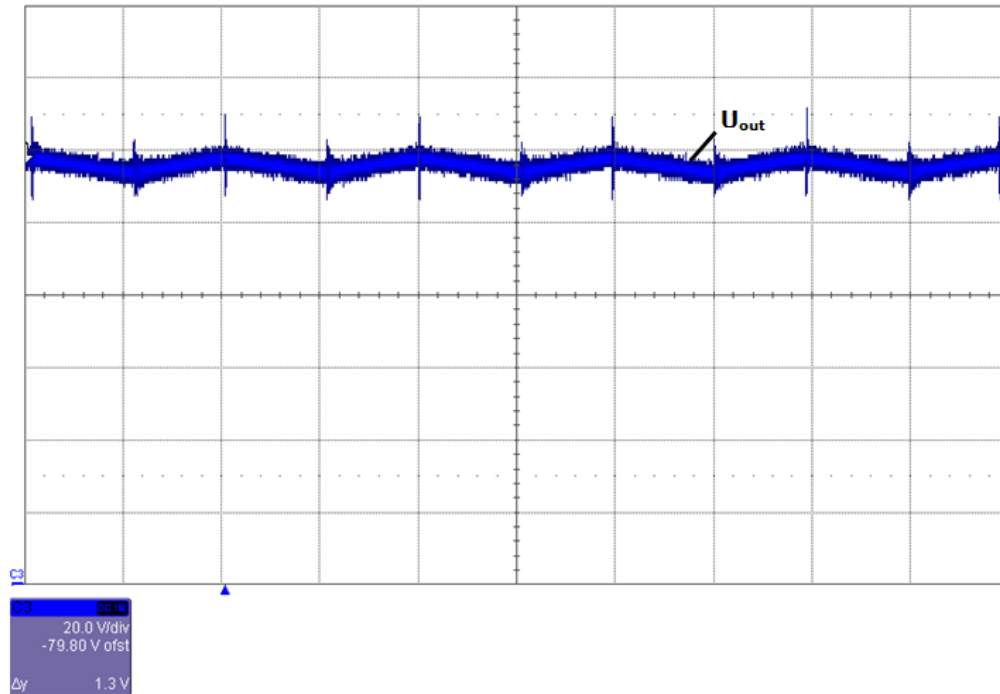


Figure 3.23. Output current waveform when  $d=1/2$

Figure 3.24. Output voltage waveform when  $d=1/2$ 

Finally the voltage and current waveforms of the converter for a duty cycle  $d=2/3$  are presented. In Figure 3.25, the input voltage is shown. The duty cycle of the converter is obvious from the Figure 3.26, where the switch current is shown. In Figure 3.27 the input phase current is represented. The current in the two inductors is represented in Figure 3.28. The output phase current is presented in Figure 3.29. In Figure 3.30 and Figure 3.31, the current and output voltages respectively are shown.

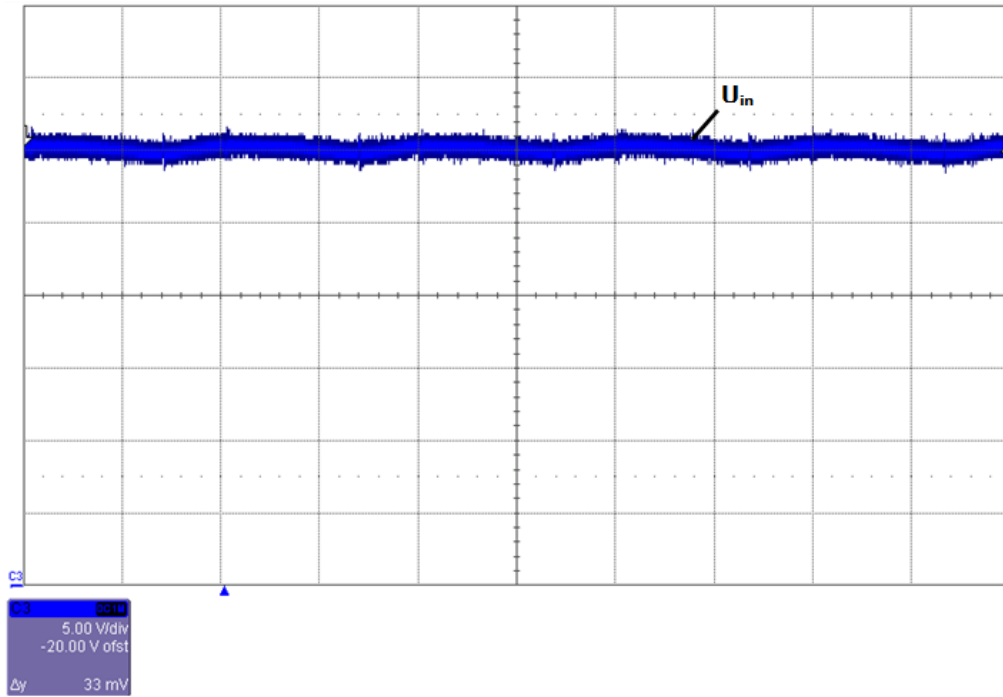


Figure 3.25. Input voltage waveform when  $d=2/3$

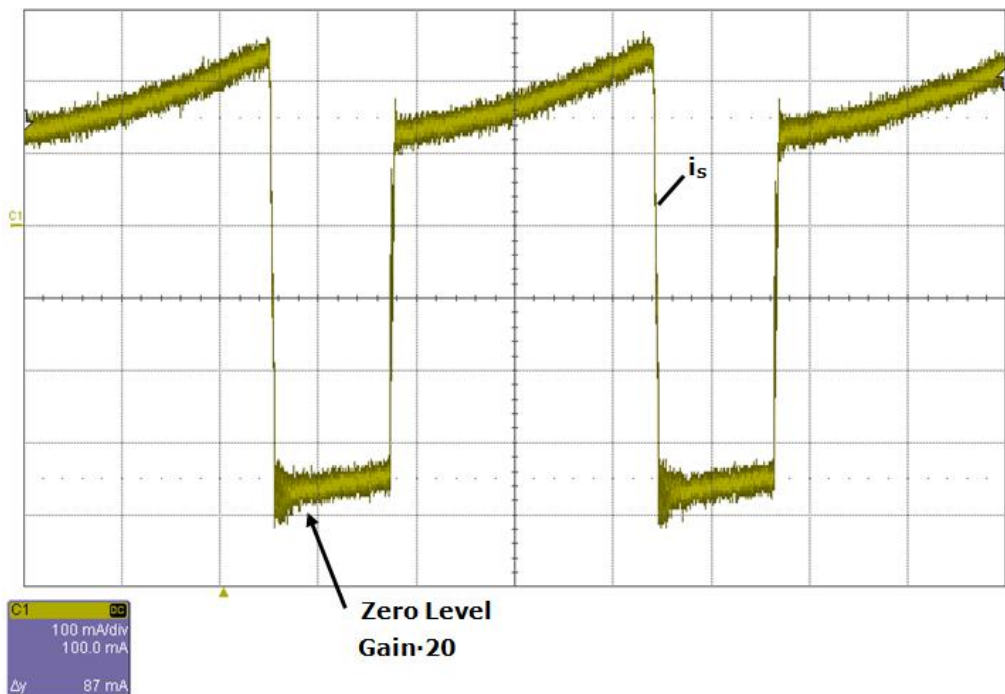


Figure 3.26. MOSFET current waveform when  $d=2/3$

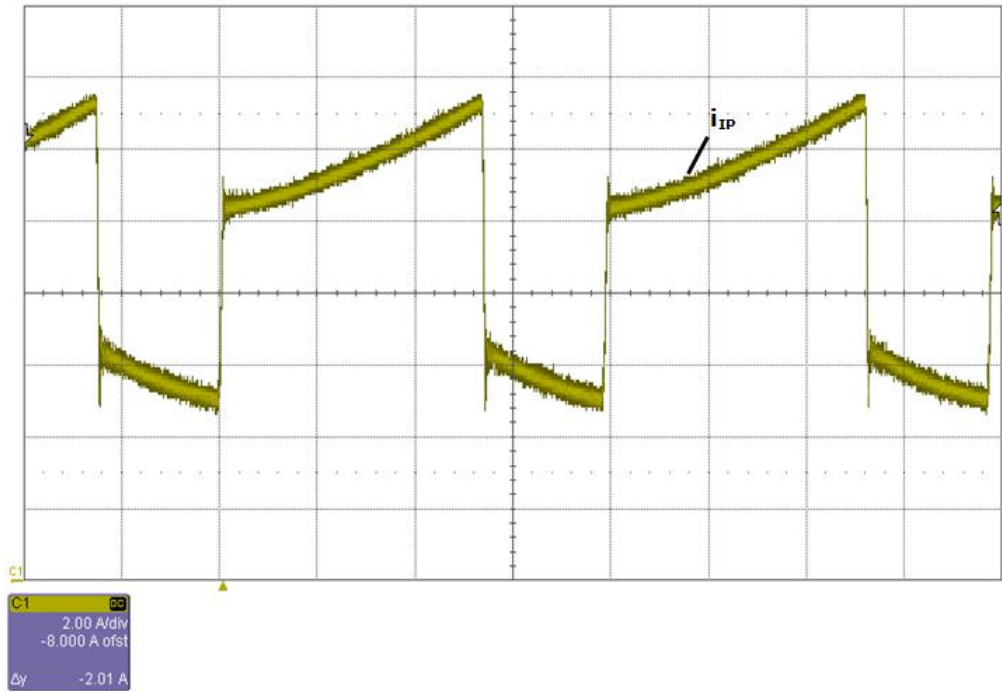


Figure 3.27. Input phase current waveform when  $d=2/3$

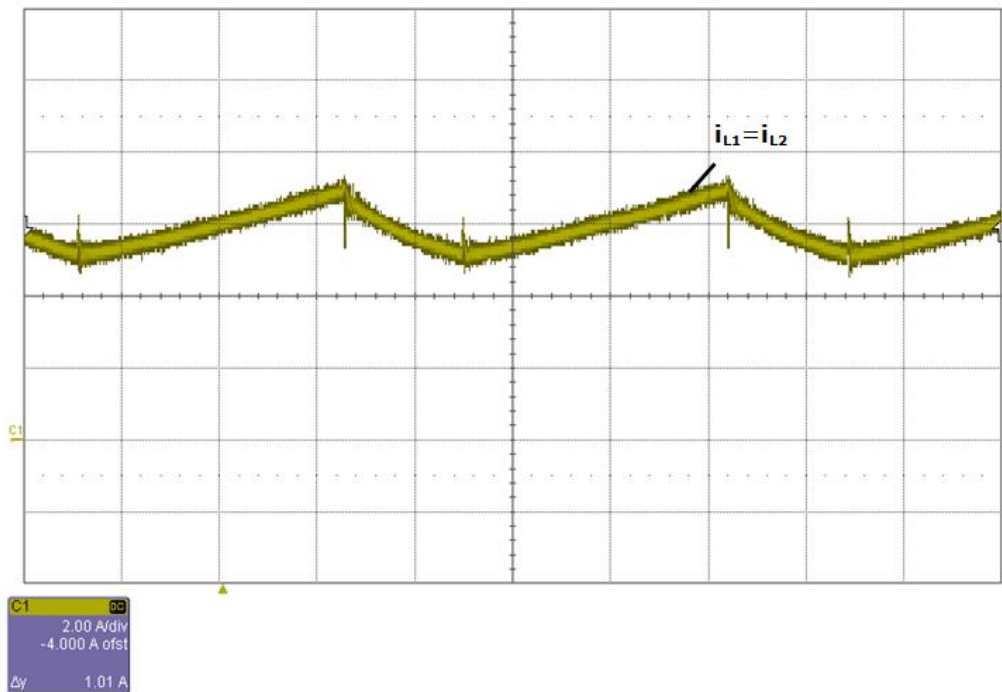


Figure 3.28. Current in the inductors when  $d=2/3$

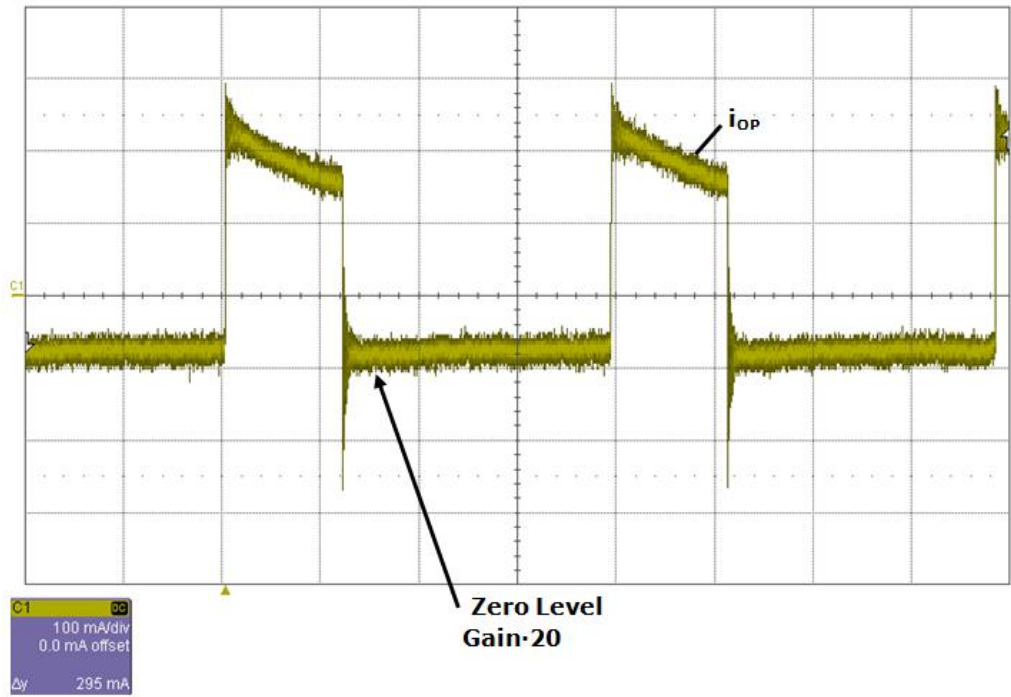


Figure 3.29. Output phase current waveform when  $d=2/3$

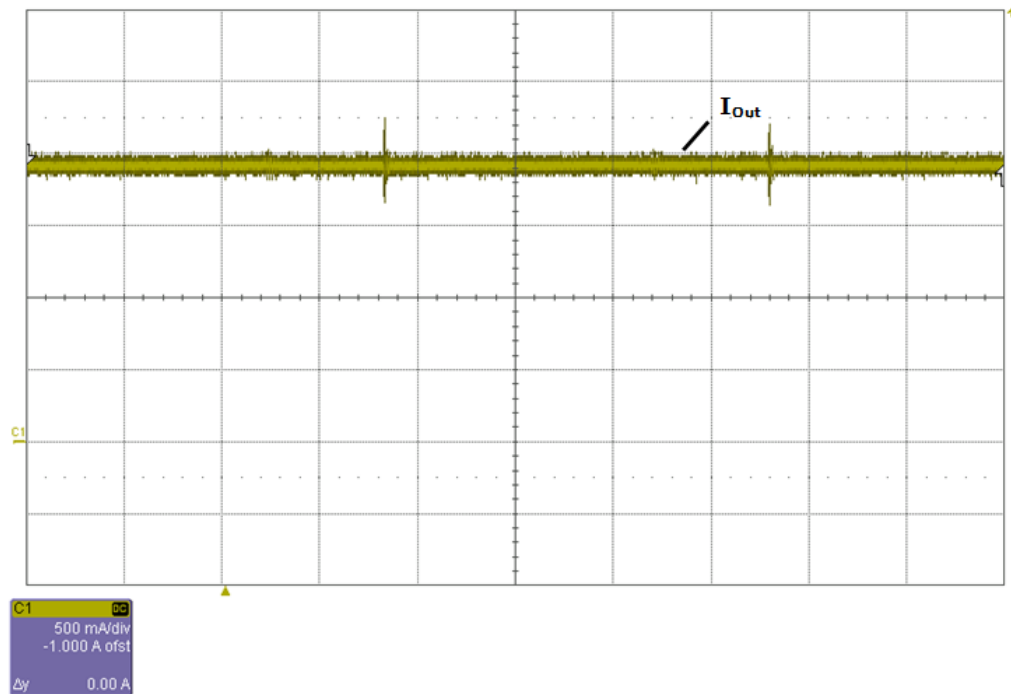


Figure 3.30. Output current waveform when  $d=2/3$

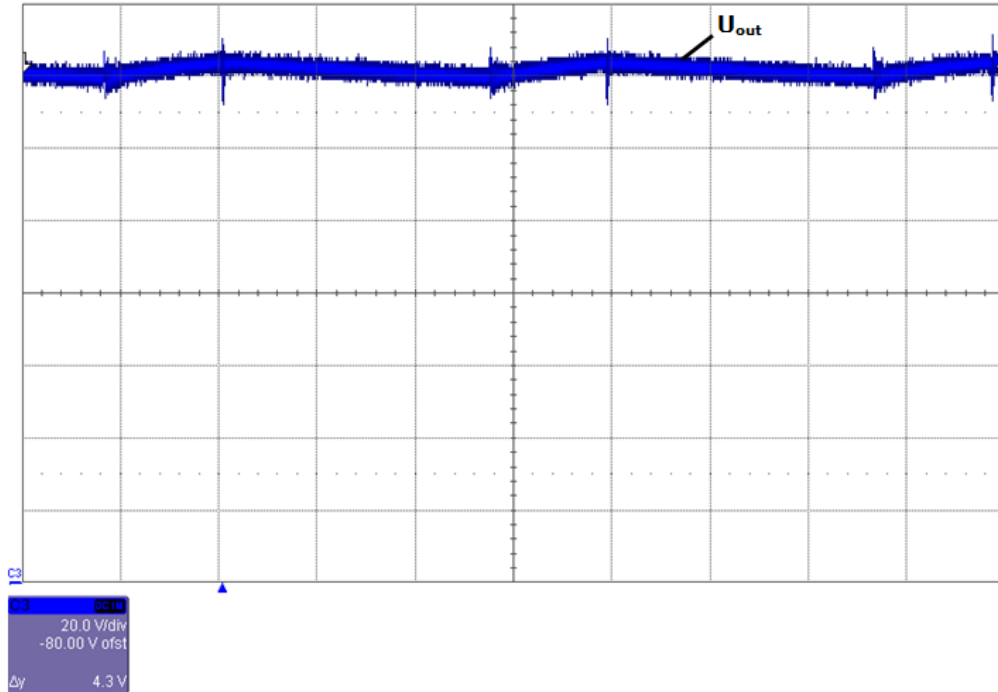


Figure 3.31. Output voltage waveform when  $d=2/3$

The experimental results obtained validate the simulation results and the theoretical consideration. Thereby a very good accordance between them is shown.

The current, voltage and power from the input and output are measured, and with these results the efficiency is calculated, Figure 3.34. The measurements were performed starting from the output power of 30W up to the rated power of 300W and a little beyond. The output voltage of the converter is approximately 120V and the input voltage is 60V at  $d=1/3$ . A comparison with the simulation is presented in Figure 3.34. The simulation was done in SABER, Figure 3.32, with the real model of the component. Even that, small difference is obvious from the figure. These differences are due to semiconductor devices, switching and conduction losses, and temperature and component tolerances that affect the efficiency.

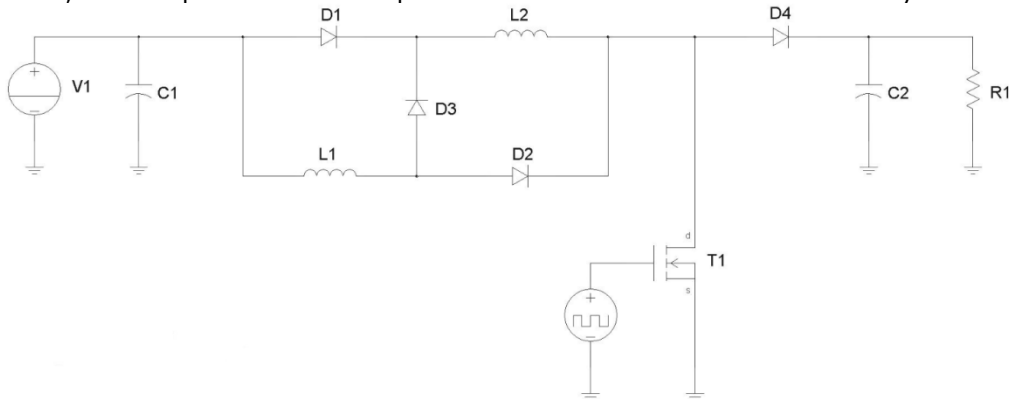


Figure 3.32. Saber simulation diagram for the hybrid Boost DC-DC L-converter

To calculate the efficiency from Saber simulator we measured the average of the output power and input power. The measurements were performed starting from the output power of 30W until approximately 320W. One measurement from simulation it is presented in Figure 3.33. First waveform it is the output power and last one it is the input power (from up to down order).

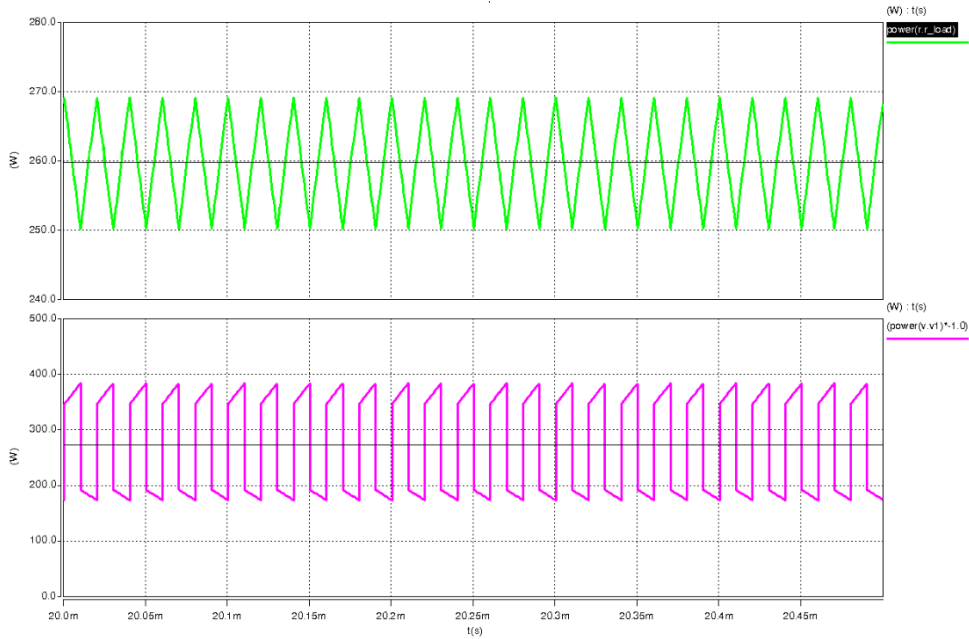


Figure 3.33. Simulation results for the hybrid Boost DC-DC L-converter

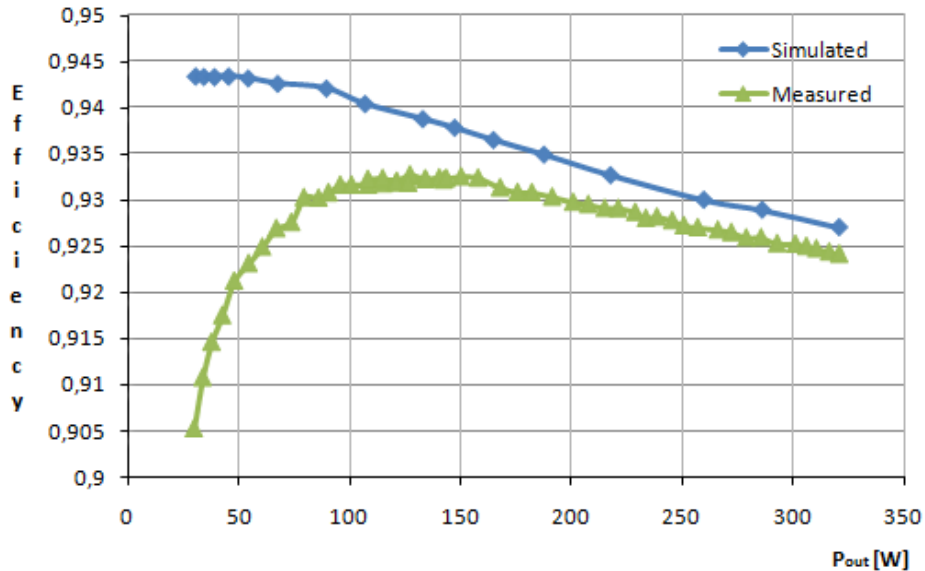


Figure 3.34. Efficiency vs output power  $d=1/3$

The maximum efficiency reached is 94.3% for simulation for an output power of 90W, and 93.2% for measured for an output power between 100W and 150W. The efficiency at rated power is 92.5% respective 92.8% from simulated. Over the whole power range efficiency is higher than 90.5%.

The effort for the input and output capacitor in case of a single-phase DC-DC Boost L-converter is very high.

In the next chapter a method for reducing the capacitor currents is presented.

### 3.5. Conclusions and contributions

This chapter describes a hybrid Boost L-converter. The analytical description, the design formulae and the waveforms of the circuit it was presented. A comparative analysis based on the ripple current of the hybrid converters with coupled and uncoupled inductors was performed before making a choice for the multiphase hybrid converter. The coupled inductors reduce the current ripple compared to that of uncoupled inductors at half. Also, using coupled inductors it is possible to decrease the phase switching frequency without increasing the inductor current ripple or to have the same frequency and reduce the value of the inductor. This means that the inductor size is decreased, resulting in an increase in efficiency and lower price in the same time.

To validate and confirm the theoretical calculations, the author designed a single phase Boost L-converter and simulated this circuit in CASPOC simulation program. Two different levels of the input voltage were set to compare the properties of this converter through simulation. The values of the input voltages were  $U_{in}=40V$  and  $U_{in}=60V$ , and the duty cycle were  $d=50\%$  and  $d=33.3\%$  respectively. The simulation waveforms are compared to theoretical calculations and to the waveforms associated to them, and a very good agreement is accomplished. A laboratory prototype is implemented. The experimental results validated the concept and the waveforms of the prototype are shown.

The chapter ends with the diagrams of the efficiency for the implemented laboratory prototype and simulated circuit in Saber with "real" models, in the case of  $U_{out}=120V$ ,  $d=1/3$ , and an output power variation between 30W to 300W.

The most important contribution from this chapter is the modification of the hybrid converter proposed by A. Ioinovici in [4] by coupling the inductors and obtained a new hybrid converter with a single core, instead of two cores for inductor, and with reduced current ripple at half. Other contribution result from this one, and they can be summarized as follows:

- deduction of the design relationship;
- deduction of the operating condition for CCM and static characteristic;
- the analytical study, validated by simulation of the hybrid converters with coupled inductor, made in Caspoc Simulation Program;
- Matlab and Mathcad program for theoretical study and data processing;
- comparative analysis between hybrid converter with coupled and uncoupled inductors;
- the laboratory prototype built in order to validate the theoretical results;
- Saber simulation with "real" component for efficiency calculation and comparison with the measurements from the laboratory prototype;



- the scientific validation of this hybrid structure with coupled inductor by publishing them in [103] indexed **ISI** – Web of Knowledge – Thomson Reuters, and published in Hindawi Publishing Corporation, International Journal of Photoenergy, 2014.

## CHAPTER 4. Multiphase Hybrid Boost DC-DC L-converter

A new multiphase hybrid Boost converter, with wide conversion ratio as a solution for a renewable energy system is presented in this chapter. The proposed converter can be used as an interface between the renewable energy system (PV or fuel cell system) and the dc load/inverter/battery.

With a multiphase design, the filter circuit effort can be significantly reduced. In this circuit the different phases are connected in parallel both at the input and at the output at a common input and output capacitor of the converter and are controlled with phase shift, Figure 4.1. The hybrid Boost DC-DC L-converter presented in the previous chapter is used in a multiphase design [103], [120].

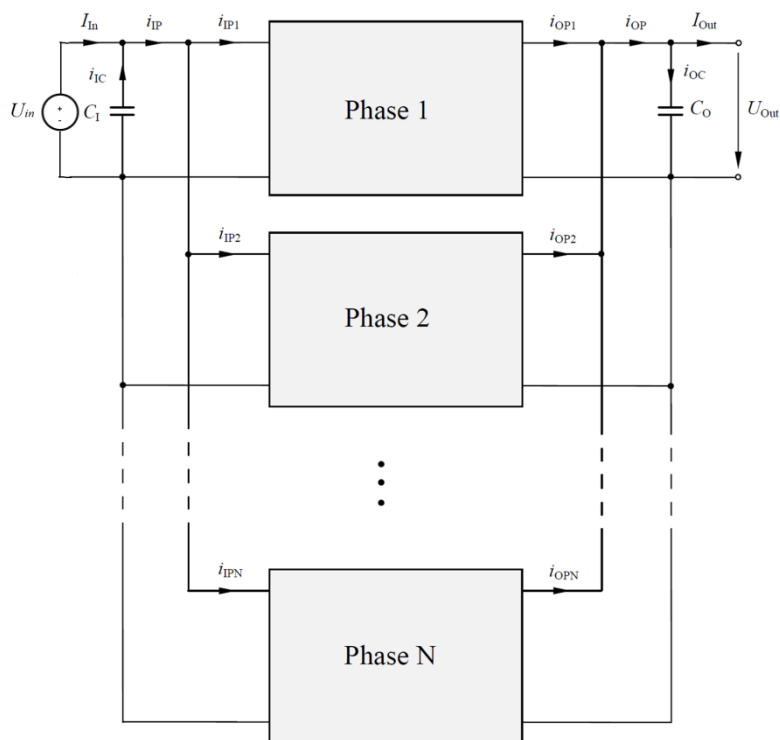


Figure 4.1. The architecture of a multiphase hybrid boost DC-DC converter [120]

The total input current is divided in the different phases with  $1/n$ . Because of the interleaved switching, the multiphase converters exhibit several benefits compared to conventional converters. The AC-currents in the input and output capacitors can be substantially reduced. In addition, the frequency of the capacitor currents is increased.

With suitable circuit design the effort of the inductances can also be decreased. Another advantage of the multiphase converter is that the load current is divided between the phases of the multiphase converter, so it allows the heat generation to be spread across a larger area.

To prove the operation of the two-phase converter the mathematical analysis is provided that is validated by several circuit simulations and practical measurements in a two-phase converter prototype, Figure 4.2. Also, the efficiency measurements of the two-phase converter are presented.

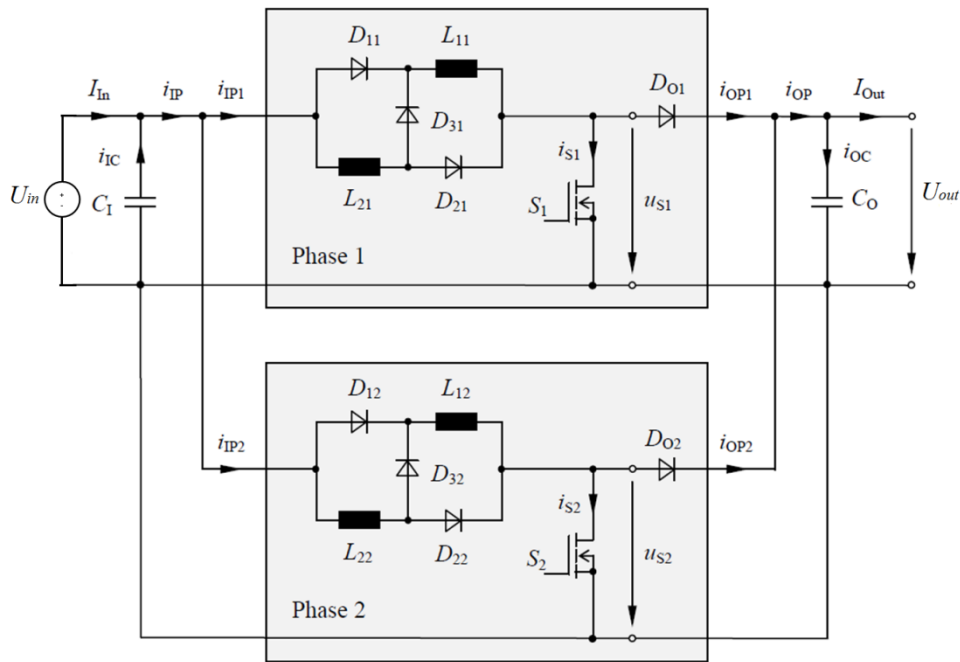


Figure 4.2. Schematics of a two-phase hybrid boost DC-DC converter [120]

To ensure a better understanding the input and output circuits of the multiphase DC-DC converter will be calculated. The current ripple in the circuit for single-phase and two-phase hybrid Boost converter will be compared to each other.

This multiphase converter has the advantage of reduced value and physical size of the input and output capacitors as well as reduced effort for the inductors.

#### 4.1. Multiphase hybrid Boost DC-DC L-converter – input circuit

For a two-phase hybrid Boost converter the currents waveforms at the input of the circuit are shown in Figure 4.3, for  $d=0.3$ ,  $d=0.5$ , and  $d=0.7$ . The first waveform shows the currents in both inductances of phase one,  $L_{11}$  ( $i_{L11}$ ),  $L_{21}$  ( $i_{L21}$ ). The second waveform shows the input current of phase one  $i_{IP1}$ . Represented underneath with green are the currents in both inductances  $L_{12}$  ( $i_{L12}$ ),  $L_{22}$  ( $i_{L22}$ ), and input current of phase two  $i_{IP2}$  respectively. The triangle shaped inductance currents of the two phases are shifted with half period. During the on state the input current

of each phase is half of the inductor current in a single-phase converter. In this circuit the overall input phase current  $I_{IP}$  consists of the sum of all the input phase currents. The overall input phase current  $I_{IP}$  with the dc-component  $I_{In}$  is the fifth waveform, Figure 4.3.

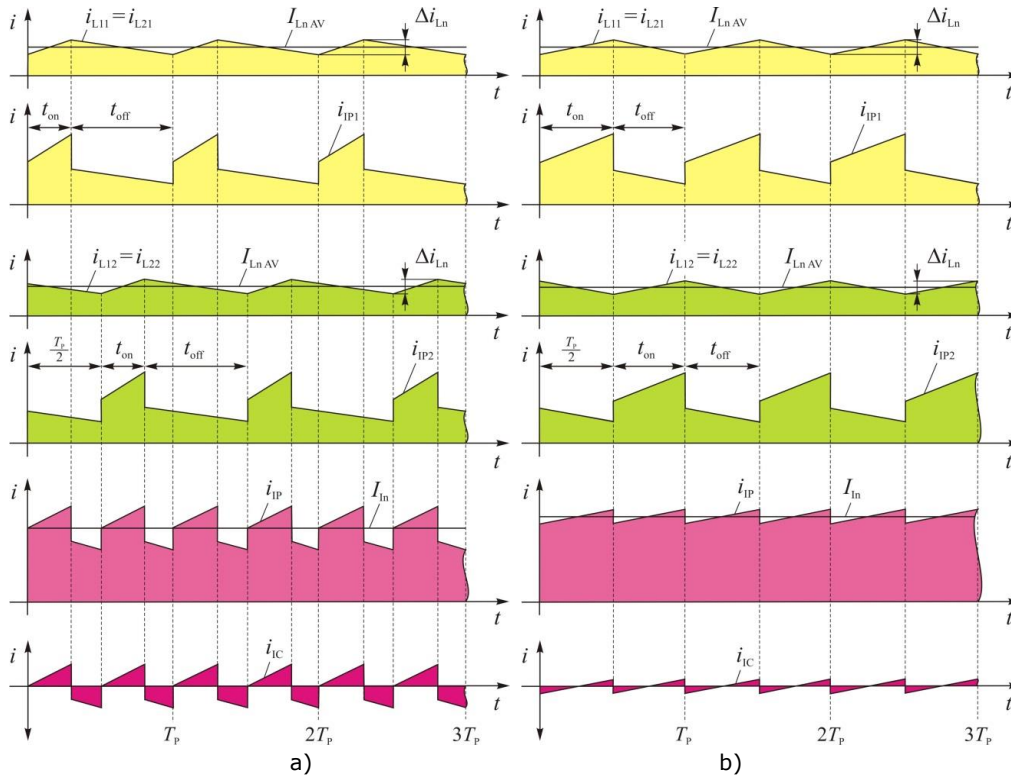


Figure 4.3. Input currents of a two-phase DC-DC converter with duty cycles a)  $d=0.3$ , b)  $d=0.5$ , c)  $d=0.7$  [120]

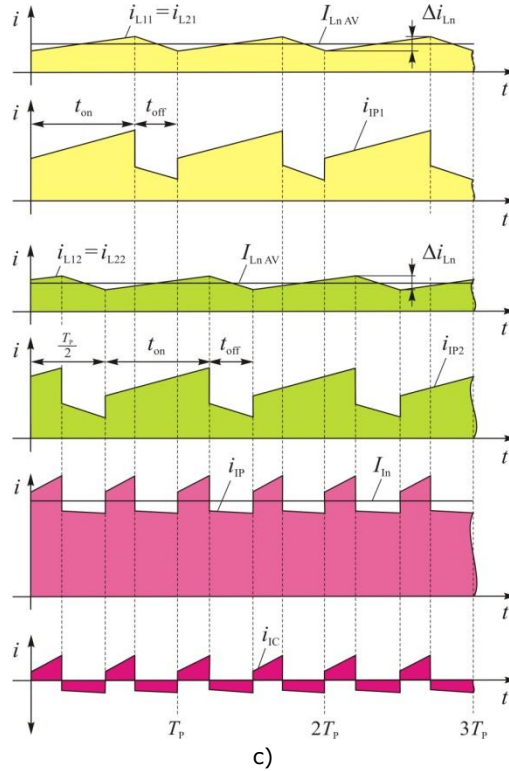


Figure 4.3. (continued 1) Input currents of a two-phase DC-DC converter with duty cycles a)  $d=0.3$ , b)  $d=0.5$ , c)  $d=0.7$  [120]

For this circuit it is assumed that only the dc-current is flowing in the circuit input. In these conditions, the relationship between the input current  $I_{In}$  and the dc inductor current of the individual phases,  $I_{LnAV}$ , can be calculated resulting in [103]:

$$I_{LnAV} = \frac{I_{In}}{n \cdot (1 + d)} \quad (4.1)$$

The AC-component of the overall input phase current  $I_{IP}$  is flowing through the input capacitor. This current is clearly smaller compared to a single-phase hybrid Boost converter. Additionally, the capacitor current frequency is doubled. For these reasons the filter effort is reduced.

The calculation of the circuit inductances and capacitors for an n-phase design can be accomplished in the same way as for single-phase circuits. The same approach for a single-phase converter is applied. Taking into account that the input current is divided between the different phases, the maximum current variation in the inductances of the individual phases is estimated at the maximum dc current and rated power [103].

$$L_{1n} = L_{2n} = \frac{U_{out} \cdot T_s}{\Delta i_{L_n max}} \cdot (3 - 2\sqrt{2}) \quad (4.2)$$

For design, the maximum current variation  $\Delta i_{L_{nmax}}$  is selected between 10%-30% of the dc phase current in the inductances at rated power [103].

$$\Delta i_{L_{nmax}} = (0.1 \div 0.3) \cdot I_{LnAVR} \quad (4.3)$$

The amplitude of the triangular current variation in the inductors is dependent on the duty cycle of the converter. Because the duty cycle in all phases has the same value, the current variations in all inductors are the same.

$$\Delta i_{L_n} = \frac{d \cdot (1-d)}{(1+d) \cdot (3-2\sqrt{2})} \cdot \Delta i_{L_{nmax}} \quad (4.4)$$

Compared to the single-phase design, the capacitor current is reduced and the current frequency is increased by the number of phases. For the capacitor design in general, the allowable static voltage variation is selected smaller than 1% of the rated input voltage. For this value, the input capacitance of the multiphase hybrid boost converter will be calculated as [103]:

$$C_I = \frac{I_{LnAVR} \cdot T_s}{4 \cdot n \cdot \Delta U_{In_{max}}} \text{ with } \Delta U_{In_{max}} \leq 0.01 \cdot U_{inR} \quad (4.5)$$

For these DC-DC converters, electrolytic capacitors are used often. The main design criterion of these capacitors is the RMS-current load. For this reason the RMS-current in the input capacitor  $C_I$  will be calculated. It is assumed that the switching processes in the phases are ideal, and it is accepted that the input current is an ideal dc-value. The worst case scenario will occur if the capacitor is loaded with the total AC-current component. In Figure 4.3 the input capacitor current is represented for a two-phase DC-DC hybrid Boost converter. It is obvious that the capacitor current can be split into two different components: a rectangular part and a triangular part. The RMS-current of these two components have been calculated in [103].

In the formula below is shown the RMS current result of the rectangular part for multiphase converters.

$$I_{IC \text{ II}} = \begin{cases} \sqrt{I_{LnAV}^2 \cdot n^2 \cdot \left(d - \frac{0}{n}\right) \cdot \left(\frac{1}{n} - d\right)} & \text{if } \frac{0}{n} \leq d \leq \frac{1}{n} \\ \sqrt{I_{LnAV}^2 \cdot n^2 \cdot \left(d - \frac{1}{n}\right) \cdot \left(\frac{2}{n} - d\right)} & \text{if } \frac{1}{n} \leq d \leq \frac{2}{n} \\ \sqrt{I_{LnAV}^2 \cdot n^2 \cdot \left(d - \frac{2}{n}\right) \cdot \left(\frac{3}{n} - d\right)} & \text{if } \frac{2}{n} \leq d \leq \frac{3}{n} \\ \vdots & \vdots \\ \sqrt{I_{LnAV}^2 \cdot n^2 \cdot \left(d - \frac{n-1}{n}\right) \cdot \left(\frac{n}{n} - d\right)} & \text{if } \frac{n-1}{n} \leq d \leq \frac{n}{n} \end{cases} \quad (4.6)$$

For the RMS current of the rectangular part for a multiphase circuit design it is necessary to consider that the dc inductor current  $I_{L_{nAV}}$  becomes smaller as the number of phases is increased. For example, the dc inductor current  $I_{L_{nAV}}$  in a two-phase converter is only half of the corresponding current in a single-phase converter. With this fact in mind the rectangular component of the input capacitor current can clearly be reduced with a multiphase design.

In the formula below is shown the RMS current result of the triangular part for multiphase circuit design [103].

$$I_{IC \Delta} = \begin{array}{l} \sqrt{\Delta i_{L_{nmax}}^2 \cdot \frac{n \cdot \left[ 2 - (n+1) \cdot d \right]^2 \cdot \left( d - \frac{0}{n} \right)^3 + \left[ 0 - (n+0) \cdot d \right]^2 \cdot \left( \frac{1}{n} - d \right)^3}{12 \cdot (3 - 2\sqrt{2})^2 \cdot (1+d)^2}} \quad \text{if } \frac{0}{n} \leq d \leq \frac{1}{n} \\ \sqrt{\Delta i_{L_{nmax}}^2 \cdot \frac{n \cdot \left[ 4 - (n+2) \cdot d \right]^2 \cdot \left( d - \frac{1}{n} \right)^3 + \left[ 2 - (n+1) \cdot d \right]^2 \cdot \left( \frac{2}{n} - d \right)^3}{12 \cdot (3 - 2\sqrt{2})^2 \cdot (1+d)^2}} \quad \text{if } \frac{1}{n} \leq d \leq \frac{2}{n} \\ \sqrt{\Delta i_{L_{nmax}}^2 \cdot \frac{n \cdot \left[ 6 - (n+3) \cdot d \right]^2 \cdot \left( d - \frac{2}{n} \right)^3 + \left[ 4 - (n+2) \cdot d \right]^2 \cdot \left( \frac{3}{n} - d \right)^3}{12 \cdot (3 - 2\sqrt{2})^2 \cdot (1+d)^2}} \quad \text{if } \frac{2}{n} \leq d \leq \frac{3}{n} \\ \vdots \\ \sqrt{\Delta i_{L_{nmax}}^2 \cdot \frac{n \cdot \left[ 2 \cdot n - (n+n) \cdot d \right]^2 \cdot \left( d - \frac{n-1}{n} \right)^3 + \left[ (2 \cdot n - 2) - (n+n-1) \cdot d \right]^2 \cdot \left( \frac{n}{n} - d \right)^3}{12 \cdot (3 - 2\sqrt{2})^2 \cdot (1+d)^2}} \quad \text{if } \frac{n-1}{n} \leq d \leq \frac{n}{n} \end{array} \quad (4.7)$$

The current variation  $\Delta i_{L_{nmax}}$  is selected according to the rated average inductor current  $I_{L_{nAV}}$  for the circuit design. This means that with the same circuit design and an increased number of phases, the current variation is reduced.

The geometrical addition of rectangular and triangular RMS-components results in the total capacitor current for an n-phase hybrid boost DC-DC converter [103].

$$I_{IC} = \sqrt{I_{IC \Pi}^2 + I_{IC \Delta}^2} \quad (4.8)$$

## 4.2. Multiphase hybrid Boost DC-DC L-converter – output circuit

The current waveforms at the output of a two-phase hybrid Boost converter are presented in Figure 4.4, for different duty cycles. The first waveform shows the current in both inductances of phase one,  $L_{11}$  ( $i_{L11}$ ),  $L_{21}$  ( $i_{L21}$ ). The output current of phase one  $i_{OP1}$ , is shown in the second waveform. Represented underneath with green are the currents in both inductances  $L_{12}$  ( $i_{L12}$ ),  $L_{22}$  ( $i_{L22}$ ), and output current of phase two  $i_{OP2}$  respectively. The triangular inductor current of the two phases is shifted half period to each other. During the off state the inductors are connected in series and the current flows to the output phase, similar to the single-phase converter. In this circuit the overall output phase current  $i_{OP}$  consists of the sum of all the output phase currents. The overall output phase current  $i_{OP}$  with the dc-component  $I_{Out}$  is shown as the fifth waveform in the figure. It is assumed that only the DC-current is flowing in the circuit output and the total AC-component of the overall output phase current  $i_{OP}$  is flowing in the output capacitor. This current is clearly smaller and the frequency of the capacitor current is doubled compared to a single-phase hybrid Boost converter [103].

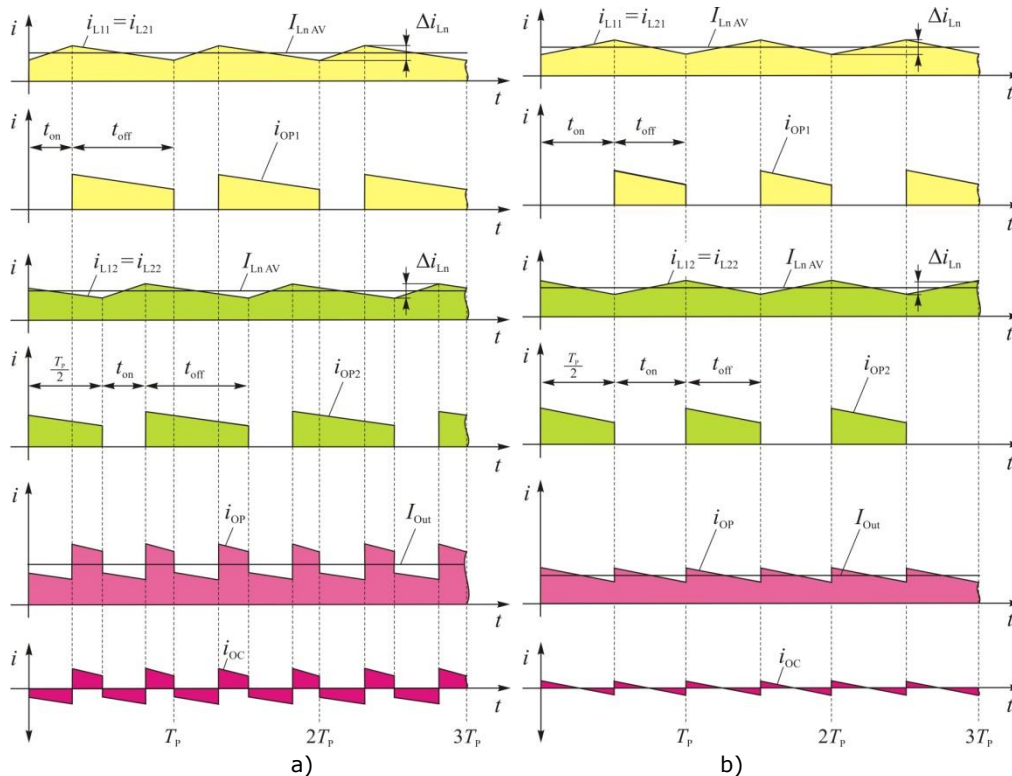


Figure 4.4. Output currents of a two-phase DC-DC converter with duty cycles: a)  $d=0.3$ , b)  $d=0.5$ , c)  $d=0.7$  [120]



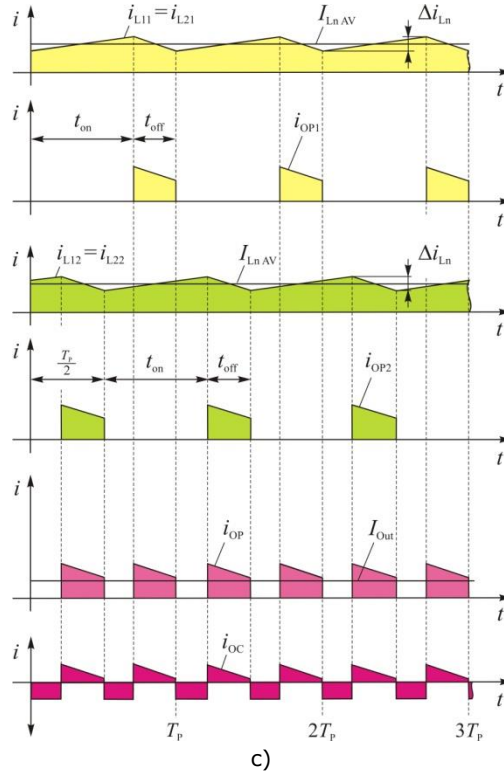


Figure 4.4. (continued 1) Output currents of a two-phase DC-DC converter with duty cycles: a)  $d=0.3$ , b)  $d=0.5$ , c)  $d=0.7$  [120]

Compared to a single-phase design, the output capacitor current is reduced and the current frequency is increased by the number of phases. For capacitor design in general, the allowable static voltage variation is selected smaller than 1% of the rated output dc voltage. The necessary output capacitance of the multiphase hybrid Boost converter is calculated as [103]:

$$C_O = \frac{I_{LnAV} \cdot T_s}{4 \cdot n \cdot \Delta u_{Out_{max}}} \text{ with } \Delta u_{Out_{max}} \leq 0.01 \cdot U_{OutR} \quad (4.9)$$

With similar considerations related to the input capacitor, for these DC-DC converters electrolytic capacitors are used often and the main design criterion of these capacitors is the RMS-current. For this reason the RMS-current in the output capacitor  $C_O$  will be calculated. The output capacitor current can also be split in a rectangular and a triangular part.

The RMS-current of the rectangular part is given by the formula below [103]:

$$I_{OC II} = \begin{cases} \sqrt{I_{LnAV}^2 \cdot n^2 \cdot \left(d - \frac{0}{n}\right) \cdot \left(\frac{1}{n} - d\right)} & \text{if } \frac{0}{n} \leq d \leq \frac{1}{n} \\ \sqrt{I_{LnAV}^2 \cdot n^2 \cdot \left(d - \frac{1}{n}\right) \cdot \left(\frac{2}{n} - d\right)} & \text{if } \frac{1}{n} \leq d \leq \frac{2}{n} \\ \sqrt{I_{LnAV}^2 \cdot n^2 \cdot \left(d - \frac{2}{n}\right) \cdot \left(\frac{3}{n} - d\right)} & \text{if } \frac{2}{n} \leq d \leq \frac{3}{n} \\ \vdots & \vdots \\ \sqrt{I_{LnAV}^2 \cdot n^2 \cdot \left(d - \frac{n-1}{n}\right) \cdot \left(\frac{n}{n} - d\right)} & \text{if } \frac{n-1}{n} \leq d \leq \frac{n}{n} \end{cases} \quad (4.10)$$

The output capacitor RMS-current that is produced by the rectangular component is exactly the same as that in the input capacitor. Also, in this formula must be assumed that the average inductor current  $I_{LnAV}$  becomes smaller when the number of phases is increased.

The next formula shows the output capacitor RMS component produced by the triangular part in multiphase converters [103].

$$I_{OC \Delta} = \begin{cases} \sqrt{\frac{\Delta i_{L_{nmax}}^2 \cdot n \cdot d^2 \cdot \left[ (n-1)^2 \cdot \left( d - \frac{0}{n} \right)^3 + (n-0)^2 \cdot \left( \frac{1}{n} - d \right)^3 \right]}{12 \cdot (3-2\sqrt{2})^2 \cdot (1+d)^2}} & \text{if } \frac{0}{n} \leq d \leq \frac{1}{n} \\ \sqrt{\frac{\Delta i_{L_{nmax}}^2 \cdot n \cdot d^2 \cdot \left[ (n-2)^2 \cdot \left( d - \frac{1}{n} \right)^3 + (n-1)^2 \cdot \left( \frac{2}{n} - d \right)^3 \right]}{12 \cdot (3-2\sqrt{2})^2 \cdot (1+d)^2}} & \text{if } \frac{1}{n} \leq d \leq \frac{2}{n} \\ \sqrt{\frac{\Delta i_{L_{nmax}}^2 \cdot n \cdot d^2 \cdot \left[ (n-3)^2 \cdot \left( d - \frac{2}{n} \right)^3 + (n-2)^2 \cdot \left( \frac{3}{n} - d \right)^3 \right]}{12 \cdot (3-2\sqrt{2})^2 \cdot (1+d)^2}} & \text{if } \frac{2}{n} \leq d \leq \frac{3}{n} \\ \vdots & \vdots \\ \sqrt{\frac{\Delta i_{L_{nmax}}^2 \cdot n \cdot d^2 \cdot \left[ (n-n)^2 \cdot \left( d - \frac{n-1}{n} \right)^3 + [n-(n-1)]^2 \cdot \left( \frac{n}{n} - d \right)^3 \right]}{12 \cdot (3-2\sqrt{2})^2 \cdot (1+d)^2}} & \text{if } \frac{n-1}{n} \leq d \leq \frac{n}{n} \end{cases} \quad (4.11)$$

The geometrical addition of rectangular and triangular RMS-components results in the total RMS capacitor current for an n-phase hybrid boost DC-DC converter [103].

$$I_{OC} = \sqrt{I_{OC \Pi}^2 + I_{OC \Delta}^2} \quad (4.12)$$

In Figure 4.5, the normalized RMS-current in the input capacitor  $C_I$  and in Figure 4.6 the RMS-current in the output capacitor  $C_O$  of a multiphase DC-DC converter is shown. The current load of the capacitor decreases with the increasing number of phases. The influence of the rectangle RMS-component in both capacitors is the same and clearly dominates (see dotted lines,  $\Delta i_{L_{nmax}} = 0$ ). The maximum capacitor current component produced by the rectangular part is smaller by a factor of  $n$  for n-phase converters compared to the single phase design. The load in the input and output capacitors produced by the triangular current is imposed by the inductor design. This capacitor current is not dependent on the power processed. If the converter is operated with rated output power this current has only a small influence on the overall capacitor current.

The capacitor currents are represented in the figure with a current variation of:

$$\Delta i_{L_n N \max} = 0.5 \cdot I_{L_n AV} \quad (4.13)$$

The influence of the triangular current in the output capacitors is smaller as in the input side of the converter. The calculations demonstrate that the triangular current component has only a small influence on the total current in the input and output capacitor of multiphase converters. Therefore, in practice the triangular current in the inductances can be selected larger. Therefore the dynamics of the hybrid boost DC-DC converter can be improved and beyond that the inductor and capacitor efforts of the circuit can be substantially reduced.

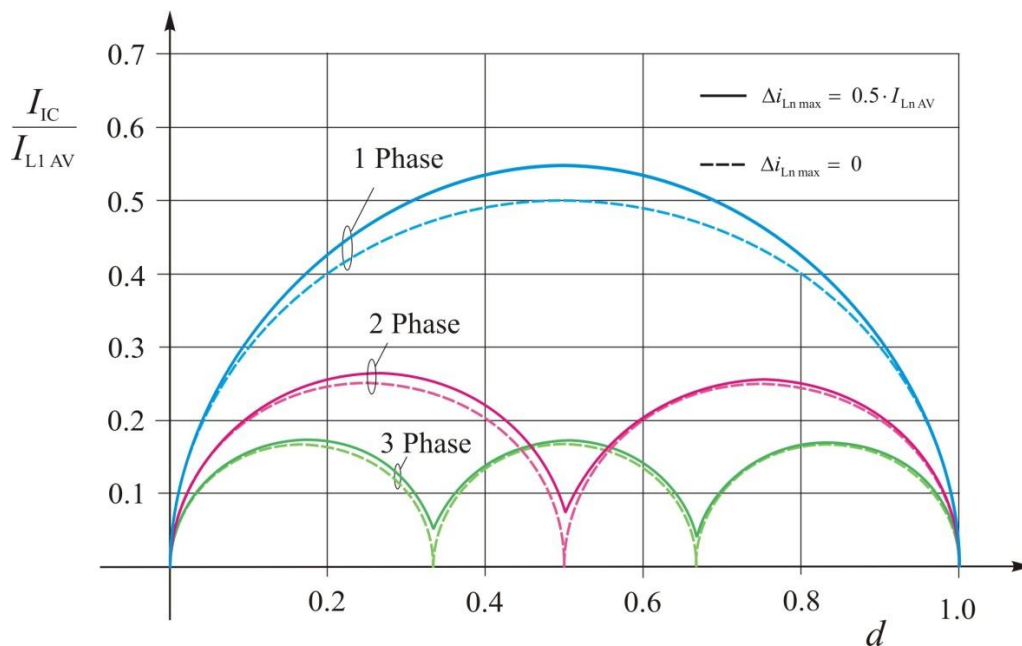


Figure 4.5. RMS input capacitor currents of a one-, two- and three-phase converter [103]

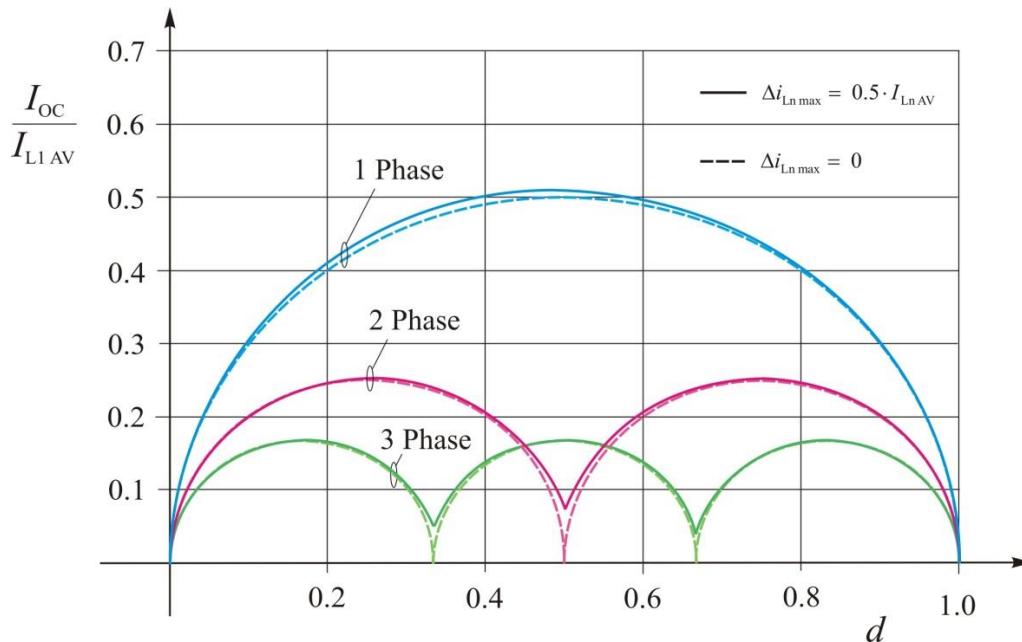


Figure 4.6. RMS output capacitor currents of a one-, two- and three-phase converter [103]

Besides the calculated current in the capacitors, also is flowing harmonics current produced by switching processes of the phases [124]. This current has been examined also in [125] - [127] for another converter. These results can also be used for a hybrid Boost converter. The additional current can substantially contribute in the output capacitors, heating up the capacitors at small loads. But, with higher output power the calculated capacitor current dominates. However, it can't be made a statement for all semiconductor types. Beyond that, this additional current is dependent on the switching frequency of the converter.

The multiphase interleaved Boost L-converter design involves the selection of the number of phases, the inductors, the input and output capacitors, the power switches and the diodes.

The multiphase interleaving structure has more inductors than the single phase converters. Since the inductor is the largest and heaviest component in a power converter this will lead to an increase in the complexity of this converter. In previous chapter a solution was found to reduce the number of core and the complexity of the converter, through the coupling of the inductors. With this solution, like in the case for a single phase, it is also possible to decrease the inductor current ripple and to have the same frequency, or to have the same value of the inductor and reduce the switching frequency. Both situations will lead to an increase in efficiency.

Advantages, disadvantages as well as possible improvements of the proposed topology will be presented. The most important features are: simplicity, cost, efficiency and size. In order to evaluate this, the proposed multiphase two-phase Boost L-converter is designed, simulated and practically implemented for the following values:

## 150 Multiphase Hybrid Boost DC-DC L-converter

- $U_{in}=40V$ ;
- $f_s=50\text{ KHz}$ ;
- duty cycle  $d=50\%$ .

After calculations the following parameters resulted for the Boost L-converter:

- $L_{11}=L_{21}=L_{12}=L_{22}=823.55\ \mu\text{H}$ ;
- $C_1=15.625\ \mu\text{F}$ ;
- $C_0=5.208\ \mu\text{F}$ .

For a fair comparison, the two-phase Boost L-converter is designed and simulated with the same value of the inductors, input and output capacitors, like the one that is practical realized.

Also:

- $L_{11}=L_{21}=822\ \mu\text{F}$ ;
- $L_{12}=L_{22}=830\ \mu\text{F}$ ;
- $C_1=22\ \mu\text{F}$ ;
- $C_0=5.5\ \mu\text{F}$ .

The proposed system with coupled and uncoupled inductors will be designed and tested by computer simulations. Detailed simulations analysis for the current and voltage ripple of the converter will be performed and, a laboratory prototype will be built and tested for coupled inductors to validate the improved converter.

### 4.3. Simulation of the two-phase hybrid Boost DC-DC L-converter

The simulation models of the two-phase hybrid Boost L-converter with coupled and uncoupled inductors were created in Caspoc simulation program to verify its theoretical properties. The input power supply is modelled by a constant voltage source  $U_{in}$ . The gate signals for the MOSFETs are generated by using 2 squarewave signal generators. According to the duty ratio, switching sequences of each phase can be overlapped or not. All the components, including MOSFETs, diodes, coupled inductors are assumed to be ideal. It is important to note that components used in the simulation have the same values to the components purchased for the hardware prototype.

Models of multiphase boost converters with uncoupling and direct coupling will be compared through simulation.

Table 4.1, Table 4.2, and Table 4.3 compare the simulation results for multiphase hybrid Boost L-converter in the case of uncoupled and directly coupled inductors.

Table 4.1. Simulation results for uncoupled and directly coupled inductor  $d=1/3$

Parameters	Two-phase converter uncoupled inductor			Two-phase converter coupled inductor		
	Average	Ripple	Ripple [%]	Average	Ripple	Ripple [%]
$i_{L11}$	1.856	0.485	23.1	1.856	0.245	12.37
$i_{L12}$	1.833	0.487	23.4	1.859	0.244	12.31
$I_{Out}$	2.477	0.019	0.76	2.485	0.017	0.68
$U_{out}$	118.9155	0.911	0.76	119.3	0.84	0.70

Table 4.2. Simulation results for uncoupled and directly coupled inductor  $d=1/2$ 

Parameters	Two-phase converter uncoupled inductor			Two-phase converter coupled inductor		
	Average	Ripple	Ripple [%]	Average	Ripple	Ripple [%]
$i_{L11}$	2.501	0.485	17.67	2.505	0.243	9.25
$i_{L12}$	2.498	0.486	17.73	2.496	0.243	9.28
$I_{Out}$	2.499	0.002	0.08	2.499	0.001	0.04
$U_{out}$	119.96	0.118	0.09	119.96	0.063	0.05

Table 4.3. Simulation results for uncoupled and directly coupled inductor  $d=2/3$ 

Parameters	Two-phase converter uncoupled inductor			Two-phase converter coupled inductor		
	Average	Ripple	Ripple [%]	Average	Ripple	Ripple [%]
$i_{L11}$	2.993	0.493	15.21	2.939	0.247	8.06
$i_{L12}$	2.979	0.493	15.28	2.934	0.247	8.07
$I_{Out}$	1.977	0.023	1.15	1.976	0.019	0.95
$U_{out}$	148.301	1.698	1.13	148.25	1.412	0.94

The results presented in the Table 4.1, Table 4.2, and Table 4.3 demonstrates that the inductor current ripple is not reduced even with the interleaved PWM method, unless the inductors are coupled.

The directly coupled interleaved Boost L-converter effectively reduces the inductors current ripple by approximately two times compared to that of uncoupled inductors. Therefore, two-phase Boost L-converter with coupled inductors provide a reduced inductor current ripple, two cores for the inductors instead of 4, which lead to reduced parts count, volume and weight of the converter.

The simulated waveforms of two-phase Boost L-converter in the case of coupled inductors are presented. In Figure 4.7 the circuit diagram of the converter is presented.

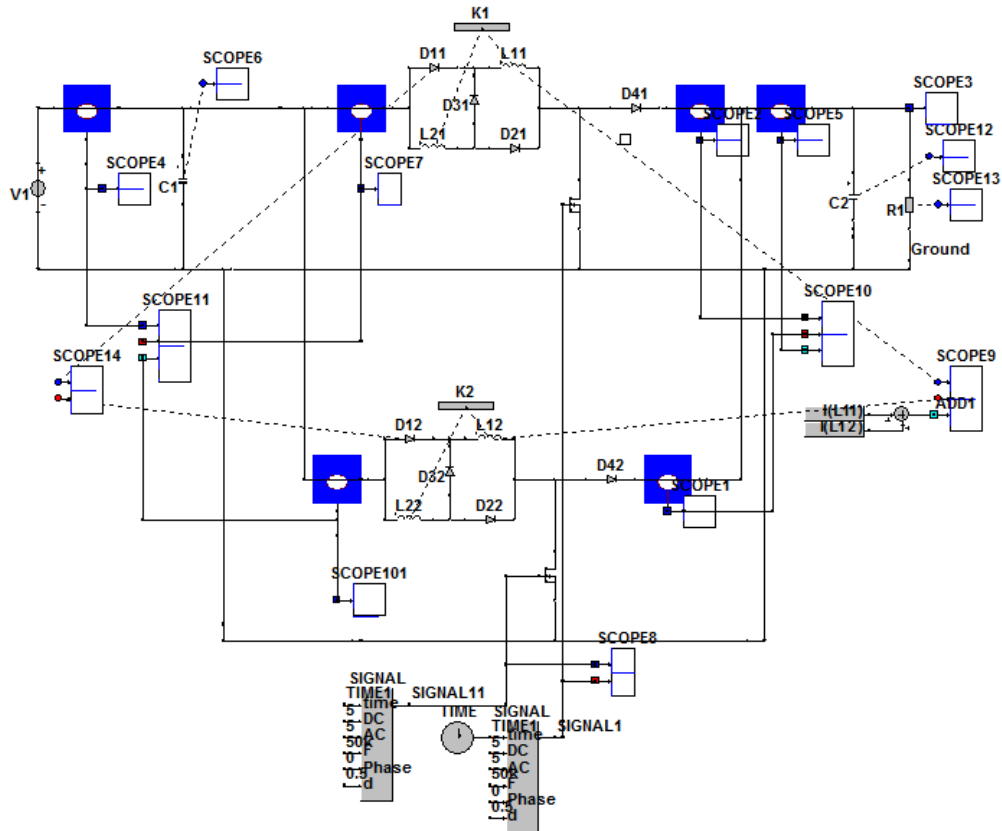


Figure 4.7. CASPOC circuit diagram for the two-phase hybrid Boost DC-DC L-converter coupled inductor

Figure 4.8 shows the resulted waveforms from Caspoc Simulation, based on the design parameters.  $U_{in}$ , in this case it is 60V,  $I_{In}=5A$ , resulting an input power  $P_{in}=300W$ .

In Figure 4.8 are presented the PWM pulses applied to switch 1, Signal 1, corresponding to first phase of the converter, respective the PWM pulses applied to switch 2, Signal 11, corresponding to the second phase of the converter. Further it is presented the overall input phase current which consists of the sum of all the input phase currents, in our case phase one and phase two. There is  $180^\circ$  phase shift between Signal1 and Signal11, so the inductor current  $I_{L11}$  and  $I_{L12}$  also exhibit  $180^\circ$  phase shift. The currents of phase one through inductors  $L_{11}$  and  $L_{21}$  are equal, also the currents of phase two through inductors  $L_{12}$  and  $L_{22}$  are equal. Here in Figure 4.8, fifth waveform is represented just one of them. It is continuing with the figure of switching current, and the voltage stresses of the switch which is the same value to that the output voltage.

Output current of phase 1, and phase 2 and the overall output phase current which consists of the sum of all the output phase currents, in our case phase one and phase two, are presented after voltage of the switch from Figure 4.8. In the last images the output capacitor current, and the output current and voltage of the converter are presented.



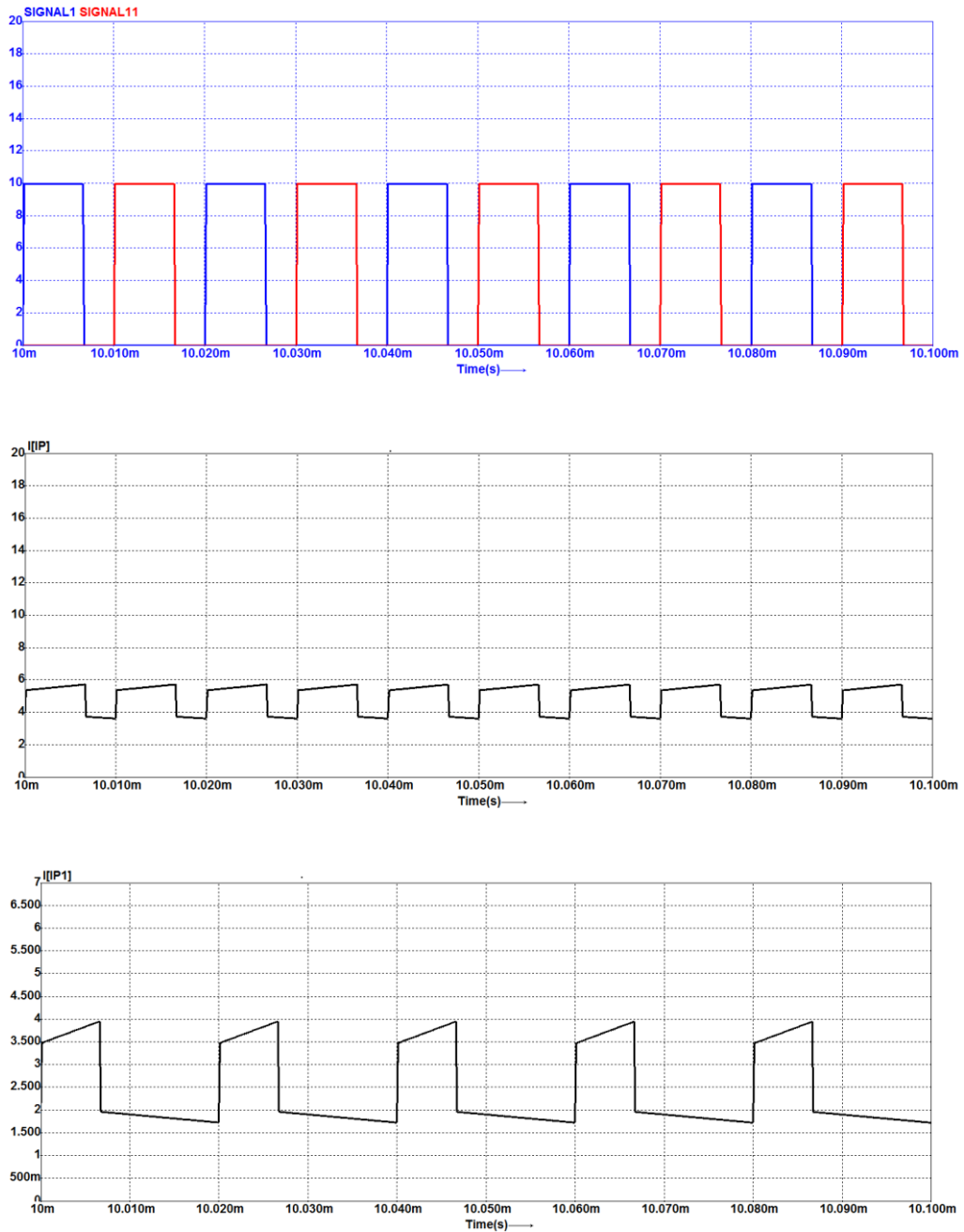


Figure 4.8. Simulation results for the two-phase hybrid Boost DC-DC L-converter with coupled inductors,  $d=33.3\%$

154 Multiphase Hybrid Boost DC-DC L-converter

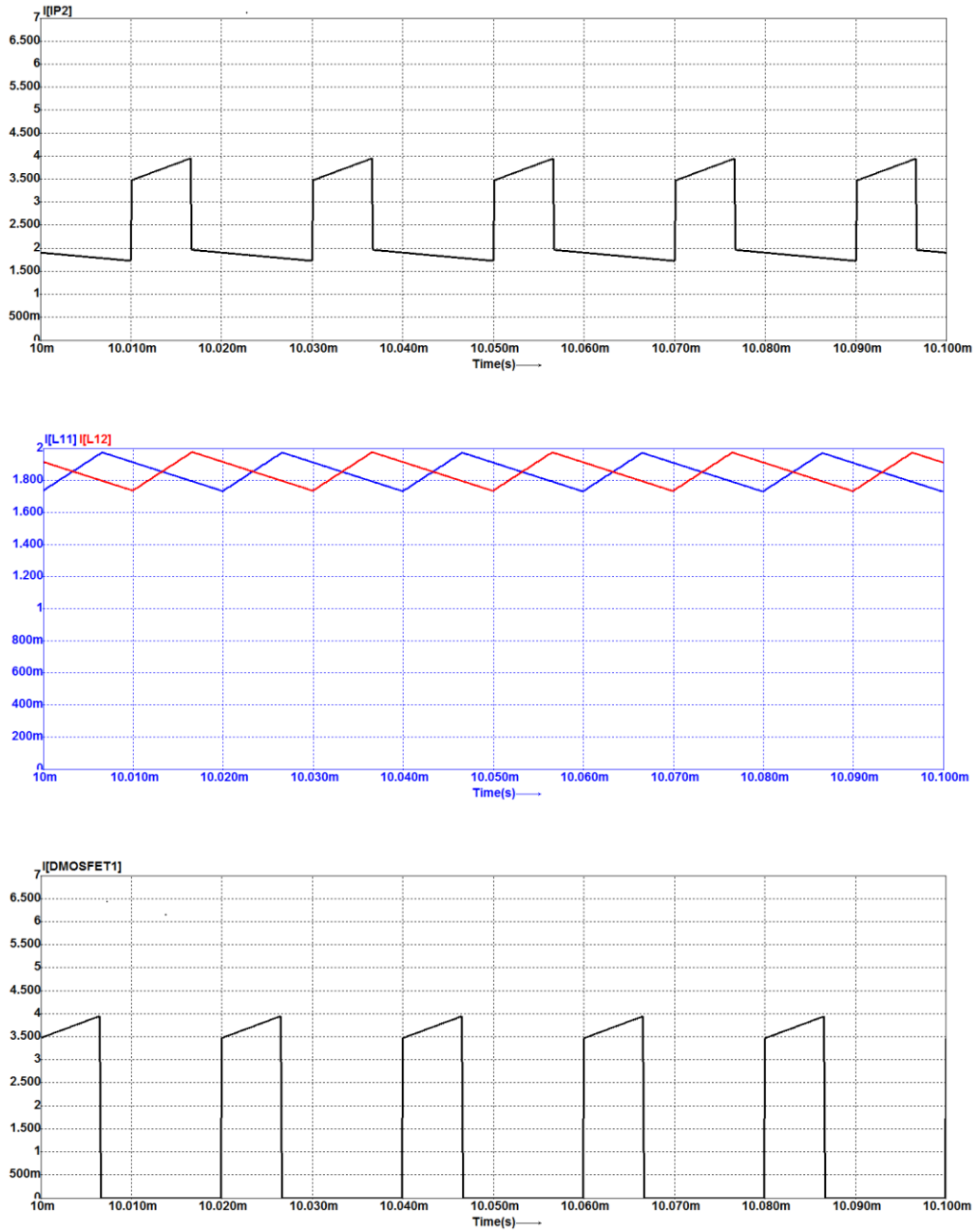


Figure 4.8. (continued 1) Simulation results for the two-phase hybrid Boost DC-DC L-converter with coupled inductors,  $d=33.3\%$

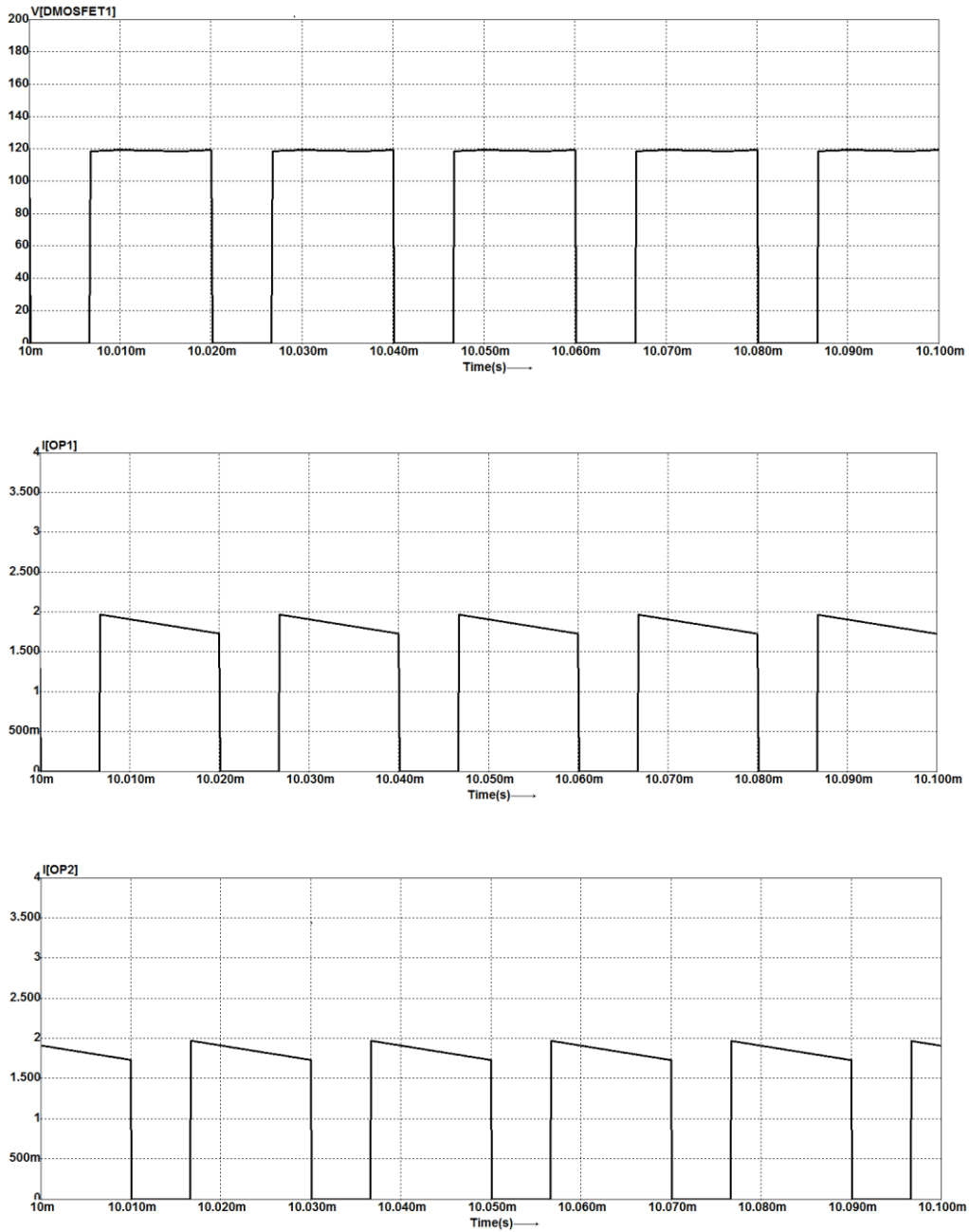


Figure 4.8. (continued 2) Simulation results for the two-phase hybrid Boost DC-DC L-converter with coupled inductors,  $d=33.3\%$

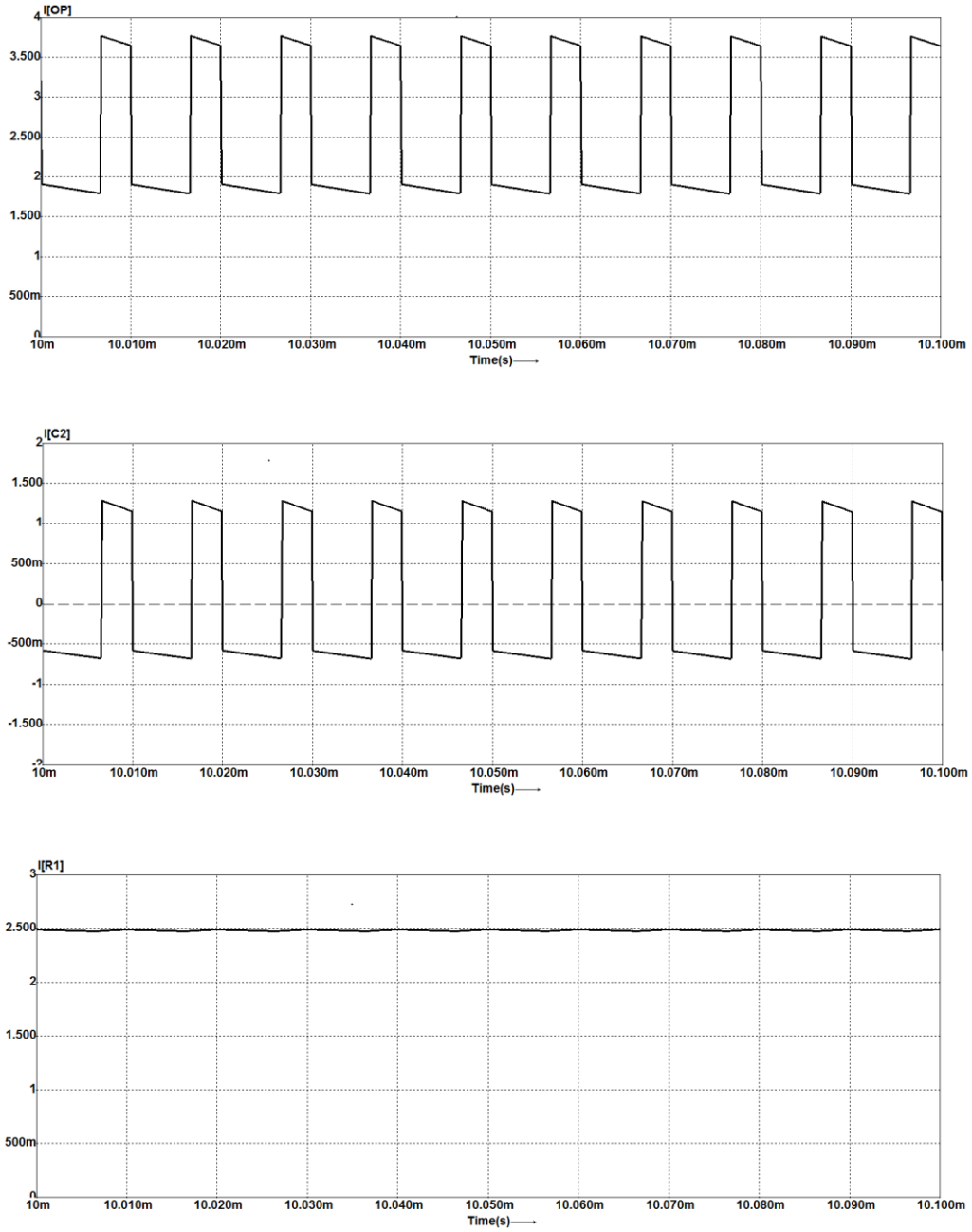


Figure 4.8. (continued 3) Simulation results for the two-phase hybrid Boost DC-DC L-converter with coupled inductors,  $d=33.3\%$

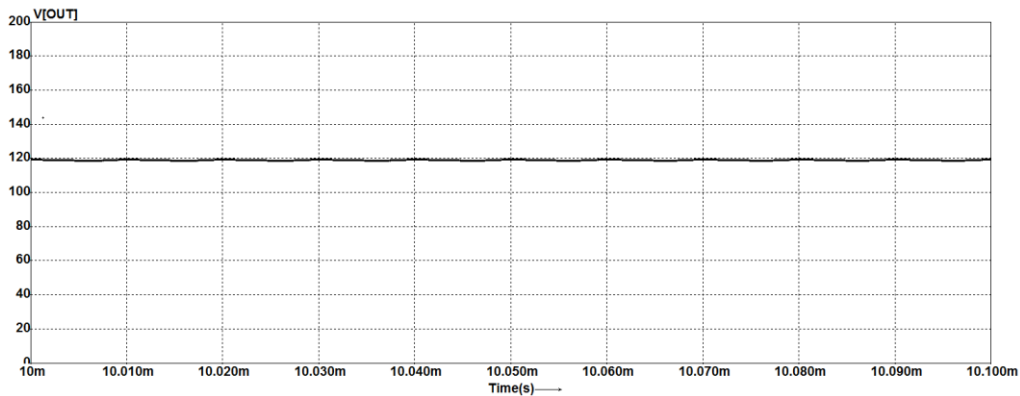


Figure 4.8. (continued 4) Simulation results for the two-phase hybrid Boost DC-DC L-converter with coupled inductors,  $d=33.3\%$

This up to down order: signal and signal 2,  $i_{IP}$ ,  $i_{IP1}$ ,  $i_{IP2}$ ,  $i_{L11}$  and  $i_{L12}$ ,  $i_{S1}$ ,  $U_{S1}$ ,  $i_{OP1}$ ,  $i_{OP2}$ ,  $i_{OP}$ ,  $i_{OC}$ ,  $i_{out}$  and  $U_{out}$

In the multiphase topology each inductance value is larger by a factor of "n". Also, the current in each inductor is smaller by a factor of "n", compared to a single phase Boost converter. In practice this means that the value of "n" inductors is almost equal to the value of single stage inductor.

The inductor current peak-to-peak ripple is measured to be 0.245A in first phase of the converter, and 0.244A in the second phase of the converter, fulfilling the 10-30% ripple requirement.

The peak-to-peak ripple input current is substantially reduced by interleaving. The current magnitude reduction can either reduce the input filter capacitor size or prolong the input capacitor life time by reducing the power loss of the electrolytic capacitor. Considering both the magnitude and the frequency factors, the input capacitor filter requirements can be significantly reduced.

In addition, the capacitor current ripple and the overall input and output phase current ripple frequency is increased 2 times compared to the switching frequency. However, the input and output phase currents of phase 1 and 2 are still at switching frequency.

For an n-phase converter the improvement in frequency will be even more. The capacitor current ripple and the overall input and output phase current ripple frequency will be  $n \cdot f_s$ , where  $f_s$  is the operating/switching frequency of each converter.

Figure 4.9 shows the resulted waveforms from Caspoc Simulation, for an input voltage  $U_{in}=40V$ ,  $I_{in}=7.5A$ , resulting an input power  $P_{in}=300W$ .

First, in Figure 4.9 the PWM pulses applied to switch 1, Signal 1, and the PWM pulses applied to switch 2, Signal 11, are presented. There is  $180^\circ$  phase shift between Signal1 and Signal11. Further it is presented the overall input phase current, the input current of phase 1, and the input current of phase 2.

The inductor current  $I_{L11}$  and  $I_{L12}$  has  $180^\circ$  phase shift. The currents of phase one through inductors  $L_{11}$  and  $L_{21}$  are equal, also the currents of phase two through inductors  $L_{12}$  and  $L_{22}$  are equal. Here in the figure is represented only one of them. Current and the voltage associated to the switch which is depicted in Figure 4.9. The switch voltage stress equals the output voltage.

Output current of phase 1, and 2 and the overall output phase current, are presented after the switch voltage. It is obvious from the figure that the ripple peak-

to-peak input and output currents at this duty cycle are the smallest. In the last images are presented the output capacitor current, and the output current and voltage of the converter. The ripple of the output current and voltage of the converter at this duty cycle is minimal, almost inexistent.

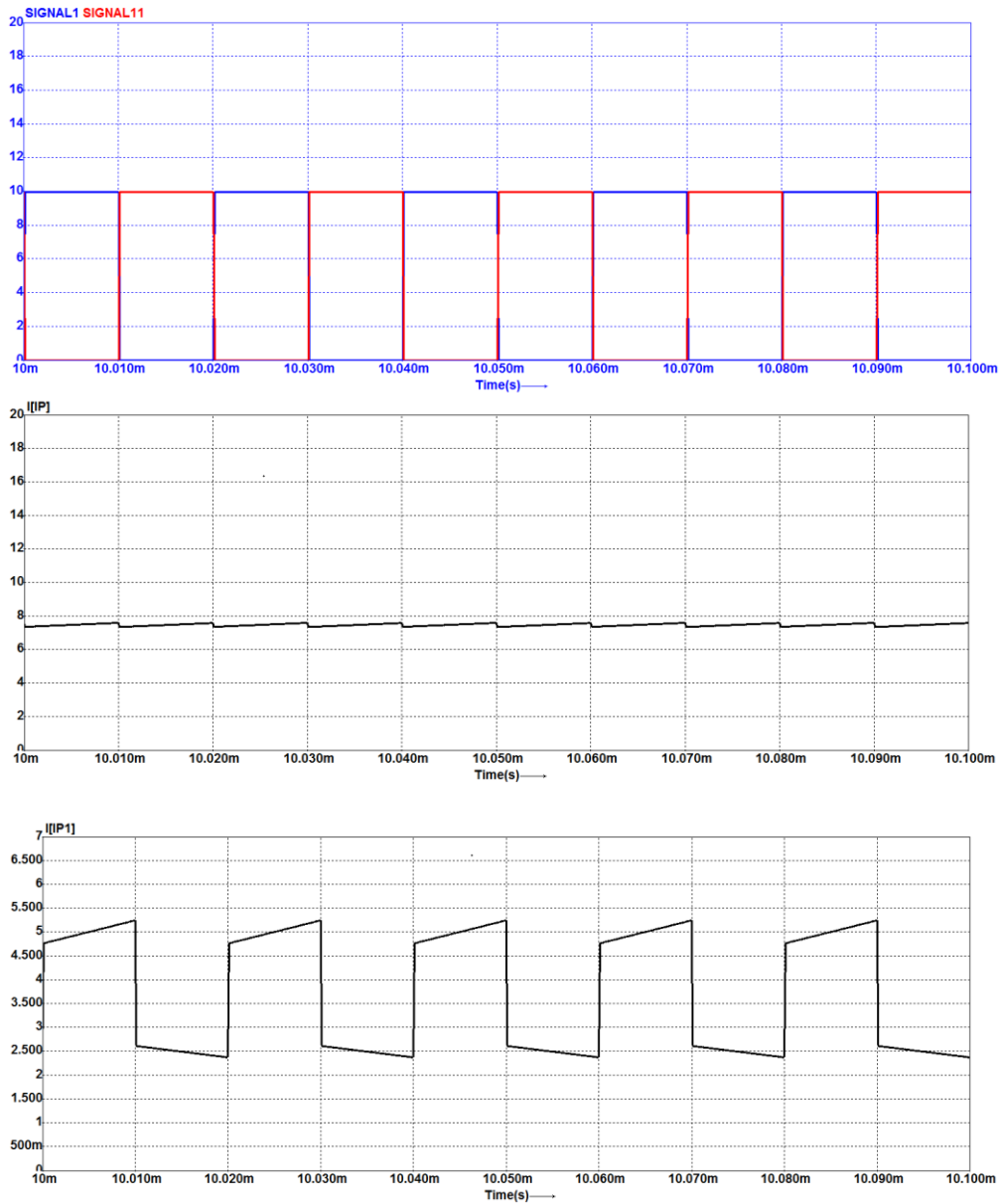


Figure 4.9. Simulation results for the two-phase hybrid Boost DC-DC L-converter with coupled inductors,  $d=50\%$

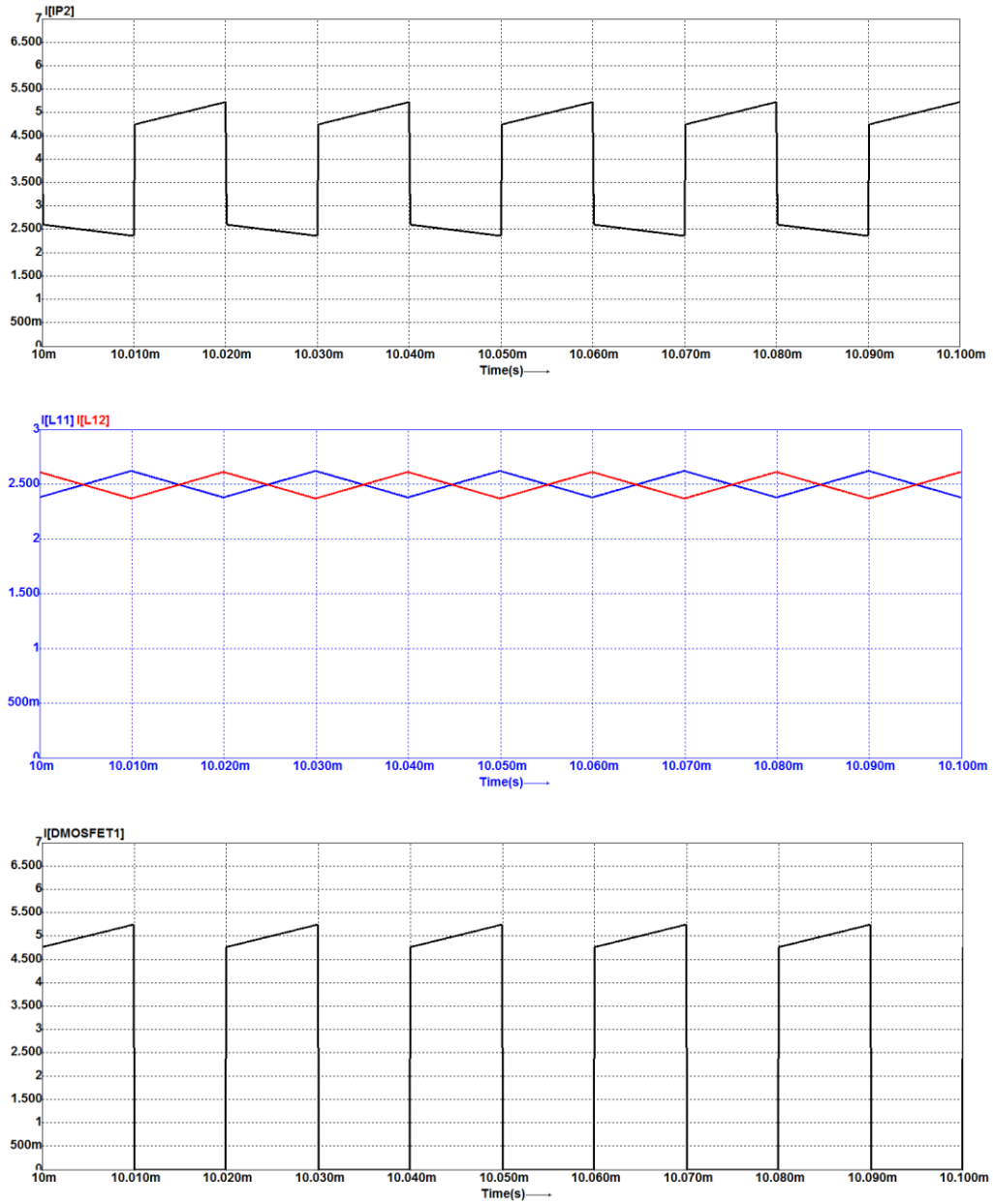


Figure 4.9. (continued 1 ) Simulation results for the two-phase hybrid Boost DC-DC L-converter with coupled inductors,  $d=50\%$

## 160 Multiphase Hybrid Boost DC-DC L-converter

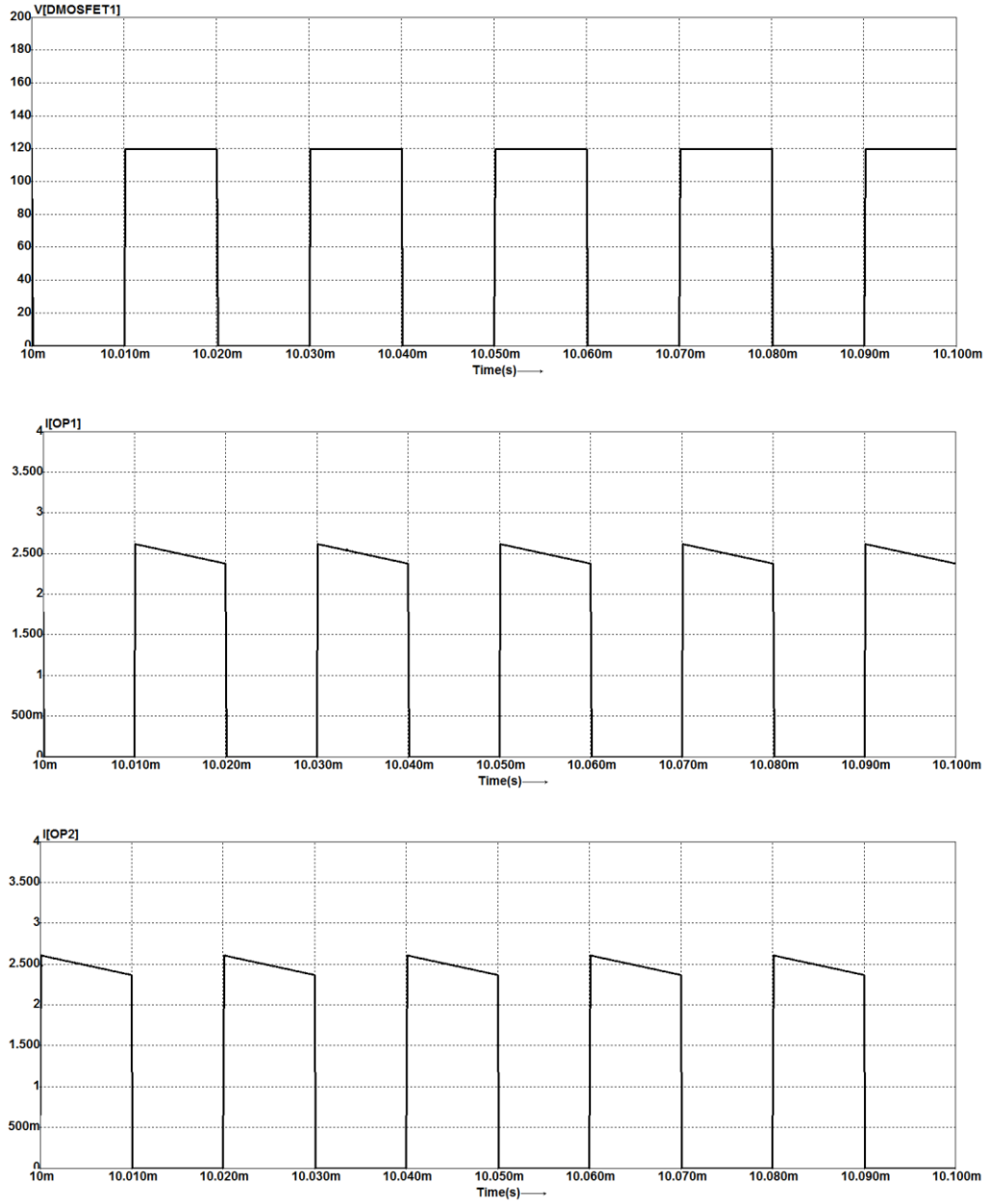


Figure 4.9. (continued 2 ) Simulation results for the two-phase hybrid Boost DC-DC L-converter with coupled inductors,  $d=50\%$



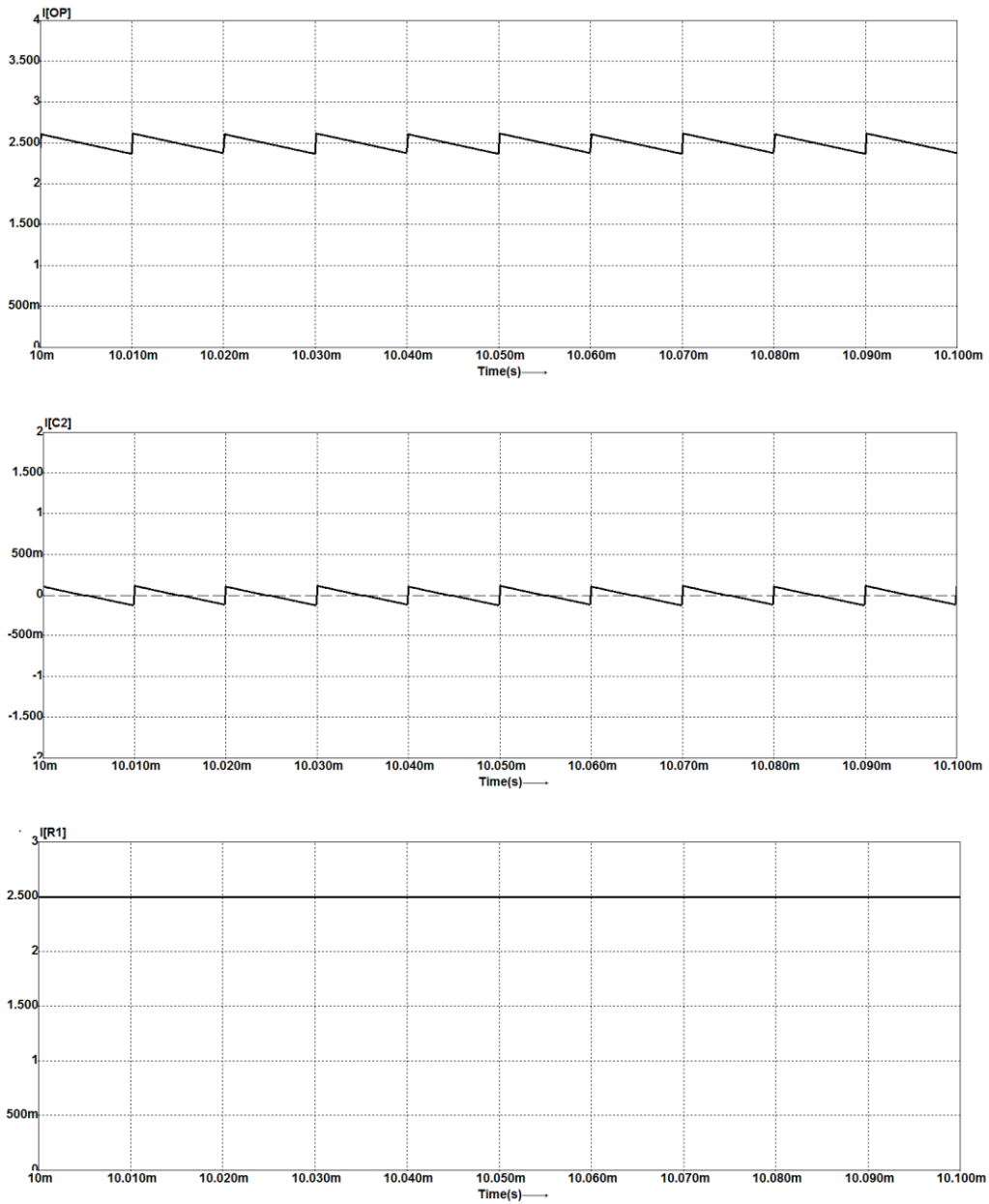


Figure 4.9. (continued 3 ) Simulation results for the two-phase hybrid Boost DC-DC L-converter with coupled inductors,  $d=50\%$

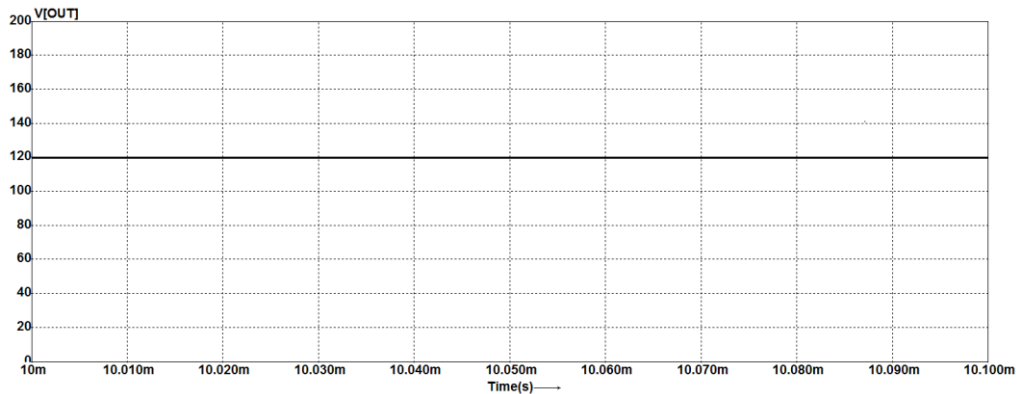


Figure 4.9. (continued 4 ) Simulation results for the two-phase hybrid Boost DC-DC L-converter with coupled inductors,  $d=50\%$

This up to down order: signal 1 and signal 2,  $i_{IP}$ ,  $i_{IP1}$ ,  $i_{IP2}$ ,  $i_{L11}$  and  $i_{L12}$ ,  $i_{S1}$ ,  $U_{S1}$ ,  $i_{OP1}$ ,  $i_{OP2}$ ,  $i_{OP}$ ,  $i_{OC}$ ,  $i_{out}$  and  $U_{out}$

The amount of ripple current cancellation depends on the operating duty cycle. The sum of the ripple input phase currents is smaller than the individual ripple phase currents of phase 1, and phase 2. In case of a 50% duty cycle operation, the ripple of the output current and the output voltage of a two-phase Boost converter cancel out completely.

The value of the currents and the ripple of the current is approximately the same to the one resulted from the calculations. This means that the simulation validated the theoretical considerations.

The resulted waveforms from Caspoc Simulation, for  $U_{in}=30V$ ,  $I_{in}=10A$ , resulting an input power  $P_{in}=300W$  is presented in Figure 4.10.

In Figure 4.10 the PWM pulses applied to switch 1, Signal 1, and the PWM pulses applied to switch 2, Signal 11, are presented first. How it is obvious from the figure the PWM pulses are overlapped. Further it is presented the overall input phase current, the input current of phase 1, and the input current of phase 2.

The phase shift between Signal1 and Signal11 is  $180^\circ$ , so the inductor current  $i_{L11}$  and  $i_{L12}$  also has  $180^\circ$  phase shift. The currents of phase one through inductors  $L_{11}$  and  $L_{21}$  are equal, also the currents of phase two through inductors  $L_{12}$  and  $L_{22}$  are equal. Here in the figure is represented only one of them. Current and the voltage associated to the switch are depicted in Figure 4.10. The switch voltage stress equals the output voltage.

Output current of phase 1, and 2 and the overall output phase current are presented after the switch voltage. The output capacitor current, and the output current and voltage of the converter are presented in the last images.

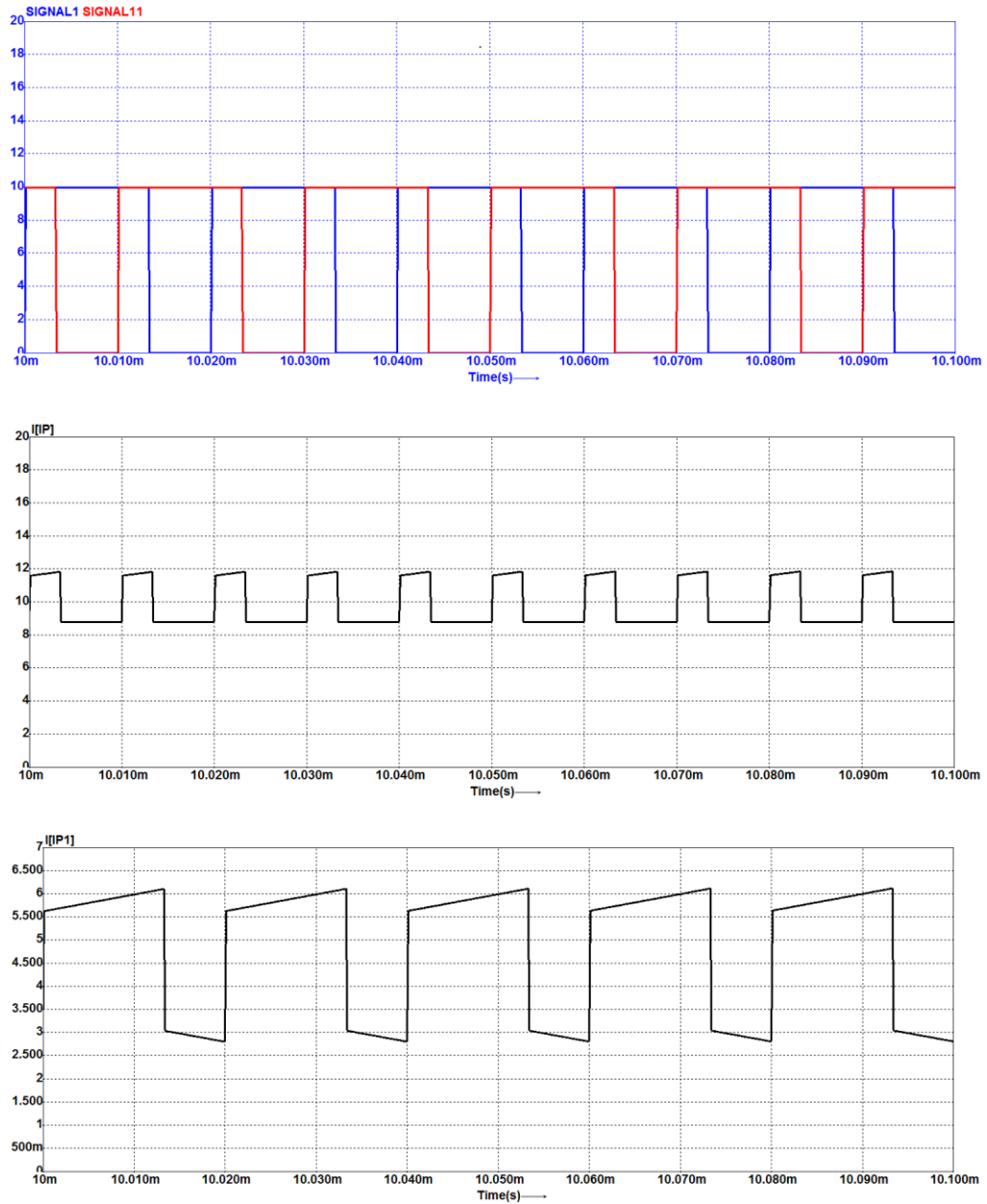


Figure 4.10. Simulation results for the two-phase hybrid Boost DC-DC L-converter with coupled inductors,  $d=66.7\%$

## 164 Multiphase Hybrid Boost DC-DC L-converter

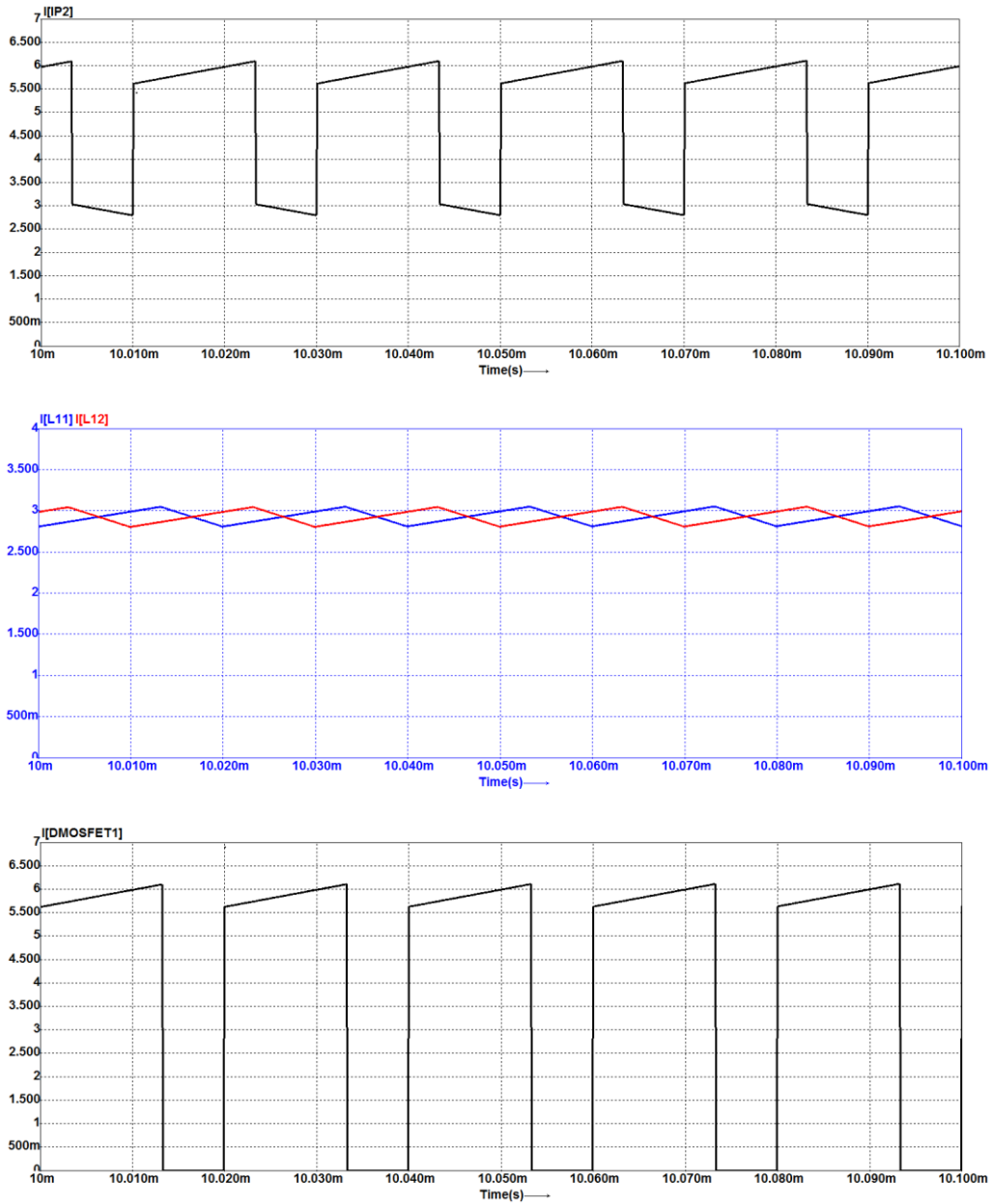


Figure 4.10. (continued 1) Simulation results for the two-phase hybrid Boost DC-DC L-converter with coupled inductors,  $d=66.7\%$

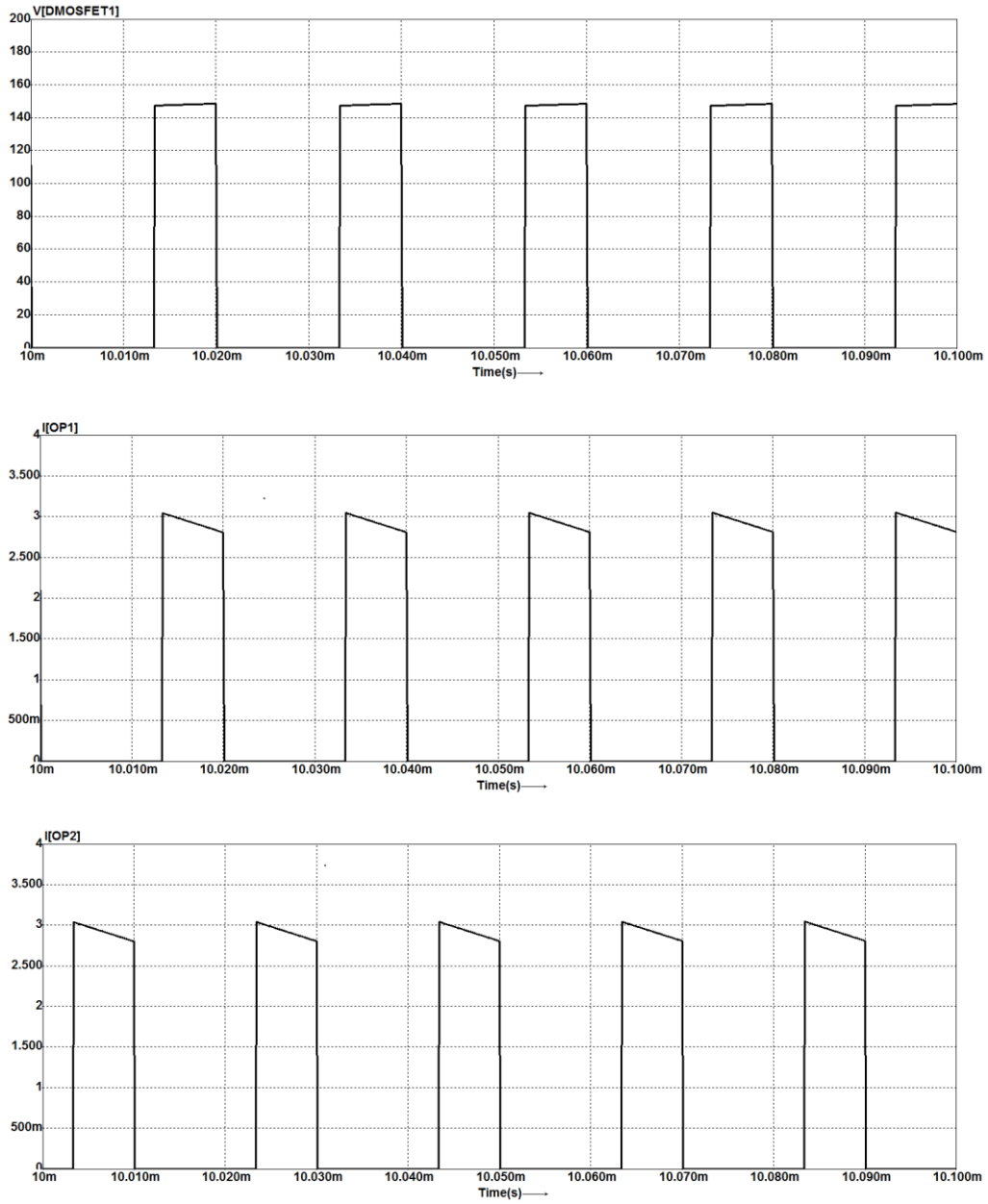


Figure 4.10. (continued 2) Simulation results for the two-phase hybrid Boost DC-DC L-converter with coupled inductors,  $d=66.7\%$

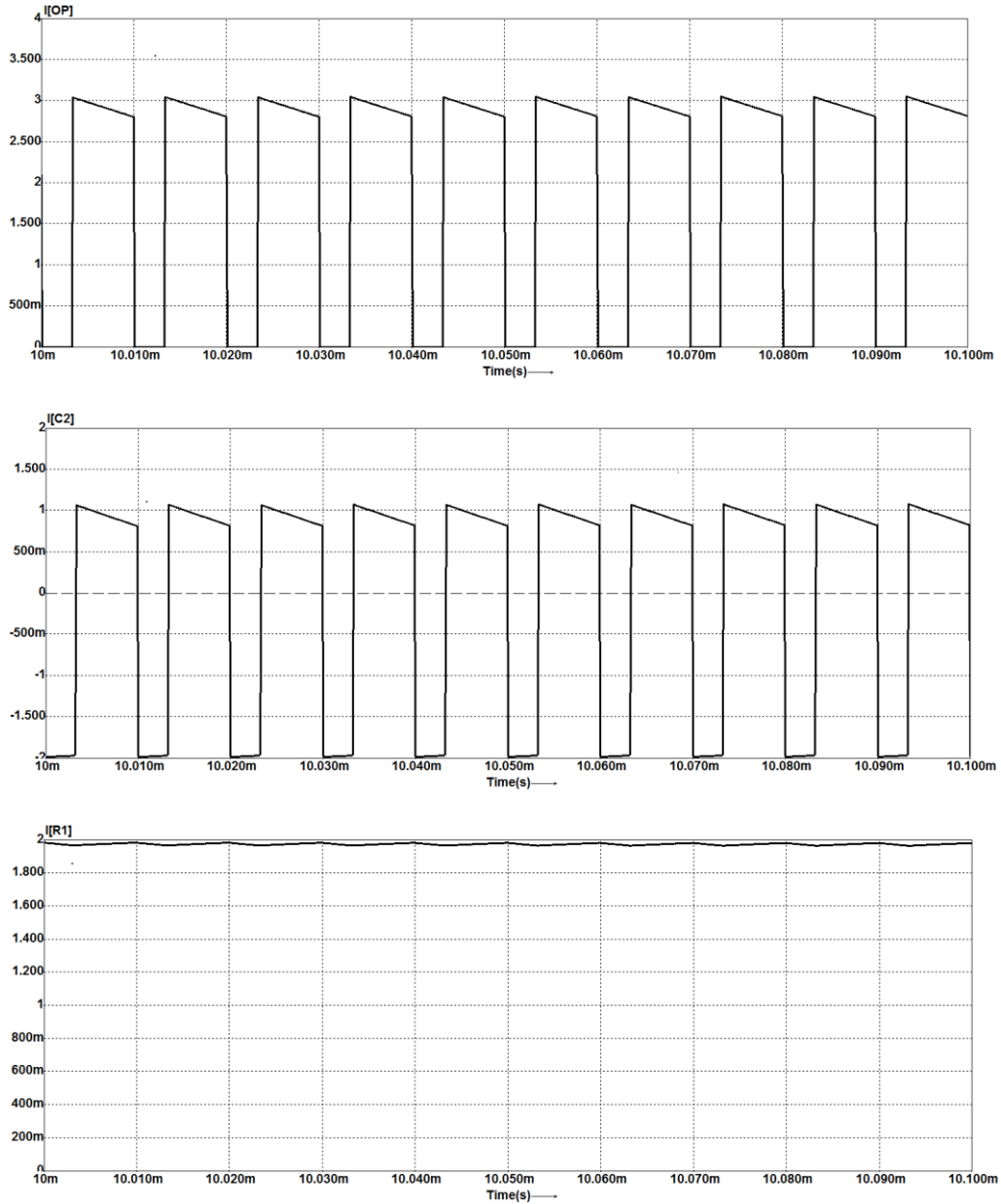


Figure 4.10. (continued 3) Simulation results for the two-phase hybrid Boost DC-DC L-converter with coupled inductors,  $d=66.7\%$

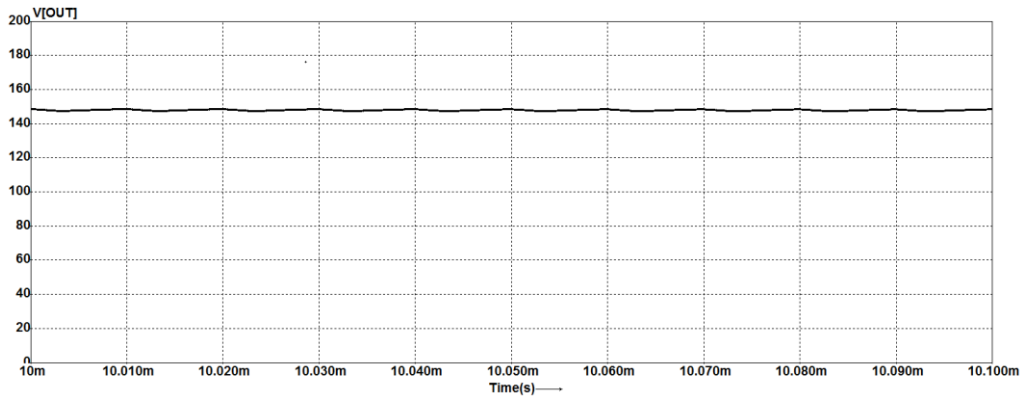


Figure 4.10. (continued 4) Simulation results for the two-phase hybrid Boost DC-DC L-converter with coupled inductors,  $d=66.7\%$   
 This up to down order: signal 1 and signal 2,  $i_{IP}$ ,  $i_{IP1}$ ,  $i_{IP2}$ ,  $i_{L11}$  and  $i_{L12}$ ,  $i_{S1}$ ,  $U_{S1}$ ,  $i_{OP1}$ ,  $i_{OP2}$ ,  $i_{OP}$ ,  $i_{OC}$ ,  $i_{out}$  and  $U_{out}$

Two-phase Boost L-converter operates with the same switching frequency like the single phase Boost L-converter, but, the switches operate with a phase shift between them.

The switching signals for the main switches of two-phase Boost L-converter having a phase shift of 180 degrees between the switching signals is presented in Figure 4.9. The result of the phase delay allows multiphase configurations to exhibit higher overall efficiency due to ripple cancellation; smaller input filter requirements, smaller output filter requirements and smaller output voltage ripple. The output voltage ripple is reduced because the output frequency is increased by the number of phases compared to the individual switching frequency.

Higher frequency makes the output ripple easier to be filtered which allows for smaller components and further increase in efficiency. The switching frequency of each phase is 50 kHz, thus creating an expected output frequency of 100 kHz due to frequency multiplication effect of two-phase topology. Looking at Figure 4.10, a full period occurs approximately between 10.013ms and 10.023ms and therefore:

$$F_{Out} = \frac{1}{(10.023 - 10.013) \cdot 10^{-3}} = 100kHz \quad (4.14)$$

Through this it is demonstrated the frequency multiplication that takes place at the output phase of the converter.

In the same way the author demonstrates that interleaving can also reduce significantly the input filter capacitor requirement or prolong the input capacitor life time by reducing the power loss of the electrolytic capacitor. The comparison between the interleaved two-phase hybrid Boost L-converter and the single phase hybrid Boost L-converter has been done using simulation and through the measurements on a laboratory prototype.

The input ripple current waveform of a single-phase Boost L-converter and of a two-phase Boost L-converter is shown in Figure 4.11 and Figure 4.12 respectively.

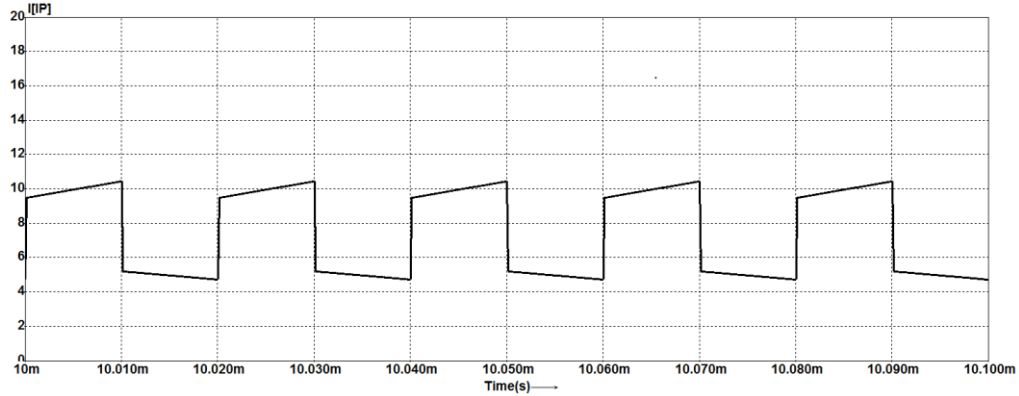


Figure 4.11. Simulation waveform for input current for the single phase hybrid Boost L-converter in the case of  $d=50\%$

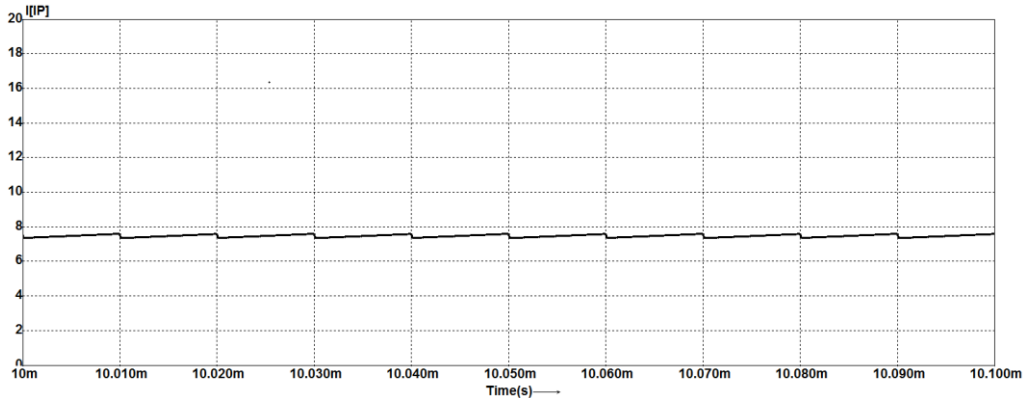


Figure 4.12. Simulation waveform for input current for the two-phase hybrid Boost L-converter in the case of  $d=50\%$

In Figure 4.11 the higher magnitude of ripple from single phase is obvious. Through multiphase not only the ripple magnitude is reduced, but the ripple frequency is increased with the number of phases, in this example two times. Considering both the magnitude and the frequency factors, the input capacitor filter can significantly be reduced.

Figure 4.13 and Figure 4.14 show the output current ripple for single phase and two-phase respectively.



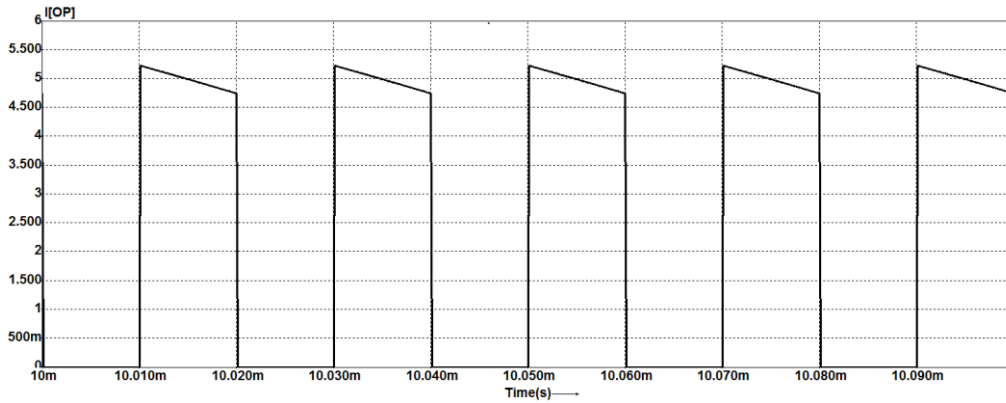


Figure 4.13. Simulation waveform for output current for a single phase hybrid Boost L-converter in the case of  $d=50\%$

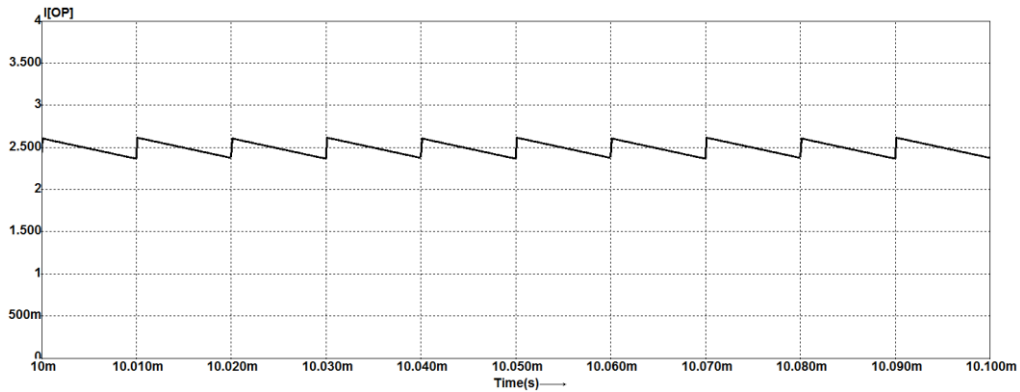


Figure 4.14. Simulation waveform for output current for a two-phase hybrid Boost L-converter in the case of  $d=50\%$

The output current ripple for single phase is again higher than that of the coupled two-phase converter. This leads to increased filtering effort at the output of the single phase converter. In Table 4.4 a comparison between the single phase converter and the two-phase Boost L-converter, at  $d=33.3\%$  is presented.

Table 4.4. Simulation results for the coupled inductor single and two-phase Boost L-converters when  $d=1/3$

Parameters	Single phase converter coupled inductor		Two-phase converter coupled inductor	
	Average	Peak-to-peak Ripple	Average	Peak-to-peak Ripple
$i_{IP}$	5.613	4.069	4.706	2.116
$i_{IP1}$			2.847	2.22
$i_{IP2}$			2.851	2.23
$i_{L11}$	3.702	0.244	1.856	0.245
$i_{L12}$			1.859	0.244
$i_{OP1}$	1.911	3.822	0.988	1.977

170 Multiphase Hybrid Boost DC-DC L-converter

$i_{OP2}$			0.989	1.979
$i_{OP}$			2.785	1.983
$i_{OC}$			0.308	1.983
$I_{Out}$	2.474	0.068	2.485	0.017
$U_{out}$	118.74	3.244	119.3	0.84

Table 4.4. (continued 1) Simulation results for the coupled inductor single and two-phase Boost L-converters when  $d=1/3$

From Figure 4.11 - Figure 4.14 it can be observed that the ripple frequency at the input and output is twice than that in single phase case, therefore increasing the number of phases, the frequency of input and output currents also increases. This allows for a faster transient response, and less filtering capacitors at both the input and the output. The peak-to-peak ripple of the input current, output current and output voltage of the converter is lower in the two-phase case. The input current ripple in single phase is  $\sim 50\%$  higher than that in two-phase. The ripple in the output voltage of two-phase converter is approximately  $\sim 75\%$  lower than that in single phase, Table 4.4. Also the output current ripple is  $\sim 75\%$  lower than that in single phase.

As observed from Table 4.4, for the same value of the inductance, the inductor current in two phase is shared equally among the inductors, and peak-to-peak ripple has the same value in the case of single and two-phase converter because both converters use the coupled inductors. The value of the capacitor decreases to half than the value in single phase, due to the use of multiphase interleaving.

Even if the converter has more components than in single phase, the value of the components is optimized, making the converter more compact.

The current ripples of the switches and the diodes are still large. The switch voltage stress is equal to the output voltage, which is large in high output voltage applications. The factor that decides in choosing the number of phases is that the ripple content, which is reduces with the increase the number of phases. Also there is a restriction to the increase in the number of phases because if the number of phases is further increased without significant reduction in ripple content, the number of the components increases and hence the cost increases, too.

Examining the above data the advantages of multiphase Boost L-converter are evident. One important advantage provided by the multiphase converter is that the load current splits among the  $n$ -phases of the multiphase converter, allowing the heat generation on each of the switches to be spread across a larger area. The output current and voltage ripples are reduced in multi-phase with an increase in efficiency.

Therefore, through this, the author demonstrates that two-phase converter is a better choice. The laboratory prototype was built and tested to demonstrate the concept.

#### 4.4. Practical Measurements for the two-phase hybrid Boost DC-DC L-converter

The technical description and the components value of the experimental prototype of a two-phase Boost L-converter were presented in Chapter 4.3. In order to verify and validate the simulation results already presented an actual hardware implementation has been developed.

In Figure 4.15 the experimental setup of the converter is shown. The rated power of the circuit is 300W and the output voltage is 120V. In the circuit, the inductor coils of the same phase are coupled to each other. Because of this, the effort of the inductors is clearly reduced. The connections to the inductors are provided with loops for simple current measurements. For the measurements of the current in the capacitors semiconductor current transformers were used. The transformer-transmission factor of 20 is used in each case. At the output of the transformers, the currents are measured with current probes.

The semiconductor devices chosen for constructing the two-phase interleaved Boost L-converter are the HiPerFET IXFT50N20 power MOSFET transistor and HiPerFRED DPG10J200PM diode.

All switches operate at a constant switching frequency,  $f_s$  equal to 50 kHz. Each phase is driven by gate drive signals and for gate driving the TLP250 circuit is used.

The cores used are ETD 59N87 from Siemens Matsushita Components. In the two-phase converter the author used two cores. Each channel shares a core. The phases of the converter have the same switching frequency  $f_s$ , but the phases are shifted by  $360^\circ/n$ . The input and output of the each converter are paralleled such that the ripple frequency at the input and output is  $n \cdot f_s$ .

The efficiency plot resulted from the hardware measurements will also be presented.

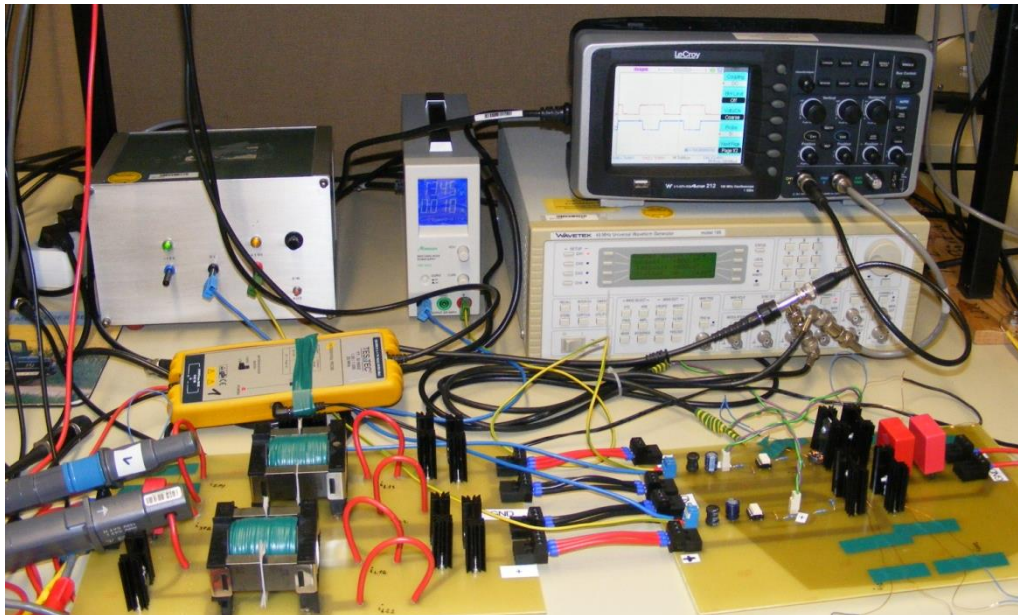


Figure 4.15. Image of the experimental two-phase hybrid Boost DC-DC L-converter [120]

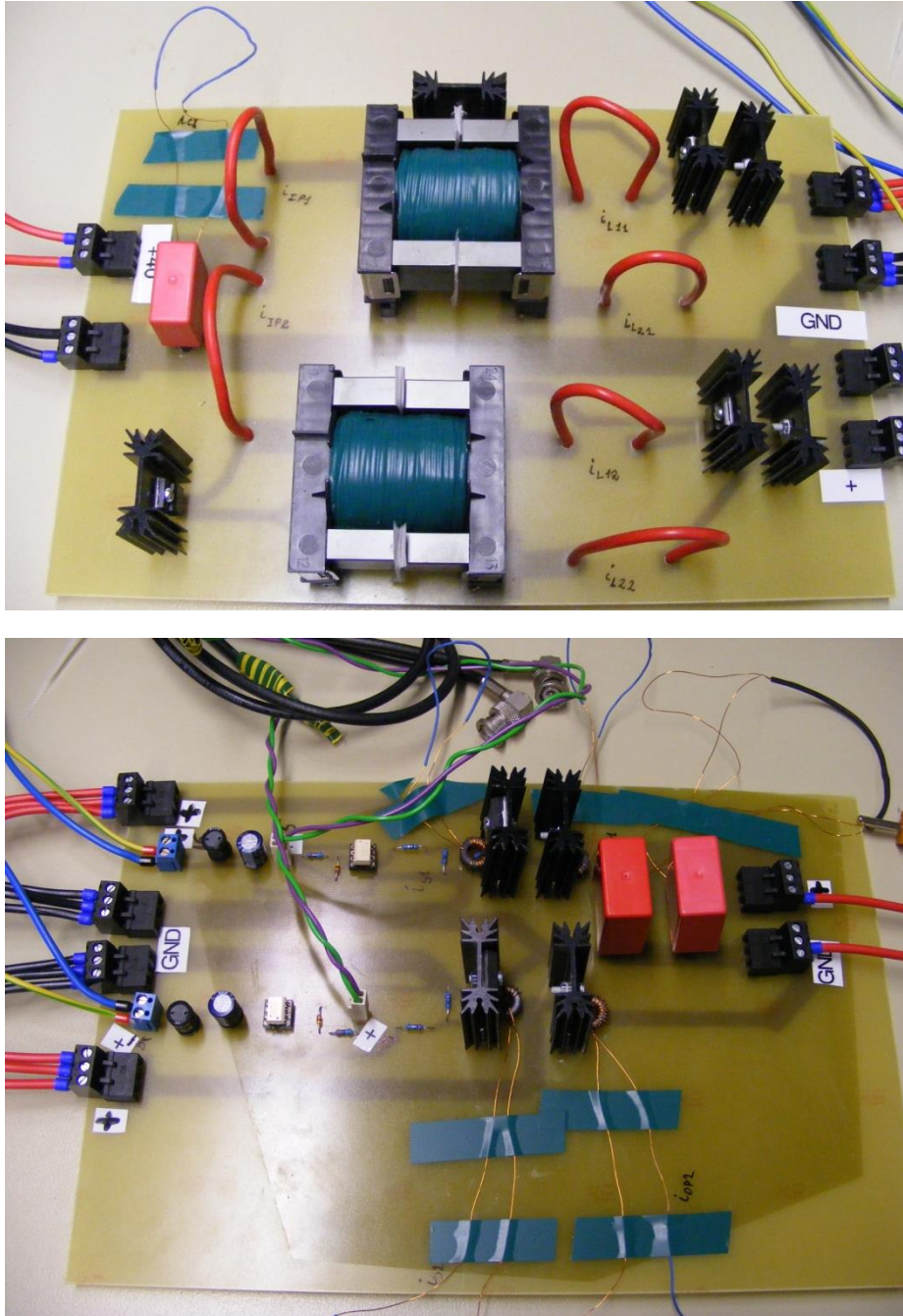


Figure 4.15 (continued 1) Image of the experimental two-phase hybrid Boost DC-DC L-converter [120]

The voltage and current waveforms of the converter with duty cycle  $d=1/3$  are first presented.

In Figure 4.16 the input current and voltage are shown. The input voltage is 60V and the dc-current is 5A. With these values, obviously the power is 300W. The switches operate with a phase shift between the switch gate drivers. For two phase converter the shift between the phases is half of the switching period. This can be seen better from the Figure 4.17 and Figure 4.18, where the current and voltage of the switch in the first and second phase are respectively represented. During the on state the current is twice the current in the inductor coils. In Figure 4.19 the input phase current  $i_{IP}$  which consists of the sum of the currents  $i_{IP1}$  and  $i_{IP2}$  are represented. The current in the two inductor coils of first and the second phases is represented in Figure 4.20. The dc values of the inductor currents are slightly smaller than 2A, approximately equal with the simulated value. The output currents of the individual phases are presented in Figure 4.21. In Figure 4.22 the output current and output voltage are shown.

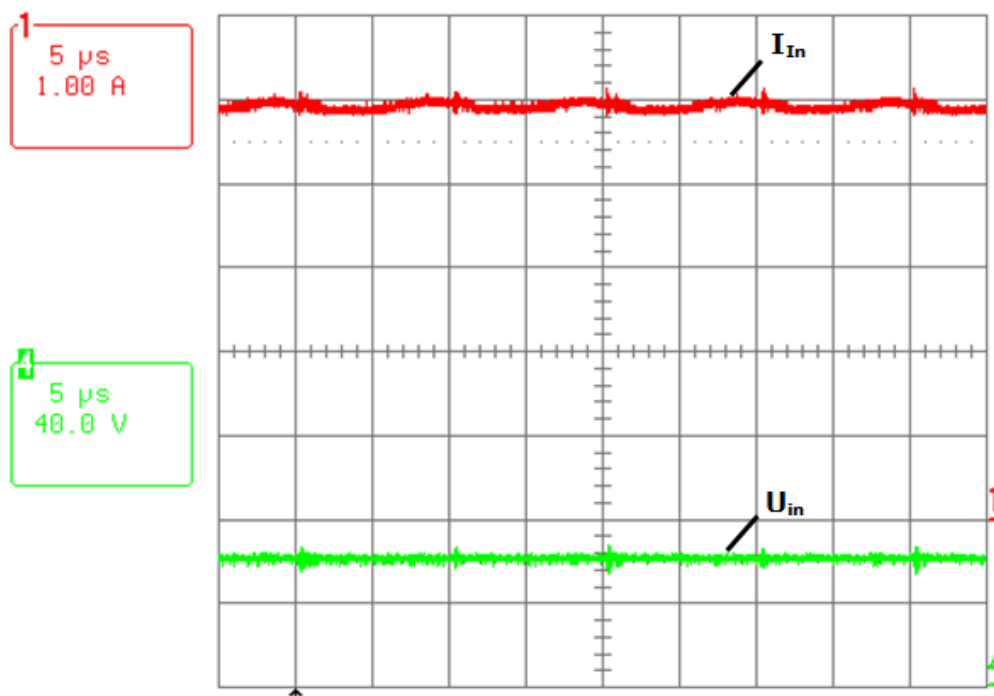


Figure 4.16. Input current and voltage waveforms when  $d=1/3$  [120]

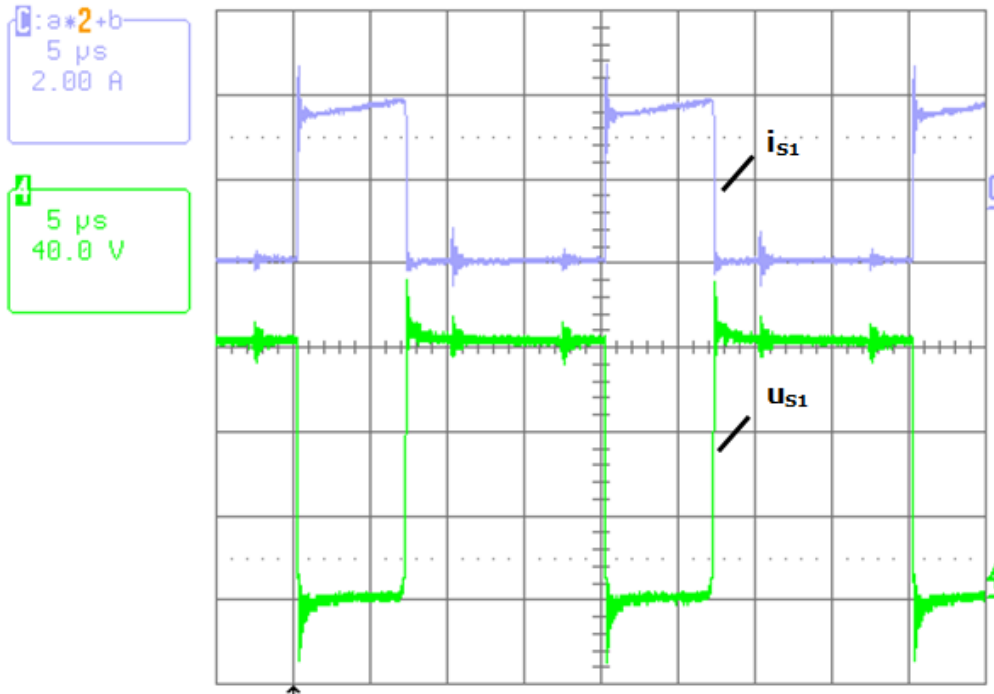


Figure 4.17. MOSFET current and voltage of first phase switch when  $d=1/3$  [120]

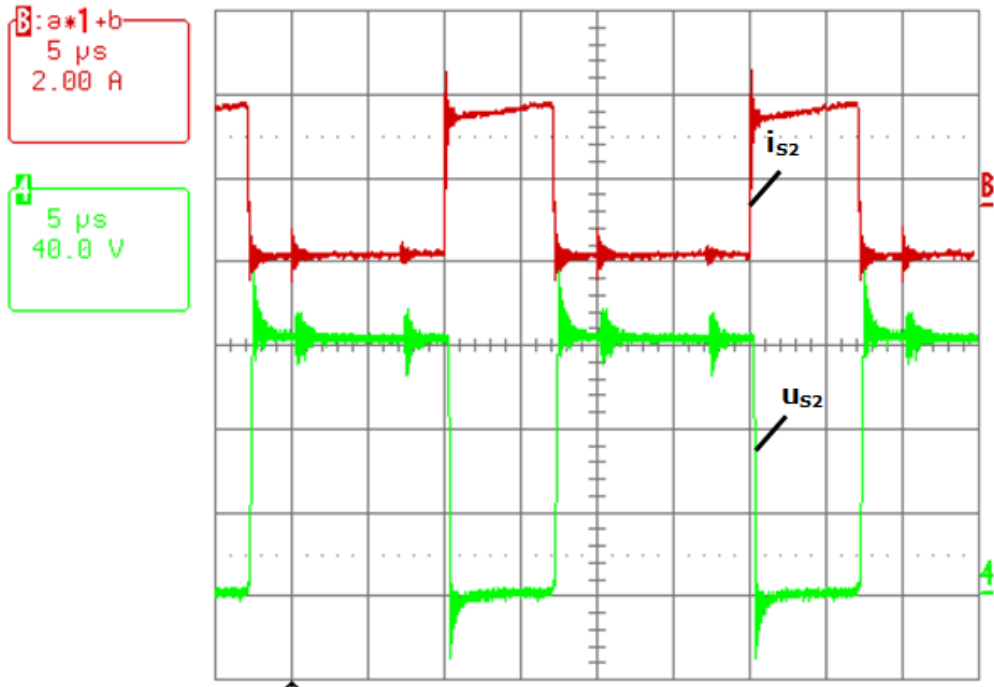


Figure 4.18. MOSFET current and voltage of second phase switch when  $d=1/3$

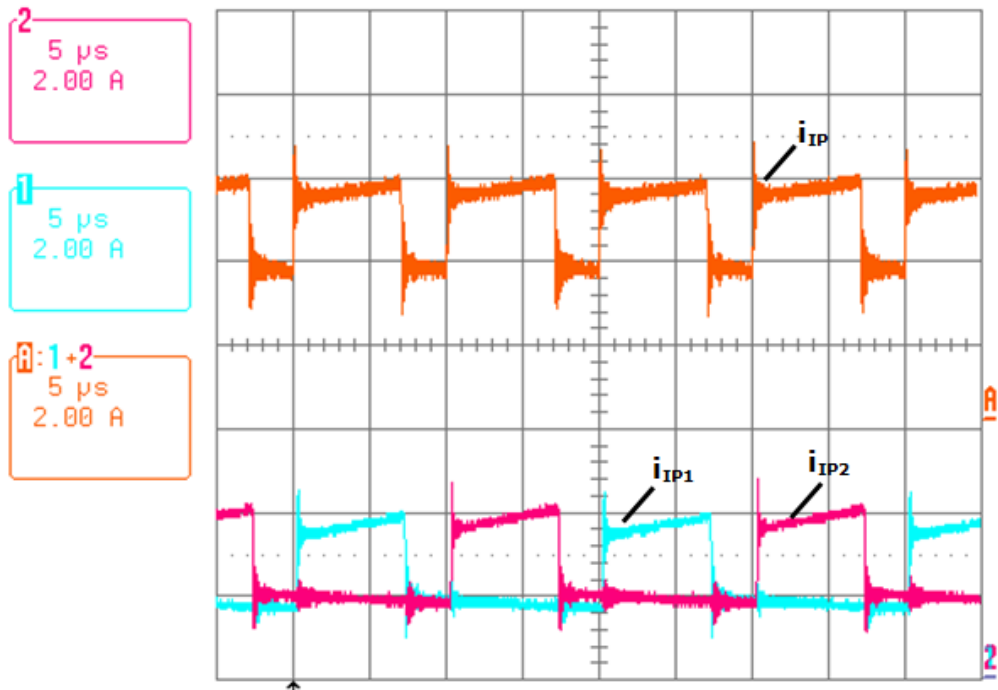


Figure 4.19. Input current and input phase current of the first and second phase when  $d=1/3$  [120]

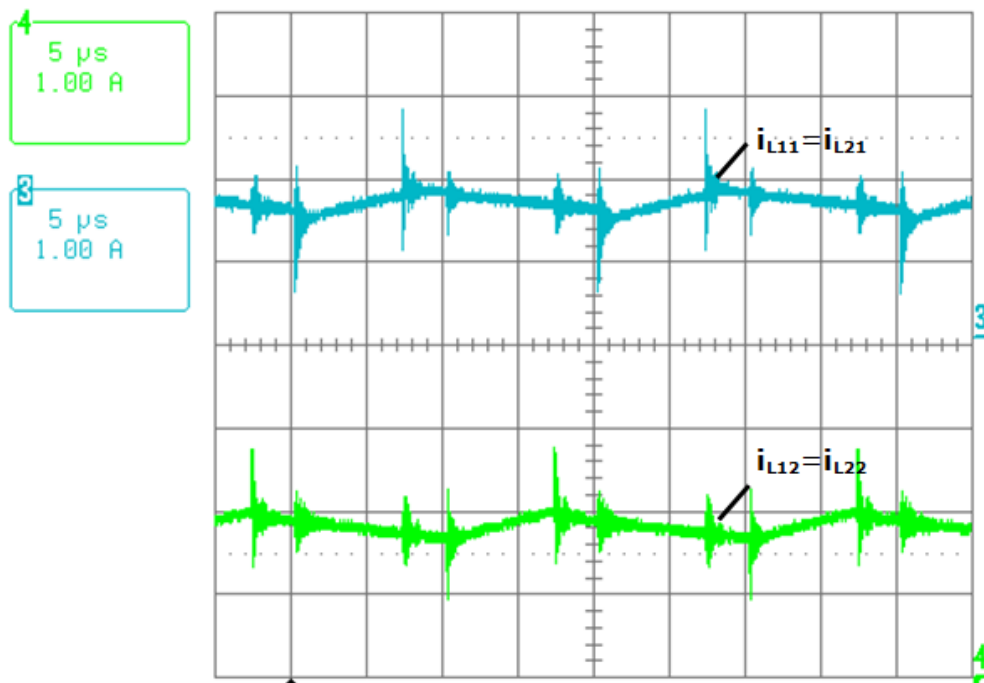


Figure 4.20. Current in the inductors of the first phase and second phases when  $d=1/3$  [120]

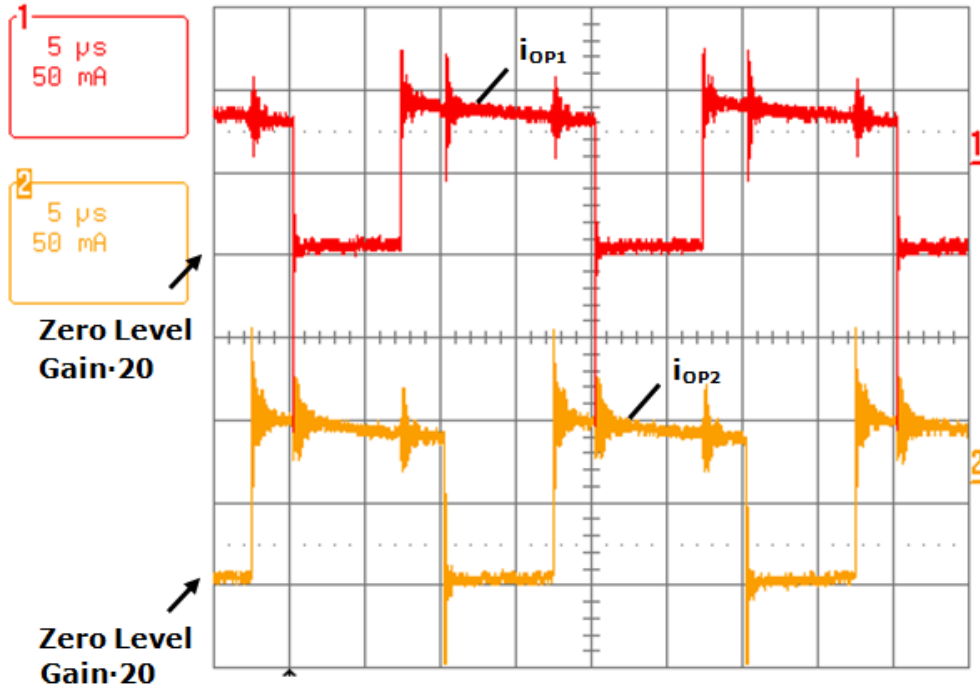


Figure 4.21. Output phase current of the first and second phases when  $d=1/3$

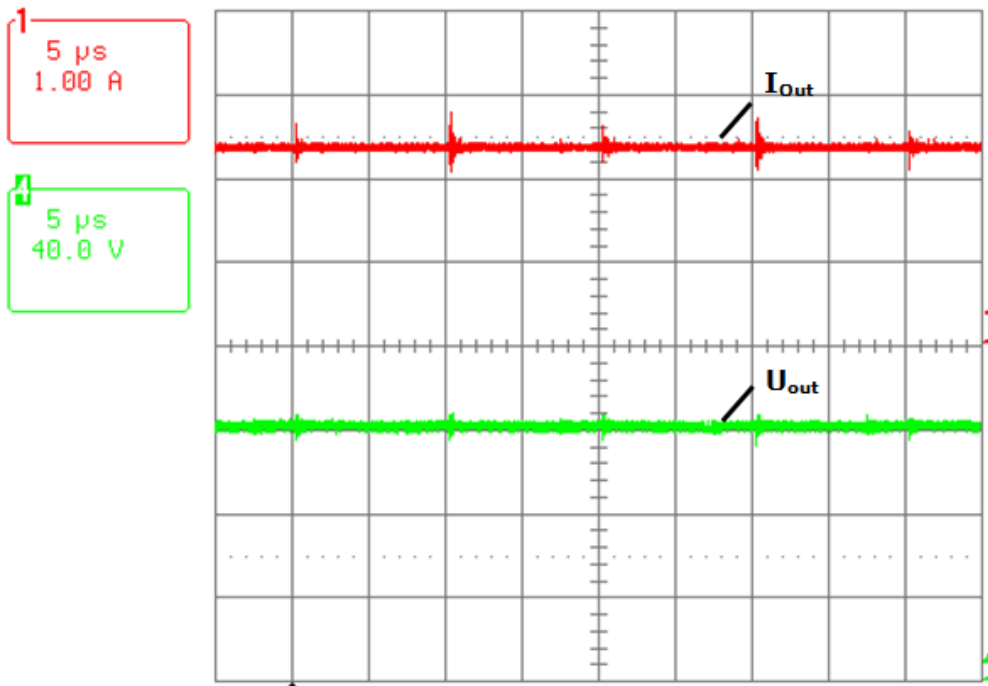


Figure 4.22. Output current and output voltage waveforms when  $d=1/3$  [120]



We continue with the voltage and current waveforms of the converter with a duty cycle  $d=1/2$ , input voltage 40V and the dc-current 7.25A. With these values, the input power is 290W. The input current and voltage is represented in Figure 4.23. For two phase converter the shift between the phases is half of the switching period, and can be seen in Figure 4.24.

The current and voltage of the switch in first and second phase are represented in Figure 4.25 and Figure 4.26 respectively. During the on state the current is twice as the current in the inductor coils. In Figure 4.27 the input phase current  $i_{IP}$  which consists of the sum of the currents  $i_{IP1}$  and  $i_{IP2}$  is represented. At this duty cycle the AC-component of current  $i_{IP}$  is only a triangle waveform. In Figure 4.28 the current in the two inductor coils of first and the second phase is shown. The dc values of the inductor currents are approx. 2.5A. The output currents of the individual phases are presented in Figure 4.29 and Figure 4.30. In Figure 4.31 the output current and output voltage are represented.

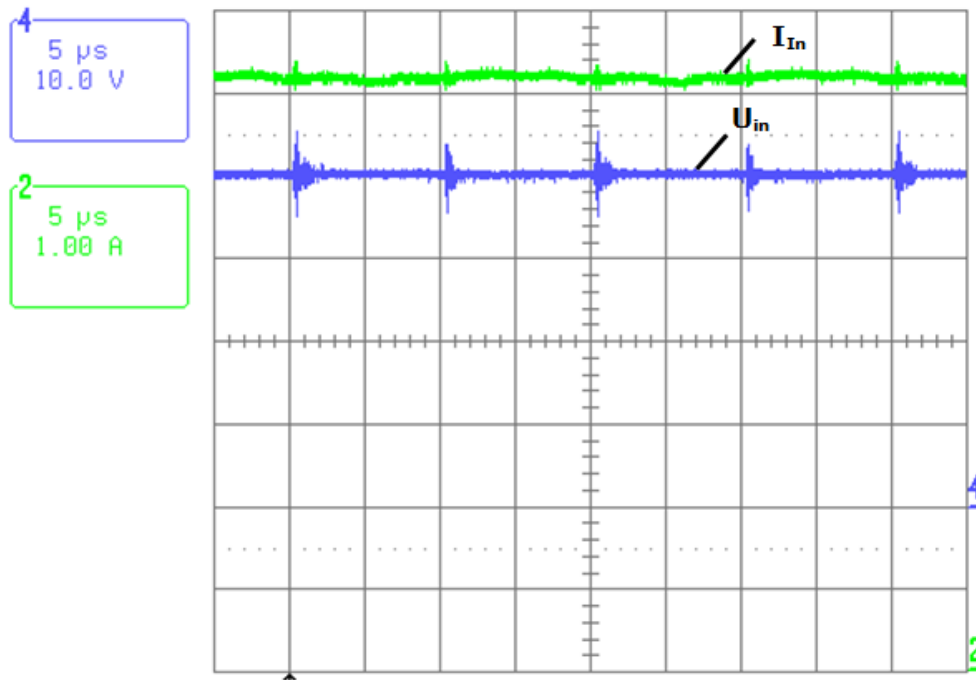


Figure 4.23. Input current and voltage waveforms when  $d=1/2$  [120]

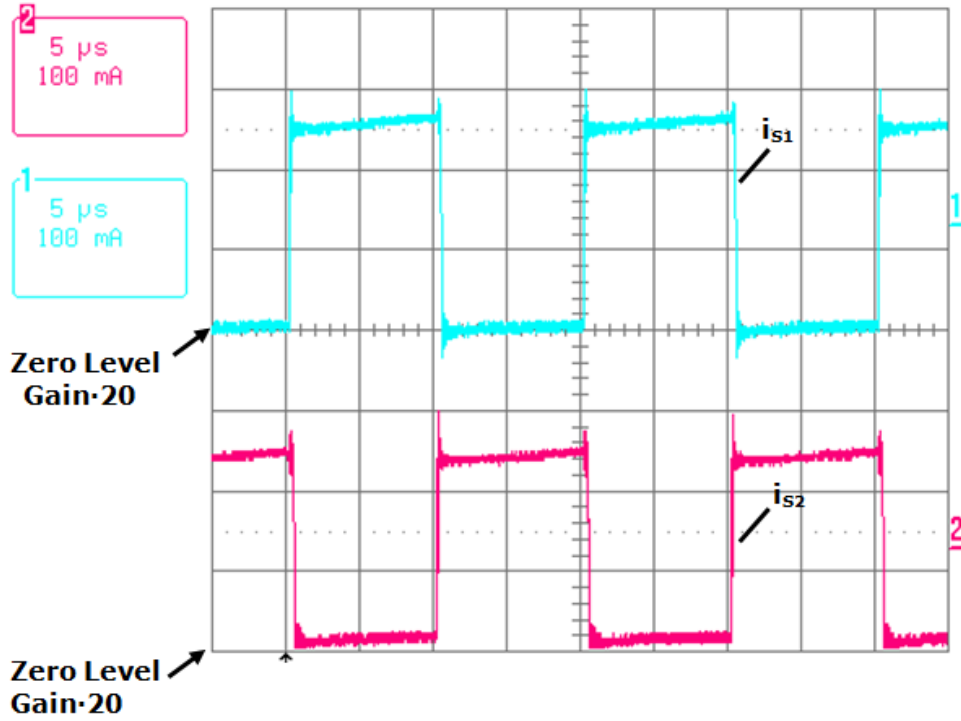


Figure 4.24. MOSFET current of first and second phase when  $d=1/2$

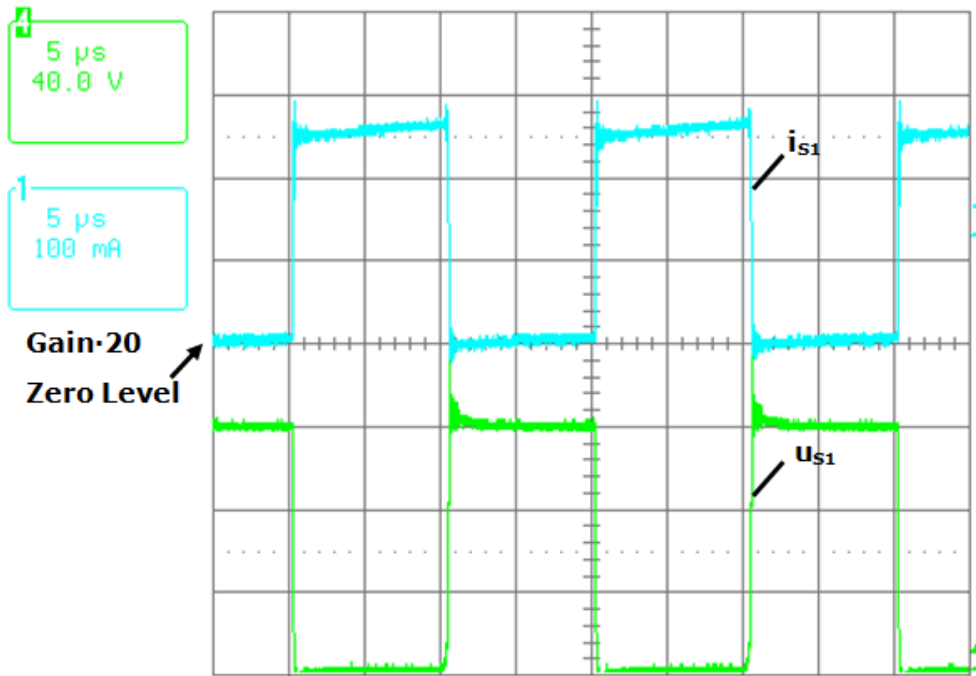


Figure 4.25. MOSFET current and voltage of the first phase when  $d=1/2$  [120]

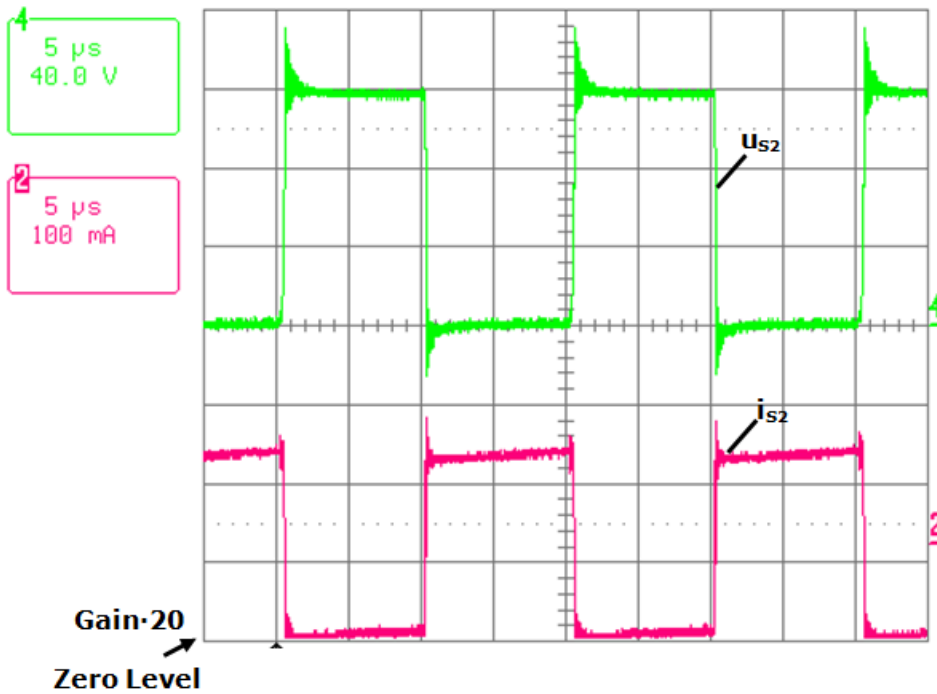


Figure 4.26. MOSFET voltage and current for the second phase when  $d=1/2$

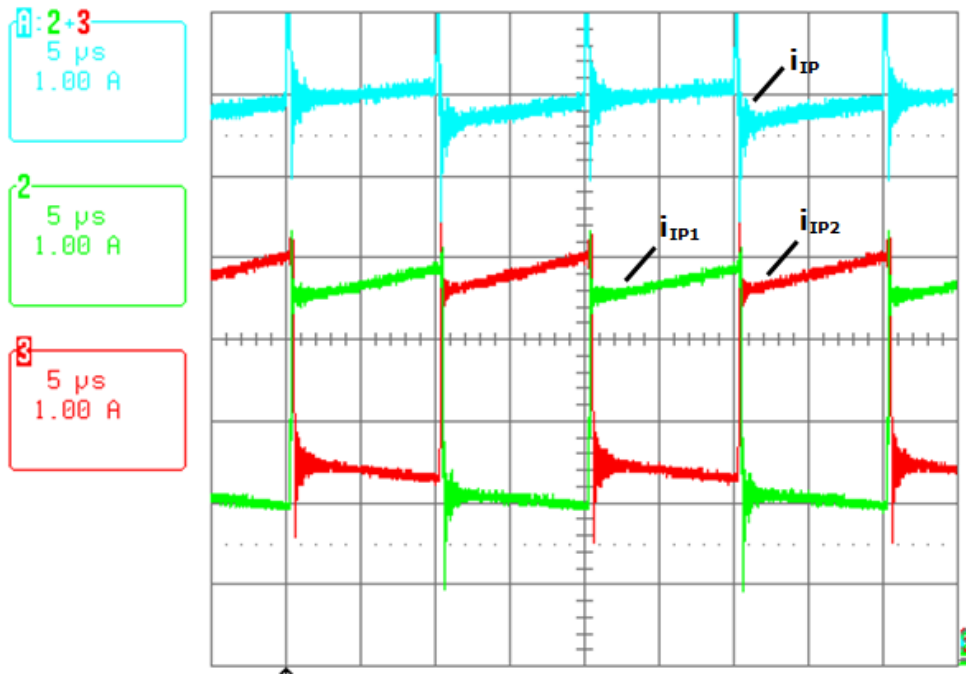


Figure 4.27. Input current and input phase current of first and second phases when  $d=1/2$   
[120]

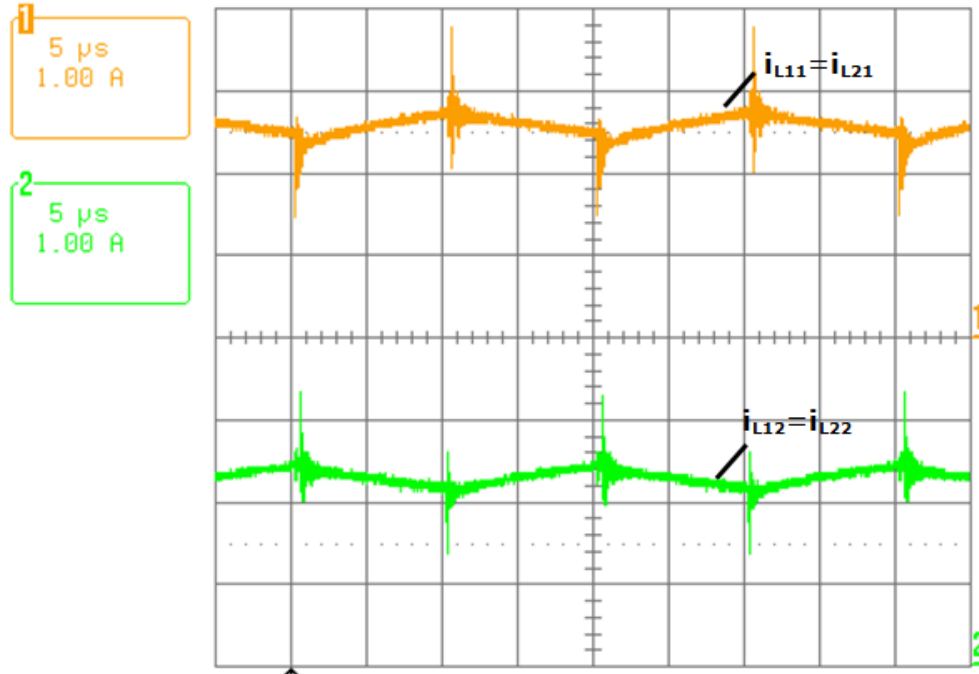


Figure 4.28. Current in the inductors of first and second phase when  $d=1/2$  [120]

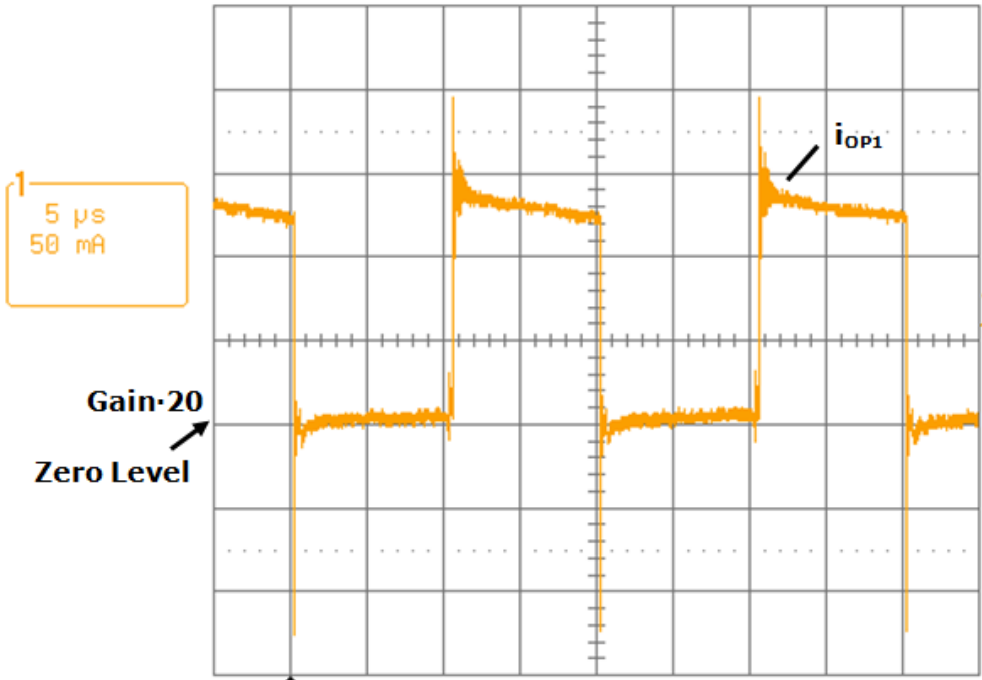


Figure 4.29. Output phase current of first phase when  $d=1/2$

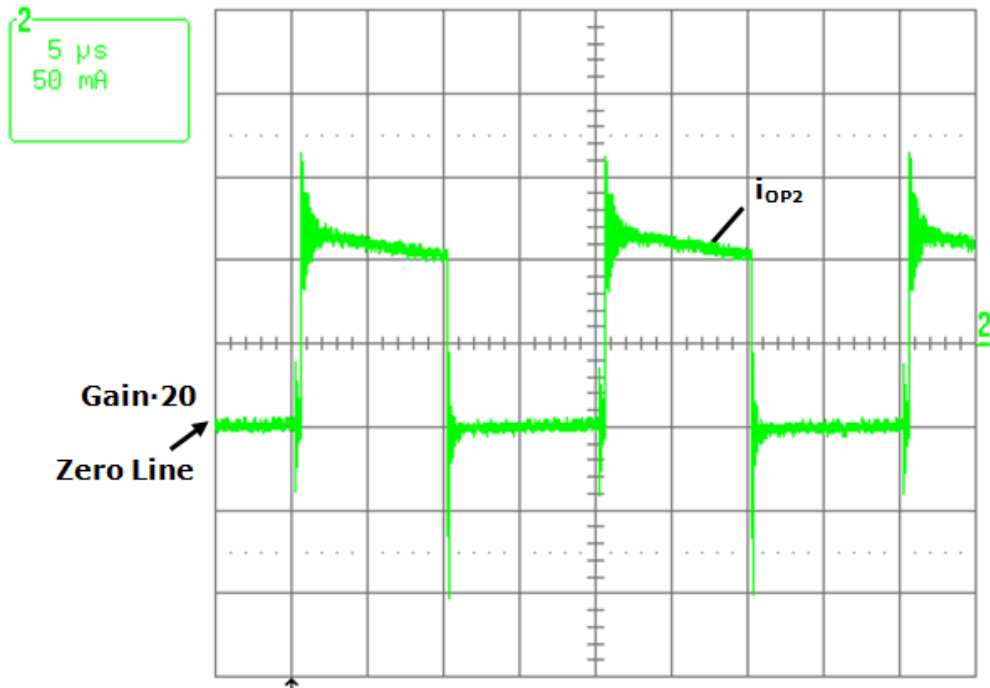


Figure 4.30. Output phase current of second phase when  $d=1/2$

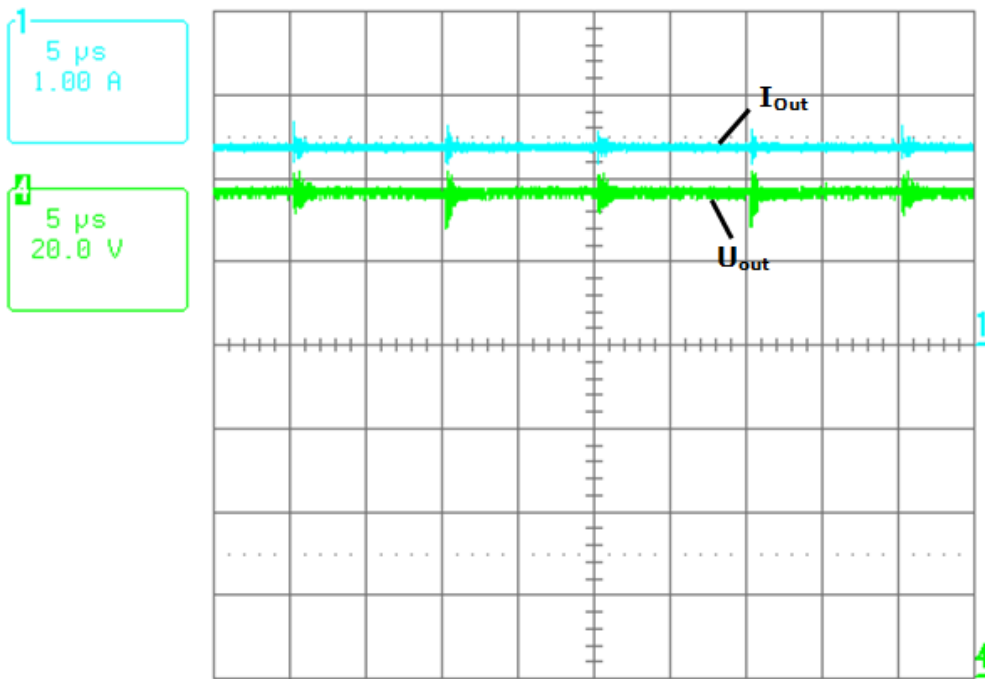


Figure 4.31. Output current and voltage waveforms when  $d=1/2$  [120]

Finally voltage and current waveforms of the two-phase hybrid Boost L-converter for a duty cycle of  $d=2/3$  are presented. The input voltage is 30V and the dc-current is 10A, Figure 4.32. With these values, the input power is 300W. The current and voltage of the switch in first and second phase are represented in Figure 4.33 and Figure 4.34. During the switched-on state the current is twice the current in the inductor coils. In Figure 4.35 the input phase current  $i_{IP}$  which consists of the sum of the currents  $i_{IP1}$  and  $i_{IP2}$  is represented. The current in the two inductor coils of first and the second phase is represented in Figure 4.36. The dc values of the inductor currents are approx. 3A.

The output currents of the individual phases are presented in Figure 4.37. In Figure 4.38 the output current and output voltage are shown.

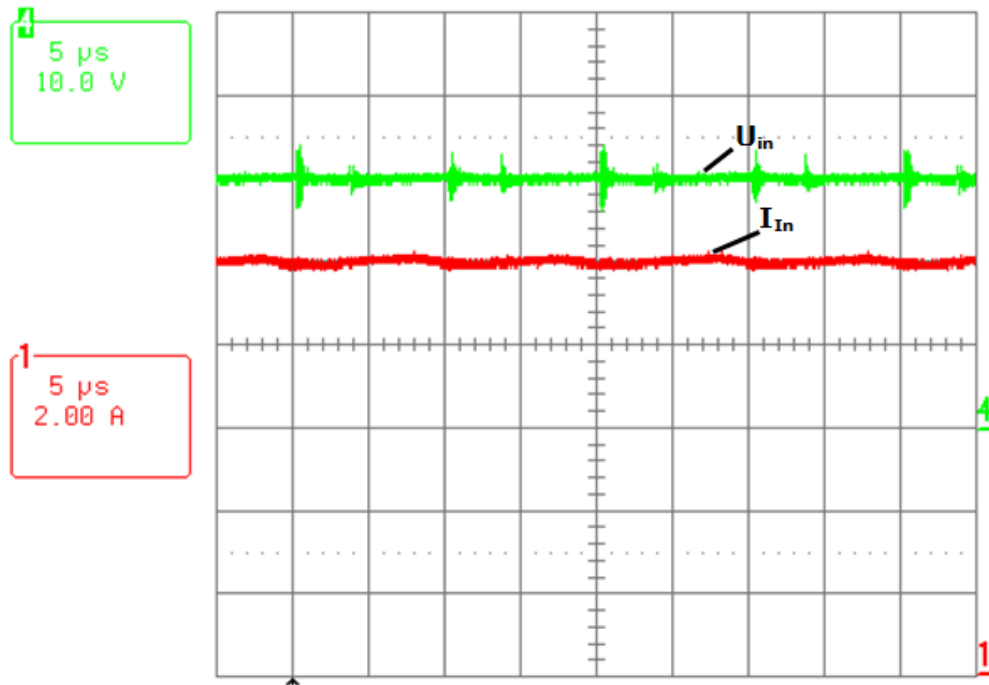


Figure 4.32. Input voltage and current waveforms when  $d=2/3$

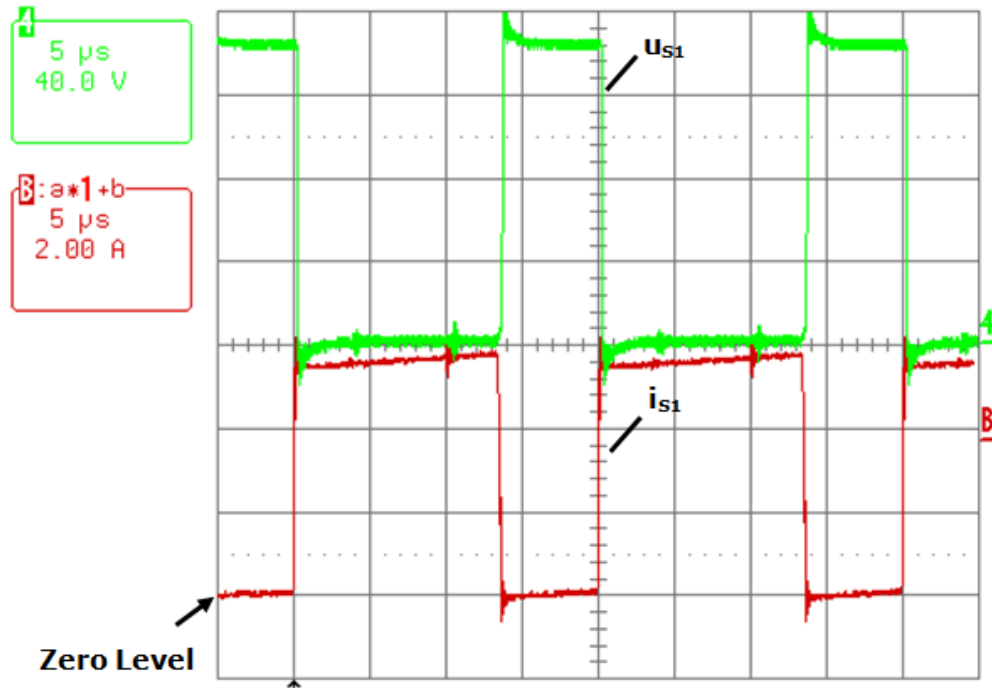


Figure 4.33. MOSFET voltage and current of the first phase when  $d=2/3$

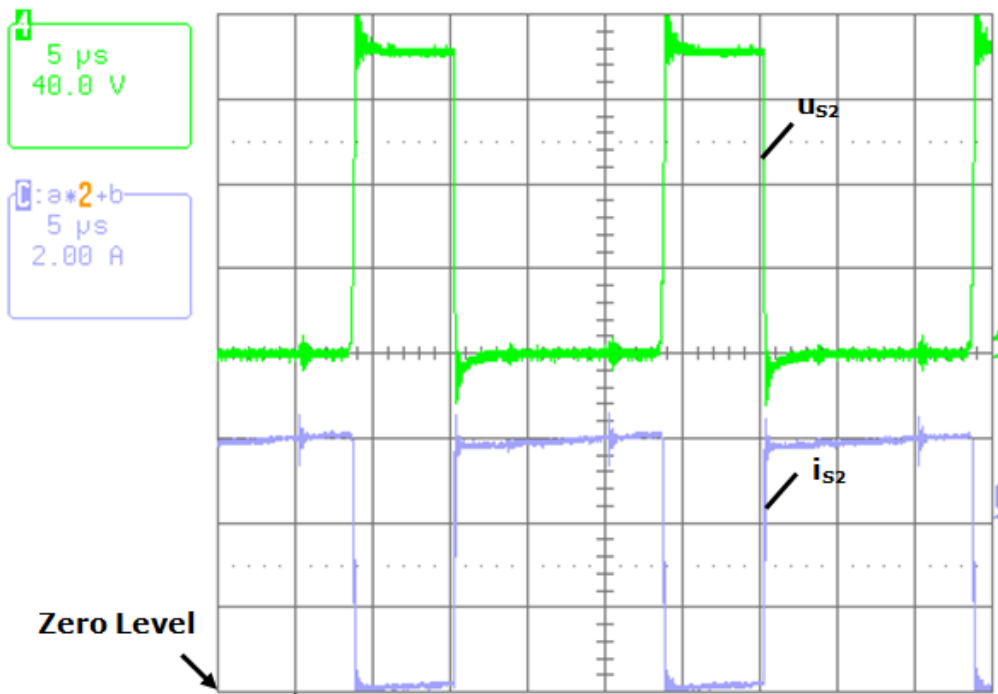


Figure 4.34. MOSFET voltage and current of the second phase when  $d=2/3$

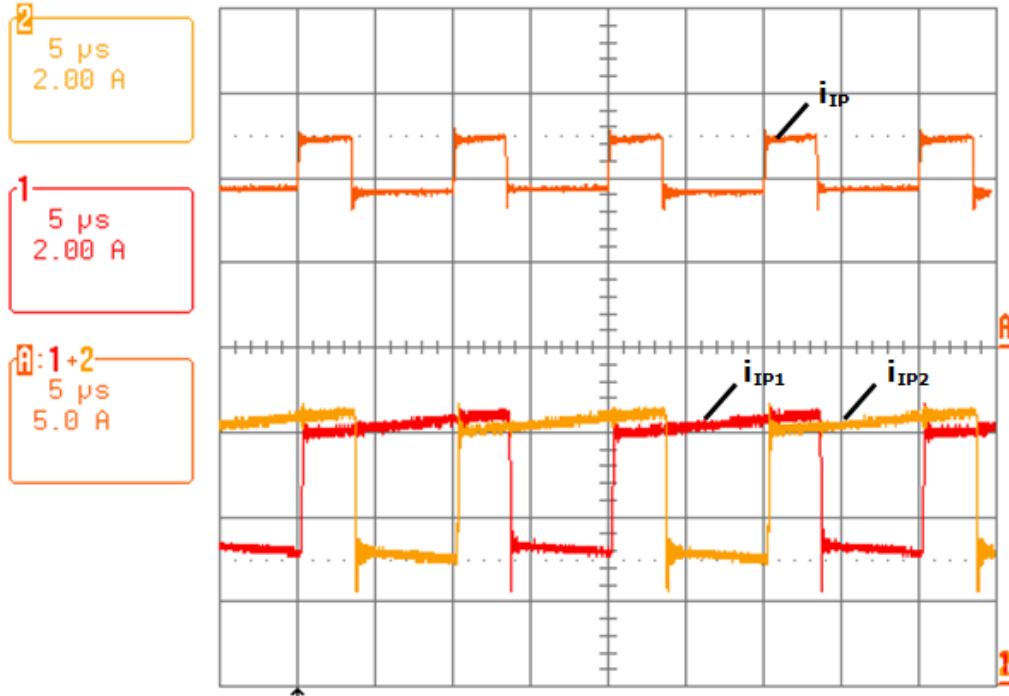


Figure 4.35. Input current and input phase current of the first and second phase when  $d=2/3$

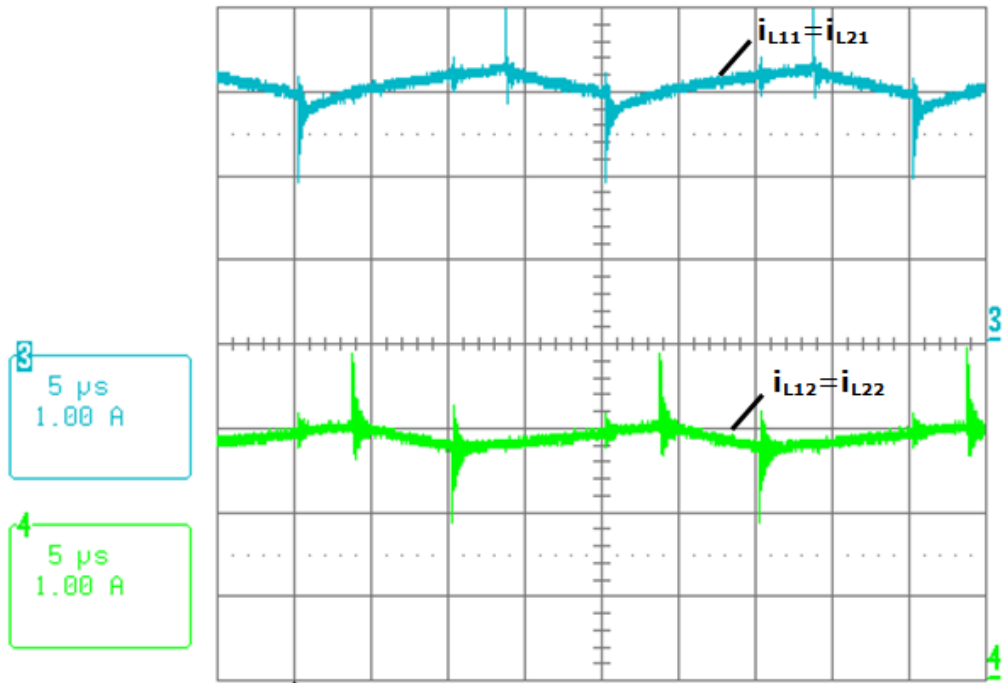


Figure 4.36. Current in the inductors of first phase and second phase when  $d=2/3$



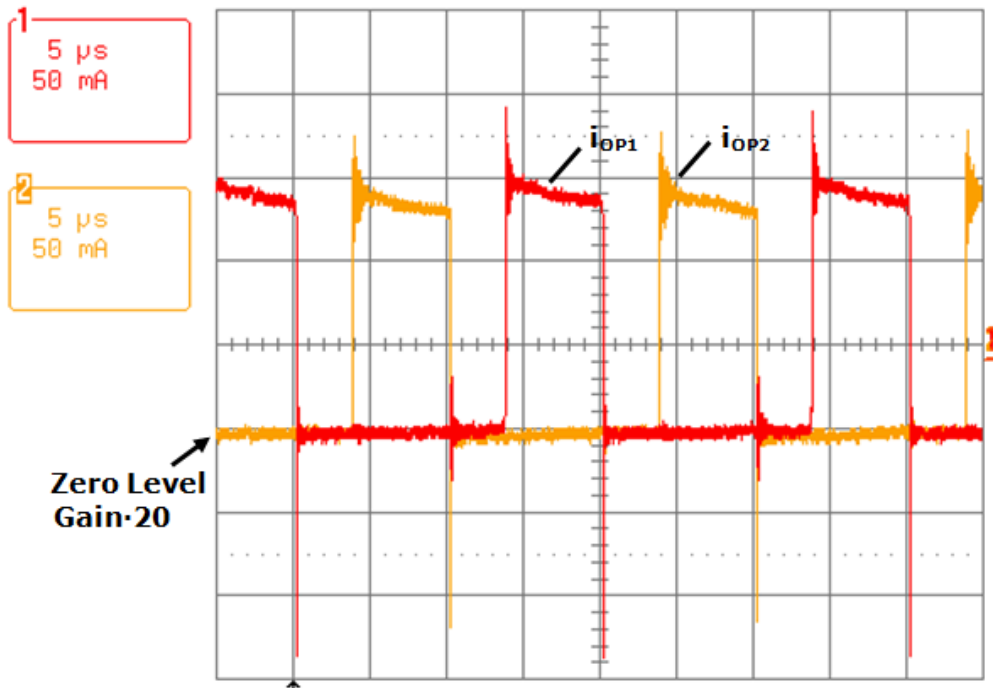


Figure 4.37. Output phase current of first and second phase when  $d=2/3$

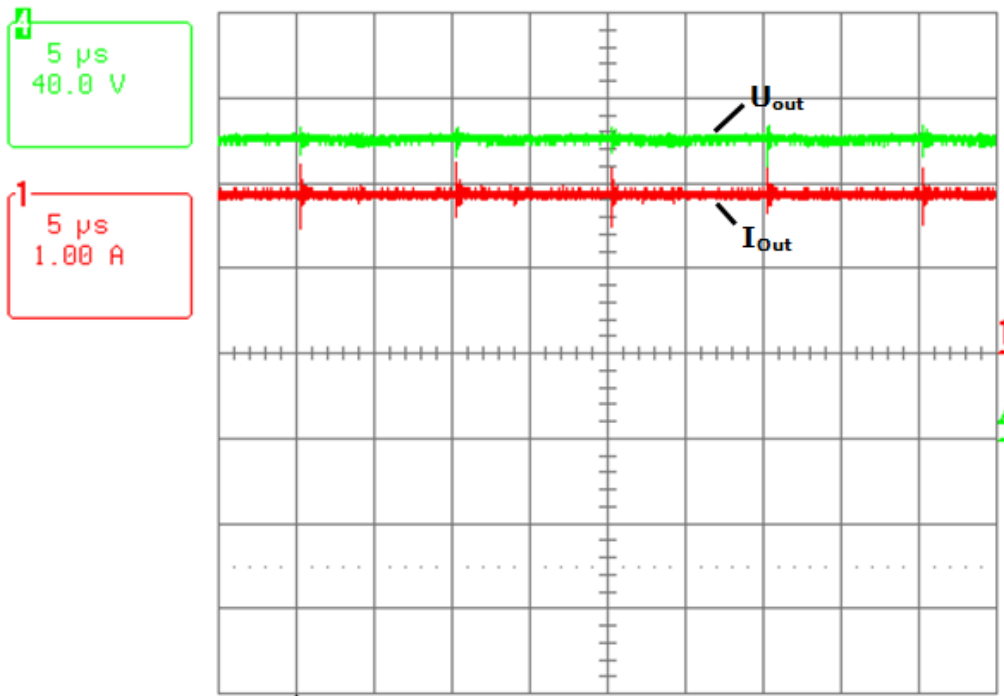


Figure 4.38. Output current and voltage waveforms when  $d=2/3$

The values from calculations and simulations are compared with practical measurements. Thereby a very good accordance between them is shown. Besides the numerous current and voltage waveforms, the efficiency of the complete circuit is calculated for each duty cycle and is presented in Figure 4.41 and Figure 4.42.

For this purpose, current, voltage and power from the input and output are measured, and with these results the efficiency is calculated in each case. The measurements were performed starting from the output power of 30W up to the rated power of 300W and a little beyond. The output voltage of the converter is approximately 120V in each case and the input voltage is 60V in the case of  $d=1/3$  and 40V in the case of  $d=1/2$ .

The simulations for comparison the efficiency of the converter were made in Saber simulator in the same conditions like the measurements. In Figure 4.39 is presented the circuit diagram of the Saber simulation, and in Figure 4.40 it is shown one result of the measurements. The average value of the output and input power was taken in account.

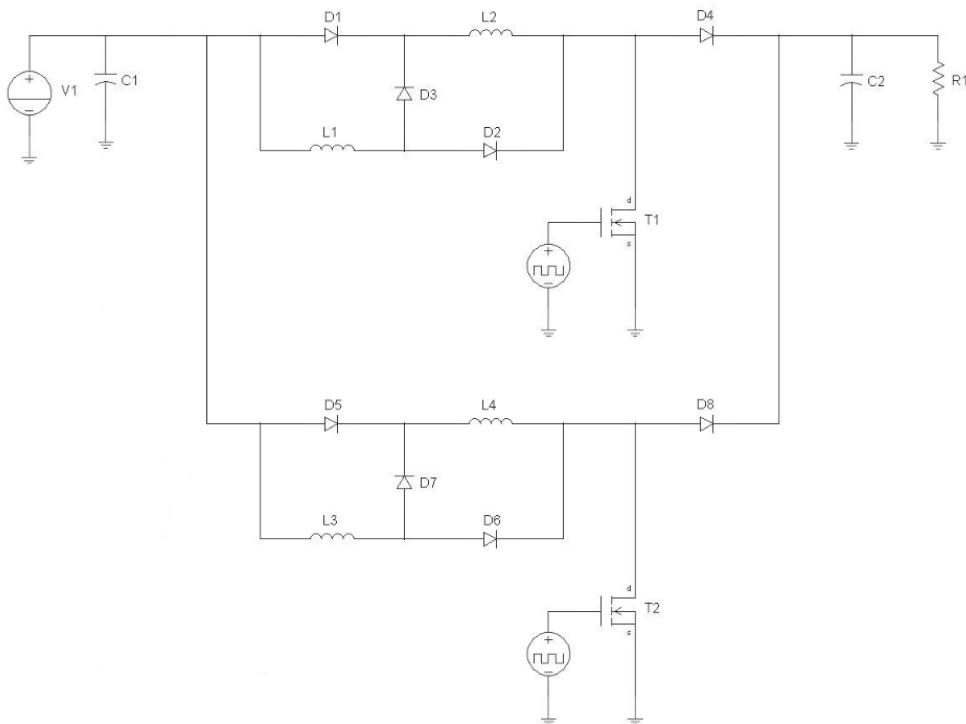


Figure 4.39. Saber circuit diagram for the two-phase hybrid Boost DC-DC L-converter

First waveform it is the output power and last one it is the input power (from up to down order).

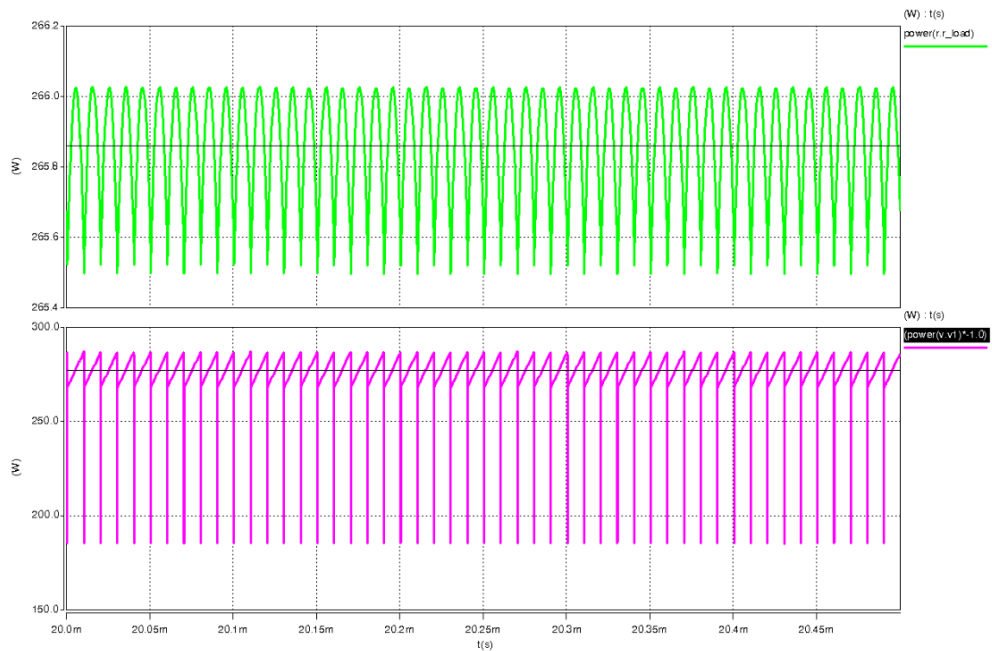


Figure 4.40. Simulation results for the two-phase hybrid Boost DC-DC L-converter, output and input power

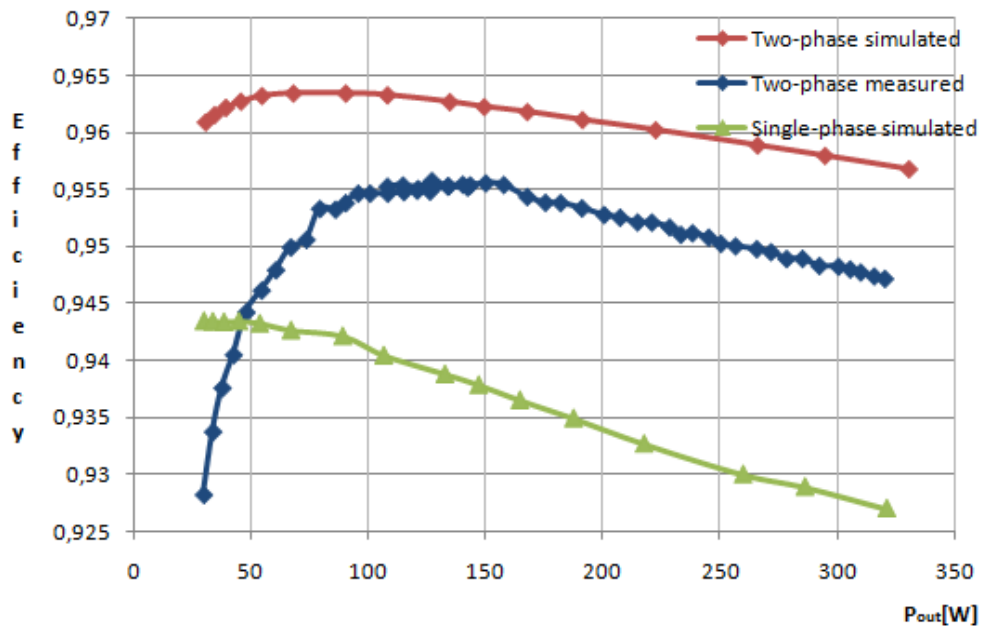


Figure 4.41. Efficiency vs output power  $d=1/3$

At the input voltage of 60V and  $d=1/3$ , the efficiency is higher in the case of two-phase converter compared with the single-phase converter. This is due to the lower effort for the input and output capacitor and faster transient performance.

Also, from the Figure 4.41 can be seen a small difference between efficiency for simulated two-phase converter and measured two-phase converter. Even if the simulations are made in Saber with the "real" models of the semiconductor devices, appear small difference due to the real component, switching losses and conduction losses.

The maximum efficiency reached is 95.5% between the output power of 100W and 150W. The efficiency at rated power is 94.8%. Anyway, efficiency is higher than 92% over the whole power range.

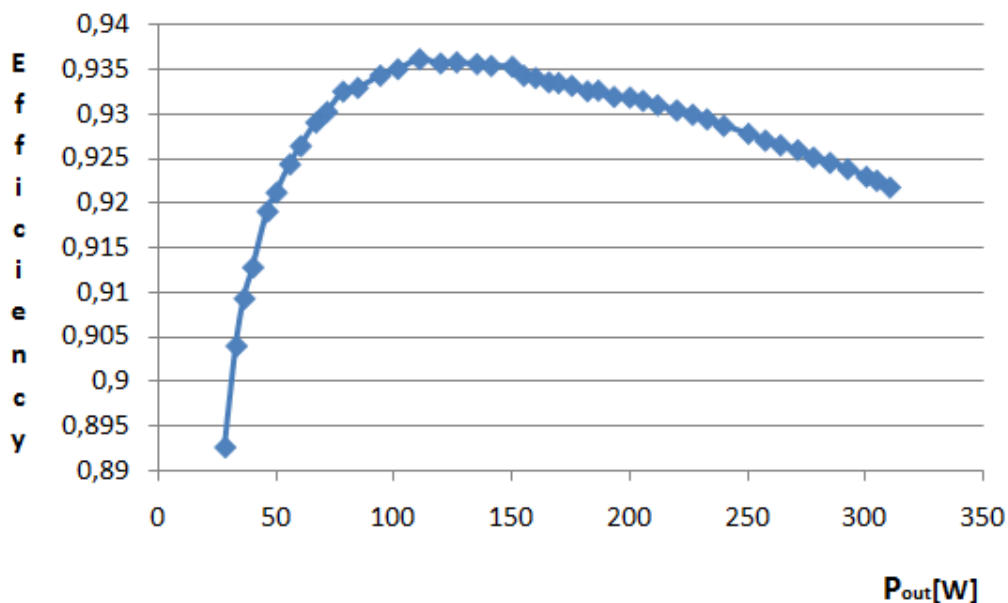


Figure 4.42. Efficiency vs output power  $d=1/2$

Because the conduction losses of the main switches and diodes increase with  $d$ , the efficiency of the converters get lowers with  $d$ . For this reason, at the input voltage of 40V and  $d=1/2$ , the converter efficiency is 93.6% at 120W, and 92.3% at rated output power.

#### 4.5. Conclusions and contributions

This chapter describes a hybrid multiphase Boost L-converter proposed by the author. The kernel of this circuit is the step-up hybrid Boost L-converter which was presented in Chapter 3, but built in a multiphase design. To ensure that all phases of the converter operate at the same switching frequency and with phase-shift between them, the author used interleaving switching strategy.

After analyzing this new multiphase hybrid Boost L-converter, developing the theoretical quantitative relationships, and sketching the waveform, the validation of

the new structure was performed. The frequency of the capacitor currents is increased by the number of phases.

To validate and confirm the theoretical equations, the author designed a two-phase Boost L-converter and simulated this circuit in CASPOC simulation program. The simulated waveforms were compared to theoretical one, and a very good agreement both qualitatively and quantitatively is obvious.

One advantage, that is evident from the Figure 4.2, is that the multiphase configuration allows the combination of output capacitor from each individual Boost into just a single output capacitor. Another major advantage of multiphase is the improvement of input and output characteristics due to frequency multiplication produced by multiphasing of input and output current. This produces smaller input and output filtering requirements as well as faster transient performance compared to the single phase converter. Due to the frequency multiplication property of the multiphase, the output voltage will actually have the frequency of the ripple component twice (in our case) than operating switching frequency of each individual boost converter,  $n \cdot f_s$ . In turns this property doesn't have any effect on the inductors, diode and switches.

The numbers of the inductors are increased due to the multiphase structure. This will lead to an increase in the complexity of the converter. The author applies the solution that was found in Chapter 3, of coupling the inductors to reduce the cores number and the complexity of the converter. The analysis and simulation of the circuit in the case of coupled and uncoupled inductors are presented. A comparison between them is made. The conclusion is that the coupled interleaved Boost L-converter effectively reduces the inductors current ripple by approximately half compared to that of uncoupled inductors and it is only two cores for the inductors instead of four, which will lead to reduced parts count, volume and weight of the converter.

A comparison based on the ripple current in the case of single and two-phase Boost L-converter was made as well.

Experimental waveforms from hardware measurement are presented at the end of this chapter and validated the theoretical and simulation analyses. The disadvantages of this circuit are the increased number of components compared with single-phase hybrid converter.

The measured efficiency for two-phase converter is compared with the simulated efficiency from Saber simulator for two- and single-phase converter, and is obvious that for two-phase converter the efficiency is higher. The measured efficiency is above 94% when  $d=1/3$  and above 92%, when  $d=1/2$  over the whole power range.

The most important contribution brought in this chapter is the validation, as an example for the family, of one of the multiphase hybrid converters proposed by the author. The important number of advantages compared with single-phase hybrid converters is stressed out.

Other contributions to this chapter are:

- the analytical study of the multiphase hybrid converter;
- developing the theoretical quantitative relationships, the operating condition for CCM, static characteristic and the waveforms of the multiphase hybrid converter;
- Matlab and Mathcad program for theoretical study and data processing in case of coupled and uncoupled inductors;
- design and simulation in Caspoc Simulation Program, of the two-phase hybrid converter, in case of coupled and uncoupled inductors;

- comparative analysis between two-phase hybrid converter with coupled and uncoupled inductors through simulation;
- comparative analysis between two-phase hybrid converter with coupled inductors and single-phase hybrid converter through simulation;
- validation and confirmation of the theoretical equation, through simulation. Also, a very good accordance between the simulated waveforms compared to theoretical one for two-phase converter, is shown;
- a laboratory prototype built in order to validate the theoretical and simulated results;
- Saber simulation with “real” component for efficiency calculation, and comparison with the measurements from the laboratory prototype for two- and single-phase converter;
- the scientific confirmation of this two-phase hybrid structure with coupled inductor by publishing them in [103] and [120]. [103] is indexed **ISI** – Web of Knowledge – Thomson Reuters, and published in Hindawi Publishing Corporation International Journal of Photoenergy, 2014, and [120] is indexed **IEEE** at “16th European Conference on Power Electronics and Applications, EPE’14-ECCE Europe”, Lappeenranta 2014.

## **CHAPTER 5. Conclusions and Contributions**

### **5.1. Conclusions**

The focus of this thesis is to extend the existing knowledge and techniques in the field of multiphase DC-DC converters for use in renewable energy systems, from classical multiphase converters, to the hybrid multiphase converters. For this, the author presents the L- and C-switching structures proposed by Boris Axelrod, Yefim Berkovich and Adrian Ioinovici. These structures are inserted in classical and bidirectional converters resulting in 17 new hybrid structures, and these structures are studied and simulated by the author. Also a comparative analysis of the hybrid converters is performed. The results of simulation of 6 of the hybrid converters, one with each switching cell, are presented in the thesis.

A method for increasing the efficiency, reducing the size through reducing the numbers of inductors in the hybrid Boost L-converter without affecting the circuit operation and the dc voltage transfer function, is also proposed. The design and simulation of the proposed converter was performed and explained. Moreover, to exhibit the potential of the proposed converter, a hardware prototype was built and tested.

A synthesizing method for multiphase hybrid converters is proposed. Based on synthesizing method, from 17 hybrid converters that were analysed, just 11 can be used in multiphase design. So, 11 new topologies of multiphase hybrid DC-DC converter were proposed, and 1 was analytically studied, simulated, and practical implemented. All the equations necessary for the design of such a circuit is presented. Laboratory prototype of Boost converters has been built to confirm the theoretical results. The design methods are validated through simulation and experimental results. Comparison between the specification of single phase and multiphase is thoroughly examined.

### **5.2. Contributions**

The author contributions summarized below are in fact a reunion of contributions from each chapter, and can be summarized as follows:

1. The comprehensive literature survey of the DC-DC converters used in RE systems, from all the points of view, is discussed in Chapter 1. Including this study in the thesis is justified by the fact that the new L- or C-switching structures are inserted in the classical, bidirectional or associated converters resulting the new hybrid converters.

2. A synthesizing method, 11 new multiphase converters with hybrid structures that are possible to be implemented and the dc voltage transfer function, is proposed by the author in Chapter 2. It begins with the analytical study of the hybrid converter, continued with a comparative analysis of the hybrid with classical converters and ends with the validating of these converters by simulations in Caspoc Simulation Program.

3. After coupling the inductors of the hybrid converter proposed by A. Ioinovici in [4], a new hybrid converter with a single core, instead of two cores for inductor, and with reduced current ripple at half is obtained;

- a comparative analysis between coupled and uncoupled inductors, was given for a duty cycle of 1/2, respectively 1/3. From this analysis, the importance of the coupled inductors resulted;

- a analytical study, validated by simulation, and confirmed by laboratory prototype of the hybrid converters with coupled inductor, was made;

- the output voltage is increased  $(1+d)$  times compared to classical Boost converter.

- the efficiency at rated power is 92.5% from measurements, respective 92.8% from Saber simulation with real components.

- the effort for the input and output capacitor is very high.

4. A validation of one of the multiphase hybrid Boost converter proposed by the author is the most important contribution from Chapter 4.

The **advantages** of the proposed topology are as follows:

- ripple of the input and output current are reduced;

- ripple frequency of the input and output current are increased with the number of phases;

- provide a reduced inductor current ripple;

- two cores for the inductors instead of 4;

- with these multiphase hybrid converter the effort for the input and output capacitor is reduced compared with the single phase hybrid converter.

- smaller voltage ripple with the same filter, or we can use a smaller sized filter to obtain the same ripple performance;

- increase converter power rating by paralleling phases not by paralleling multiple devices;

- reduced thermal losses;

- the converter has an efficiency above 94% when  $d=1/3$  and above 92%, when  $d=1/2$  over the whole power range, determined from laboratory prototype, and 95.5% when  $d=1/3$  from Saber simulation with real components.

### 5.3. Future works

The thesis leaves open the following research direction:

1. To further improve the efficiency of the multiphase Boost converter, a solution will be to investigate the soft switching techniques. If the soft switching techniques can be applied to the main switch, the switching frequency can may go up to few MHz. As a result, the filter and the inductors will be much smaller compared with that of 50 kHz multiphase hybrid Boost converter proposed in the thesis.

2. The extension of application for the proposed converter in other power conversion systems or other industries, like telecommunication, bio-medical which is dominant by series-parallel resonant converter, and automotive.



3. Analytical study, simulation and practical implementation for the other 10 multiphase configurations.
4. Investigate whether is possible to develop small signal models for the new proposed topologies

## References

- [1] B. Axelrod, Y. Berkovich, and A. Ioinovici, "Transformerless dc-dc Converters with a Very High dc Line-to-Load Voltage Ratio," in *International Symposium on Circuits and Systems 2003, ISCAS '03*, 2003, pp. III-435 - III-438.
- [2] B. Axelrod, Y. Berkovich, and A. Ioinovici, "Transformerless dc-dc converters with a very high dc line-to-load voltage ratio," *Journal of Circuits, Systems and Computers*, vol. 13, no. 03, pp. 467-475, Jun 2004.
- [3] Boris Axelrod, Yefim Berkovich, and Adrian Ioinovici, "Hybrid switched-capacitor-Cuk/Zeta/Sepic converters in step-up mode," in *IEEE International Symposium on Circuits and Systems (ISCAS), 2005*, 2005, pp. 1310-1313.
- [4] Boris Axelrod, Yefim Berkovich, and Adrian Ioinovici, "Switched-Capacitor/Switched-Inductor Structures for Getting Transformerless Hybrid DC-DC PWM Converters," *IEEE Transactions on Circuits and Systems*, vol. 55, pp. 687-696, March 2008.
- [5] Boris Axelrod, Yefim Berkovich, and Adrian Ioinovici, "Switched-capacitor (SC)/switched inductor (SL) structures for getting hybrid step-down Cuk/Sepic/Zeta converters," in *2006 IEEE International Symposium on Circuits and Systems, ISCAS2006*, 2006, pp. 5063-5066.
- [6] Adrian Ioinovici, *Power Electronics and Energy Conversion Systems-Fundamentals and Hard-switching Converters*, 1st ed.: 2013, John Wiley & Sons, Ltd, 2013.
- [7] Muhammad H. Rashid, *Power Electronics Handbook*, 3rd ed.: Elsevier, 2011.
- [8] **Pop-Calimanu Ioana-Monica**, "Solar energy used in buildings," in *IP „Materials Energy and sustainable Growth*, Vilnius, 2011.
- [9] F. Bordry, "Power converters:definitions, classifications and converter topologies," CAS -CERN Accelerator School and CLRC Daresbury Laboratory, Geneva, Switzerland, Specialised CAS Course on Power Converters May 2004.
- [10] **Ioana-Monica Pop-Calimanu**, "Converters Used in Solar Energy Systems," in *Spre cariere de cercetare prin studii doctorale*, Timisoara, 2011.
- [11] Florin Prutianu, Ioana-Monica Pop-Calimanu, and Viorel Popescu, "Validation system for power supply module part of automotive ECUs," in *10th International Symposium on Electronics and Telecommunication, ISETC '12*, Timisoara, 2012, pp. 75-78.
- [12] Florin Prutianu, **Ioana-Monica Pop-Calimanu**, and Viorel Popescu, "Semi-automated power supply efficiency measuring system," in *10th International Symposium on Electronics and Telecommunication, ISETC '12*, Timisoara, 2012, pp. 45-48.
- [13] A. Rufer, "Passive components," CERN Accelerator School (CAS), Warrington, Power Converters for Particle Accelerators 2004.
- [14] E. Duran, M. Sidrach-de-Cardona, J. Galán, and J.M. Andujar, "Comparative analysis of buck-boost converters used to obtain I-V characteristic curves of photovoltaic modules," in *PESC 2008 - IEEE Power Electronics Specialists Conference*, Rhodes, 2008, pp. 2036-2042.

- [15] R. W Erickson, "DC-DC Power Converters," *Wiley Encyclopedia of Electrical and Electronics Engineering*, JUN 2007.
- [16] Eladio Duran Aranda, Juan Antonio G Mez Galan, Mariano Sidrach de Cardona, and Jose Manuel Andujar Marquez, "Measuring the I-V Curve of PV Generator-Analyzing Different dc-dc Converter Topologies," *IEEE Industrial Electronics Magazine*, pp. 4-14, Sept 2009.
- [17] Syafrudin Masri and Pui-Weng Chan, "Development of a Microcontroller-Based Boost Converter for Photovoltaic System," *European Journal of Scientific Research*, vol. 41, no. 1, pp. 38-47, 2010.
- [18] Prutianu Florin, **Pop-Calimanu Ioana-Monica**, and Popescu Viorel, "Power factor Correction Inductor Design From a Wind Turbine Boost Converter," in *The 11th International Conference on Engineering of Modern Electric Systems, EMES'11*, Oradea, 2011, pp. 199-202.
- [19] **Pop-Calimanu Ioana-Monica**, Prutianu Florin, and Popescu Viorel, "Boost Converter Used in Solar Energy Systems," in *The 11th International Conference on Engineering of Modern Electric Systems, EMES'11*, Oradea, 2011, pp. 195-198.
- [20] R. Gules, J. De Pellegrin Pacheco, H.L. Hey, and J. Imhoff, "A Maximum Power Point Tracking System With Parallel Connection for PV Stand-Alone Applications," *IEEE Transactions on Industrial Electronics*, vol. 55, no. 7, pp. 2674-2683, Jul. 2008.
- [21] Zhiling Liao and Xinbo Ruan, "A novel power management control strategy for stand-alone photovoltaic power system," in *IPEMC '09-IEEE 6th International Power Electronics and Motion Control Conference*, Wuhan, 2009, pp. 445-449.
- [22] S. Inoue and H. Akagi, "A Bidirectional DC-DC Converter for an Energy Storage System With Galvanic Isolation," *IEEE Transactions on Power Electronics*, vol. 22, no. 6, pp. 2299- 2306 , Nov. 2007.
- [23] Seung-Yo Lee, A.G. Pfaelzer, and J.D. van Wyk, "Comparison of Different Designs of a 42-V/14-V DC/DC Converter Regarding Losses and Thermal Aspects," *IEEE Transactions on Industry Applications*, vol. 43, no. 2, pp. 520 - 530 , Mar./Apr. 2007.
- [24] R. Gules, J. De Pellegrin Pacheco, H.L. Hey, and J. Imhoff, "A Maximum Power Point Tracking System With Parallel Connection for PV Stand-Alone Applications," *IEEE Transactions on Industrial Electronics*, vol. 59, no. 2, pp. 2674 - 2683, FEBRUARY 2012.
- [25] "Control of energy storage interface with a bidirectional converter for photovoltaic systems," in *AUPEC'08- Australasian Universities Power Engineering Conference* , Sydney, 2008, pp. 1-6.
- [26] D. Ramesh Babu and M. Ram Prasad Reddy, "A Extensive Non-Isolated Bidirectional Zero-Voltage Switching DC-DC Converterfor PV Cell Application to Grid Connected System," *International Journal of Engineering & Science Research*, vol. 2, no. 9, pp. 1251-1266, Sept. 2012.
- [27] Chih-Chiang Hua, Chih-Wei Chuang, Chun-Wei Wu, and Deng-Jie Chuang, "Design and Implementation of a Digital High-Performance Photovoltaic Lighting System," in *ICIEA 2007-2nd IEEE Conference on Industrial Electronics and Applications*, Harbin, 2007, pp. 2583 - 2588.

- [28] H. Matsuo and F. Kurokawa, "New Solar Cell Power Supply System Using a Boost Type Bidirectional DC-DC Converter," *IEEE Transactions on Industrial Electronics*, vol. IE-31, no. 1, pp. 51-55, Feb. 1984.
- [29] Jih-Sheng Lai and D.J. Nelson, "Energy Management Power Converters in Hybrid Electric and Fuel Cell Vehicles," *Proceedings of the IEEE*, vol. 95, no. 4, pp. 766- 777, April 2007.
- [30] H. Tao, A. Kotsopoulos, J.L. Duarte, and M.A.M. Hendrix, "Multi-input bidirectional DC-DC converter combining DC-link and magnetic-coupling for fuel cell systems," in *Fourtieth IAS Annual Meeting. Conference Record of the 2005 Industry Applications Conference*, Hong Kong, 2005, pp. 2021- 2028.
- [31] Y. Hu, J. Tatler, and Z. Chen, "A bidirectional dc-dc power electronic converter for an energy storage device in an autonomous power system," in *IPEMC 2004 - The 4th International Power Electronics and Motion Control Conference*, Xi'an, 2004, pp. 171 - 176.
- [32] T. Mishima, E. Hiraki, T. Tanaka, and M. Nakaoka, "A New Soft-Switched Bidirectional DC-DC Converter Topology for Automotive High Voltage DC Bus Architectures," in *VPPC '06- IEEE Vehicle Power and Propulsion Conference*, Windsor, 2006, pp. 1-6.
- [33] J.L. Duarte, M. Hendrix, and M.G. Simoes, "Three-Port Bidirectional Converter for Hybrid Fuel Cell Systems," *IEEE Transactions on Power Electronics*, vol. 22, no. 2, pp. 480-487, March 2007.
- [34] Huang-Jen Chiu and Li-Wei Lin, "A bidirectional DC-DC converter for fuel cell electric vehicle driving system," *IEEE Transactions on Power Electronics*, vol. 21, no. 4, pp. 950-958, July 2006.
- [35] Nimrod Vazquez, Claudia Hernandez, and Esli Vazquez, *A DC/DC Converter for Clean-Energy Applications, Clean Energy Systems and Experiences*, Kei Eguchi, Ed., 2010.
- [36] Junseok Song, Ruichen Zhao, and A. Kwasinski, "Design considerations for energy storage power electronics interfaces for high penetration of renewable energy sources," in *2011 IEEE 8th International Conference on Power Electronics and ECCE Asia (ICPE & ECCE)*, Jeju, 2011, pp. 2160 - 2167.
- [37] Valluri Satya Srinivas, E.Vargil Kumar, and K.Bhavya, "A Two Input Single Output Z-Sourced Dc-Dc Converter for," *International Journal of Modern Engineering Research (IJMER)*, vol. 2, no. 5, pp. 3861-3868, Sep-Oct 2012.
- [38] Yan Li, Xinbo Ruan, Dongsheng Yang, and Fuxin Liu, "Modeling, analysis and design for hybrid power systems with dual-input DC/DC converter," in *ECCE 2009- IEEE Energy Conversion Congress and Exposition*, San Jose, 2009, pp. 3203 - 3210.
- [39] Yaow-Ming Chen, Yuan-Chuan Liu, Shih-Chieh Hung, and Chung-Sheng Cheng, "Multi-Input Inverter for Grid-Connected Hybrid PV/Wind Power System," *IEEE Transactions on Power Electronics*, vol. 22, no. 3, pp. 1070 - 1077, May 2007.
- [40] N. Vazquez et al., "A double input DC/DC Converter for photovoltaic/wind systems," in *PESC 2008-IEEE Power Electronics Specialists Conference*, Rhodes, 2008, pp. 2460 - 2464.

- [41] Yaow-Ming Chen, Chung-Sheng Cheng, and Hsu-Chin Wu, "Grid-connected hybrid PV/wind power generation system with improved DC bus voltage regulation strategy," in *APEC '06- Twenty-First Annual IEEE Applied Power Electronics Conference and Exposition*, Dallas, 2006, pp. 1-7.
- [42] M.SubbaRao, Ch.Sai Babu, and S.Satynarayana, "Analysis and Control of Double-Input Integrated Buck-Buck-Boost Converter for Hybrid Electric Vehicles," *International Journal of Advances in Engineering & Technology (IJAET)*, vol. 1, no. 4, pp. 40-46, Sep. 2011.
- [43] L. Solero, A. Lidozzi, and J.A. Pomilio, "Design of multiple-input power converter for hybrid vehicles," *IEEE Transactions on Power Electronics*, vol. 20, no. 5, pp. 1007- 1016 , Sept. 2005.
- [44] Zhihao Li, O. Onar, A. Khaligh, and E Schaltz, "Design and Control of a Multiple Input DC/DC Converter for Battery/Ultra-capacitor Based Electric Vehicle Power System," in *APEC 2009. Twenty-Fourth Annual IEEE Applied Power Electronics Conference and Exposition*, Washington, 2009, pp. 591-596.
- [45] L. M. Tolbert and F. Z. Peng, "Multilevel Converters as a Utility Interface for Renewable Energy System," in *Proceedings of 2000 IEEE Power Engineering Society Summer Meeting*, 2000, pp. 1271-1274.
- [46] J. Rodriguez et al., "Multilevel Converters: An Enabling Technology for High-Power Applications," *Proceedings of the IEEE*, vol. 97, no. 11, pp. 1786-1817, Nov. 2009.
- [47] L.M. Tolbert, Fang Zheng Peng, and T.G. Habetler, "A multilevel converter-based universal power conditioner," *IEEE Transactions on Industry Applications*, vol. 36, no. 2, pp. 596 - 603, Mar/Apr 2000.
- [48] L. M. Tolbert, F. Z. Peng, and T. G. Habetler, "Multilevel Inverters for Electric Vehicle Applications," in *IEEE*, Dearborn, 1998, pp. 1424-1431.
- [49] M. F. Escalante, J. C. Vannier, and A. Arzande, "Flying Capacitor Multilevel Inverters and DTC Motor," *IEEE Transactions on Industrial Electronics*, vol. 49, no. 4, pp. 809 - 815, Aug 2002.
- [50] L. M. Tolbert, F. Z. Peng, and T. G. Habetler, "Multilevel Converters for Large Electric Drives," *IEEE*, vol. 35, no. 1, pp. 36 - 44, Jan/Feb 1999.
- [51] M. F. Aiello, P. W. Hammond, and M. Rastogi, "Modular Multi-Level Adjustable Supply with Parallel," U.S. Paten 6 301 130, Oct. 2001.
- [52] A.H. El Khateb, N.A. Rahim, and J. Selvaraj, "Cascaded DC-DC Converters as a Battery Charger and Maximum Power Point Tracker for PV Systems," in *2013 International Renewable and Sustainable Energy Conference (IRSEC)*, Ouarzazate, 2013, pp. 426- 429.
- [53] Wei Zhao, Hyuntae Choi, G. Konstantinou, M. Ciobotaru, and V.G. Agelidis, "Cascaded H-bridge multilevel converter for large-scale PV grid-integration with isolated DC-DC stage," in *2012 3rd IEEE International Symposium on Power Electronics for Distributed Generation Systems (PEDG)*, Aalborg, 2012, pp. 849- 856.
- [54] A. Santoja et al., "High voltage gain DC-DC converter for micro and nanosatellite electric thrusters," in *2013 Twenty-Eighth Annual IEEE Applied Power Electronics Conference and Exposition (APEC)*, Long Beach, 2013, pp. 2057-2063.

- [55] J.A. Abu-Qahoug, H.Mao, S. Deng, and I. Batarashe, "Interleaved Current Doublers with Parallel Connected Transformers' Primary and Secondary Sided," in *APEC 2004 - Applied Power Electronics Conference and Exposition*, 2004, pp. 641-646.
- [56] J.M. Guerrero, L. Hang, and J. Uceda, "Control of Distributed Uninterruptible Power Supply Systems," *IEEE Transactions on Industrial Electronics*, vol. 55, no. 8, pp. 2845-2859, Aug. 2008.
- [57] T. Hosi, "Control circuit for parallel operation of self-commutating inverters," Japanese Patent S56-13101, Apr. 10, 1975.
- [58] P. Alou, J. A. Cobos, O. García, R. Prieto, and J. Uceda, "Input Voltage influence on Voltage Regulator Modules based on Multiphase Buck and Multiphase Half Bridge topologies," in *APEC 2004-Applied Power Electronics Conference and Exposition*, 2004, pp. 1282-1288.
- [59] Taufik Soepraptob, Satwiko Sidopeksoc, and Mohammad Taufik, "A Comparison of multiple boost configurations for small renewable energy battery storage systems," in *International Conference on Sustainable Energy Engineering and Application*, Yogyakarta, 2012, pp. 93-96.
- [60] Yang Zhang, Regan Zane, and Dragan Maksimovic, "Current Sharing in Digitally Controlled Masterless Multi-Phase DC-DC Converters," in *PESC '05-IEEE 36th Power Electronics Specialists Conference*, Recife, 2005, pp. 2722-2728.
- [61] (2006, July) On Semiconductor - NCP5316 4-5-6 phase converter datasheet. [Online]. [http://www.onsemi.com/pub\\_link/Collateral/NCP5316-D.PDF](http://www.onsemi.com/pub_link/Collateral/NCP5316-D.PDF)
- [62] S. Ogasawara, J. Takagaki, H. Akagi, and A. Nabae, "A novel control scheme of duplex current-controlled PWM inverters," *IEEE Transactions on Industry applications*, vol. , pp. 330-337, 1987.
- [63] I. Takahashi and M. Yamane, "Multiparallel asymmetrical cycloconverter having improved power factor and waveforms," *IEEE Transactions on Industry applications*, vol. IA-22, no. 6, pp. 1007-1016, Nov 1986.
- [64] Takao Kawabata and S. Higashino, "Parallel operation of voltage source inverters," *IEEE Transactions on Industry applications*, vol. 24, no. 2, pp. 281-287, Mar/Apr 1988.
- [65] J.W. Dixon and B.T Ooi, "Series and parallel operation of hysteresis current-controlled PWM rectifiers," *IEEE Transactions on Industry applications*, vol. 25, no. 4, pp. 644-651, July-Aug 1989.
- [66] Y. Komatsuzaki, "Cross current control for parallel operating three-phase inverter," in *PESC '94 Record-25th Annual IEEE Power Electronics Specialists Conference*, Taipei, 1994, pp. 943-950.
- [67] **Pop-Calimanu Ioana-Monica**, Anna Tom, Popescu Viorel, and Muntean. Gheorghe, "A Low Cost System for Testing and Monitoring the Performance of Photovoltaic Module," *Advances in Electrical and Computer Engineering*, vol. 13, no. 4, pp. 93-98, November 2013, JCR Impact Factor: 0.642.

- [68] Aloña Berasategi Arostegi, "New Optimized Electrical Architectures of Photovoltaic Generators with High Conversion Efficiency," Université Toulouse 3 Paul Sabatier (UT3 Paul Sabatier), PhD Thesis 2013.
- [69] Tasi-Fu Wu and Yu-Kai Chen, "Modeling PWM DC/DC converters out of basic converter units," *IEEE Transactions on Power Electronics*, vol. 13, no. 5, pp. 870-881, Sep 1998.
- [70] Dariusz Czarkowski, "DC-DC Converters," in *Power electronics handbook : devices, circuits, and applications handbook*, 3rd ed.: Elsevier, 2011, ch. 13, pp. 249-264.
- [71] **Pop-Calimanu Ioana-Monica**, Prutianu Florin, and Popescu Viorel, "Design and Simulation of DC/DC Boost Converter used for a Distributed Sensing System Based on a Multidrop Sensor Network with RS485 Interface," in *10th International Symposium on Electronics and Telecommunication, ISETC '12*, Timisoara, 2012, pp. 79-82.
- [72] **Ioana-Monica Pop-Calimanu**, "Design and Simulation of DC/DC Boost Converter used for a Distributed Sensing System," in *Interdisciplinaritatea si managementul cercetarii*, Oradea, 2012.
- [73] Amtex Electronics. [Online]. [http://www.amtex.com.au/application\\_notes\\_pdf/CHP1-Princ.\\_Power\\_Convers.pdf](http://www.amtex.com.au/application_notes_pdf/CHP1-Princ._Power_Convers.pdf)
- [74] Gang Chen, Dehong Xu, and Y.-S. Lee, "A family of soft-switching phase-shift bidirectional DC-DC converters: synthesis, analysis, and experiment," in *PCC-Osaka 2002 - Proceedings of the Power Conversion Conference, Osaka, 2002*, pp. 122- 127.
- [75] Gang Chen, Dehong Xu, Yousheng Wang, and Y.-S. Lee, "A new family of soft-switching phase-shift bidirectional DC-DC converters," in *PESC. 2001 - IEEE 32nd Annual Power Electronics Specialists Conference*, vol. 2, Vancouver, 2001, pp. 859- 865.
- [76] F. Caricchi, F. Crescimbeni, F. Giulii Capponi, and L. Solero, "Study of bi-directional buck-boost converter topologies for application in electrical vehicle motor drives," in *APEC '98- Conference Proceedings 1998., Thirteenth Annual Applied Power Electronics Conference and Exposition*, vol. 1, Anaheim, 1998, pp. 287-293.
- [77] Lung-Sheng Yang and Tsorng-Juu Liang, "Analysis and Implementation of a Novel Bidirectional DC-DC Converter," *IEEE Transactions on Industrial Electronics*, vol. 59, no. 1, pp. 422 - 434, Jan. 2012.
- [78] Ruseler Adriano and Barbi Ivo, "Modeling and Digital Control Implementation of the Bidirectional Zeta-Sepic DC-DC Converter," in *PCIM 2012 - Power Electronics South America 2012*, 2012.
- [79] Ruseler Adriano and Barbi Ivo, "Modeling and digital control implementation of bidirectional step-up step-down DC-DC converters featuring the Zeta-Sepic," in *PCIM 2012 - Power Electronics South America 2012*, 2012.
- [80] M. Jain, M. Daniele, and P.K. Jain, "A bidirectional DC-DC converter topology for low power application," *IEEE Transactions on Power Electronics*, vol. 15, no. 4, pp. 595-606, JULY 2000.

- [81] Muhammed Shamveel and Vinod John, "Isolated Bidirectional DC-DC Power Supply for Charging and Discharging Battery," in *Sixth National Power Electronics Conference 2013 (NPEC 2013)*, Kanpur, 2013.
- [82] Marian K. Kazimierczuk, *Pulse-width Modulated DC-DC Power Converters*, 1st ed.: 2008 John Wiley & Sons, Ltd, 2008.
- [83] Popescu Viorel, *Electronica de putere*, 2nd ed. Timisoara: Editura de Vest, 2009.
- [84] Robert W. Erickson, *Fundamentals of Power Electronics*, Second Edition ed.: Kluwer Academic Publishers, 2000.
- [85] Raja Ayyanar, Ramesh Giri, and Ned Mohan, "Active input-voltage and load-current sharing in input-series and output-parallel connected modular DC-DC converters using dynamic input-voltage reference scheme," *IEEE Transactions on Power Electronics*, vol. 19, no. 6, pp. 1462-1473, September 2004.
- [86] R. Haroun, A. Cid-Pastor, A. El Aroudi, and L. Martinez-Salamero, "Cascade connection of DC-DC switching converters by means of self-oscillating dc-transformers," in *EPE/PEMC, 2012 15th International Power Electronics and Motion Control Conference*, Novi Sad, 2012, pp. DS1b.14-1- DS1b.14-5.
- [87] Dragan Maksimovic and Slobodan Cuk, "Switching Converters with Wide DC Conversion Range," *IEEE Transactions on Power Electronics*, vol. 6, no. 1, pp. 151-157, Jan. 1991.
- [88] D.S. Wijeratne and G. Moschopoulos, "Quadratic Power Conversion for Power Electronics: Principles and Circuits," *IEEE Transactions on circuits and systems*, vol. 59, no. 2, pp. 426-438, Febr. 2012.
- [89] L. Huber and M.M. Jovanovic, "A design approach for server power supplies for networking applications," in *APEC 2000 - Fifteenth Annual IEEE Applied Power Electronics Conference and Exposition*, New Orleans, 2000, pp. 1163-1169.
- [90] Carlos Andrés Torres-Pinzón, Roberto Giral, and Ramon Leyva, "LMI-Based Robust Controllers for DC-DC Cascade Boost Converters," *Journal of Power Electronics*, vol. 12, no. 4, pp. 538-547, July 2012.
- [91] S. Sumathi, L. Ashok Kumar, and P. Surekha, *Solar PV and Wind Energy Conversion Systems, An Introduction to Theory, Modeling with MATLAB/SIMULINK, and the Role of Soft Computing Techniques.*: Springer International Publishing Switzerland 2015, 2015.
- [92] J. Leyva Ramos, M.G. Ortiz-Lopez, J.A. Morales-Saldana, and L.H. Diaz-Saldierna, "Control of a cascade boost converter with a single active switch," in *PESC 2008-IEEE Power Electronics Specialists Conference*, Rhodes, 2008, pp. 2383- 2388.
- [93] Tsai-Fu Wu and Te-Hung Yu, "Unified approach to developing single-stage power converters," *IEEE Transactions on Aerospace and Electronic Systems*, vol. 34, no. 1, pp. 211-223, Jan 1998.
- [94] L. Linares, R.W. Erickson, S. MacAlpine, and M. Brandemuehl, "Improved Energy Capture in Series String Photovoltaics via Smart Distributed Power Electronics," in *Twenty-Fourth Annual IEEE Applied Power Electronics Conference and Exposition*, 2009, pp. 15-19.



- [95] K.P. Yalamanchili, M. Ferdowsi, and K. Corzine, "New Double Input DC-DC Converters for Automotive Applications," in *VPPC '06- IEEE Vehicle Power and Propulsion Conference*, Windsor, 2006, pp. 1-6.
- [96] M. Gavris, O. Cornea, and N. Muntean, "Multiple input DC-DC topologies in renewable energy systems - A general review," in *IEEE 3rd International Symposium on Exploitation of Renewable Energy Sources (EXPRES), 2011*, Subotica, 2011, pp. 123-128.
- [97] Manuel Jesús Vasallo Vázquez, José Manuel Andújar Márquez, and Francisca Segura Manzano, "A Methodology for Optimizing Stand-Alone PV-System Size Using Parallel-Connected DC/DC Converters," *IEEE TRANSACTIONS ON INDUSTRIAL ELECTRONICS*, vol. 55, no. 2, pp. 2664-2673, July 2008.
- [98] Sudip K. Mazumder, "Stability Analysis of Parallel DC-DC Converters," *IEEE Transactions on Aerospace and Electronic Systems*, vol. 42, no. 1, pp. 50-69, January 2006.
- [99] S. V. G. Oliveira and I. Barbi, "A three-phase step-up DC-DC converter with a three-phase high frequency transformer," in *Proceedings of the IEEE International Symposium on Industrial Electronics 2005 (ISIE '05)*, 2005, pp. 571-576.
- [100] H. B. Shin, J. G. Park, S. K. Chung, H. W. Lee, and T. A. Lipo, "Generalised steady-state analysis of multiphase interleaved boost converter with coupled inductors," in *IEE Proceedings Electric Power Applications*, 2005, pp. 584-594.
- [101] G. Y. Choe, J. S. Kim, H. S. Kang, and B. K. Lee, "An optimal design methodology of an interleaved boost converter for fuel cell applications," *Journal of Electrical Engineering and Technology*, vol. 5, no. 2, pp. 319-328, 2010.
- [102] P. Thounthong and B. Davat, "Study of a multiphase interleaved step-up converter for fuel cell high power applications," *Energy Conversion and Management*, vol. 51, no. 4, pp. 826-832, 2010.
- [103] **Pop-Calimanu Ioana-Monica** and Renken Folker, "New Multiphase Hybrid Boost Converter with Wide Conversion Ratio for PV System," *International Journal of Photoenergy*, vol. 2014, pp. 1-16, April 2014, JCR Impact Factor: 2.663.
- [104] Wenxun Xiao, Bo Zhang, and Dongyuan Qiu, "Analysis and Design of an Automatic-Current-Sharing Control Based on Average-Current Mode for Parallel Boost Converters," in *Power Electronics and Motion Control Conference*, 2009, pp. 1-5.
- [105] Taufik T., Prasetyo R., Dolan D., and Garinto D., "A New Multiphase Multi-Interleaving Buck Converter With Bypass LC," in *The 36th Annual Conference of the IEEE Industrial Electronics Society*, Phoenix, 2010, pp. 291- 295.
- [106] Z. Lukic, S.S. Ahsanuzzaman, A. Prodić, and Zhenyu Zhao, "Self-Tuning Sensorless Digital Current-Mode Controller with Accurate Current Sharing for Multi-Phase DC-DC Converters," in *APEC 2009-Twenty-Fourth Annual IEEE Applied Power Electronics Conference and Exposition*, Washington, 2009, pp. 264- 268.
- [107] Pit-Leong Wong, Peng Xu, B. Yang, and F.C. Lee, "Performance improvements of interleaving VRMs with coupling inductors," *IEEE Transactions on Power Electronics*, vol. 16, no. 4, pp. 499- 507, July 2001.

- [108] M. Nagano M. Hirakawa, Y. Watanabe, S. Nakatomi K. Ando, S. Hashino, and and T. Shimizu, "High power density interleaved DC/DC converter using a 3-phase integrated close-coupled inductor set aimed for electric vehicles," in *In Energy Conversion Congress and Exposition, ECCE* , 2010, pp. 2451-2457.
- [109] J.C. Schroeder, B. Wittig, and and F.W. Fuchs, "High efficient battery backup system for lift trucks using interleaved-converter and increased edlc voltage range," in *36th Annual Conference on IEEE Industrial Electronics Society, IECON 2010*, 2010, pp. 2334 -2339.
- [110] J.C. Schroeder and F.W. Fuchs, "Design of a power management for a battery buffer system in an electric lift truck by means of fuzzy control and genetic algorithm ," in *Proceedings of the 2011-14th European Conference on In Power Electronics and Applications (EPE 2011)*, 2011, pp. 1-10.
- [111] Jong-Pil Lee et al., "Analysis and Design of Coupled Inductor for Two-Phase Interleaved DC-DC Converters," *Journal of Power Electronics*, vol. 13, no. 3, pp. 339-348, May 2013.
- [112] Taufik Taufik, Tadeus Gunawan, Dale Dolan, and Makbul Anwari., "Design and Analysis of Two-Phase Boost DC-DC Converter," *World Academy of Science, Engineering and Technology*, pp. 912-916, 2010.
- [113] Mounica Ganta, Pallamreddy Nirupa, Thimmadi Akshitha, and R. seyezhai, "Design And Simulation Of Pwm Fed Two-Phase Interleaved Boost Converter For Renewable Energy Source," *International Journal of Electrical, Electronics and Data Communication*, vol. 1, no. 1, pp. 18-23, March 2013.
- [114] **Ioana-Monica Pop-Calimanu**, "Designing a distributed sensing system based on a multidrop sensor network with RS485 interface," in *International Conference "Technical Students Day"*, No. XIV, Timisoara, 2010, pp. 171-176.
- [115] O. Cornea, O. Pelan, and N. Muntean, "Comparative Study of Buck and Hybrid Buck "Switched-Inductor" DC-DC Converters," in *13th International Conference on Optimization of Electrical and Electronic Equipment (OPTIM), 2012* , Brasov, 2012, pp. 853 - 858.
- [116] N Muntean, O Cornea, O Pelan, and C Lascu, "Comparative Evaluation of Buck and Hybrid Buck DC-DC Converters for Automotive Applications," in *15th International Power Electronics and Motion Control Conference*, Novi Sad, 2012, pp. DS2b.3-1 - DS2b.3-6.
- [117] O. Pelan, N. Muntean, and O Cornea, "Comparative Evaluation of Buck and Switched-Capacitor Hybrid Buck DC-DC converters," in *International Symposium on Power Electronics, Electrical Drives, Automation and Motion, SPEEDAM2012*, Sorrento, 2012, pp. 1330 - 1335.
- [118] Iman Rezaei and Mahdi Akhbari, "Transformerless Hybrid Buck Converter with Wide Conversion Ratio," in *2nd Power Electronics Drive Systems and Technologies Conference* , Tehran, 2011, pp. 599-603.
- [119] Hiroshi Nomura, Kenichiro Fujiwara, and Masanobu Yoshida, "A New DC-DC Converter Circuit with Larger Step-up/down Ratio," in *37th IEEE Power Electronics Specialists Conference, 2006. PESC '06.* , Jeju, 2006, pp. 1-7.
- [120] Folker Renken, **Ioana-Monica Pop-Calimanu**, and Udo Schürmann, "Novel Multiphase Hybrid Boost Converter with Wide Conversion Ratio," in *The 16th European Conference on Power Electronics and Applications, EPE'14 ECCE Europe* , Lappeenranta, 2014, pp. P.1-P.10.

- [121] O. Abdel-Rahim, M. Orabi, E. Abdelkarim, M. Ahmed, and M.Z. Youssef, "Switched inductor boost converter for PV applications," in *2012 Twenty-Seventh Annual IEEE Applied Power Electronics Conference and Exposition (APEC)*, Orlando, 2012, pp. 2100-2106.
- [122] Lung-Sheng Yang, Tsorng-Juu Liang, and Jiann-Fuh Chen, "Transformerless DC-DC Converters With High Step-Up Voltage Gain," *IEEE Transactions on Industrial Electronics*, vol. 56, no. 8, pp. 3144-3152, August 2009.
- [123] Renken F. and Karrer V., "DC/DC Converters for Automotive Board-Net Structures," in *EPE-PEMC2004 Meeting*, Riga, 2004.
- [124] F. Renken, "Analytic Calculation of the DC-Link Capacitor Current for Pulsed Single-Phase H-Bridge Inverters," *EPE Journal*, vol. 13, no. 4, 2003.
- [125] F. Renken, "Analytic Calculation of the DC-Link Capacitor Current for Pulsed Single-Phase H-Bridge Inverters," in *EPE2003*, Toulouse, 2003.
- [126] F. Renken, "Analyses of the DC-Link Current in Discontinuous Modulated Three-Phase Inverters," in *EPE-PEMC 2006 Meeting*, Portorož, 2006.
- [127] F. Renken, "DC-Link Current in Pulsed H-bridge Inverters," in *PCIM Conference*, Nürnberg, 2009.
- [128] E. Hiraki, K. Yamamoto, and T. Mishima, "An Isolated Bidirectional DC-DC Soft Switching Converter for Super Capacitor Based Energy Storage Systems," in *PESC 2007 - IEEE Power Electronics Specialists Conference*, Orlando, 2007, pp. 390-395.

## Author's papers related to the thesis

### 1. Scientific papers published in ISI Journals

1. **Ioana-Monica Pop-Calimanu**, F. Renken, "New Multiphase Hybrid Boost Converter with Wide Conversion Ratio for PV System", Hindawi Publishing Corporation, International Journal of Photoenergy, vol 2014, Article ID 637468, 17 pages, Accession Number: WOS:000335769800001, ISSN: 1110-662X, eISSN: 1687-529X, doi: 10.1155/2014/637468, JCR Impact Factor: 2.663, JCR 5-Year Impact Factor: 2.240, *Journal Citation Reports® 2012 Science Edition (Thomson Reuters)*

2. **Ioana-Monica Pop-Calimanu**, T. Anna, V. Popescu, G. Muntean, "A Low Cost System for Testing and Monitoring the Performance of Photovoltaic Module", Advances in Electrical and Computer Engineering, vol 13, issue 4, pp. 93-98, 2013, Accession Number: WOS:000331461300016, ISSN: 1582-7445, eISSN: 1844-7600, doi: 10.4316/AECE.2013.04016, JCR Impact Factor: 0.642, JCR 5-Year Impact Factor: 0.580, *Journal Citation Reports® 2013 Science Edition (Thomson Reuters)*

### 2. Scientific papers published in the Proceedings from scientific meetings/conference indexed ISI Proceedings

1. **Ioana-Monica Pop-Calimanu**, F. Prutianu, V. Popescu, "Design and Simulation of DC/DC Boost Converter used for a Distributed Sensing System Based on a Multidrop Sensor Network with RS485 Interface", 2012 10th International Symposium on Electronics and Telecommunication, ISETC '12, Timisoara, Romania, ISBN: 978-1-4673-1175-5(IEEE catalog number: CFP1203LCDR), doi: 10.1109/ISETC.2012.6408077, Noiembrie 2012, pp.79-82, indexed IEEE Romanian Sect, IEEE ComSoc Germany Chapter, Romanian Academy of Technical Sciences, (Web of Knowledge-Thomson Reuters)

2. F. Prutianu, **Ioana-Monica Pop-Calimanu**, V. Popescu, "Validation system for power supply module part of automotive ECUs", 2012 10th International Symposium on Electronics and Telecommunication, ISETC '12, Timisoara, Romania, ISBN: 978-1-4673-1175-5(IEEE catalog number: CFP1203L-CDR), doi: 10.1109/ISETC.2012.6408069, Noiembrie 2012, pp.75-78, indexed IEEE Romanian Sect, IEEE ComSoc Germany Chapter, Romanian Academy of Technical Sciences, (Web of Knowledge-Thomson Reuters)

3. F. Prutianu, **Ioana-Monica Pop-Calimanu**, V. Popescu, "Semi-automated power supply efficiency measuring system", 2012 10th International Symposium on Electronics and Telecommunication, ISETC '12, Timisoara, Romania, ISBN: 978-1-4673-1175-5 (IEEE catalog number: CFP1203LCDR), doi: 10.1109/ISETC.2012.6408067, Noiembrie 2012, pp.45-48, indexed IEEE Romanian Sect, IEEE ComSoc Germany Chapter, Romanian Academy of Technical Sciences, (Web of Knowledge-Thomson Reuters)

### **3. Scientific papers published in BDI Journals -**

#### **4. Scientific papers published in the Proceedings from scientific meetings/conference indexed BDI Proceedings**

1. **Ioana-Monica Pop-Calimanu**, F. Prutianu, V. Popescu, "Boost Converter Used in Solar Energy Systems", The 11th International Conference on Engineering of Modern Electric Systems, EMES'11, Oradea, Romania, ISSN 1844 – 6035, Volum 4, Mai 2011, pp. 195-198, Index Copernicus International, Scopus

2. F. Prutianu, **Ioana-Monica Pop-Calimanu**, V. Popescu, "Power factor Correction Inductor Design From a Wind Turbine Boost Converter", The 11th International Conference on Engineering of Modern Electric Systems, EMES'11, Oradea, Romania, ISSN 1844 – 6035, Volum 4, Mai 2011, pp. 199- 202, Index Copernicus International, Scopus

#### **5. Scientific papers published in the Proceedings volumes from international scientific meetings/conference from abroad**

1. F. Renken, **Ioana-Monica Pop-Calimanu**, U. Schurmann "Novel multiphase hybrid Boost converter with wide conversion ratio", 2014 16th European Conference on Power Electronics and Applications, EPE'14-ECCE Europe, Lappeenranta, doi: 10.1109/EPE.2014.6910967, August 2014, pp. 1-10, indexed IEEE

#### **6. Scientific papers published in the Proceedings volumes of scientific meetings**

1. **Ioana-Monica Pop-Calimanu**, O.A. Ciurdar, D. A. Dinca, V. Malcoci, A. Radu, "Solar energy used in buildings", IP „Materials Energy and sustainable Growth”, Vilnius, Lituania, 27.02-12.03.2011

2. **Ioana-Monica Pop-Calimanu**, "Converters Used in Solar Energy Systems", Workshop-ul numarul 1, din cadrul proiectului „Spre cariere de cercetare prin studii doctorale”, Timisoara, Romania, Noiembrie 2011.

3. **Ioana-Monica Pop-Calimanu**, "Design and Simulation of DC/DC Boost Converter used for a Distributed Sensing System Based on a Multidrop Sensor Network with RS485 Interface", Workshop-ul nr. 2, „Interdisciplinaritatea si Managementul cercetarii in studiile doctorale, Oradea, Romania, 7-8 iunie 2012.